AD-773 886

RESEARCH IN MATERIALS SCIENCE

D. J. Epstein, et al

Massachusetts Institute of Technology

Prepared for:

Defense Supply Service
Advanced Research Project Agency

31 December 1973

DISTRIBUTED BY:

NTIS

National Technical Information Service
U. S. DEPARTMENT OF COMMERCE
5285 Port Royal Road, Springfield Va. 22151

UNCLASSIFIED

SECURITY CLASSIFICATION OF THIS PAGE (When Data Entered)

AD-773 886

REPORT DOCUMENTATION PAGE		READ INSTRUCTIONS BEFORE COMPLETING FORM
1. REPORT NUMBER #1	2. GOVT ACCESSION NO.	3. RECIPIENT'S CATALOG NUMBER
4. TITLE (and Subtitle) RESEARCH IN MATERIALS SCIENCE		5. TYPE OF REPORT & PERIOD COVERED Semi-Annual Technical 1 July 1973 - Dec. 31, 1973
		6. PERFORMING ORG. REPORT NUMBER
7. AUTHOR(s) D. J. Epstein, R. M. Rose, M. MacVicar, R. Lagow, R. Pelloux, G. Benedek		8. CONTRACT OR GRANT NUMBER(s) DAHC 15-73-C-0316
9. PERFORMING ORGANIZATION NAME AND ADDRESS Massachusetts Institute of Technology Center for Materials Science & Engineering Cambridge, Mass. 02135		10. PROGRAM ELEMENT, PROJECT, TASK AREA & WORK UNIT NUMBERS 3D10
11. CONTROLLING OFFICE NAME AND ADDRESS Defense Supply Service - Washington Room 1D 245- The Pentagon Washington, D. C. 20310		12. REPORT DATE 31 December 1973
		13. NUMBER OF PAGES ~~885~~ 299
14. MONITORING AGENCY NAME & ADDRESS (if different from Controlling Office) ONR Resident Representative Massachusetts Institute of Technology Room E19-629 Cambridge, Mass. 02135		15. SECURITY CLASS. (of this report) Unclassified
		15a. DECLASSIFICATION/DOWNGRADING SCHEDULE

16. DISTRIBUTION STATEMENT (of this Report)

Distribution of this document is unlimited.

17. DISTRIBUTION STATEMENT (of the abstract entered in Block 20, if different from Report)

Unlimited

18. SUPPLEMENTARY NOTES

19. KEY WORDS (Continue on reverse side if necessary and identify by block number)

Optoelectronic Materials and Components: Miniaturized Thin Film Laser Sources and Modulators; Superconducting Transition Metal Alloys;

Chemical Synthesis/High Temperature Lithium Vapor Species; Fatigue and Fracture of Austenitic Steels; Materials Characterization/Laser light Scattering Spectroscopy

20. ABSTRACT (Continue on reverse side if necessary and identify by block number)

This report presents the results and status of work after the first six month period of work on this research program which consists of five separate tasks involving research in materials scinece.

I Optoelectronic Materials and Components: Miniaturized and Thin Film Laser Sources and Modulators

Laser action at 2μm in a single mode has been demonstrated.

Films of KTN have been successfully grown. Silicon and antimony doped

DD FORM 1 JAN 73 1473 EDITION OF 1 NOV 65 IS OBSOLETE S/N 0102-014-6601

1<

SECURITY CLASSIFICATION OF THIS PAGE (When Data Entered)

GaAs diodes have been fabricated and tested. A "clean chemistry" laboratory has been installed. A Single zone furnace for the growth of KTN by CVD has been constructed. An instrument for precision measurement of refraction index over a wave length range extending from the visible to the near infrared has been built.

II Superconducting Transition Metal Alloys

Progress towards the solution of the complex problem of superconductivity of high-T_c A15 materials by tunneling experiments.

III Chemical Synthesis Using High Temperature Lithium Vapor Species

New synthetic routes to polylithiocarbons, per lithiocarbons and inorganic polylithium species, synthesis of the first perlithioalkanes, tetralithiomethane, $C(Li)_4$ and hexalithiorthane, C_2Li_6, preparation of hexalithiobenzene C_6Li_6 and study thereof.

IV Fatigue and Fracture Properties of Austenitic Steels

Fatigue crack growth rates (FCGR) of two unstable austenitic stainless steels are determined and results discussed in terms of the influence of phase structures, stacking fault energy and work hardening exponent on the FCGR.

V Materials Characterization Using Laser Light Scattering Spectroscopy

Study of the spectrum of light scattered quasi-elastically from gels and the accurate measurement of state of a two-dimensional gas of pentadecylic acid water molecules on the surface of water.

SEMI-ANNUAL TECHNICAL REPORT #1

Period: July 1, 1973 - Dec. 31, 1973

Title: Research In Materials Sciences

Project Title: Optoelectronic Materials and Components: Miniaturized and Thin Film Laser Sources and Modulators

Contract Number: DAHC 15-73-C-0316

ARPA Order Number: 2469

Program Code Number: 3D10

Name of Contractor: Massachusetts Institute of Technology
Cambridge, Mass. 02139

Principal Investigator: N. J. Grant (617) 253-5638

Project Scientists or Engineers: D. J. Epstein (617) 253-4676;
A. Linz (617) 253-[illegible], C. G. Sonstad, Jr. (617) 253-4634,
H. P. Jenssen (617) 253-6878

Effective Date of Contract: June 1, 1973

Contract Expiration Date: May 31, 1974

Amount of Contract: $425,000

Amount of Project: $152,000

Sponsored By

Advanced Research Projects Agency

ARPA Order No. 2469

OPTOELECTRONIC MATERIALS AND COMPONENTS: MINIATURIZED AND THIN FILM LASERS AND MODULATORS

SUMMARY

The research being carried out under the subject contract is directed toward the development of miniaturized lasers and modulators compatible with dielectric waveguide and fiber optic transmission elements. Specific objectives include:

1. development of rare earth doped fluoride and oxide materials suitable for miniaturized and thin film lasers;
2. development of techniques for the epitaxial growth of KTN compositions in structural configurations appropriate for electro-optical light modulation;
3. development of light-emitting diodes as pump sources for miniaturized lasers;
4. design, fabrication and evaluation of miniaturized and thin film laser-source "packages" which include the associated pump and modulator.

The following listing summarizes our achievements during the first six months of the program:

1. We have demonstrated laser action at 2 μm in a single mode Ho:YLF minilaser 0.2 x 0.6 x 0.9 mm in dimension. Lasing occurred at a threshold power of 20 mw; an output power of 5 mw was obtained at 150 mw pump power. The laser was operated in a dielectric-cavity mode which is particularly well adapted for coupling to optical waveguides (Section II).
2. Films of KTN have been successfully grown on $KTaO_3$ substrates by

carried out (Section V).

We expect by the end of the first year of the program to have an LED pumped 2 μm Ho:YLF laser operating cw at, or near, room temperature. We believe that in this miniiaser we will have a prototype of a class of lasers that will be extremely useful for integrated optical systems. The only serious competitive source on the scene is the diode laser, and its future, as a room-temperature source, appears clouded by problems involving reliability and lifetime.

I. INTRODUCTION

When we began this program we believed that we had sufficient knowledge of energy transfer and fluorescence in lithium yttrium fluoride (YLF) to allow us to predict with some confidence that the development of a miniaturized 2 μm Ho:YLF laser was a realistic prospect. Our work to date, described in Section II, bears out this initial confidence. We have demonstrated lasing action in a crystal of volume 0.2 x 0.5 x 0.6 mm The threshold for lasing was low, about 20 mw, and we were able to get a cw output of about 5 mw at a pump power of 150 mw. This laser appears to be the smallest dielectric laser ever to operate at such low thresholds. Our goal is to achieve lasing action in samples of even smaller dimensions. The laser is side pumped and operates in an internal reflection, two-dimensional, dielectric cavity mode. A mode analysis is given in the Appendix. Output coupling occurs via the evanescent fields established outside the dielectric boundaries by the totally reflected internal waves. This electromagnetic configuration appears particularly attractive for integrated optics because it allows coupling to a waveguide structure merely by placing the cavity in close proximity to the guide. Coupling structures such as prisms, wedges or gratings are not required. We are continuing this work with emphasis on obtaining a Ho:YLF composition operable at or near room temperature in the near term, and are investigating the feasibility of utilizing other activators such as Tm^{3+} and Er^{3+} in YLF as well as improving the pumping efficiency and other factors by going to a high refractive index oxide host. Further miniaturization is also a goal in order to match the size of the diode pumps.

The work to date on the diode pumps is described in Section III. The thrust of the program has been the design and fabrication of specialized diode geometries; the growth, testing and evaluation of Si-doped GaAs

LED's with emission tailored to the Yb:YLF minilaser absorption band and with efficient high intensity output; and the growth and characterization of Zn and Si doped GaAsSb LED's with the objectives of understanding the system for use vs more sophisticated heterostructure diode geometries.

The technology development to permit the growth of desired geometries in the GaAs:Si system is virtually complete and several runs have been made to explore the emission wavelength and bandwidth as a function of various parameters. It is expected that useful pump diodes from this system will be available before the end of the next reporting period.

The growth of thin KTN films for electro-optical waveguide modulators is described in Section IV. Films have been grown on $KTaO_3$ substrates by a liquid phase epitaxy technique and have shown waveguiding in preliminary experiments. Masks are being fabricated for appropriate electrodes to permit evaluation of a wave deflection-modulation scheme as well as a simple step phase modulator. Chemical vapor deposition growth experiments have been made and a method for generating and transporting KCl vapor has been developed. An improved two-zone furnace is being constructed and we expect by the end of the next reporting period to be able to evaluate this technique for the growth of KTN.

Instrumentation for accurate measurement of refractive indices of crystals is described in Section V, together with a description of the newly installed clean air chemistry laboratory.

A mode calculation for the dielectric resonator minilaser is given in the Appendix.

II. MINILASER DEVELOPMENT

2.1 Prototype Minilaser

To obtain an efficient minilaser it is necessary for the laser crystal to have a high absorption coefficient at the pump wavelength. This objective can be achieved by employing a high concentration of the active ion as in the NdLa pentaphosphate laser[1] or by incorporating into the host a high concentration of sensitizer ions. The latter approach, which we are following in our work, has proved successful in the 2.06 μm Ho:YLF laser sensitized with Er and Tm.[2]

Additional problems encountered in the minilaser involve the design of the resonator and output coupling scheme. One resonator configuration that has been employed[3] is simply a scaled down version of the usual rod laser with reflecting end plates. A laser of this type would have to be coupled to a thin film waveguide by a prism or grating. We believe that a more attractive route is to use a configuration capable of sustaining resonant modes confined to the cavity volume by total internal reflection (Fig. 1). The evanescent field associated with total internal reflection can be used to couple to an output structure. Using such a scheme we have succeeded in obtaining single mode cw laser action at 2.06 μm in a single crystal of $LiY_{0.462}Er_{0.5}Tm_{0.035}Ho_{0.003}F_4$. The laser transition is from the lowest level of Ho^{3+} $^5I_7$ to the upper $^5I_8$ level.

The experimental details are shown in Fig. 2. The laser crystal with its four long sides polished and with dimensions 0.94 mm x 0.60 mm and 5 mm long was mounted over an undoped $LiYF_4$ prism. A tapered gap was formed by resting one end of the crystal on top of a 20 micron thick evaporated indium pad while the other end rested on the prism. A 0.2 mm wide region of the crystal was pumped with the output of a cw krypton ion laser (6471 Å). By

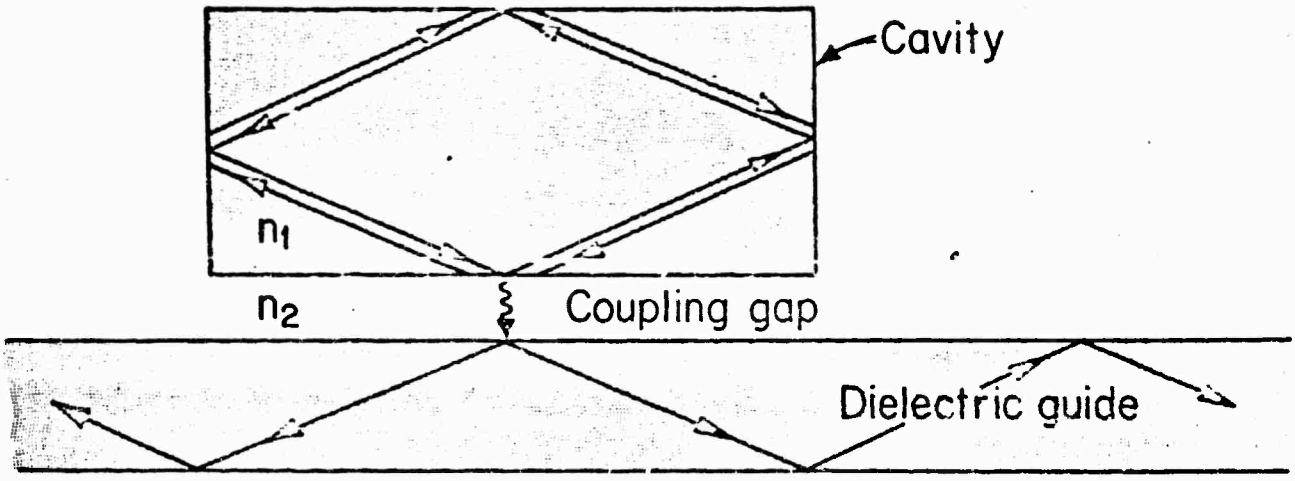

Fig. 1 Internal refl ction mode in cavity coupled to dielectric waveguide via evanescent field in coupling gap.

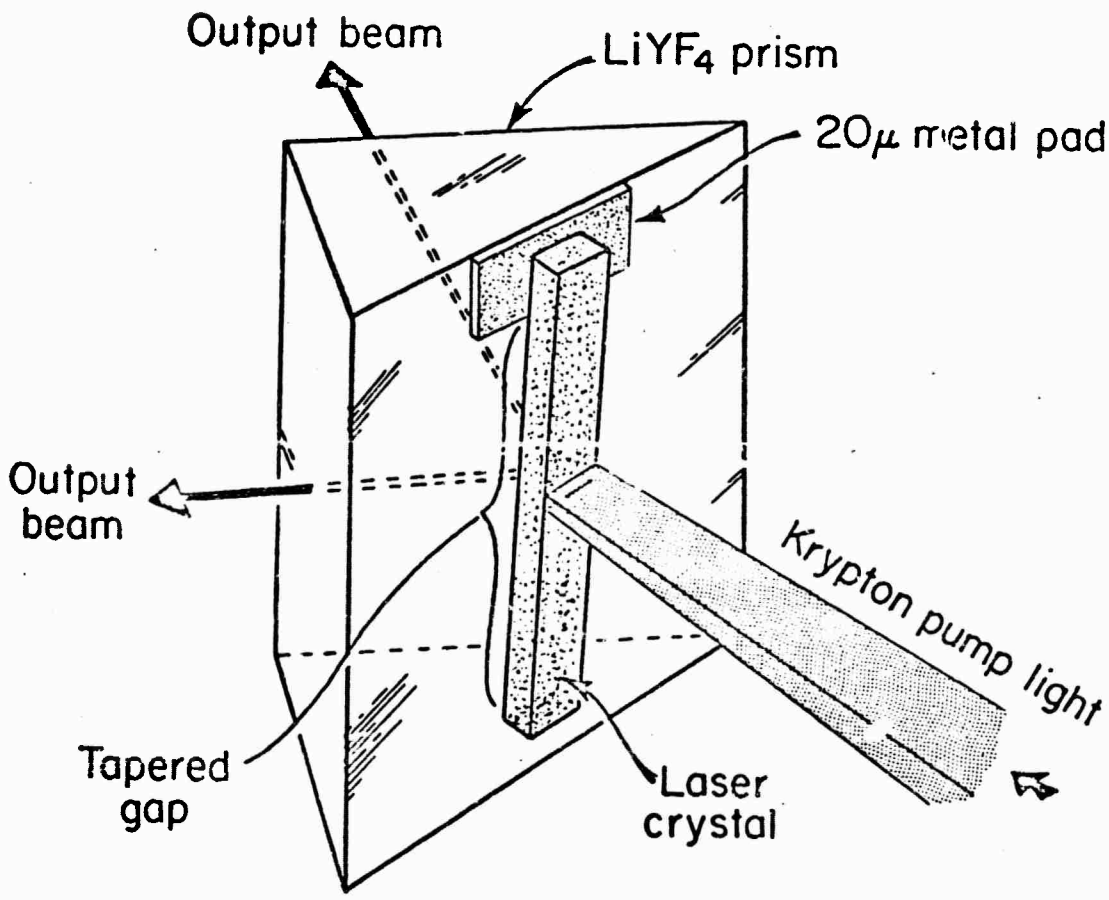

Fig. 2 Experimental arrangement for test of prototype minilaser using internal reflection mode. The rod cross section is 0.94 x 0.60 mm. The pump light is confined to a beam 0.2 mm wide.

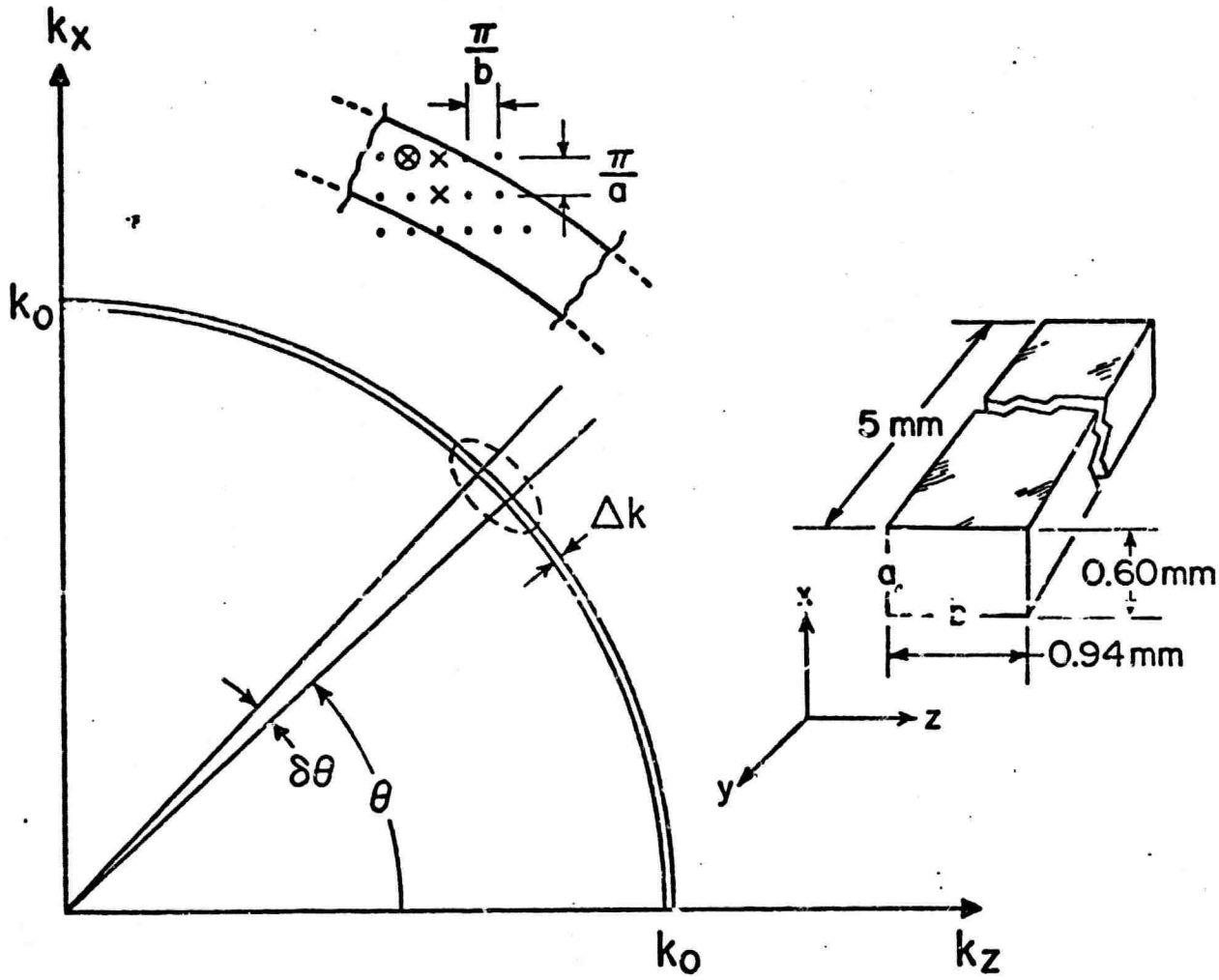

Fig. 3 Internal reflection modes in k-space for the Ho:YLF minilaser. Total internal reflection occurs for those modes within the sector $\delta\theta$. The mode marked ⊗ is the one appearing at threshold; the nearby modes marked x appear above threshold (see Fig.4).

varying the position of the pumped region along the length of the crystal, the output could be observed as a function of coupling strength. The laser crystal and prism were mounted in vacuum in a liquid N_2 dewar.

The resonator is closed on four sides by total internal reflecting dielectric boundaries and open on the other two sides. Since only a small segment of the active material is pumped, only those modes with propagation vector transverse to the long axis of the crystal are excited. It is shown in the Appendix that, in a rectangular crystal, the condition for total internal reflection modes to exist is $n_1 > \sqrt{2}\, n_2$, where n_1 is the refractive index of the crystal and n_2 is the index of the surrounding medium. Figure 3 shows the region of k-space available for internal reflection modes in a rectangular crystal with $n_1 = 1.46\, n_2$, a situation which applied to a crystal of $LiYF_4$ (n_1) in vacuum (n_2). The angle $\delta\theta$ (see Appendix) is given functionally as

$$\delta\theta = 2 \tan^{-1} \left[\left(\frac{n_1}{n_2}\right) - 1\right]^{\frac{1}{2}} - \frac{\pi}{2}, \qquad (1)$$

and for our experimental situation is numerically equal to 3.5°.

Light is coupled out of the resonator into the prism through the evanescent field in the gap.

Output spectra of the laser are shown in Fig.4. Threshold was reached with approximately 20 mW pump power. Near threshold laser action took place in only one mode, as is evident from the single line in the spectrum. The linewidth is determined by the resolution limit of our spectrometer. With pump power about twice threshold, two other modes appear. The unequal spacing of the modes can be explained by considering the modes of a two-dimensional resonator as is done in the Appendix. The theoretical analysis shows that the modes which appear at increasing pump

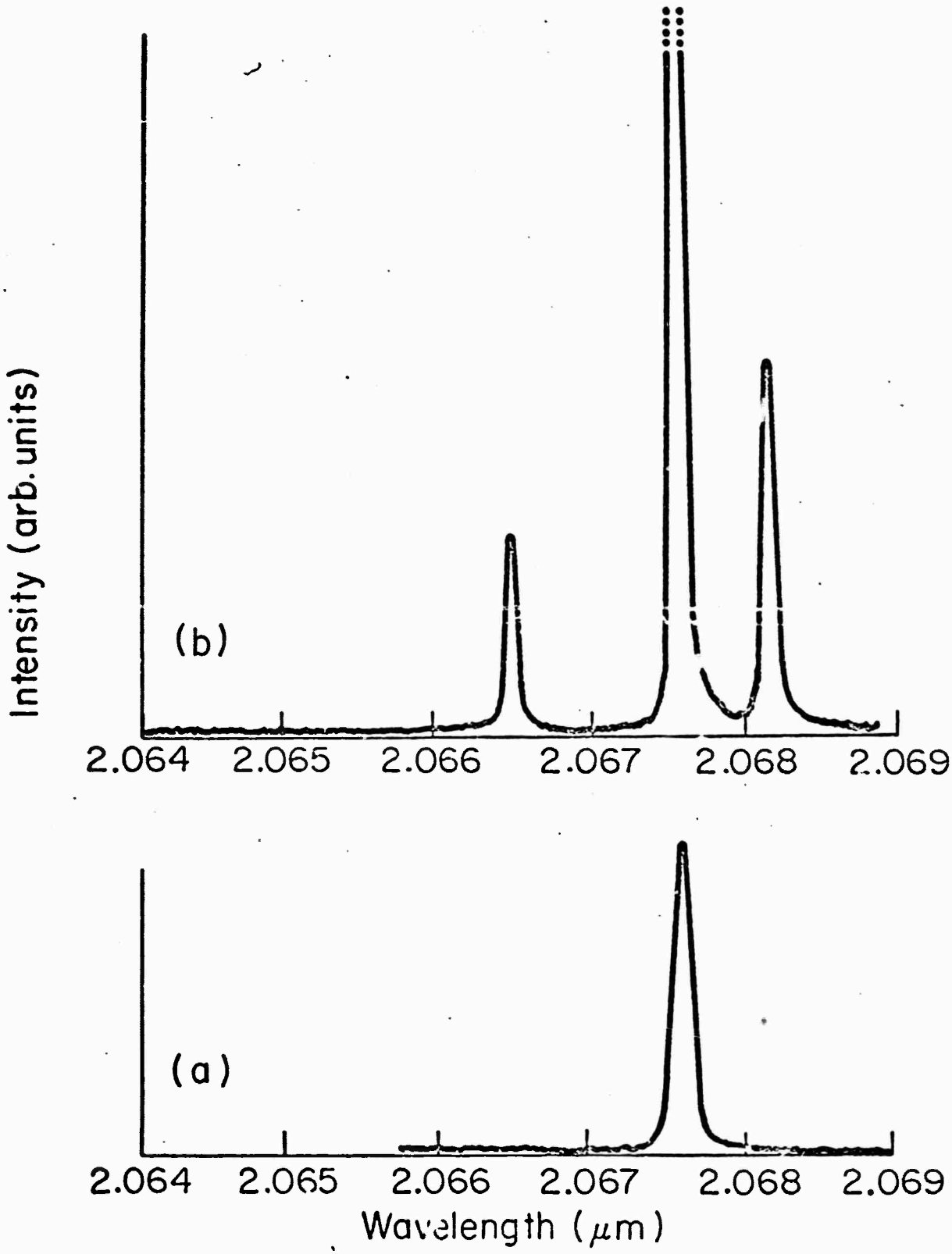

Fig. 4 Output spectra of Ho:YLF minilaser: (a) near threshold; (b) twice threshold.

power are separated from the initial mode by

$$\Delta\lambda_o = \frac{-\lambda_0^2}{2\sqrt{2}n_1}\left(\frac{\Delta p}{a} + \frac{\Delta q}{b}\right) \qquad (2)$$

where Δp, Δq = 0, ±1, ±2, ±3, etc. The modes appearing in Fig.4 correspond to $\Delta\lambda_o$ (Δp = 0, Δq = 1) = -1.1×10^{-3} μm and $\Delta\lambda_o$ (Δp = -1, Δq = 1) = 0.62×10^{-3} μm. The experimental values are in precise agreement with theoretical predictions. The relative positions of these modes in k-space are shown in the inset in Fig. 3.

Output powers of 5 mW were measured with 150 mW pump power and a gap size of 5 microns. The threshold did not increase monotonically with decreasing gap size, indicating that losses associated with edge chipping and other crystal defects partially determined the threshold. Lower thresholds are expected with more careful sample preparation.

The transmission through the coupling gap is largest for modes whose propagation vector is incident on the base of the crystal at the critical angle, and decreases rapidly with increasing incident angle. Figure 5 shows the calculated transmission loss versus mode angle for a TE cavity mode coupled across a 5 μm gap. Only the lowest loss modes will reach laser threshold. Note that internal reflection modes exist only in the interval between 43.3° and 46.7°. When the mode angle increases above 43.3° (the critical angle) we enter the region of internal reflection, and transmission of energy out of the cavity modes occurs via the evanescent field at the output coupling face. In our experiments this was the narrow face of the crystal (dimension a). With increasing angle there is progressively less transmission across the gap. At 46.7° evanescent fields still exist at the coupling face, where the condition for internal reflection is still maintained. However, we no longer satisfy this condition on the

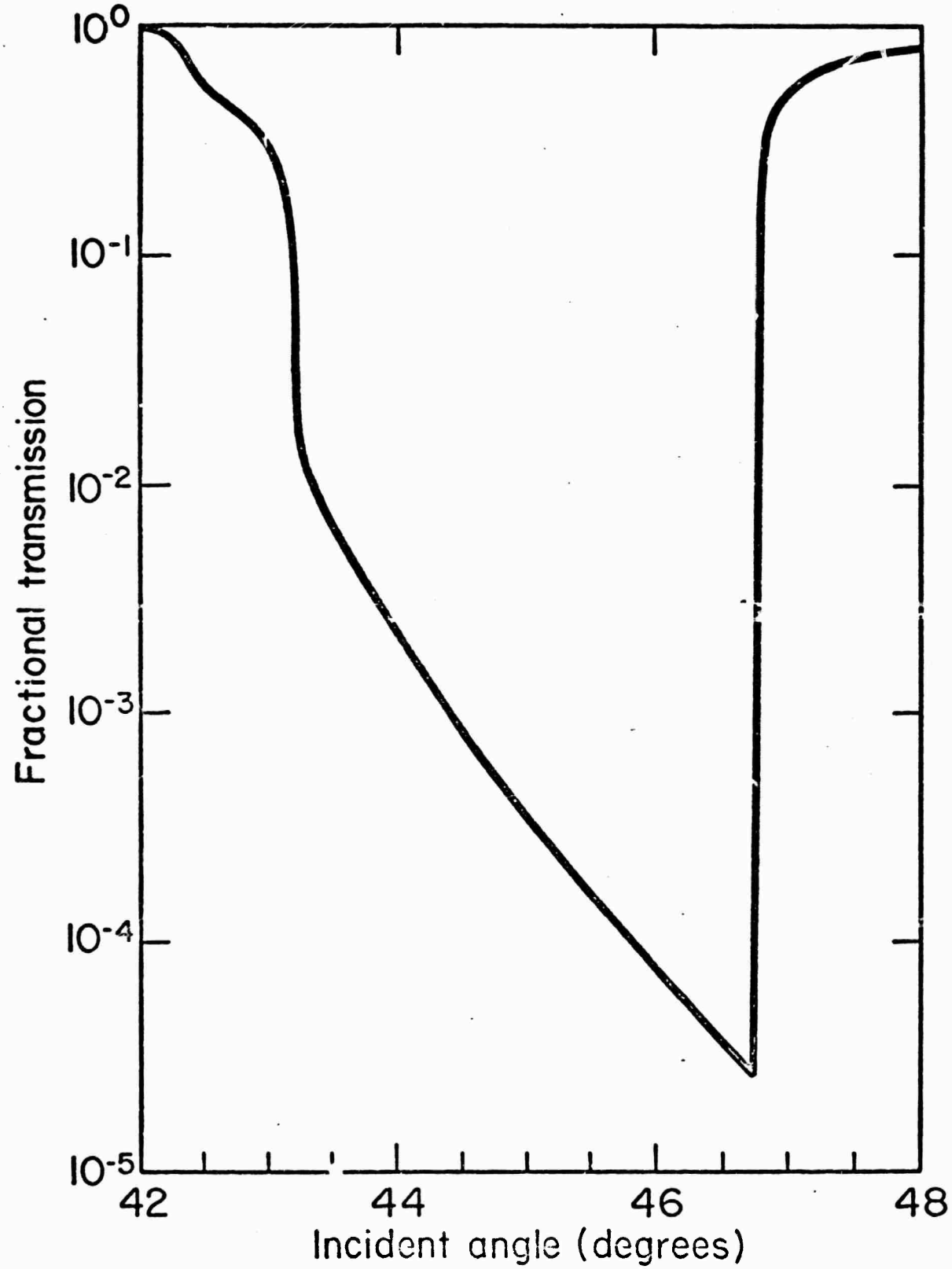

Fig. 5 Cavity transmission loss as a function mode angle (measured as angle of incidence at output face of cavity).

orthogonal b face and, consequently, the transmission loss rapidly increases as energy is radiated from the two b faces.

We see in Fig. 3 that the cavity modes which are excited above threshold have an angle of incidence θ (measured from the normal to the a face) which is less than the angle for the mode with lowest threshold. This result is consistent with loss curve shown in Fig. 5.

As a source for integrated optical networks, this type of minilaser has the advantage of much higher efficiency than proposed thin film rare earth lasers.[4] The largest absorption coefficient of a rare earth ion transition that can be pumped by a light-emitting diode is about $\alpha = 200\ cm^{-1}$. Thus, for a thin film 1 micron thick, only 2% of the incident light can be absorbed when transversely pumped. With the dielectric resonator, the dimension in the pumping direction can be made about $1/\alpha$, so that most of the pump light will be absorbed, leading to an increase in pumping efficiency by a factor of about 50.

The number of possible resonant modes can always be made arbitrarily small in this scheme by proper control of the indices n_1 and n_2. Decreasing the size of the resonator increases the mode separation in k-space. Thus, with smaller resonators single mode operation should be obtainable even at pump powers many times threshold.

The Ho:alphabet YLF laser materials studied so far have run cw only at liquid N_2 temperature. Future work will be directed toward a room temperature miniature cw holmium laser. To obtain room temperature cw operation the Ho^{3+} concentration must be low (< 0.5%) so that the terminal laser level will have a small population, but there are two factors limiting how low the Ho^{3+} concentration can be made: (1) resonator loss, and (2) energy transfer rates.

If laser resonators with losses of 0.01% can be made, materials with less than 0.01% Ho^{3+} would have sufficient gain for cw laser operation. Conventional Fabry-Perot resonators have a minimum loss of about 1% from mirror scattering and diffraction losses. The miniature total internal reflection resonator should have much less loss. Future work will be done on measuring and reducing the losses of this resonator. Edge chipping is a problem in fabricating these small crystals; scattering losses from these defects will be less from resonators of different geometries than those previously used.

In the Ho-alphabet YLF laser material energy transfer between the Tm:$^3H_4$ and the Ho:$^5I_7$ levels is very fast compared to the fluorescent lifetimes of the levels so that the populations of the levels can be described by a thermal equilibrium. Therefore, a low Ho^{3+} concentration necessitates a low Tm^{3+} concentration so that the quantum efficiency of the Ho^{3+} fluorescence will remain high. It is not yet known how low the Tm^{3+} and Ho^{3+} concentration can be made before energy transfer from Er^{3+} is inefficient.

Single mode laser operation is needed for integrated optics applications. The total internal reflection resonator has been operated single-mode for pump powers up to twice threshold. Further work will be done to obtain single mode operation over a larger range of pump powers by making the resonator smaller, which will also make it more compatible with the LED pump.

2.2 Fluoride Crystal Growth

Alphabet YLF samples of the following compositions have been utilized for this program:

#159f $LiY_{0.487}Er_{0.5}Tm_{0.01}Ho_{0.003}F_4$

#171f $LiY_{0.462}Er_{0.5}Tm_{0.01}Ho_{0.003}F_4$

#193f $LiY_{0.628}Er_{0.20}Yb_{0.1}Tm_{0.067}Ho_{0.005}F_4$

#213f $LiYb_{0.495}Er_{0.4945}Ho_{0.0005}Tm_{0.01}F_4$

#217f $LiErF_4$: 0.005 Tm

#219f $LiErF_4$: 0.01 Tm

Sample #171f was used for the minilaser described in Section 2.1, while sample #213f has yet to be tested. Measurements on samples #217f and 219f indicated that the Tm fluorescence was almost completely quenched by back transfer (Tm $^3H_4 \rightarrow$ Er $^4I_{13/2}$) and subsequent impurity quenching of the Er $^4I_{13/2}$ via energy migration to an impurity center. The impurity center could be a transition element such as Fe or, more probably, trace amounts of Dy^{3+}. It is evident that higher purity ErF_3 than is currently commercially available will have to be used when low activator concentrations are necessary. Zone refining experiments are in progress.

2.3 New Materials

A considerable amount of exploratory research has been devoted to finding suitable oxide rare earth hosts with high refractive indices to provide a better optical match to the pump LED and to give more flexibility for coupling into modulator and wave guide structures. These have included CAMGAR ($CaY_2Mg_2Ge_3O_{12}$), $n_D = 1.83$, and $Y_2Ti_2O_7$, $n_D \sim 2.35$. The latter material is of the most interest, not only for the higher index but also because this pyrochlore structure places the rare earth ion in a site with a center of inversion symmetry ($3\bar{m}$ D_{3d}). This results in only magnetic dipole transitions being allowed and may provide better branching

ratios for some transitions.

$Yb_2Ti_2O_7$ crystals with Er^{3+} compositions of 0.1, 1 and 2 atomic % have been grown. The refractive index as a function of wavelength is shown in Section V, Fig. 19. As with Tm^{3+} in $LiErF_4$ the Er^{3+} fluorescence in the 0.1% sample was completely quenched by impurities and much purer feed materials will have to be used. We propose to use solvent extraction as well as conversion to chlorides for zone refining as methods of purification. The new clean air chemistry laboratory described in Section V makes these procedures practical.

III. DIODE PUMPS

3.1 Diode Pump Requirement

The solid state minilaser excitation source, or pump, will be a semiconductor light-emitting diode which has been designed specifically to pump the laser geometries already discussed. The diodes to be used will be designed to have planar emitting surfaces to which the lasers can be intimately attached. Two possible structures are illustrated in Fig. 6. The diode geometry will further be such that the junction can be well heat sunk to permit operation at high current levels, 3-400 A/cm^2, and the junction area will be slightly greater than that of the laser to maximize the pump energy entering the minilaser. General diode structures have been designed and fabrication techniques are being developed.

The diode emission, as well as geometry, is being tailored for optimum pumping. An intense, efficient emission is, of course, important, but the emission spectrum too must be adjusted to match the pump band of the minilaser. This requires as narrow an emission band as possible peaking at the laser absorption maximum. To achieve this two approaches are being followed: (1) the use of silicon-doped gallium arsenide diodes, and (2) the use of silicon and/or zinc-doped gallium arsenide antimonide diodes. Both systems, as will be discussed in detail in the following section, emit further into the infrared than do conventional zinc-doped GaAs LED's, which is what is required, and each has its own particular advantages. The GaAs;Si system has been the subject of considerable study[5-9] so that our work here is as much development as research. We have been concerned in this program with developing our own capability in growing the required diode layers, with tailoring the pump diode emission spectrum, and with maximizing the emission intensity and overall pump efficiency. The GaAsSb system, on the

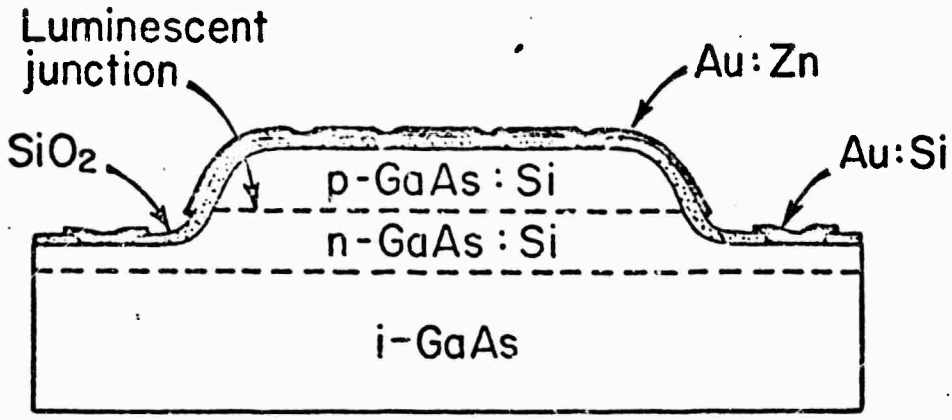

a) Pump diode, mesa geometry

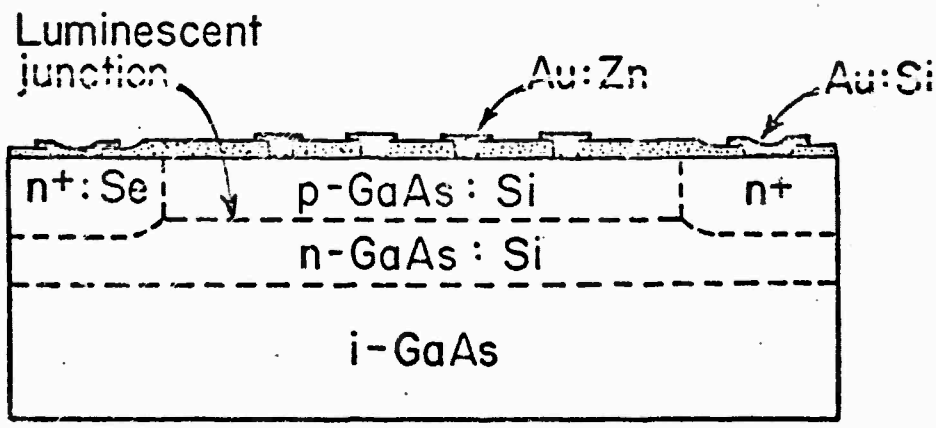

b) Pump diode, planar-diffused geometry

Figure 6- Cross section drawings of two possible pump diode structures.

other hand, is much more poorly understood[11] and the work on this system is considerably more basic, starting with the determination of parameters in the growth system and the behavior of dopants in the alloy system.

To summarize then, the diode minilaser pumps program has three areas of emphasis, or thrusts: (1) the design and fabrication (including technology development) of specialized diode geometries; (2) the growth, testing, and evaluation of Si-doped GaAs LED's with emission tailored to pump the Yb:YLF minilaser absorption band and with efficient, high intensity output; and (3) the growth and characterization of Zn and Si doped GaAsSb LED's with the objectives of fully understanding this system and evaluating it for ultimate use in the pump diodes. Initial pump diodes and minilaser-diode structures will evolve from a combination of the results of programs 1 and 2 above. Future structures will involve more sophisticated, heterostructure diode geometries and materials developed in the third effort.

3.2 Emission Tailoring

The minilaser we intend to build has a strong pump band at 0.97 μm and it is this band that the pump diode emission will be matched to. Because conventional GaAs diodes emit at 0.90 μm[10] this requires the use of either silicon-doped GaAs diodes, which with sufficient silicon-doping will emit at 0.97 μm, or the use of an alloy compound system such as GaAsSb with silicon doping in homostructures or with zinc doping in heterostructures, i.e., between GaAs layers.

Silicon doping has attractive features for the pump diode application. First, silicon can enter the GaAs lattice either at gallium sites where it acts as a donor or at arsenic sites where it behaves as an acceptor.[7] Which position it enters depends on the temperature the crystal is grown at, and by growing an epitaxial layer through a transition temperature (∿ 900°C

for GaAs[6]) a p-n junction is grown "automatically". The junction grown is never exposed to contamination at the junction interface as it would be if it were grown from two melts, so it is of very high quality. This feature is being exploited in our diode programs and one of the first things to be determined in the GaAsSb program is this transition temperature as a function of silicon and antimony concentrations. The gradual junction formed has desirable features for efficient device production as well. In particular, the p region which grows at the lower temperature is heavily compensated, resulting in a conduction band with a fairly deep tail of donor states even in the p region near the junction. These states are usually filled. Thus, radiative transitions occur between the lower tip of the "tail" and the valence band or acceptor states, whereas the absorption edge corresponds to the energy between the valence band and the empty conduction states above the tail. This effectively increases the energy difference between the emission peak and the absorption edge. The GaAs is therefore much more transparent at the emitted wavelength than at energies nearer the bandgap, so reabsorption of the light is greatly reduced and the external efficiency similarly improved. Diodes with overall efficiencies greater than 30% have been reported.[10]

The final important feature of silicon doping is the fact that because the levels introduced by silicon are deeper than other "shallow" dopants such as zinc, emission via these levels occurs at a lower energy, therefore longer wavelength. This is desirable for pumping into the laser absorption band and is why GaAs:Si diodes can emit at 0.97 μm.

One potential disadvantage of relying on large silicon doping concentrations, 1-3%, to get the longer wavelength emission desired, is that the emission peak may become broader as the silicon concentration is increased.

There is some evidence in the literature[7-9] that this is the case, but other factors such as the width of the n to p transition region, that is, the junction grading constant, must also be considered. One of our main objectives, in fact, is to determine the effect of the grading constant on the emission spectrum and diode efficiency. It is definitely the case that the Si-doped GaAs emission peak is broader than the emission peak of Zn-doped GaAs, roughly 40 nm vs 25 nm. To get the desired 0.97 μm emission using Zn-doping or lower levels of Si-doping, however, a lower bandgap semiconductor must be used, and for this purpose the alloy GaAsSb is being studied. The room temperature bandgap of $GaAs_xSb_{1-x}$ decreases from 1.425 eV in GaAs to 0.725 eV in GaSb[11], and for $x \approx 0.97$, for example, should be sufficiently lowered to give the desired emission for a low 0.5% Si doping. In homostructure diodes there will clearly be a compromise required between the width of the emission line and the level of silicon doping needed to get emission sufficiently far below the absorption edge so that reabsorption is not a problem. If heterostructures are used, the reabsorption problem can be minimized by surrounding the emitting GaAsSb layer by wider bandgap GaAs layers, and that problem can be effectively separated from the problem of the emission linewidth.

3.3 Liquid Phase Epitaxy of Diode Layers

The pump diodes are fabricated in epitaxial layers grown by liquid phase epitaxy, LPE. A typical device might require a p-type layer on an n-type layer all on an n-type or semi-insulating GaAs substrate. As was described above, when silicon is used as a dopant only one growth is necessary to produce both of the layers. If zinc, a p-type dopant, is used, however, an n-layer may have to be grown first from, for example, a tin-doped melt, and then the p-type layer grown from a second zinc-doped

melt. Multiple growths would also be required if more complicated heterostructure devices are being fabricated.

We currently have two LPE growth systems dedicated to this program. Both are horizontal, sliding furnaces similar to the one illustrated in Fig. 7. In such a system, the substrate and melt are contained in a graphite boat like that in Fig. 8. As can be seen in the cutaway sketch of another boat in Fig. 9, the substrate rests in a depression in the bottom of the boat. The melt consisting of gallium saturated (at the growth initiation temperature) with arsenic (and antimony when growing GaAsSb) is contained in the well in the graphite slider. The slider illustrated in Fig. 8 has several wells and thus can be used to grow multiple layers; the boat in Fig. 9 has only one well.

To see how these boats are used in an LPE growth, it is illustrative to outline the steps in an actual growth. The growth run starts with the substrate. Careful preparation of the substrate is one of the singularly most important parts of a successful epitaxial growth. High quality material must be used, although grown layers tend to have higher crystalline perfection than the substrate, and the substrate surface must be highly polished and chemically etched. Our substrates are given a five minute etch in 5:1:1 etch (five parts by volume H_2SO_4, one part H_2O_2, and one part H_2O) rinsed, dried, and placed in the boat. The boat at this stage contains the gallium for the melt. The gallium is loaded into the boat first where it is baked at 1000°C in hydrogen for twelve hours to deoxidize it prior to loading the other items. The arsenic, antimony, and dopants are added after the substrate and then the boat is sealed in the furnace. Growth is performed in a hydrogen atmosphere. With the boat loaded and in position the system is flushed with hydrogen overnight. It is then heated

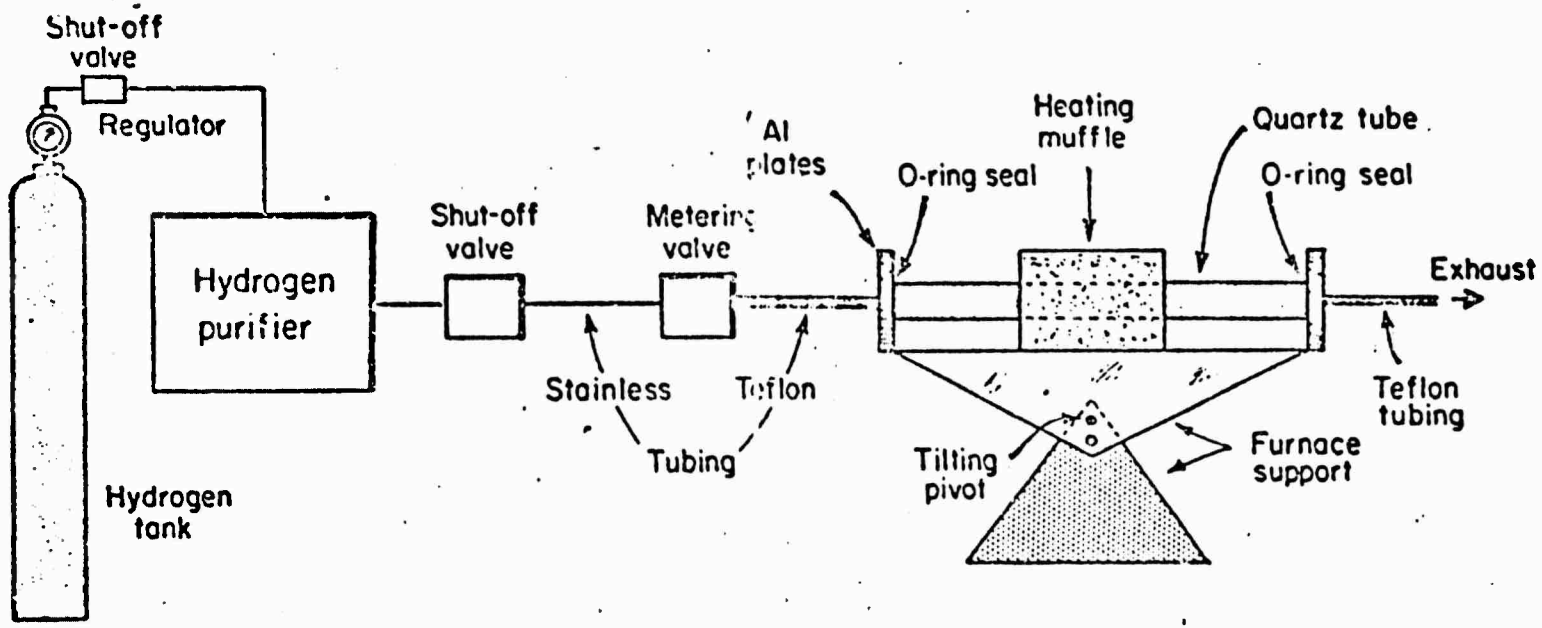

Figure 7 - Schematic diagram of the crystal growth system.

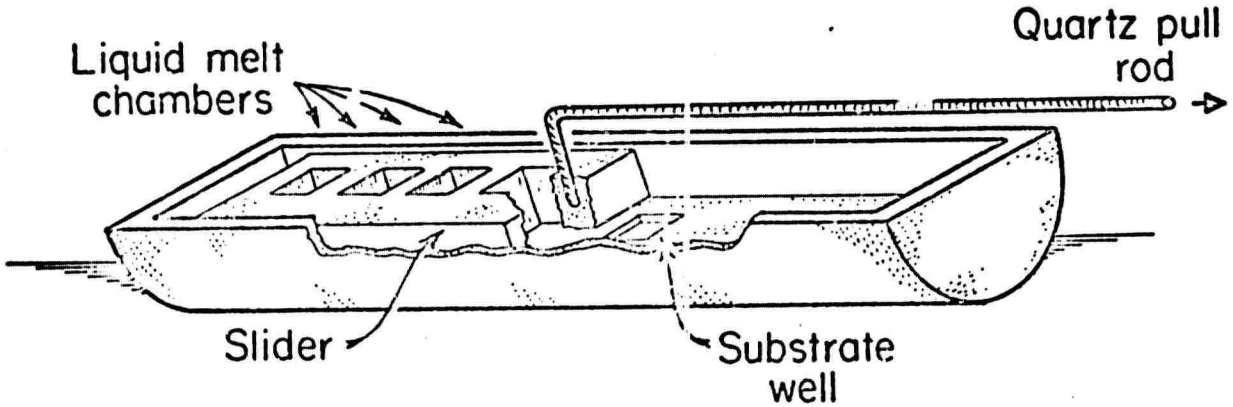

Figure 8 - Multi-well boat used to multiple hetero-layers.

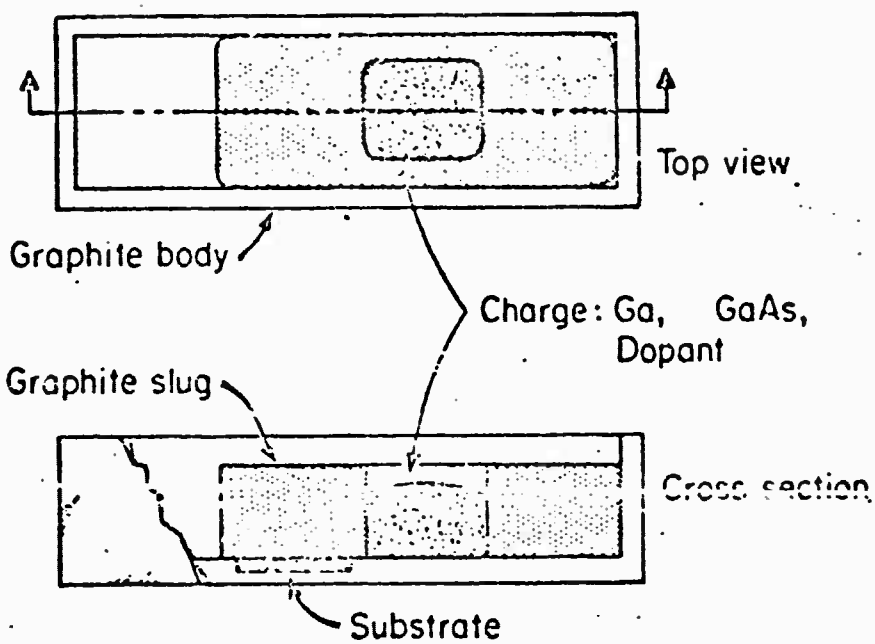

Figure 9 - Single well reaction vessel or "boat", top and cut-away views.

to approximately 20°C above the growth initiation temperature and allowed to equilibrate. The temperature is then lowered to the growth initiation temperature and once it stabilizes the slider is moved, using a quartz push rod, to bring the melt into contact with the substrate. It is often desirable to etch off a thin layer of the substrate prior to initiating the growth and this can be accomplished by either making the melt purposely undersaturated at the initiation temperature or by increasing the temperature a few degrees after the sliding. The later technique affords very good control over the etch back particularly if a second "dummy" substrate is used to equilibrate the melt at the growth initiation temperature prior to moving it onto the "good" substrate. In either case, the temperature is then lowered at a constant rate, 25°C/hour in our typical growths, until the desired layer thickness is grown. This is, of course, readily determined from solubility data for the alloy system; numbers are available in the literature.

Once the proper thickness layer has been grown, the melt is removed from the substrate by moving the slider over again with the quartz push rod. The furnace is then cooled to room temperature and the substrate is removed and used. The growth of multiple layers is done in a similar manner although etch back of the grown layers is not necessary, nor in fact desirable, and the use of a dummy substrate is essential.

The materials used in the growth are all obtained commercially. GaAs substrates are purchased from Electronic Materials Corporation in the form of (100) oriented wafers, 0.015" thick, with a chemically polished face. These are cut into substrates approximately 7 mm square on a wire saw in our laboratory. The gallium used is nominal 6-9's purity and the antimony and arsenic are added to the melts in the form of undoped polycrystalline GaAs and GaSb. The silicon is obtained in the form of standard

arsenic-doped wafers from Monsanto that are scribed and broken into small dice in the MIT Microelectronics Laboratory.

As described the LPE technique appears to be a straightforward process, as it should be. It is our experience that with certain precautions, essentially by being careful at the proper times, the commonly reported difficulties with LPE such as constitutional supercooling are not in fact encountered. The key areas of concern appear to be (1) that the gallium be prebaked and the system be carefully flushed prior to growth to avoid oxides, (2) that the substrate be carefully prepared and etched to remove surface damage prior to growth, and (3) that the melt be removed completely and cleanly after growth. The latter is accomplished by cutting the substrate to completely fill the boat substrate well and by keeping the substrate and layer thickness such that there is a small clearance between the slider bottom and the grown surface.

A modification of our standard technique described above which we have found significant for the GaAsSb growth is the use of a graphite plug in the melt well. This plug keeps the melt, which in the GaAsSb growths contains a large amount of Sb and has a large surface tension, from balling up and improves the surface coverage and layer uniformity. Most importantly, it reduces the crystallization on the upper surface of the melt which, if not controlled, can interfere with the slider motion.

3.4 Results to Date

In the initial six months of this program we have been very successful in getting two LPE growth systems functioning which are currently producing both epitaxial GaAs:Si and GaAsSb:Si layers. The grown samples are divided into several pieces, one of which is angle-lapped and stained to check junction depth uniformity and junction planarity. Small gold contacts

are evaporated through a metal mask on another piece and it is cut into test diode dice which are mounted as illustrated in Fig. 10. Spectral emission and efficiency as a function of operating current are then obtained. A typical emission spectrum for a GaAs device with 1.7% Si doping is shown in Fig. 11.

In the GaAsSb:Si program we have, with the system modification described earlier, been able to grow high quality appearing layers with good surface coverage and flat surfaces. We are currently refining this technique to improve our reproducibility and simultaneously are collecting data on the n to p transition temperature as a function of Si and Sb concentrations.

The development of pump diode geometries and fabrication techniques has also proceeded well. A David Mann photorepeater has recently been installed in our Microelectronics Laboratory and will be used to produce the necessary mask sets for the pump diode patterns. Actual diode fabrication must await growth of the LPE layers but work on development of fabrication techniques has proceeded using bulk GaAs samples, i.e., bare substrates. Techniques for etching mesas using patterned pyrolytic SiO_2 as a mask and for patterning gold contact patterns using standard photoresists and photolithographic methods have been developed. We are currently developing techniques to do the deep n+ diffusions in GaAs needed for the device structure shown in Fig. 6.

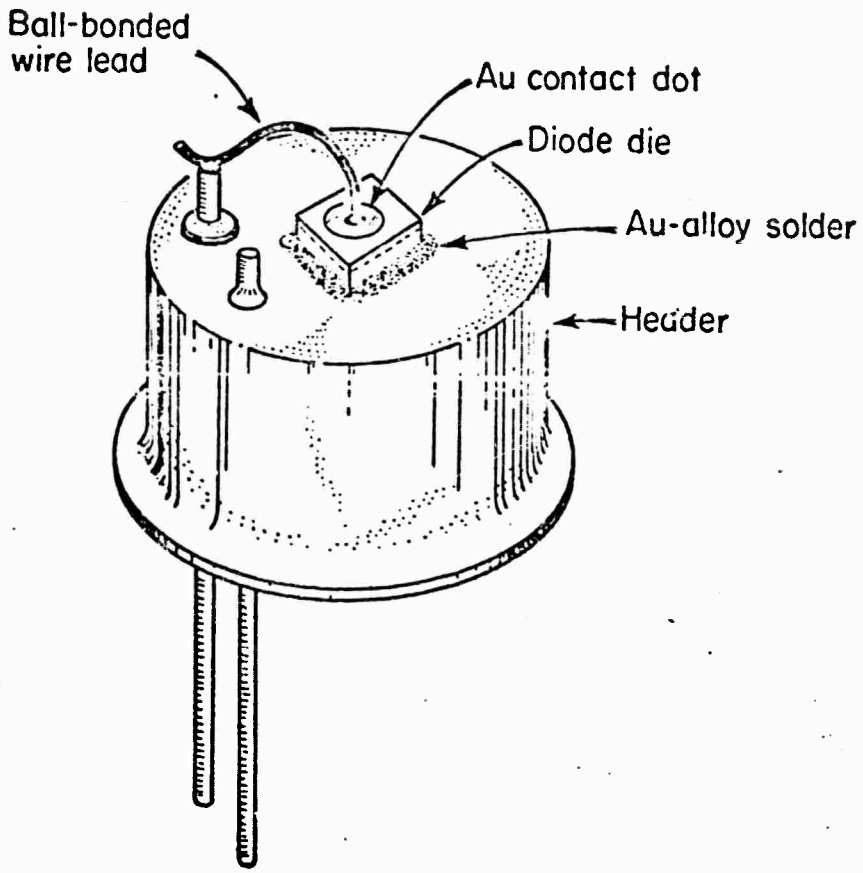

Figure 10- Artist's sketch of mounted diode chip for use in testing the diodes for emission spectrum and efficiency.

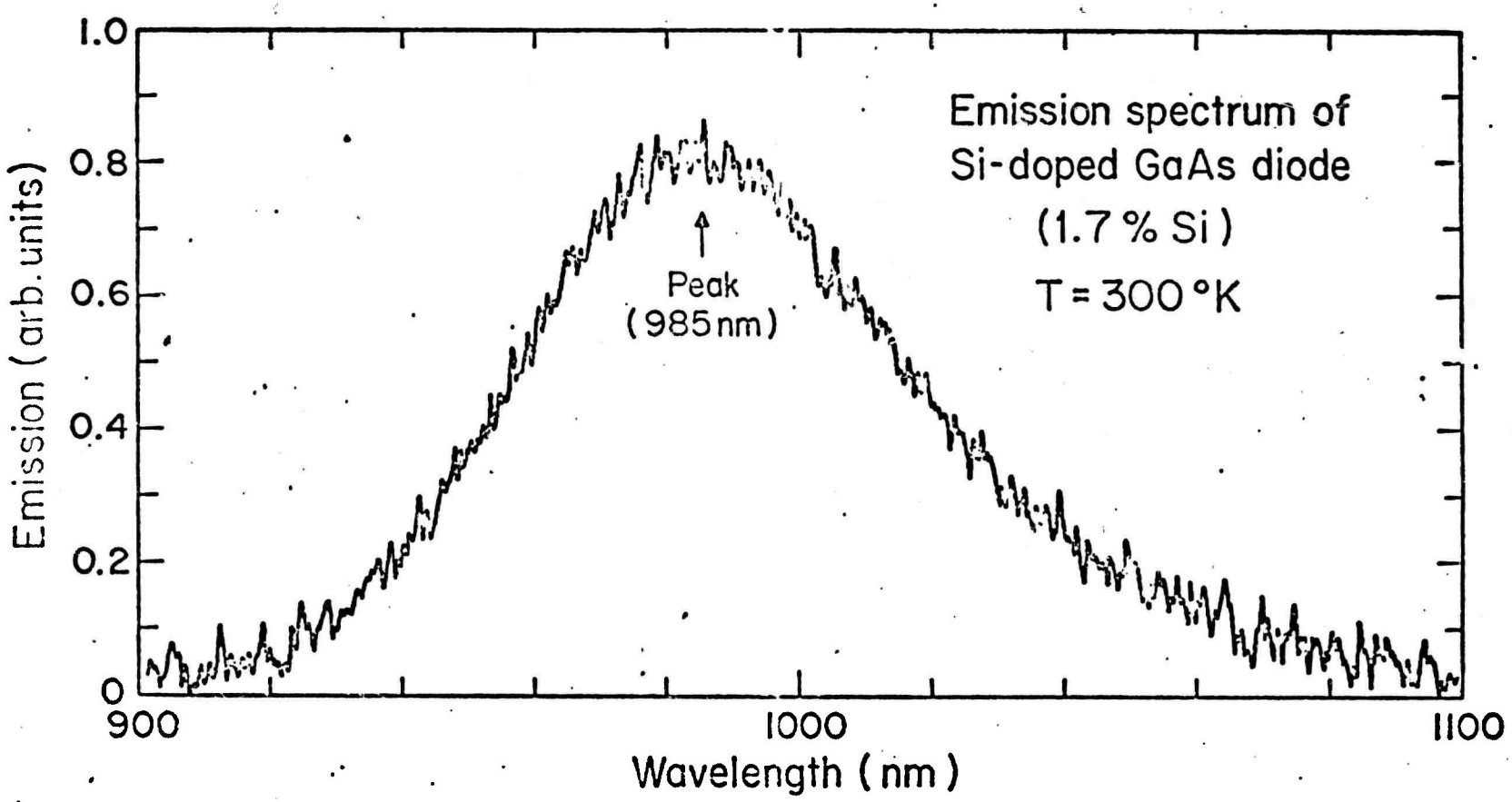

Fig. 11 Typical diode emission spectrum for a silicon-doped GaAs diode containing 1.7% silicon doping.

IV. MODULATOR PROGRAM

We describe in this section that part of our program concerned with the growth of thin films for electro-optical waveguide modulators. We have concentrated on materials in the solid solution series $KTa_{1-x}Nb_xO_3$. Compositions in this system are attractive because they possess a particularly high figure of merit for electro-optical modulation. Two distinct growth techniques are being explored: (1) chemical vapor deposition (CVD); and (2) liquid phase epitaxy (LPE).

4.1 CVD Growth

A CVD system for the growth of KTN in bulk and thin film form has been constructed. The system, shown in Fig. 12, has provision for six independent gas flows. Two chlorine flows are used for the production of $TaCl_5$ and $NbCl_5$ vapor by the controlled chlorination of Ta and Nb metal. Monitored flows are provided for the oxygen and hydrogen necessary for the reaction

$$2KCl+2(1-x)TaCl_5+(2x)NbCl_5+6H_2+3O_2 \rightarrow 2KTa_{1-x}Nb_xO_3+12HCl$$

A third chlorine flow is used to create, between the chloride streams and the H_2 and O_2 flows, a sheath which prevents the reaction from occurring at the nozzle, where it could cause clogging, and allows the reaction instead to occur downstream in the reaction zone. Finally, helium can be introduced to suppress back-diffusion of the metal vapors, and to allow for purging the system during start-up and termination of the run.

The production of the TaCl and NbCl vapors is accomplished without difficulty. The Ta and Nb are chlorinated in external reactors heated to 240°C and the vapors are transported to the furnace in heated lines. The

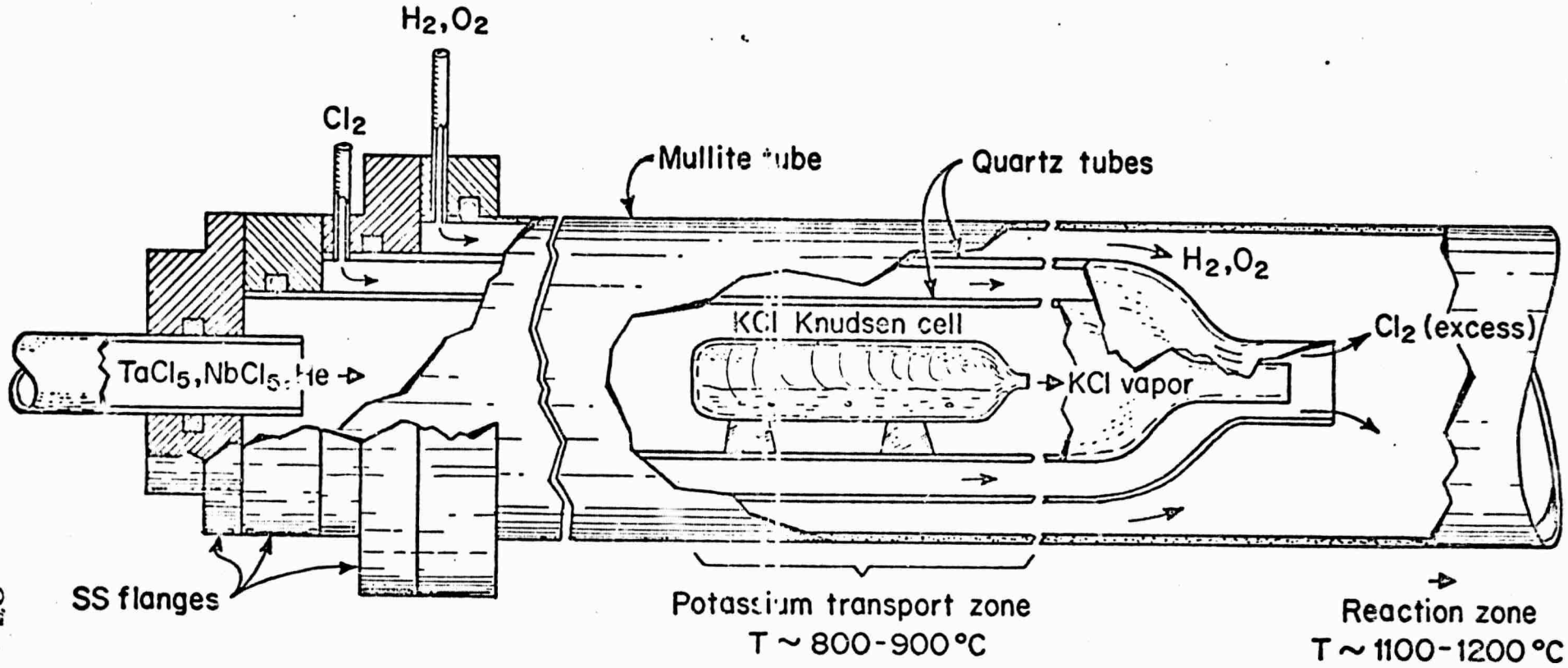

Fig. 12 System for growth of KTN by chemical vapor deposition.

production of KCl vapor is much more difficult. After a number of false starts we ended up with an arrangement in which liquid KCl is vaporized within a Knudsen cell. The cell is a cylindrical quartz vessel 3" in length, 1" in diameter, with a 0.25 mm diameter hole at the exit end. To obtain a controlled flow the cell is positioned in the furnace at a point where the temperature is slightly above the melting point of KCl (ca. 770°C). Unfortunately, in our present single zone furnace there is a substantial gradient at the point where we must position the Knudsen cell. We are in the process of constructing a new furnace which will contain two zones, one a reaction zone, the other a region for the controlled volatilization of KCl.

Work with the present furnace has been concerned with finding the appropriate conditions for KTN growth. Nineteen runs, lasting from 1 to 8 hours, have been made thus far. Runs 1 through 8 involved general testing of the system as well as checks on $TaCl_5$ and $NbCl_5$ production and flow. Runs 9 through 14 were concerned with finding a suitable scheme for the production of a controlled flow of KCl vapor. Runs 15 and 16 were tests to see whether the pentoxides of Ta and Nb could be grown. Runs 17 through 19 were unsuccessful attempts to grow KTN. It appears that if we are to be successful in growing KTN by chemical vapor deposition we need greater flexibility in control of KCl flow than we have in our present furnace. Our new two-zone furnace should provide this needed flexibility.

In our first runs with the new furnace we plan to concentrate on the growth of $KTaO_3$. Only after this composition is successfully grown shall we proceed with the growth of solid solutions in the KTN system.

4.2 Growth by Liquid Phase Epitaxy

Using the method of liquid phase epitaxy we have successfully grown

thin films of KTN on a substrate of $KTaO_3$. We are employing a dip method in which a suitably prepared substrate of $KTaO_3$ is dipped into a molten mixture of K_2CO_3, Ta_2O_5 and Nb_2O_5, held in contact with the melt for a brief period, and upon withdrawal, is rapidly spun to remove any attached droplets.

The $KTaO_3$ substrates are cut from crystals grown by the top-seeded solution technique. They are prepared as circular discs 0.5 - 1.0 mm thick and 8 - 18 mm in diameter with the face of the substrate parallel to a (100) crystallographic plane. The surface on which we desire to grow the epitaxial film is polished on a GMI, Model 1000 polishing machine using successively finer grades of diamond paste ending with 0.25 μm grit size. Flatness is maintained to within one quarter wavelength of sodium light. The sample is degreased, cleaned in a warm chromic-sulfuric acid solution, and rinsed in distilled water.

The substrate, attached to platinum seed rod with three platinum wire prongs, is slowly lowered to within 6 cm of the surface of the melt (melt temperature 1250°C) where it is allowed to stabilize for about 15 minutes and then lowered into the melt while rotating at 50 - 60 rpm. After a growth period varying from 10 - 40 minutes the sample is withdrawn and spun at 1000 rpm for 10 seconds. The seed rod is then lifted at a rate of about 2 cm/min until the substrate is fully removed from the furnace.

The growth rate of the epitaxial films produced by this procedure is quite rapid, ca 5 - 10 μm/min, suggesting that growth occurs under supersaturated conditions. The melt used for the runs we have made to date consists of

57.6 mole percent K_2CO_3

25.4 mole percent Nb_2O_5

17.0 mole percent Ta_2O_5

The "as grown" epitaxial films had rippled surfaces and when examined in polarized light showed birefringence despite the fact that films were in a compositional range where the material is structurally cubic at room temperature. Presumably the birefringence is strain-induced.

The compositional variation of the films was examined with an electron microprobe. Typical results are shown in Figs. 13 and 14 for a film having the composition $KTa_{0.69}Nb_{0.31}O_3$. The scatter in the data obtained in the traverse parallel to the surface lies within the limits of instrumental accuracy. The degree to which we can determine the abruptness of the transition from film to substrate is limited by the positional accuracy of the microprobe system, about ± 4 μm.

In our future work we plan several modifications in film preparation procedure. In order to slow down the growth rate we plan to dilute the melt somewhat by the addition of a suitable flux. We will carry out a systematic investigation of the way in which film growth and quality is affected by the various steps in the soak, dip, withdrawal and spin sequence. To reduce film strain we shall explore the possibilities of slightly modifying the substrate composition in an attempt to improve the lattice constant match between substrate and film. We also hope to reduce strain effects by ion milling the substrate subsequent to our final diamond polish.

4.3 Film Evaluation

The films as grown were not suitable for light guiding because of their rippled surfaces. These irregularities were eliminated by careful polishing. The resultant films were optically flat, scratch-free, and varied in thickness from 50 - 70 μm. Light guiding was observed using a

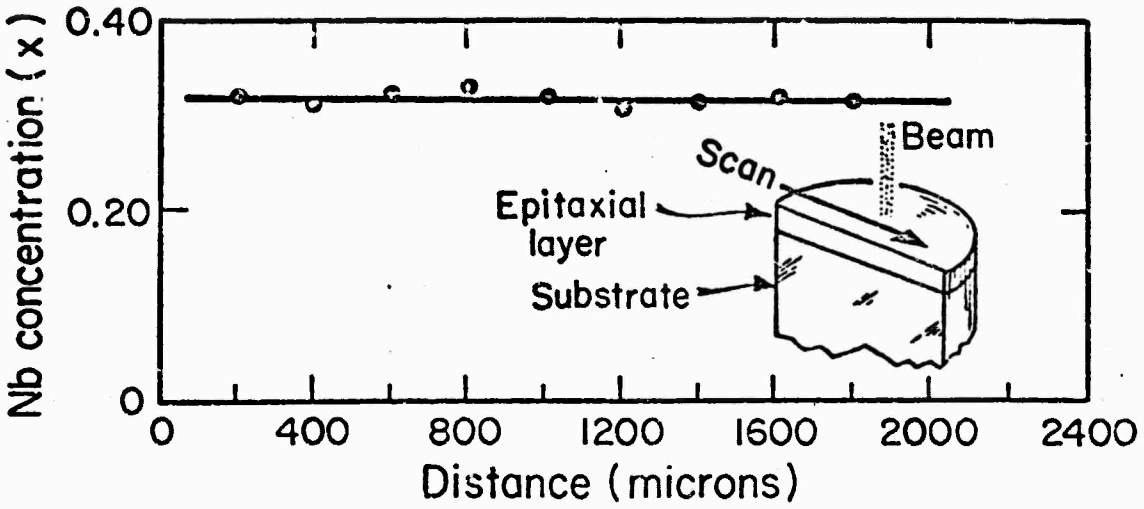

Fig. 13 Microprobe scan of KTN film on $KTaO_3$ substrate; scan is parallel to surface.

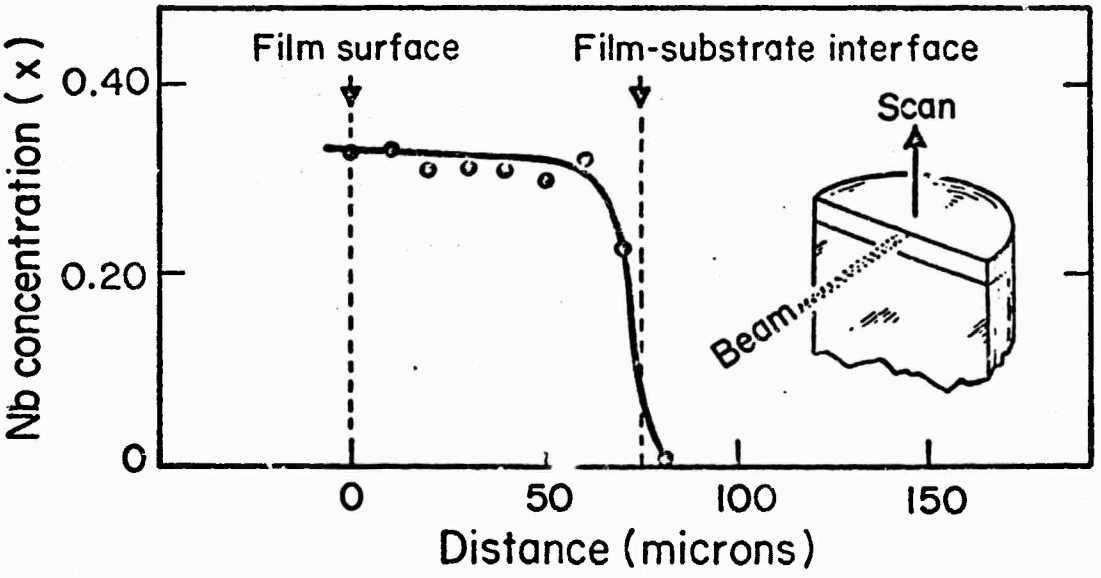

Fig. 14 Microprobe scan of KTN film on $KTaO_3$ substrate; scan is perpendicular to film edge.

rutile prism to couple into the film. By using a double-sided prism we were able to resolve a series of mode pattern "m-lines" on an output screen.[12] The patterns appeared and disappeared at approximately the angular patterns predicted by our theoretical calculations. We are now in the process of more carefully examining the guided modes in these films.

To evaluate the electro-optical properties we will initially check the performance of the films in a waveguide deflection-modulation scheme employing an interdigital electrode structure deposited on the film surface (Fig.15). We are in the process of fabricating a suitable mask for the electrode configuration. Electrode fingers will be 3 mm long, 25 μm wide, spaced 50 μm center to center. A mask is also being made for a phase modulator which employs a simple strip configuration (Fig. 16) consisting of two parallel electrodes 3 mm long separated by 3 mils. The effective depth of penetration of field into the film is the order of the film thickness; accordingly, the 3-mil separation was chosen to match the 75 μm thickness of our present films.

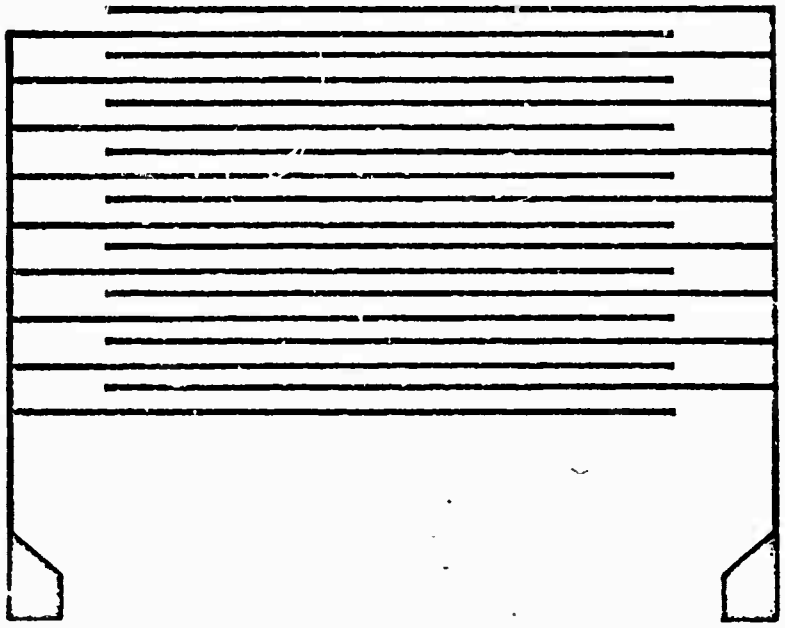

Fig. 15 Interdigital electrode structure for deflector-modulator. (Not to scale.)

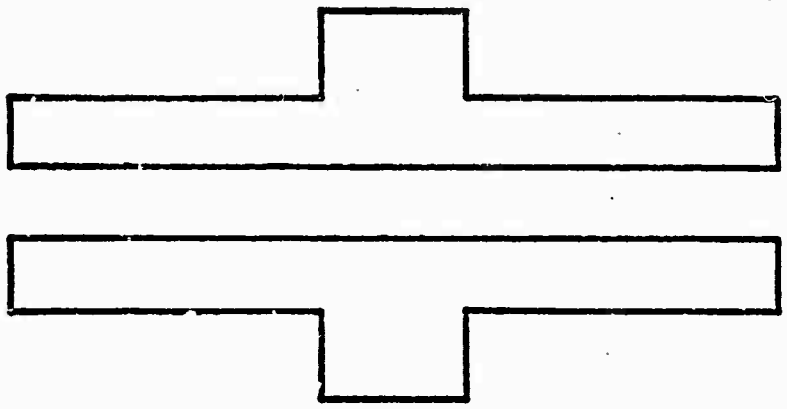

Fig. 16 Electrode configuration for phase modulation. (Not to scale.)

V. SPECIAL INSTRUMENTS AND FACILITIES

5.1 Refractive Index Instrument

In order to make precise measurements of refractive index we have built a spectrometer patterned after a design by Bond.[13] The instrument employs the method of minimum deviation. The crystal, cut in the form of a prism, is mounted on a precision goniometer table and placed in a collimated beam of monochromatic light so that the prism deflects the beam. This prism is then rotated about an axis parallel to its edge until the angular deflection D is a minimum. The refractive index is calculated from the relation

$$n = \sin [(A + D)/2]/\sin (A/2)$$

where A is the prism angle.

The instrument is now operating on a routine basis. Typical results are shown in Figs. 18 and 19. Index accuracy in these measurements is $\Delta n = \pm 0.002$.

5.2 Clean Air Chemistry Laboratory

As noted in sections 2.2 and 2.3, room temperature cw operation of our sensitized rare earth minilasers will require low activator concentrations and will place extreme constraints on the purity of the host and sensitizer combination. Our previous efforts to purify feeds have resulted in the development of a variety of methods for purification, but most of them have been of limited effectiveness due to recontamination from the laboratory atmosphere.

During this reporting period, we have completed the installation of a class 100 clean air chemistry laboratory designed and constructed by Environmental Air Control, Inc. of Hagerstown, Md. This laboratory is a room within a room, with an area of approximately 250 sq. ft. As shown in

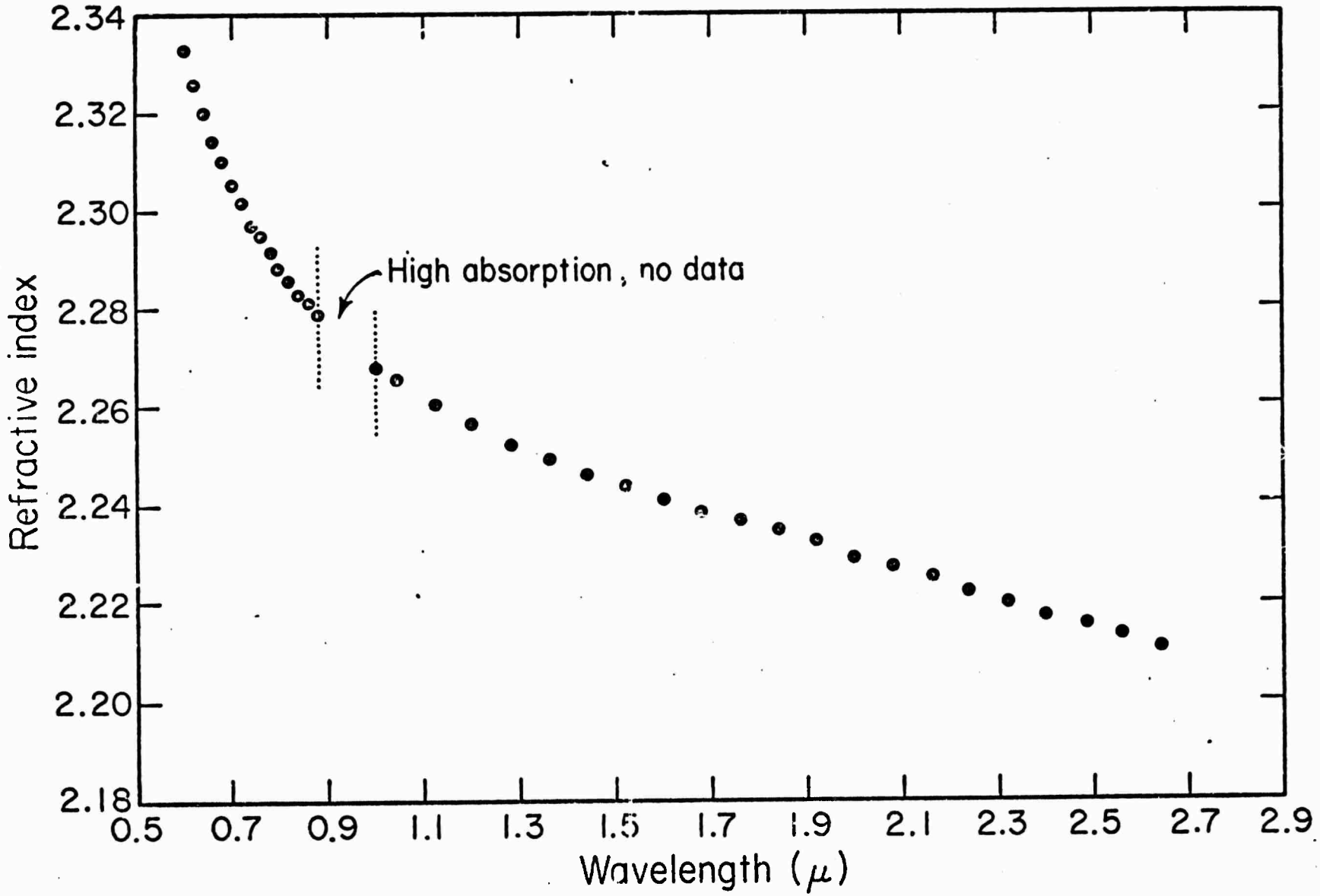

Fig. 19 Refractive index of $Yb_2Ti_2O_7$ as a function of wavelength.

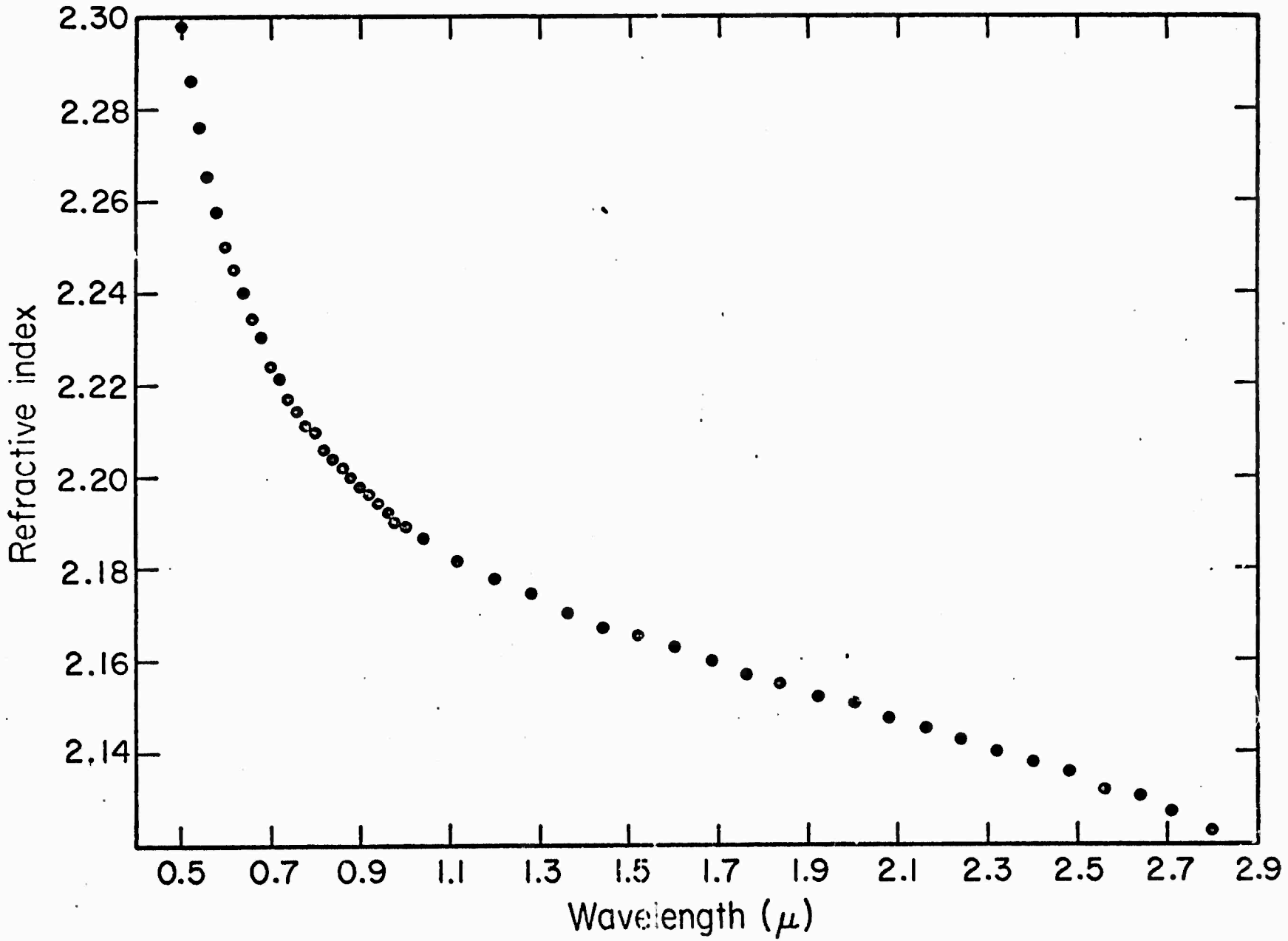

Fig. 18 Refractive index of $KTaO_3$ as a function of wavelength.

Fig. 20, there are two front air curtain type clean air hoods, one standard laboratory hood, and two eight-foot laminar flow benches, all equipped with the usual chemistry bench services. This laboratory will be used exclusively for the preparation of the very high purity fluoride and oxide feed materials needed for this program.

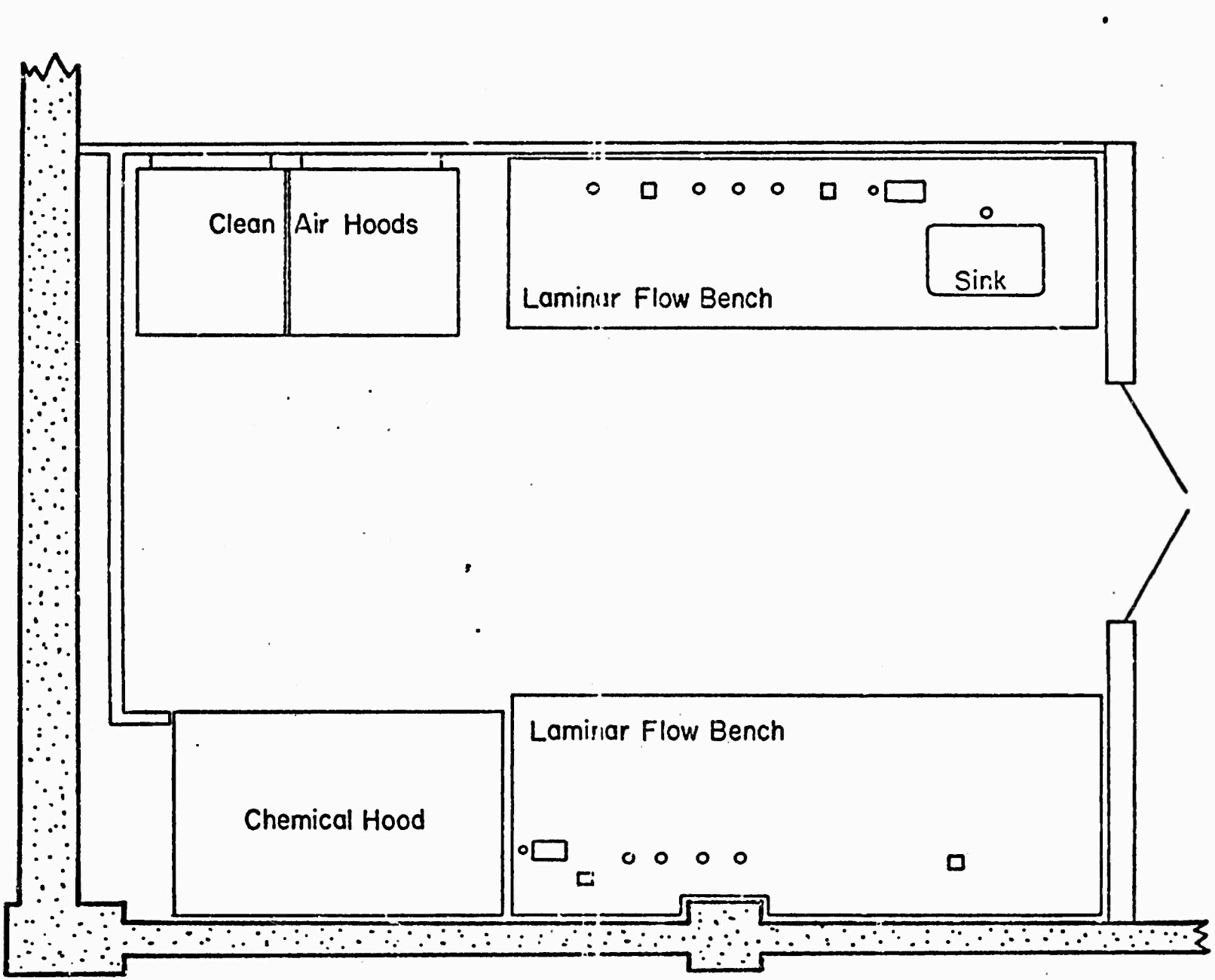

Fig. 20 Clean air chemistry room.

REFERENCES

1. H. P. Weber, T. C. Damen, H. C. Danielmeyer and B. C. Tofield, Appl. Phys. Letters 22, 534 (1973).

2. E. P. Chicklis, C. S. Naiman, R. C. Folweiler, D. R. Gabbe, H. P. Jenssen and A. Linz, Appl. Phys. Letters 19, 119 (1971).

3. R. B. Chester and D. A. Draegert, Appl. Phys. Letters 23, 235 (1973).

4. J. R. Wittke, RCA Review 33, 674 (1972).

5. H. Rupprecht, J. M. Woodall, K. Konnerth and D. G. Pettit, Appl. Phys. Letters 9, 221 (1966).

6. B. H. Ahn, R. R. Shurtz and C. W. Trussell, J. Appl. Phys. 11, 4512 (1971).

7. H. Kressel, J. V. Dunse, H. Nelson and F. Z. Hawryld, J. Appl. Phys. 39, 2006 (1968).

8. B. H. Ahn, R. R. Shurtz and C. W. Trussell, J. Electrochem. Soc. 118, 1015 (1971).

9. T. Ladany, J. Appl. Phys. 42, 654 (1971).

10. A. A. Bench and P. J. Dean, Proc. IEEE 60, 156 (1972).

11. G. A. Antypas, L. W. James, J. Appl. Phys. 41, 2165 (1970).

12. P. K. Tien, R. Ulrich and R. J. Martin, Appl. Phys. Letters 14, 291 (1969).

13. W. L. Bond, J. Appl. Phys. 36, 1674 (1965).

APPENDIX

Modes in a Two Dimensional Dielectric Resonator

Our objective is to find the normal modes that exist in the two dimensional dielectric cavity shown in Fig. A-1. The cavity has a rectangular cross-section with a length a in the x-dimension, b in the z-dimension. The cavity index, n_1, is less than n_2, the index of the surrounding medium. An "exact" solution to this electromagnetic problem can only be carried out numerically; however, a reasonably accurate closed form solution is attainable if we introduce some simplifications based on the physics of the problem. It is evident that for a cavity with dimensions large compared to a wavelength most of the energy will be confined to region 1 when the conditions for total internal reflection are satisfied. The energy stored outside the cavity is small because in this region the fields are evanescent. Within the cavity we expect the fields to be essentially harmonic. If we, in fact, take the solutions to be harmonic, we can match the fields on the four surfaces of the cavity to exponentially decaying fields outside. While this solution will match the boundary conditions on the faces, it will fail at the corners. Despite this failure the solutions should exhibit little error as long as most of the energy is confined to the cavity.

Proceeding along these lines we shall construct solutions which behave in the following way: in region 1 the field varies sinusoidally in x and z; in region 2 and 4 the variation is sinusoidal in z and exponential in x; in 3 and 5 we have sinusoidal variation along x and exponential dependence on z. These assumed fields fail as an exact solution because they are incompatible in the "corner" regions indicated by the shaded boundaries in Fig. A-1.

Our representation shall be in terms of modes TE and TM to z. For modes

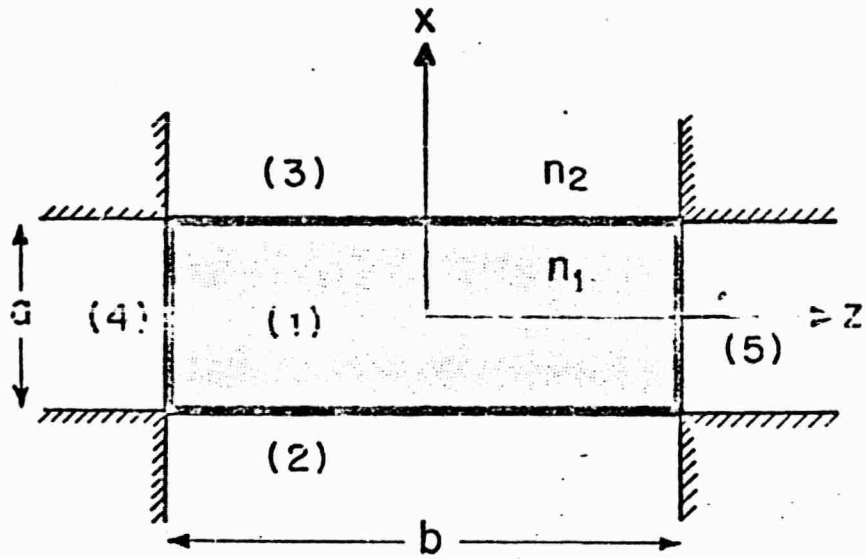

Fig. A-1 Two-dimensional dielectric cavity

TM to z, $E_z = f(x)\, g(z)$. There are four cases to consider: (1) f(x) and g(z) are even; (2) f(x) is even and g(z) is odd; (3) f(x) is odd and g(z) is even; and (4) f(x) and g(z) are odd.

For case (1), we choose in region 1

$$E_z = A \cos(k_x x) \cos(k_z z) \qquad |x| < \frac{a}{2};\ |z| < \frac{b}{2} \tag{A-1}$$

and in regions 2, 3, 4 and 5

$$E_z = Be^{-u|x|} \cos(k_z z) \qquad |x| > \frac{a}{2};\ |z| < \frac{b}{2} \tag{A-2}$$

and

$$E_z = Ce^{-v|z|} \cos(k_x x) \qquad |x| < \frac{a}{2};\ |z| > \frac{b}{2} \tag{A-3}$$

Upon substitution in Maxwell's equations we obtain for each region

$$k_x^2 + k_z^2 = k_1^2 = \omega^2 \varepsilon_1 \mu_o \tag{A-4}$$

$$k_z^2 + -u^2 = k_2^2 = \omega^2 \varepsilon_2 \mu_o \tag{A-5}$$

$$k_x^2 - v^2 = k_2^2 = \omega^2 \varepsilon_2 \mu_o \tag{A-6}$$

The field components transverse to z can be found from

$$\overline{E}_t = \frac{1}{k^2 - k_z^2} \left[\frac{\partial}{\partial z} (\nabla_t E_z) + i\omega\mu\, \nabla_t \times H_z\right] \tag{A-7}$$

$$\overline{H}_t = \frac{1}{k^2 - k_z^2} \left[\frac{\partial}{\partial z} (\nabla_t H_z) - i\omega\varepsilon\, \nabla_t \times E_z\right] \tag{A-8}$$

from which we obtain

$$H_y = A\left(\frac{i\omega\varepsilon_1}{k_x}\right) \sin(k_x x) \cos(k_z z) \qquad |x| < \frac{a}{2};\ |z| < \frac{b}{2} \tag{A-9}$$

$$H_y = B\left(\frac{-i\omega\varepsilon_o}{u}\right) e^{-u|x|} \cos(k_z z) \qquad |x| > \frac{a}{2};\ |z| < \frac{b}{2} \tag{A-10}$$

Continuity of E_z and H_y at $x = \pm\frac{a}{2}$ requires that

$$A \cos\left(\frac{k_x a}{2}\right) = Be^{-\frac{ua}{2}} \tag{A-11}$$

$$A \frac{\varepsilon_1}{k_x} \sin\left(\frac{k_x a}{2}\right) = -B\left(\frac{\varepsilon_2}{u}\right) e^{-\frac{ua}{2}} \tag{A-12}$$

The ratio of the first equation to the second gives

$$-\left(\frac{k_x a}{2}\right) \cot\left(\frac{k_x a}{2}\right) = \frac{\varepsilon_1}{\varepsilon_2}\left(\frac{ua}{2}\right) \tag{A-13}$$

Likewise, matching E_x and H_y at $z = \pm \frac{b}{2}$ yields

$$-\left(\frac{k_x b}{2}\right) \cot\left(\frac{k_z b}{2}\right) = \frac{\varepsilon_1}{\varepsilon_2}\left(\frac{vb}{2}\right) \tag{A-14}$$

Equations A-13 and A-14 determine the k_x's and k_z's and resonant frequencies of the even TM modes. These equations can be transformed to a more useful form by using equations A-4 through A-6 to express u and v in terms of k_x, k_z, ε_1, and ε_2. We obtain

$$-\left(\frac{\varepsilon_2}{\varepsilon_1}\right) k_x^2 \cot^2\left(\frac{k_x a}{2}\right) + \left(\frac{\varepsilon_1}{\varepsilon_2}\right) k_z^2 = k_x^2 + k_z^2 \tag{A-15}$$

$$-\left(\frac{\varepsilon_2}{\varepsilon_1}\right) k_z^2 \cot^2\left(\frac{k_x b}{2}\right) + \left(\frac{\varepsilon_1}{\varepsilon_2}\right) k_x^2 = k_x^2 + k_z^2 \tag{A-16}$$

Similarly, the characteristic equations for TM modes of symmetry types (2), (3) and (4) can be found. There is complete duality between the TM and TE modes of the resonator; so the characteristic equations must be dual. The results are presented in Table A-I. Although the characteristic equations cannot be solved exactly, simple graphical solutions do exist. Consider the even TM modes. From Eqs. A-15, A-16

Table A-I. Modes in Two Dimensional Dielectric Cavity

I. TM Modes $E_z = f(x)g(z)$

f(x) even: $-(\frac{\varepsilon_2}{\varepsilon_1})k_x^2\cot^2(\frac{k_x a}{2}) + (\frac{\varepsilon_1}{\varepsilon_2})\ k_z^2 = k_x^2 + k_z^2$

f(x) odd: $-(\frac{\varepsilon_2}{\varepsilon_1})k_x^2\tan^2(\frac{k_x a}{2}) + (\frac{\varepsilon_1}{\varepsilon_2})\ k_z^2 = k_x^2 + k_z^2$

g(z) even: $-(\frac{\varepsilon_2}{\varepsilon_1})k_z^2\cot^2(\frac{k_z b}{2}) + (\frac{\varepsilon_1}{\varepsilon_2})\ k_x^2 = k_x^2 + k_z^2$

g(z) odd: $-(\frac{\varepsilon_2}{\varepsilon_1})k_z^2\tan^2(\frac{k_z b}{2}) + (\frac{\varepsilon_1}{\varepsilon_2})\ k_x^2 = k_x^2 + k_z^2$

II. TE Modes $H_z = f(x)g(z)$

f(x) even: $-(\frac{\varepsilon_1}{\varepsilon_2})k_x^2\cot^2(\frac{k_x a}{2}) + (\frac{\varepsilon_1}{\varepsilon_2})\ k_z^2 = k_x^2 + k_z^2$

f(x) odd: $-(\frac{\varepsilon_1}{\varepsilon_2})k_x^2\tan^2(\frac{k_x a}{2}) + (\frac{\varepsilon_1}{\varepsilon_2})\ k_z^2 = k_x^2 + k_z^2$

g(z) even: $-(\frac{\varepsilon_1}{\varepsilon_2})k_z^2\cot^2(\frac{k_z b}{2}) + (\frac{\varepsilon_1}{\varepsilon_2})\ k_x^2 = k_x^2 + k_z^2$

g(z) odd: $-(\frac{\varepsilon_1}{\varepsilon_2})k_z^2\tan^2(\frac{k_z b}{2}) + (\frac{\varepsilon_1}{\varepsilon_2})\ k_x^2 = k_x^2 + k_z^2$

$$\left(\frac{\varepsilon_1}{\varepsilon_2}\right)k_z^2 \geq k_x^2 + k_z^2 \tag{A-17}$$

$$\left(\frac{\varepsilon_1}{\varepsilon_2}\right)k_x^2 \geq k_x^2 + k_z^2 \tag{A-18}$$

because in Eqs. A-15 and A-16 the first term on the left in both equations is a negative quantity.

Thus we obtain

$$\left[\left(\frac{\varepsilon_1}{\varepsilon_2}\right) - 1\right]k_z^2 = \left[\left(\frac{n_1}{n_2}\right)^2 - 1\right]k_z^2 \geq k_x^2 \tag{A-19}$$

$$\left[\left(\frac{\varepsilon_1}{\varepsilon_2}\right) - 1\right]k_x^2 = \left[\left(\frac{n_1}{n_2}\right)^2 - 1\right]k_x^2 \geq k_z^2 \tag{A-20}$$

Therefore there are no solutions (i.e., no resonant modes) for $\frac{n_1}{n_2} < \sqrt{2}$. Only for $\frac{n_1}{n_2} > \sqrt{2}$ do resonant modes exist and the range of k_x and k_z is limited by Eqs. A-19and A-20 to the region of k-space shown in Fig. A-2 where $\delta\theta = 2\tan^{-1}\left[\left(\frac{n_1}{n_2}\right)^2 - 1\right]^{1/2} - \frac{\pi}{2}$.

Since $\cot^2\left(\frac{k_x a}{2}\right)$ goes from $+\infty$ to 0 to $+\infty$ for $\frac{2\pi p}{a} \leq k_x \leq \frac{2\pi(p-1)}{a}$ where p is any positive integer, there are at most two solutions of Eq. A-15 in the interval $\frac{2\pi p}{a} \leq k_x \leq \frac{2\pi(p+1)}{a}$ for k_z fixed. Furthermore, only one of these solutions satisfies Eq. A-13, since u is positive. The same considerations are true for Eq. A-6. Therefore, there is only one resonant mode in the interval

$$\frac{2\pi p}{a} < k_x < \frac{2\pi(p+1)}{a} \quad \text{and} \quad \frac{2\pi q}{b} < k_z < \frac{2\pi(q+1)}{b} \tag{A-21}$$

where p and q are any positive integers and k_x and k_z also satisfy Eqs. A-19 and A-20. So the mode density is $\frac{ab}{4\pi^2}$ in the allowed region. Finally, the number of resonant modes in a frequency interval $\Delta\omega$ is

$$\Delta N = 4\left\{-1 + \frac{4}{\pi}\tan^{-1}\left[\left(\frac{n_1}{n_2}\right)^2 - 1\right]^{1/2}\right\}\frac{ab}{4\pi}\frac{n_1^2\omega}{c^2}\Delta\omega \tag{A-22}$$

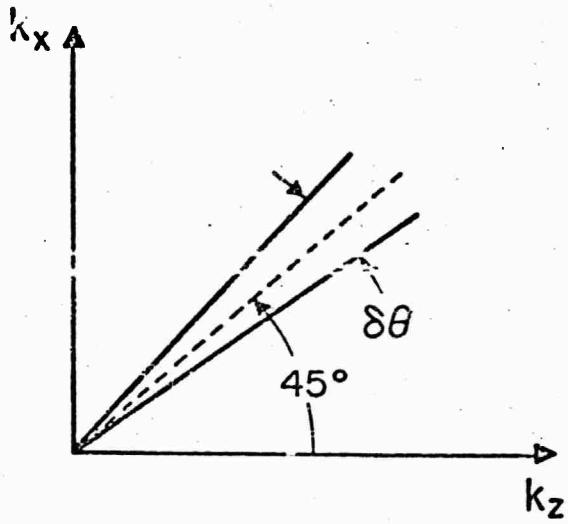

Fig. A-2 Totally reflected modes occur within the region of k-space subtended by the angle $\delta\theta$

where the factor 4 accounts for the four types of TM mode symmetry. The result is the same for TE modes.

The preceding analytical treatment of modes in a two dimensional rectangular dielectric cavity is succinctly summarized by the geometric construction shown in Fig. A-3. In k-space draw the two circles $k_1 = n_1 k_o$, $k_2 = n_2 k_o$ $(k_2 < k_1)$. Construct the horizontal and vertical tangents to the inner circle k_2. In Figure A-3 these are 1-1' and 2-2'. Find the points A, B where the tangents intersect the outer circle k_1. The radial lines drawn from the origin to A and B subtend the sector in k-space in which the totally reflecting modes are contained (the shaded region in the figure). It should be evident from the construction that the angular width of the sector decreases as k_2 increases relative to k_1 and the sector collapses to zero width when the ratio k_2/k_1 is such that the points A and B coincide. The critical ratio, evident from the geometry, is $k_2/k_1 = 1/\sqrt{2}$. For larger ratios the cavity will support no internally reflecting modes.

In Fig. A-2 the modes the shown equally spaced in intervals π/a in k_x and π/b in k_z. This representation while not exact is an excellent approximation to the mode spacing when the cavity dimensions are very large compared to the free space wavelength λ_o. In this domain, which applies to our experimental situation, we can write

$$k_1^2 = n_1^2 k_o^2 = \left(\frac{p\pi}{a}\right)^2 + \left(\frac{q\pi}{a}\right)^2 \qquad \text{(A-23)}$$

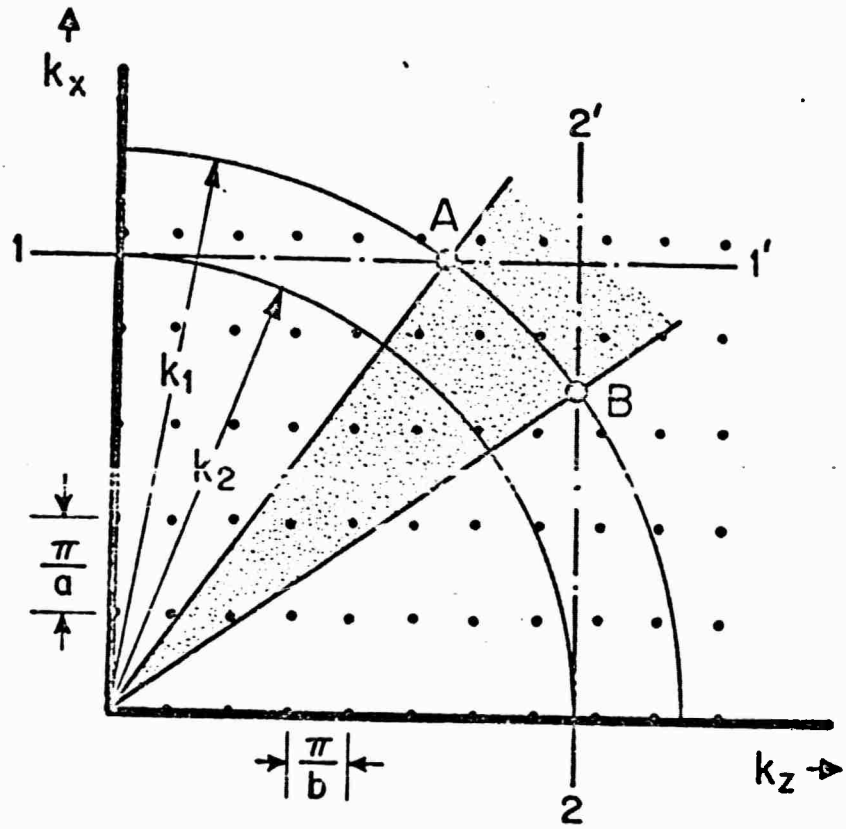

Fig. A-3 Geometric construction to find allowed k-vectors in two-dimensional dielectric resonator.

where $k_o = 2\pi/\lambda_o$ is the free space wave vector corresponding to the wavelength λ_o, and p and q are positive integers. An expression for the incremental mode spacing at large wave numbers can be obtained if we take the derivative of Eq. A-23:

$$n_1^2 k_o \Delta k_o = [(\frac{p\pi}{a})(\frac{\pi}{a})\Delta p + (\frac{q\pi}{b})(\frac{\pi}{b})\Delta q] \qquad \text{(A-24)}$$

For n_2 and n_1 chosen so that the sector of allowed modes in k-space is small we have

$$(\frac{p\pi}{a}) \approx (\frac{q\pi}{b}) \approx \frac{n_1 k_o}{\sqrt{2}} \qquad \text{(A-25)}$$

Upon substituting this result into Eq. A-24 we obtain, after some simplification,

$$\Delta\lambda_o = -\frac{\lambda_o^2}{2\sqrt{2}n_1}\left(\frac{\Delta p}{a} + \frac{\Delta q}{b}\right) \qquad \text{(A-26)}$$

where Δp and Δq are positive and negative integers and may include zero.

We note in conclusion that each point in Fig. A-3 represents eight modes: one set of 4 symmetry types for TE modes plus a similar set for TM. These 8 modes are not, in general all degenerate, but in the limit $a,b \gg \lambda$ they tend to coalesce to a single point in k-space.

SEMI-ANNUAL TECHNICAL REPORT #1

Period: July 1, 1973 - Dec. 31, 1973

Title: Research in Materials Science

Project Title: Superconducting Transition Metal Alloys

Contract Number: DAHC 15-73-C-0316

ARPA Order Number: 2469

Program Code Number: 3D10

Name of Contractor: Massachusetts Institute of Technology
Cambridge, Mass. 02139

Principal Investigator: N. J. Grant (617) 253-5638

Project Scientists or Engineers: R. M. Rose (617) 253-3230

M. L. A. MacVicar (617) 253-6261

Effective Date of Contract: June 1, 1973

Contract Expiration Date: May 31, 1974

Amount of Contract: $425,000

Amount of Project: $107,000

Sponsored By

Advanced Research Projects Agency

ARPA Order No. 2469

Summary

This project has two objectives: to unravel the complex problem of superconductivity of high-T_c A15 materials by tunneling experiments; and to develop materials for practical superconducting microwave cavities. In this report we describe our progress towards the first objective. The importance of understanding the A15 group stems from the fact that they have the highest known transition temperatures and other technologically useful properties; and, such knowledge should show the way to still higher transition temperatures and greater technical utility. Our approach to the problem is to perform high-quality tunneling experiments on A15's with the highest T_c's and to develop computer software which is capable of deconvoluting the data into phonon spectra.

Progress in the past six months has centered on two areas: (a) tunneling into $Nb_3(Al_{.8}Ge_{.2})$ and (b) deconvolution of phonon spectra from S-I-S' tunnel junctions.

(a) We have achieved, in our initial exploratory attempts, superconductive tunneling into $Nb_3(Al,Ge)$ ribbon substrates. Although ribbons of the A15 material offer good flat surfaces for barrier formation, and thus a high probability for successful tunneling, the metallurgical condition of these particular ribbons is not sufficiently bulk-like that our results can be considered representative. On the other hand, our work with the ribbons indicates that the oxides of $Nb_3(Al,Ge)$ are very fragile, deteriorating under sustained bias or temperature. The most durable barriers were formed after glow discharge

cleaning of the surface and thermal oxidation of the resulting substrate. The best quality tunneling data resulted when the ribbon, before barrier formation, was not subject to the usual low temperature ordering anneal (725 C).

(b) Our modification of the McMillan-Rowell Inversion Routine has resulted in a more (numerically) accurate set of computer programs which can be used to deconvolute the phonon spectra from S-I-S' tunnel junctions where both S and S' can simultaneously be non-BCS superconductors. The only constraint on the deconvolution program is that the phonon spectrum of one electrode must be known; i.e., both electrodes can not be total unknowns.

One implication of the above is that we can look, with greater precision than we thought possible, at more kinds of junctions than we thought possible. The initial successes at tunnel junction fabrication on ribbon substrates indicate that the goal of this research is definitely feasible, and we are now tackling the substrate surface problem, with the same optimism. We should remark at this point that recent developments in Nb_3Ge in other laboratories indicate that the potential for still higher T_c A15 compounds is very far from exhausted; thus the original premise of this research, the importance of fundamental understanding of A15 superconductivity, takes on still greater importance.

I. Introduction

In the last decade, electron tunneling has come to be recognized as the most important technique for studying the properties of metals in both the superconducting and normal metal states. In a tunnel junction, if one (or both) of the metals is in the superconducting state at least three important properties of the metal(s) can be determined from I-V and dI/dV - V characteristics: the electronic density of states of the metal in its superconducting state, the phonon density of states, and the electron-phonon coupling constant.

The purpose of the present research is to determine these three parameters for representative members of the A15 class of compounds. These materials are especially interesting for two reasons. First, the three highest known superconducting transition temperature (T_c) compounds are A15's: Nb_3Ge, Nb_3Ga, $Nb_3(Al_{.75}Ge_{.25})$. (In addition, most materials with $T_c > 15K$ are A15 compounds.) Secondly, many of the high T_c A15's are structurally unstable. It is important for future research, as well as for eventual applications of superconductivity, to know if the high T_c's attained in these materials are in any way connected with their instabilities. There is even a question as to whether the "usual" BCS pairing mechanism adequately describes the superconducting properties of these alloys.

In this report we discuss two different aspects of our research to date. The first section contains a description and analysis of the tunneling data we have obtained from $Nb_3(Al,Ge)$ ribbon-substrate tunnel

junctions with both oxide and carbon barriers.* We have found that whereas it is possible to fabricate such junctions using a lead-bismuth counterelectrode and to obtain superconductive tunneling, they are relatively fragile and deteriorate rapidly under temperature recycling and/or sustained applied bias. The methods of barrier fabrication are extensively reviewed here. The same material used to make the ribbon substrates was also rf sputtered into a superconducting film by the IBM, Thomas J. Watson Laboratory. A film junction with a carbon barrier and lead-bismuth counterelectrode was then fabricated and tested. The results from this junction are surprisingly similar to carbon junctions made on the ribbon substrate. All the carbon barrier samples have a characteristic structure in their derivatives which we have not yet identified.

The second section is a reproduction of the thesis of Alan Jay Dubin, S.B., M.I.T., August 1973. In this thesis the concepts behind superconducting tunneling are explored and a description of the method of unraveling actual tunneling data to reveal the superconducting electron spectrum, the phonon spectrum, and the electron-phonon interaction constant is given. The techniques described are a modification of the original McMillan-Rowell phonon inversion routines. Major changes have been made in two of the three programs. The first modification is a program introduction comprised of all of the software necessary to convert the output of conventional tunneling electronics

---

* A brief communication on this work will appear in Physics Letters (in press).

into absolute data characteristics. The second stage of this routine, which attempts to isolate the characteristics of the unknown (or unexplored) counter-electrode, has been extensively revised. The numerical accuracy of this stage has been improved by more than an order of magnitude and the new program will enable double superconductor junctions in which neither electrode is a BCS (or weak-coupling) material to be analyzed. The latter is absolutely necessary for tunneling investigations on transition metal elements or alloys since these are not weak-coupling materials, and because it is found experimentally that they form their best tunnel junctions with other non-BCS materials. The net result of these modifications is, we feel, an inversion routine which has greater accuracy and flexibility than the original inversion routine, is more specific in the raw data handling techniques, and, finally, has a far wider range of application than the original program.

II. Exploratory Tunneling Results on Nb-Al-Ge

We have succeeded in producing $Nb_3(Al_{.8}Ge_{.2})$ - barrier - $Pb_{.7}Bi_{.3}$ tunneling junctions on ribbon substrates of the A15 compound. In this discussion we shall discuss steps taken to date to obtain tunneling in $Nb_3(Al,Ge)$ - $Pb_{.7}Bi_{.3}$ junctions and attempt to relate these steps to the observed junction behavior.

(a) Ribbon Fabrication

The substrates were ribbons of $Nb_3(Al,Ge)$ fabricated by a process

into absolute data characteristics. The second stage of this routine, which attempts to isolate the characteristics of the unknown (or unexplored) counter-electrode, has been extensively revised. The numerical accuracy of this stage has been improved by more than an order of magnitude and the new program will enable double superconductor junctions in which neither electrode is a BCS (or weak-coupling) material to be analyzed. The latter is absolutely necessary for tunneling investigations on transition metal elements or alloys since these are not weak-coupling materials, and because it is found experimentally that they form their best tunnel junctions with other non-BCS materials. The net result of these modifications is, we feel, an inversion routine which has greater accuracy and flexibility than the original inversion routine, is more specific in the raw data handling techniques, and, finally, has a far wider range of application than the original program.

II. Exploratory Tunneling Results on Nb-Al-Ge

We have succeeded in producing $Nb_3(Al_{.8}Ge_{.2})$ - barrier - $Pb_{.7}Bi_{.3}$ tunneling junctions on ribbon substrates of the A15 compound. In this discussion we shall discuss steps taken to date to obtain tunneling in $Nb_3(Al,Ge)$ - $Pb_{.7}Bi_{.3}$ junctions and attempt to relate these steps to the observed junction behavior.

(a) Ribbon Fabrication

The substrates were ribbons of $Nb_3(Al,Ge)$ fabricated by a process

developed in our laboratory[1*]. The ribbon geometry is especially suited for tunneling work (as films are) because of the existence and accessibility of flat surfaces. The ribbons are made by first enclosing powders of Nb, Al, and Ge in the appropriate composition in a cupro-nickel tube; then reducing the tube in size by a series of swaging and rolling steps; and then finally removing the cupronickel sheath with nitric acid. (The resulting ribbons in our laboratory were 0.1 mm x 2.5 mm in cross section.) The ribbon is stored in this condition until a series of junctions is to be made. It is then heated resistively to 1700°C in an Argon atmosphere to produce the A15 compound. X-ray diffraction and metallographic studies on several of these samples showed that 90 - 95% of a given ribbon possessed the A15 structure. The typical T_c of such ribbons was 17.5 K [2].

Prior to junction fabrication at least half of the samples in the present investigation were then annealed at 725 C for 90 hours in less than 10^{-5} Torr. This is done in order to increase atomic order. After this anneal, there was a general increase of about 1.5 K in a sample's T_c [3].

The last step before the barrier fabrication was to etch the surface of the ribbons to remove the outside layers of the ribbon and, consequently, any depleted layers at the surface (and also any surface contaminants such as nickel atoms remaining after the bath in nitric acid). Both chemically etched samples[4] and those cleaned by glow discharge appeared smooth down to 1 micron. Figures 1 and 2 are the SEM

---

* References and pictures for this section of the report are found on pp 16 ff.

photographs of the ribbon surfaces after each of the two etching procedures. Both show a considerable porosity which is a remnant of the sintering process.

In the glow discharge cleaning prior to barrier formation, the ribbon was maintained at a negative potential difference greater than 1000 V in 3×10^{-2} Torr of Argon so that oxidized and cold-worked material was sputtered off. (See Fig. 3). This cleaning (or that with the potential reversed) proved to be essential to obtaining junctions which exhibited tunneling structure.

(b) Barrier Formation

As is well known, the quality of the barrier is crucial for obtaining high resolution tunneling data. Excess currents and barrier-related structure in tunneling characteristics can be so severe as to totally mask superconducting characteristics. An additional problem arises for superconductors of extremely short coherence lengths, such as A15 alloys: the interface region between barrier and bulk material constitutes a significant fraction of the region sampled by the tunneling electrons, even for interfaces which would ordinarily be considered quite sharp.

In the present work two different barrier types were tested: oxide and carbon. The oxide barrier was formed either by anodization in the glow discharge system (Fig. 3) without exposure to atmosphere, or by placing the samples in a free flow of oxygen at 150 C (thermal

oxide). In the former procedure the sample was held a few hundred volts above the cathode in 5×10^{-2} Torr of oxygen. Although it was not difficult to oxidize the samples, and they were of an insulating nature, we later found that they are apparently both physically and electrically fragile when made in the above ways. Junctions were made with carbon film barriers on 4 ribbons which had previously had a 725 C anneal. The carbon barriers were fabricated in two different ways. In one instance paracrystalline C films of about 150 Å thickness were arc-evaporated onto the cleaned ribbon as barriers[6]. In the other, an electron beam deposition technique[7] was used to fabricate barriers 100 ± 30 Å. Although the resistances and physical characteristics of these two types of carbon barriers are significantly different, their tunneling characteristics are almost indistinguishable. The lack of durability found in the oxide barriers extends to the carbon barriers as well.

After barrier fabrication by whatever technique, junction boundaries were then out-lined by a formvar mask, and a 3000 Å thick $Pb_{.7}Bi_{.3}$ counterelectrode deposited to complete the tunneling sandwich. Conventional four point probe connections were then made, and the entire junction covered with a protective layer of formvar. Two or three junctions were usually made on any one ribbon sample.

(c) $Nb_3(Al,Ge)$ Film Junctions

A number of unreacted ribbon samples were given to Mr. Walter Kateley at the IBM, Thomas J. Watson Laboratory, from which to rf

sputter $Nb_3(Al,Ge)$ films[8]. We sought to compare the quality of tunneling of the ribbon, to the film substrates The one film on which we have completed tests had an average thickness of 3000 Å, was metallic in color (not quite opaque), and had a room temperature resistivity $\sim 3 \times 10^{-2}$ Ω-cm. The transition temperature of the unannealed film was ≈ 1.6 K with a transition interval ∿0.5 K. Four carbon barrier junctions (electron beam deposition) were made on this film, only two of which were operable.

(d) Results

Our best quality results, to date have been obtained with an unannealed ribbon which had been mounted as the anode in the Ar glow discharge cleaning, and which had a thermal oxide barrier. The tunneling characteristics are shown in Figs. 4 and 5[9]. At 4.2 K this junction had a resistance of 270 Ω. It broke down shortly after the second sum peak bias was reached.

The value of 2Δ of $Nb_3(Al,Ge)$ obtained from this junction was 0.70 ± .05 meV at 4.2 K and 1.21 meV ± .05 at 2.6 K. If the energy gap followed the usual empirical temperature dependence[10], we would obtain the values: $T_c = 4.6$ K, $2\Delta(0) = 1.3$ meV and $(2\Delta/kT_c) = 3.3$. A second junction on the same ribbon yielded a value: $2\Delta = 0.65 \pm 0.1$ meV at 4.2 K. It deteriorated even more quickly, however, disintegrating before it was possible to pump from 4.2 to 2.5 K. Strangely enough it had a junction resistance of 1200Ω at 4.2 K. Several other ribbons

cleaned via glow discharge and having a thermal oxide barrier, were obtained with structure above 4 meV, but the attendent high excess currents made an accurate analysis questionable.

As discussed previously, for tunneling data to reflect the bulk properties of the sample the depth of the surface region must be less than the coherence length for superconductivity. Since in A15's the coherence length is 20-80 Å [11], we believe this study, as well as all previous ones[12], gave surface limited results. Our results are probably influenced by inadequate cleaning of the surface, the presence of segregated Al or other inhomogeneities in the ribbon surface, and/or contamination from the cupronickel tubing used in fabricating the ribbons.

(e) Discussion

In all we have investigated approximately 30 ribbons and 70 junctions. All but five of these junctions had oxide barriers. For the oxide junctions only 4 gave rise to analyzable superconductive tunneling[14]. Three oxide junctions had recognizable characteristics and all three had thermal oxide barriers; none were subjected to the low temperature (725 C) anneal. The other junctions made on unannealed ribbon were generally of poor quality but had sharp structure in the low-bias portion of the derivative curve (see Fig. 6). This might be explained either by Al segregation in the substrate or by drastic reduction of T_c and Δ for material near the ribbon surface. Subsequent evaluation of X-ray data on these ribbons indicated a rather high

percentage of unreacted Germanium. This would lead to the formation of Al-rich non-equilibrium phases in the material. In any case, the best tunneling data was observed on the ribbon subjected to the reverse glow discharge cleaning.

Junctions fabricated on annealed ribbons tended to be of even poorer quality than on the unannealed substrates. Instead of having the low bias structure shown in Fig. 6, they tended to exhibit structure at biases ∿4 meV above the gap edge, consistent with phonon structure observable in lead and lead alloys.[13] Figure 7 is one such derivative trace taken at 1.2 K. This particular trace and others with such clear-cut structure all corresponded to thermal oxide barriers, although most of the others had even higher excess currents and thus a high parabolic background in the derivative scan.

Figure 8 from an anodic barrier sample is a typical junction with the high excess current. The high excess currents of most junctions could be caused by poor surfaces (e.g., Al-depletion during annealing) or an inadequate tunneling barrier. Thus far, we have not been able to pin down the cause of this behavior. Micro-shorts and hysteresis have been present in many junctions but no evidence of Josephson behavior has been observed. All junctions have exhibited breakdown after two or three derivative scans at liquid helium temperatures; many have deteriorated in the time it takes to pump the system down from 4.2 to 1.2 K. The cause of this behavior is unknown.

All of the carbon barrier junctions had unusual structure at low temperatures. First derivative curves for both a ribbon substrate junction and the sputtered $Nb_3(Al,Ge)$ film junction are given in Fig. 9. The characteristic "three bump structure" appears in all of the dI/dV - V curves for carbon barrier junctions below 4.2 K. (In the film data it may appear at 4.2 K but the derivative is not clean enough to say unequivocally that it is there.) Just as in these two traces, however, the bias at which these "bumps" appear is not related in any obvious way to the usual derivative analysis procedures. It does not seem likely that this structure is due to the carbon alone (despite the fact that there is no evidence of its appearence) in the oxide tunnel junctions) because we have made a number of other S-I-S' junctions with carbon barriers sandwiched between In and Al, Sn, and In counterelectrodes and see absolutely no evidence for its existence in the derivative scans. We are presently looking into the possibility of interaction between the carbon and either $Nb_3(Al,Ge)$ or the lead-bismuth counterelectrode. Nonetheless, it would have to be a somewhat special type of interaction, if its characteristic energy is that fickle. Clearly if there is any kind of chemical bonding, or spreading of the barrier - material interface, then different methods of obtaining artificial barriers will have to be explored. Unfortunately, these barriers appear to be as fragile as their oxide counterparts.

(f) Summary

We have achieved superconducting tunneling on ribbon substrates of $Nb_3(Al,Ge)$; of all the samples exhibiting non-normal metal tunneling only two had ideal junction characteristics. Junction barriers were initially oxides prepared by one of a variety of methods; e.g., anodization by glow discharge and/or thermally grown in oxygen. Prior to oxidation the ribbon surfaces were cleaned by glow discharge in an Argon atmosphere and/or chemically etched. Irrespective of the combination of these procedures and whether the ribbon was annealed or not, junctions were invariably of very poor quality. Typically, when structure did appear in the derivative characteristic, it implied unusual gap values for the $Nb_3(Al,Ge)$ or the Pb-Bi alloy, or both. All characteristics with distinctive tunneling structure were thermally oxidized unannealed ribbon substrates. Although many of these junctions were not of good tunneling quality, the data from them indicated a problem of segregated Al in the ribbons, particularly after a low temperature anneal. Subsequent X-ray examination confirmed the presence of unreacted Ge in our samples.

In an effort to obtain tougher barriers, we investigated carbon as a barrier material. Although the tunneling data obtained from such junctions was clearly not that of two normal metals separated by a semiconductor, we have not yet been able to unravel what structures we have observed. Film junctions made by rf sputtering our unreacted ribbon material and then depositing both a carbon barrier and a

$Pb_{.7}Bi_{.3}$ counter-electrode have characteristics almost identical to the analogous ribbon-substrate carbon junctions. In addition, the carbon junctions have proved to be no more durable than similar ones with oxide barriers. The initial success with both the oxide and the carbon barriers, however, encourages us that further research into available fabrication techniques will probably result in more adequate barriers.

(g) Direction of Future Work

Clearly the success we have had with our preliminary investigations on the ribbon substrates dictates that in our continuing work, special care must be taken to optimize the homogeneity and smoothness of the A15 surfaces. The major emphasis in this research is on fabricating suitable barriers for the junctions. Since the film geometry also provides smooth surfaces and our results indicate a behavior analogous to that of the ribbons, we shall continue our present collaboration with IBM in the A15 film investigation.

The best-characterized form of $Nb_3(Al,Ge)$ is the arc-melted bulk material; with this in mind, we have begun to devise techniques for exposing surfaces of such material which promise to be characteristic of the bulk. Typical alternatives under investigation are controlled brittle fracture, controlled etching and various metallographic techniques. Figure 10 is a typical SEM picture of the surface of one of our recently prepared samples. The presence of such cleavage steps in quantity makes this particular surface unsuitable for our purposes. We hope to produce better surfaces soon.

References

1. R. Lohberg, T. W. Eagar, I. M. Puffer and R. M. Rose, Appl. Phys. Lett. 22, 69 (1973).

2. The J_c vs. H curves for these samples was one or two orders of magnitude less than those of sputtered films, but slightly higher than those for bulk sample with a T_c of 18.5 K. [M. A. Janocko, J. R. Gavaler, C. K. Jones, J. Vac. Sci. Tech. 9, 341 (1972)].

3. J_c vs. H decreased, as well, indicating the disappearence of flux pinning centers.

4. The etch consisted of 10 parts HF: 20 parts HNO_3: 30 parts lactic acid.

5. J. L. Miles and P. H. Smith, J. Elec. Soc. 110, 1240 (1963).

6. M. L. A. MacVicar, J. Appl. Phys. 41, 4765 (1970); M. L. A. MacVicar, S. M. Freake, and C. J. Adkins, J. Vac. Sci. Tech. 6, 717 (1969).

7. Sol Aisenberg and Ronald Chabot, J. Appl. Phys. 42, 2953 (1971).

8. This film was laid down on a sapphire substrate using conventional rf techniques: 200 watts (with 10 watts reflected power) for 4 1/4 hours in 11 μ of Argon for a water cooled target.

9. The temperature of 2.6 K for the lower trace is only approximate since the sample cooled by an additional 15 mK while this derivative scan was being taken.

10. T. P. Sheahan, Phys. Rev. 149, 368 (1966).

11. K. Hechler, G. Horn, G. Otto, and E. Saur, J. L. Temp. Phys. 1, 29 (1969).

12. H. J. Levinstein and J. E. Kunzler, Phys. Lett. 20, 581 (1966); L. Y. L. Shen, Phys. Rev. Lett. 29, 1082 (1972); and D. R. Bosomworth and G. W. Cullen, Phys. Rev. 160, 346 (1967).

13. W. L. McMillan and J. M. Rowell, Superconductivity, ed. R. D. Parks (Marcel Dekker, N.Y. 1969); J. G. Adler and S.C. Ng, Can. J. Phys. 43, 594 (1965); and T. Claeson and G. Grimvall, J. Phys. Chem. Solids 29, 387 (1968).

14. Only six junctions out of the 65 oxide barrier junctions could be shown to be superconducting.

Figure Captions

Figure 1 SEM photograph of chemically etched $Nb_3(Al,Ge)$ ribbon surface.

Figure 2 SEM photograph of the glow discharge etched ribbon surface.

Figure 3 Glow discharge configuration.

Figure 4 I-V characteristic of a $Nb_3(Al,Ge)$ - Ox - $Pb_{.7}Bi_{.3}$ junction of 270 Ω at 4.2 K.

Figure 5 dI/dV - V characteristic of the same junction as in Fig. 4.

Figure 6 Derivative scan of an unannealed ribbon junction with a thermal oxide barrier (4.2 K resistance = 12 Ω) at 1.2 K.

Figure 7 Derivative scan of an annealed ribbon junction with a thermal oxide barrier (4.2 K resistance = 10 Ω) at 1.2 K.

Figure 8 Derivative scan of an annealed ribbon junction with an anodic oxide barrier (4.2 K resistance = 4 Ω) at 1.2 K.

Figure 9 A first derivative scan of two different carbon barrier junctions. The upper curve (A) is a ribbon substrate sample at 1.2 K. The lower curve (B) is an rf sputtered film junction at 1.2 K.

Figure 10 SEM photograph of a fragment of an arc-cast $Nb_3(Al,Ge)$ ingot.

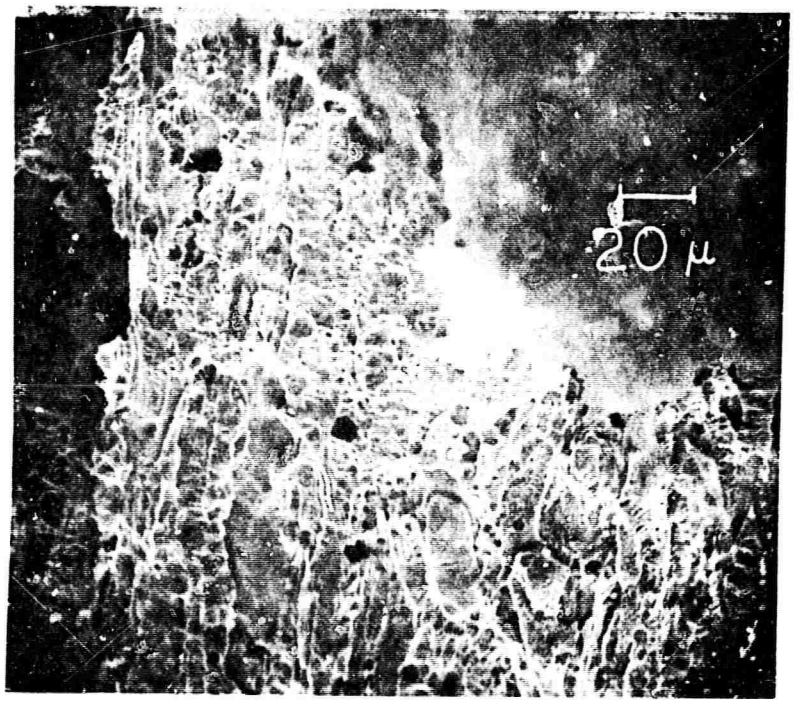

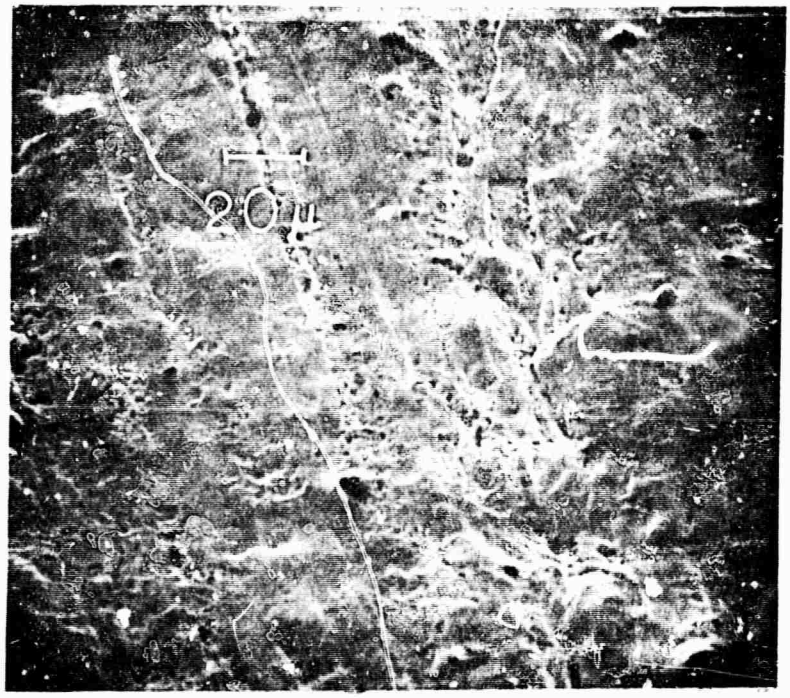
20 mi

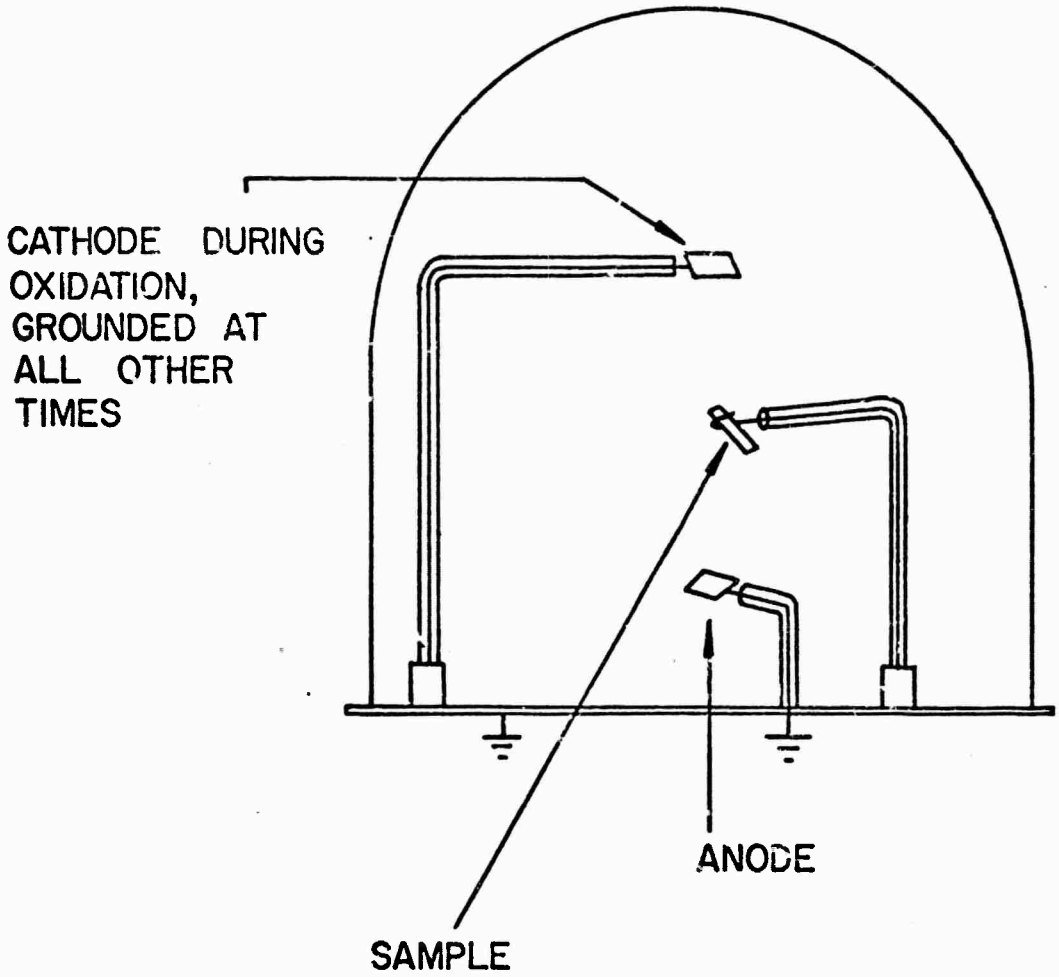

CATHODE DURING GLOW DISCHARGE
ANODE DURING OXIDATION

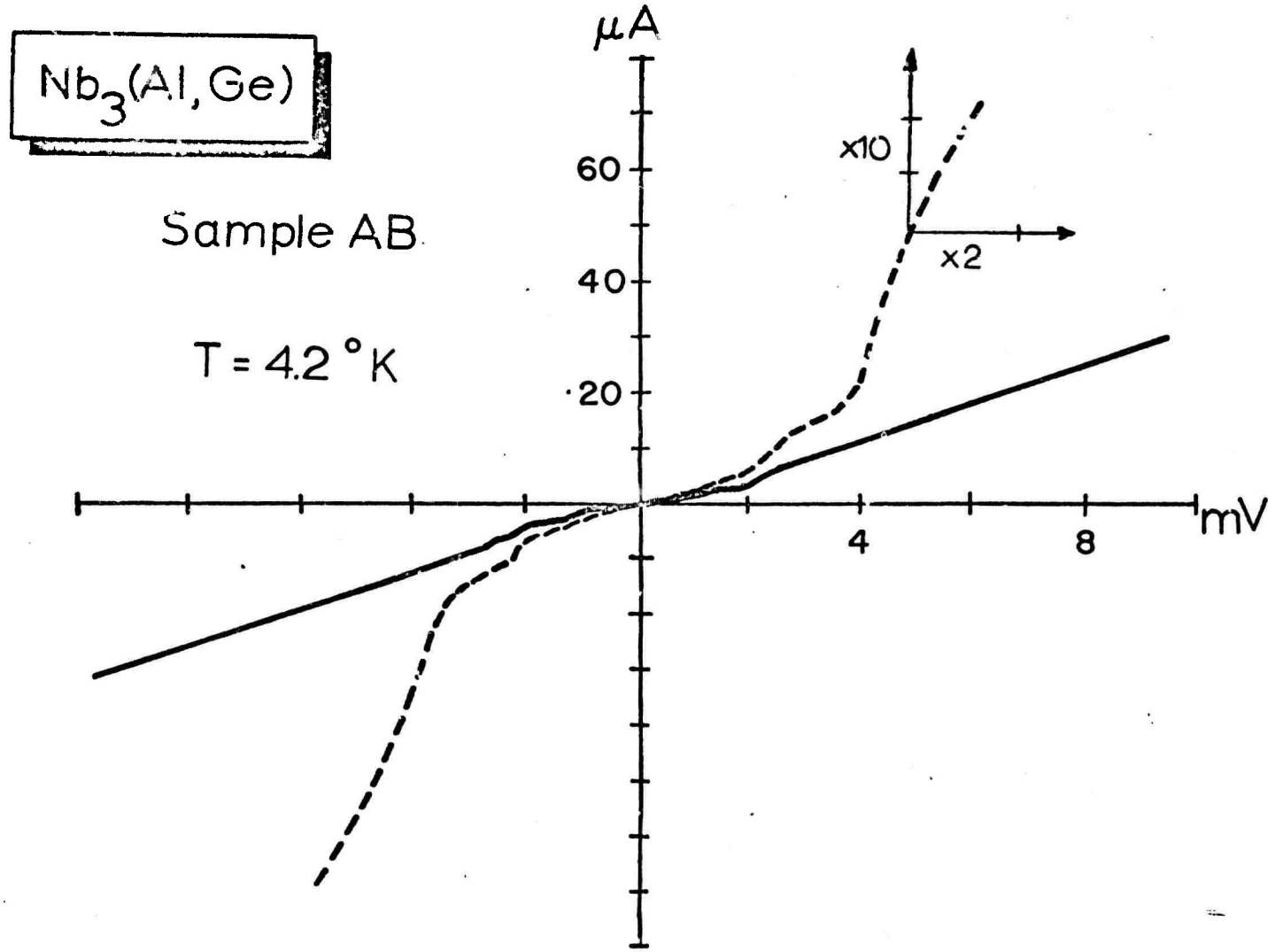
Nb3(Al,Ge)
Sample AB
T = 4.2 °K
μA
60
40
20
x10
x2
4
8
mV

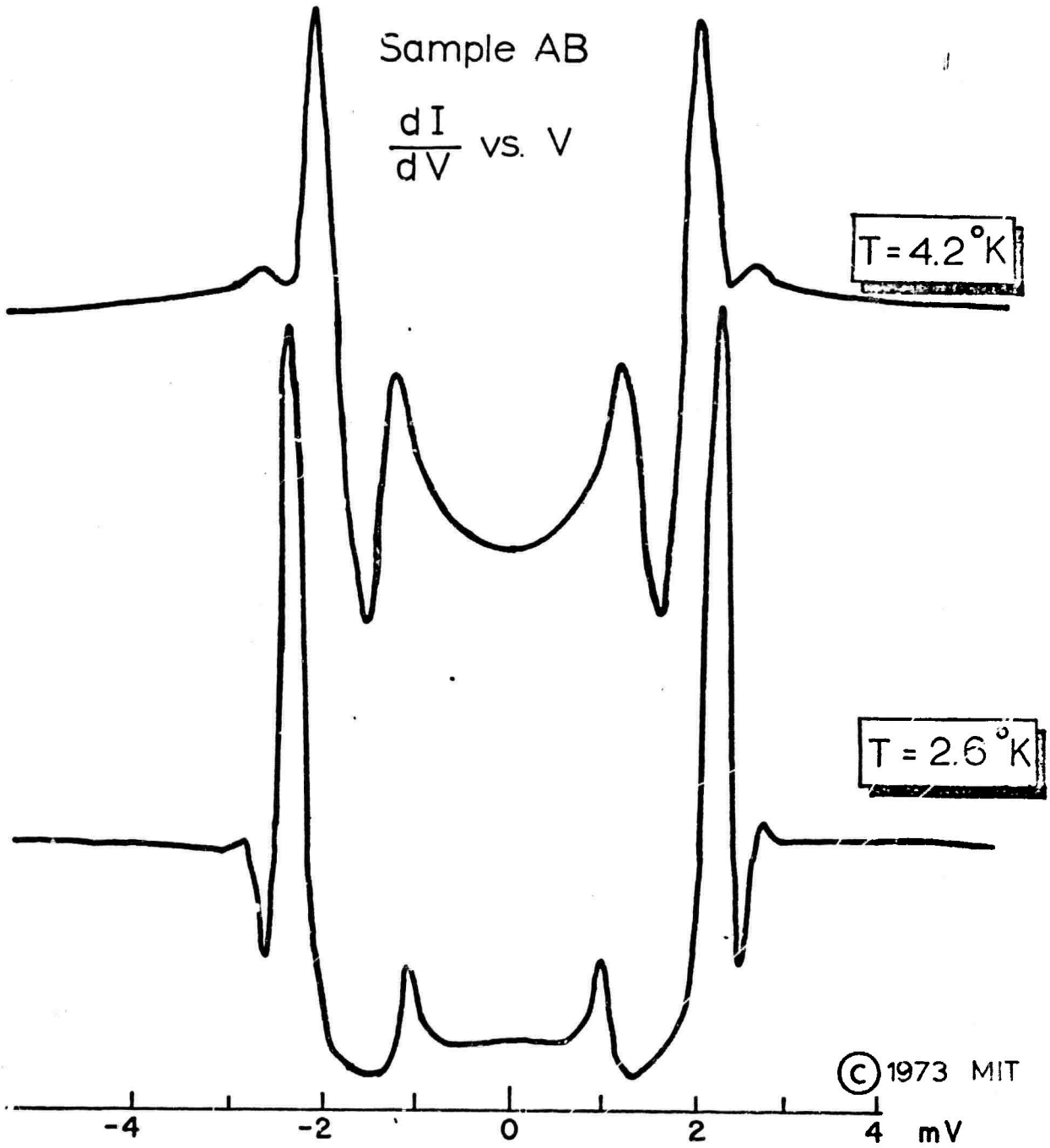
Sample AB
dI/dV vs. V
T = 4.2°K
T = 2.6°K
© 1973 MIT
-4
-2
0
2
4
mV

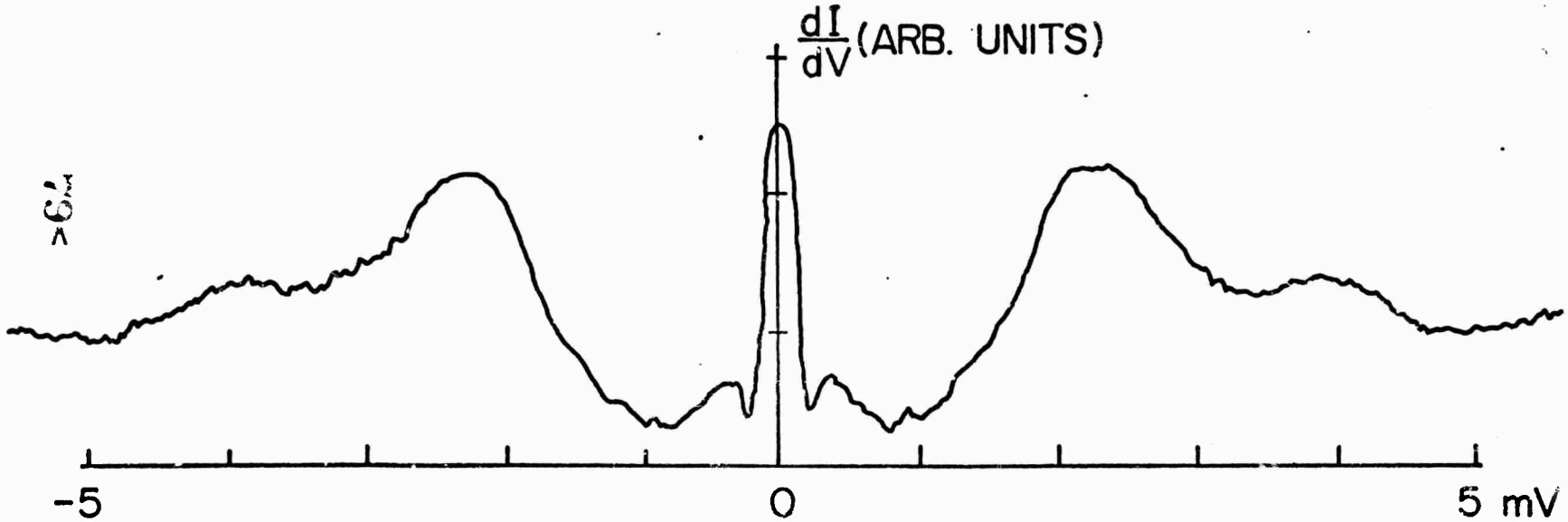

Fig. 9

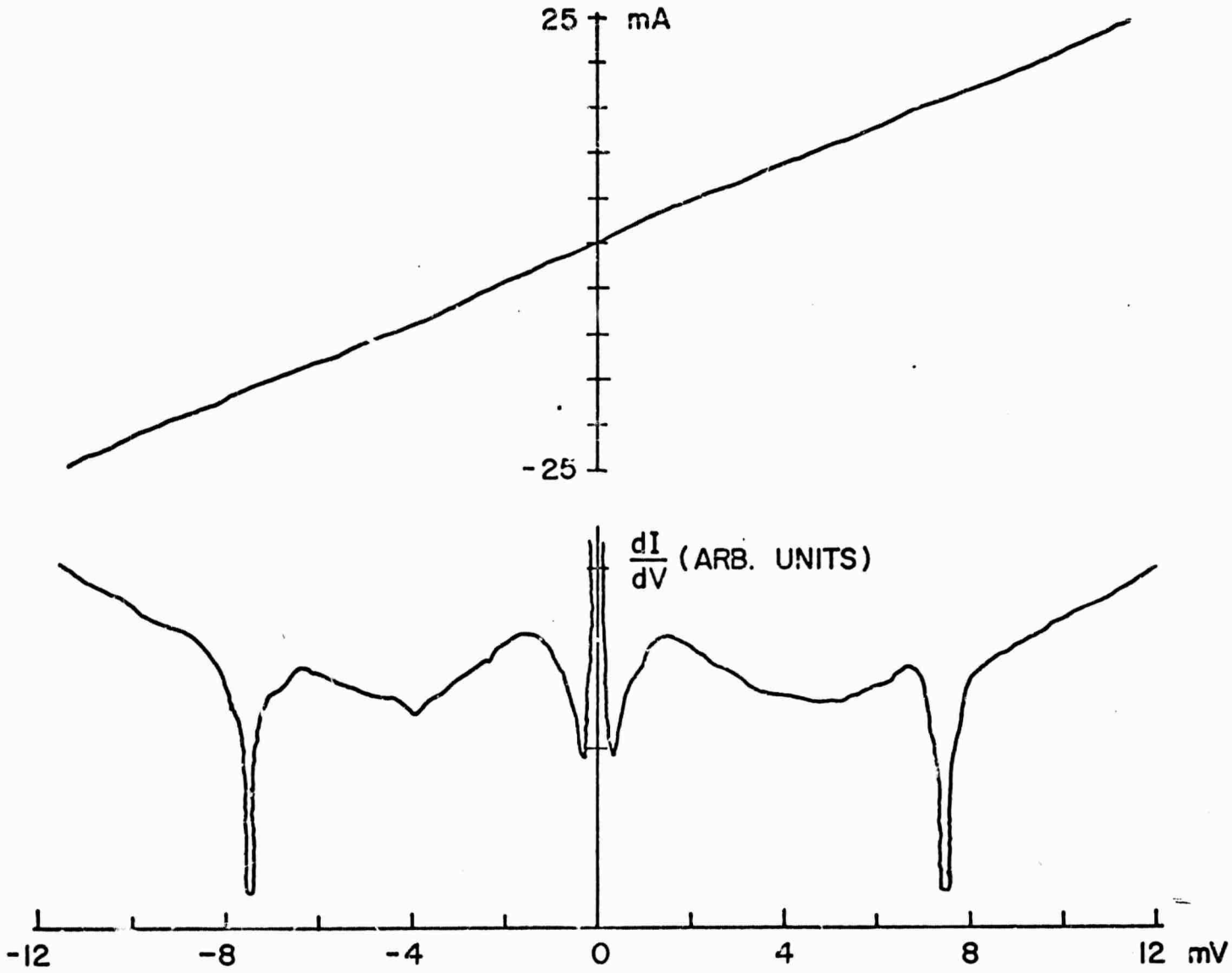
25
mA
-25
dI/dV (ARB. UNITS)
-12
-8
-4
0
4
8
12
mV

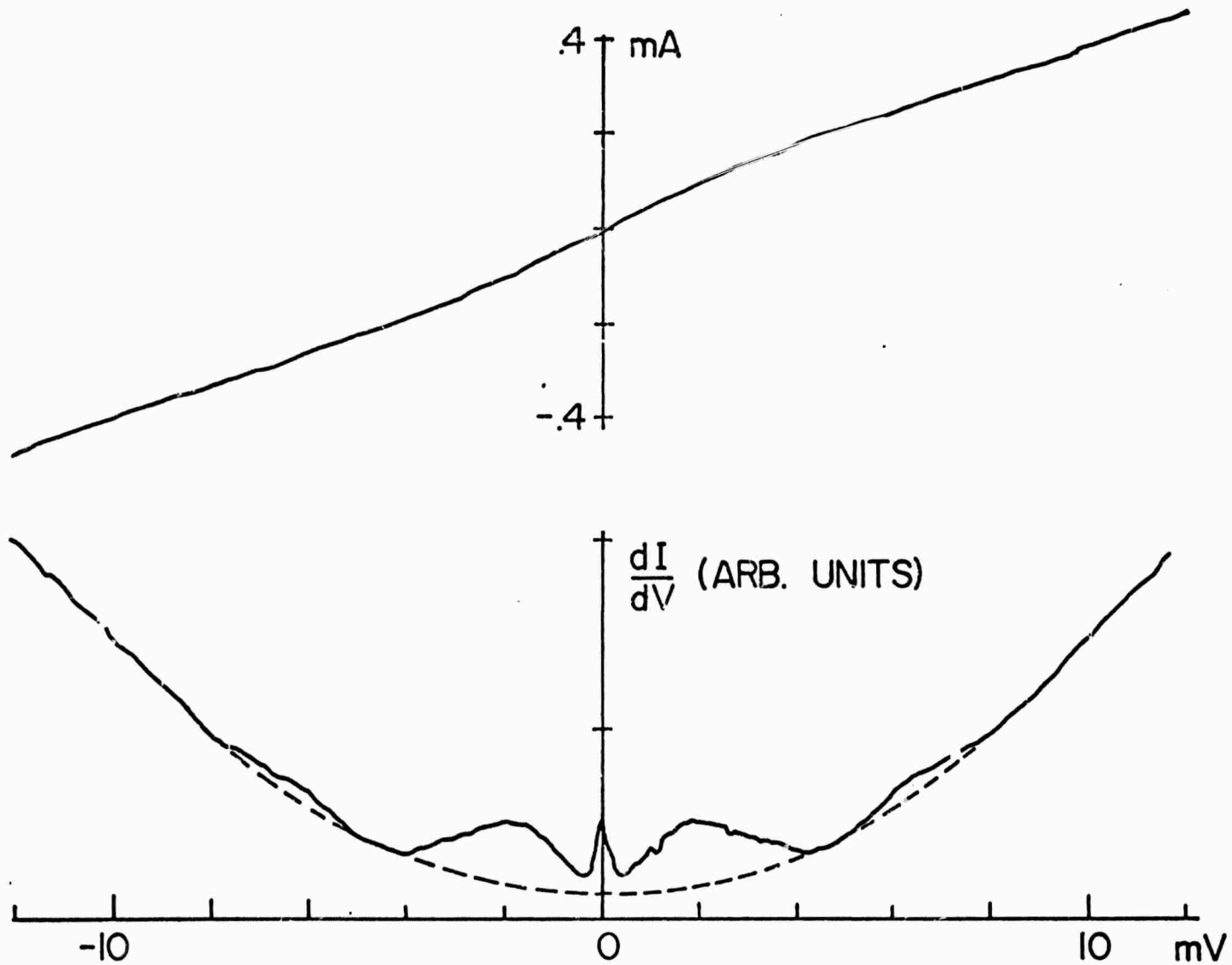
.4
mA
-.4
dI/dV (ARB. UNITS)
-10
0
10
mV

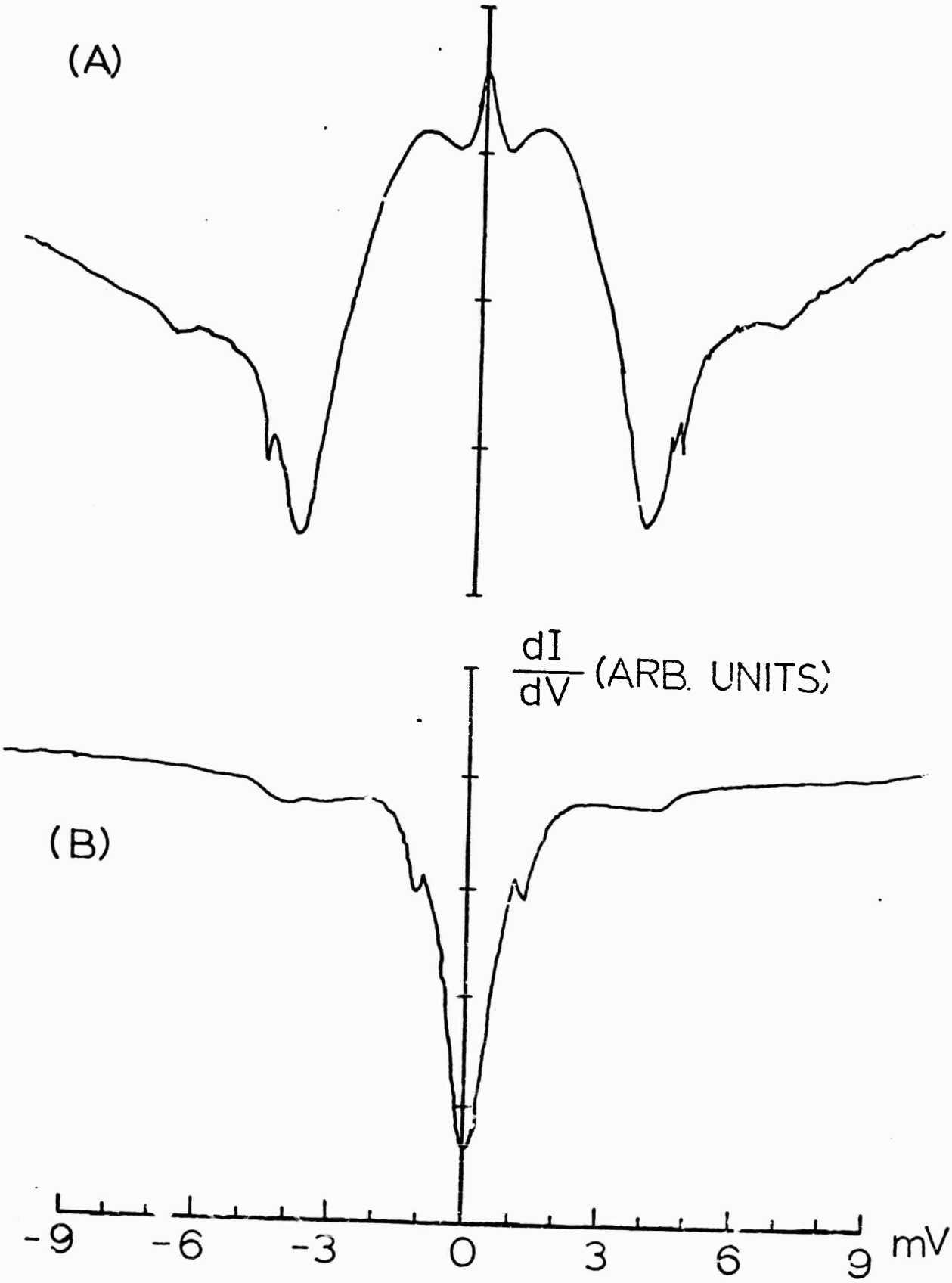
(A)
dI/dV (ARB. UNITS)
(B)
-9
-6
-3
0
3
6
9
mV

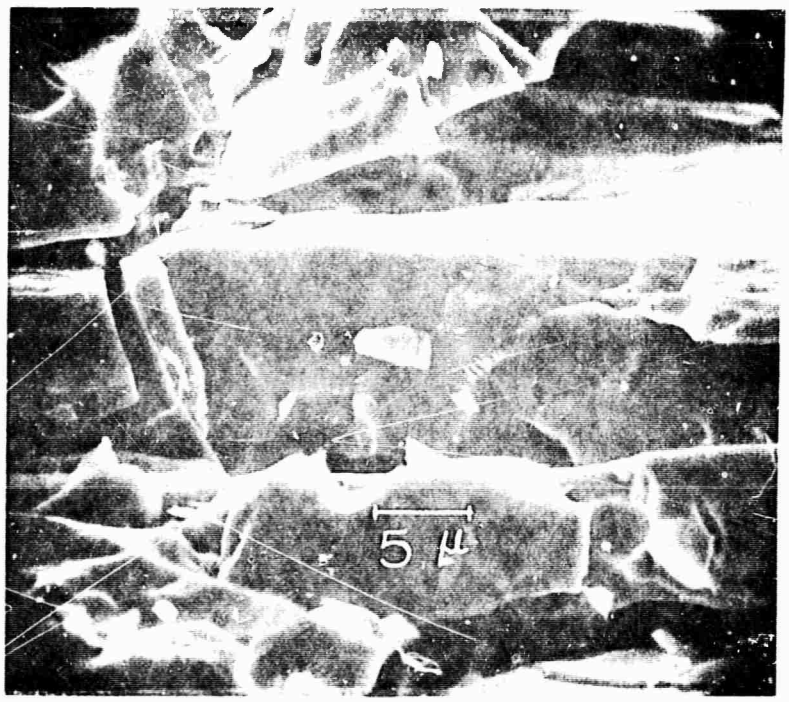
5 μ

III. An Improved Program for Deconvolution of Tunneling Data from Strong Coupled Superconductor Junctions.

A MODIFICATION OF THE McMILLAN-ROWELL TUNNELING DATA INVERSION PROGRAM

by

ALAN JAY DUBIN

Submitted in Partial Fulfillment
of the Requirements for the
Degree of Bachelor of Science
at the
MASSACHUSETTS INSTITUTE OF TECHNOLOGY
August, 1973

Signature of Author. . . . . .
Department of Electrical Engineering
August 24, 1973

Certified by . . Margaret. L. A. MacVicar
Thesis Co-Supervisor
Judith Louise Bostock
Thesis Co-Supervisor

Accepted by. . . . . .
Chairman, Departmental Committee on Theses

A MODIFICATION OF THE McMILLAN-ROWELL TUNNELING DATA INVERSION PROGRAM

ABSTRACT

The McMillan-Rowell Inversion Program for extracting phonon spectra and other normal state properties from superconducting tunnel junction data has been modified for more efficiency and greater ease of data handling. In addition, this modified program will enable double superconductor junctions in which both electrodes are strong-coupling superconductors to be analyzed. The sensitivity of the program to deviations from weak-coupling superconductivity has been increased so that previously unanalyzed materials such as Niobium can now be investigated. Having obtained the phonon spectrum of a given material, other transport properties which depend upon the electron-phonon interaction can then be calculated; various examples of such properties are given.

TABLE OF CONTENTS

List of Figures and Illustrations

ACKNOWLEDGMENTS

I wish to express my appreciation to Professor Margaret L. A. MacVicar for suggesting, directing and encouraging this work. Her interest in me and in my career has been most appreciated.

Much do I owe to Professor Judith Bostock, in particular for her contributions and tireless efforts as a critic, friend, mentor and editor. For her invaluable assistance and her warmhearted concern in my progress I am deeply grateful.

I am grateful to Professors Robert Rose and Margaret MacVicar for providing the opportunity for me to work in their group and introducing me to this area of physics.

I thank Dr. William L. McMillan of the University of Illinois, Urbana, for the use of his computer program.

Dr. Robert Dynes of Bell Research Laboratories; Murray Hill, New Jersey, was most helpful in explaining the McMillan-Rowell program and supplying various data decks that have enabled me to test my ideas.

I want to acknowledge the thesis of Dr. Wilbert

Norman Hubin which helped to simplify the writing of my own.

Above all, I wish to thank my family and my family-to-be for their continuous love, help, and support.

Finally, this thesis would not have been possible without the support of the Office of Naval Research (Contract No. ONR-039-087; Grant No. N00014-67-A-0204-0041) and of the Advanced Research Projects Agency (ARPA Contract No. DAHC 15-73-C-0316).

CHAPTER I

A. Introduction

In the last decade, electron tunneling has become recognized as one of the most important techniques for studying the properties of conductors in both the superconducting and normal metal states. A tunnel junction is a metal-insulator-metal sandwich through which current flows via a quantum mecanical tunneling process. Such devices are particularly important in the study of superconducting materials. If one (or both) of the metals is in the superconducting state at least three important properties of the metal (metals) can be determined from I-V and dI/dV - V characteristics of the junction: the electronic density of states of the metal in the superconducting state, the phonon density of states, and the electron-phonon coupling constant.

The BCS theory of superconductivity (named after the formulators: Bardeen, Cooper, and Schrieffer) (3) predicts the existence of an energy gap at the Fermi surface of a superconducting metal. In a normal metal, at T=0, the Fermi surface in energy space is sharply defined: all states below the Fermi energy,

E_F, are occupied while above E_F they are empty. In a superconductor there exists an energy gap of 2Δ in the electronic excitation spectrum centered about the Fermi energy. This gap is caused by the binding of electrons to form Cooper pairs; a phonon of energy 2Δ is required to break these pairs, that is, to excite single electron-like particles.

The purpose of this thesis is to describe how tunneling data can be processed to obtain the electronic spectrum(s), the phonon spectrum(s), and the electron-phonon interaction constant(s) appropriate to the metals comprising a superconductor junction. The initial "inversion process" was originated by McMillan and implemented by McMillan and Rowell on lead tunnel junctions (15). It has since been used by many others on various materials (1,5,12,19). Its basic limitation is that it assumes a BCS-model of electron pairing due to electron-phonon interactions in the metal. Although we have used the basic outline for inversion initiated by McMillan, substantial accuracy has been added to the program by more efficient and flexible data handling.

In this chapter the tunneling process in both normal and superconductor junctions is described. The emphasis is on how the superconducting electronic density of states is reflected in the conductance data of tunnel junctions. In Chapter II the strong-coupling modification of the BCS theory is briefly discussed and various parameters needed for the subsequent calculation of the phonon spectrum and electron-phonon coupling constant are introduced. Chapter III contains a discussion of the various stages in the computer program which enable the parameter calculations. It is hoped that the reader will obtain an overview of the total inversion process in this chapter. The appendix contains a computer printout of the inversion program along with introductory notes and comments intended to help the experimenter implement this program in his own laboratory. Finally, a brief section devoted to ideas for improving the present program has been included.

B. Tunneling

A simple theory of single particle tunneling explains how junction curves reflect the electron density of states of the metals comprising the junction (31,10).

In thermal equilibrium, the Fermi level of the two metals across the junction are the same.* A voltage, V, is applied so that the left side is at a higher potential than the right side. The current through the junction can be calculated as if the single particles were electrons. The number of electrons available to flow across the barrier from left to right in the energy interval dE will be equal to $N_1(E - eV)f(E - eV)dE$ where N_1 is the electron density of states on the left side and f is the Fermi function which gives the probability that a given state of energy $(E - eV)$ is occupied. On the other hand, there must be unoccupied states on the right hand side to receive these electrons. The number of these states equals $N_2(E)[1 - f(E)]$ where N_2 is the electron density of states of the metal on the right hand side. Therefore the current flowing from right to left is

$$I_1 = \int_{-\infty}^{\infty} P_{12}(E)\left[N_1(E-eV)f(E-eV)\right]\left[N_2(E)\left[1-f(E)\right]\right]dE \qquad (1)$$

where P_{12} equals the probability that an electron of energy E will tunnel through the barrier from left to right.

* See Fig. 1, p. 20.

By particle-hole symmetry $\{N(E) = N(-E)\}$ and since $f(E) = \{1 - f(-E)\}$ the current flowing from right to left is

$$I_2 = \int_{-\infty}^{\infty} P_{21}(E)\{N_1(E-eV)[1-f(E-eV)]\}\{f(E)N_2(E)\}dE$$

where $P_{21}(E)$ is the probability that an electron will tunnel through the barrier from right to left.

Assuming that an electron has just as much chance to go either way across the barrier [or $P_{12}(E)=P_{21}(E)$] the total current through the barrier, I, equals:

$$I = I_1 + I_2 = \int_{-\infty}^{\infty} P_{12}(E)N_1(E-eV)N_2(E)[f(E-eV)-f(E)]dE \qquad (2)$$

Assuming $P_{12}(E)$ is a constant, A, and that for a normal metal the density of states remains constant for a small applied bias voltage, then $N_1(E - eV) = N_1(0)$ and $N_2(E) = N_2(0)$ where energies are now measured from the Fermi energy. For small applied V,

$$\frac{f(E-eV)-f(E)}{-eV} \simeq \frac{df}{deV} \text{ at } T=0 \text{ and } \frac{df}{deV} = \text{Dirac delta function}$$

Hence, in the limit of small applied voltages,

$$I = AN_1(0)N_2(0)eV = DeV \qquad (3)$$

such that $D = AN_1(0)N_2(0)$, a constant. In other words, the tunnel junction obeys Ohm's law. In practice, this rule is only approximately obeyed (20,17,31) so

that $(dI/dV)_N$, the current derivative for the "normal state junction", is not a constant, as predicted by Eqn.(3).

If one of the metals of the junction is superconducting then one normal metal density of states, N(E), must be replaced by a superconducting density of states.* Using the BCS theory, the current becomes:

$$I = D\int_{-\infty}^{\infty} \frac{E}{\sqrt{E^2-\Delta_0^2}} \left[f(E-eV) - f(E)\right] dE \qquad (4)$$

where the BCS density of states is given by

$$N(0)\frac{E}{\sqrt{E^2-\Delta_0^2}} \qquad (5)$$

and N(0) is the density of the electrons of the metal in the normal state at the Fermi level (3). Upon integration (10),

$$I = 2D\frac{\Delta}{e}\sum_{1}^{\infty}(-1)^{m+1} K_1\left(\frac{m\Delta_0}{kT}\right)\sinh\left(\frac{eV}{kT}\right) \qquad (6)$$

where K_1 is a modified Bessel function of the second kind; k is Boltzman's Constant; and T is temperature.

* See Fig. 2, p. 22.

It is particularly convenient to evaluate the current Eqn.(4) at T=0. Here

$$f(E)=1 \quad E<0 \; ; \; f(E)=0 \quad E>0$$

therefore,

$$f(E-eV)-f(E)=1, \quad 0<E<eV$$
$$=0, \quad 0>E, \; E>eV$$

Taking into account that for a superconductor, due to the gap, there are no electron states for $0<E<\Delta_0$, then

$$I = D\int_{\Delta}^{eV} \frac{E}{\sqrt{E^2-\Delta_0^2}}\,dE \qquad (7)$$

and

$$\left(\frac{dI}{dV}\right)_S = D\frac{eV}{\sqrt{(eV)^2-\Delta_0^2}} \qquad (8)$$

Clearly, then, the conductance curve for the junction does reflect the superconducting density of states. In practice, however, because D is not really constant (see discussion page 11) it is usual to take conductance curves for both states of the metal, superconducting and normal. The ratio of these two quantities at a given bias V is then:

$$\frac{eV}{\sqrt{(eV)^2-\Delta_0^2}}$$

If both metals of the junction are in the superconducting state,* Eqn. (2) becomes:

$$I = \int_{-\infty}^{-\infty} A N_1(0) \frac{(E-eV)}{[(E-eV)^2 - \Delta_{01}^2]^{1/2}} \; N_2(0) \frac{E}{\sqrt{E^2-\Delta_{02}^2}} [f(E-eV) - f(E)] dE$$

or

$$I = D \int_{-\infty}^{\infty} \frac{(E-eV)}{\sqrt{(E-eV)^2 - \Delta_{01}^2}} \; \frac{E}{\sqrt{(E^2 - \Delta_{02}^2)}} [f(E-eV) - f(E)] dE \quad (9)$$

where Δ_{01} is the energy gap value of one of the metals and Δ_{02} that of the other. When T=0 and $\Delta_{01}=\Delta_{02}=\Delta_0$, (31)

$$I = D\left[2\Delta_0 + eV\mathcal{E}(\alpha) - \frac{4\Delta_0(\Delta_0 + eV)}{2\Delta_0 + eV} \times K(\alpha)\right] \quad (10)$$

for

$$eV \geq 2\Delta_0 \quad \text{and} \quad 0 \quad \text{for} \quad eV < 2\Delta_0$$

where

$$\alpha = \frac{(eV - 2\Delta_0)}{(eV + 2\Delta_0)} \quad \text{and} \quad K(\alpha) \text{ and } \mathcal{E}(\alpha) \text{ are}$$

complete elliptic integrals of the first kind. Then dI/dV at T=0 is

$$D \frac{d}{dV} \int_{\Delta_{01}}^{V-\Delta_{02}} \frac{E}{\sqrt{E^2 - \Delta_{01}^2}} \; \frac{E-eV}{\sqrt{[(E-eV)^2 - \Delta_{02}^2]}} \, dE \, .$$

* See Fig. 3, p. 24.

Therefore, if both metals of the junction are in the superconducting state the conductance curve of the junction, dI/dV - V, represents a convolution* of the densities of states of both metals. In practice, because D is not a constant, it is usual to consider the ratio

$$\frac{\left(\frac{dI}{dV}\right)_s}{\left(\frac{dI}{dV}\right)_N} = \frac{d}{dV}\int_{\Delta_{01}}^{V-\Delta_{02}} \frac{E}{\sqrt{E^2-\Delta_{01}^2}}\,\frac{E-eV}{\sqrt{(E-eV)^2-\Delta_{02}^2}}\,dE \qquad (11)$$

In principle if both Δ_{01} and Δ_{02} are known the normalized experimental data, $\left(\frac{dI}{dV}\right)_s \Big/ \left(\frac{dI}{dV}\right)_N$ should equal the calculated value of this ratio as given by Eqn.(11).

On the other hand, the superconducting behavior of most metals does deviate somewhat from that predicted by the BCS theory (28). Thus, depending on the state of the metals on both sides of the junction, the experimental "normal derivative" data will not agree with that calculated using either Eqn.(8) or Eqn. (11). The amount by which the experimental and calculated values differ is then used as a measure of how "weak-coupling" or BCS-like the given material(s) are.

* In the mathematically rigorous sense the current integral is not a convolution integral because the upper limit of the integral is a function of V. We will refer to Eqn.(11) as a convolution, however.

In fact, there exists a whole class of superconductors which are not well-described by the BCS theory of superconductivity, the so-called "strong-coupling" superconductors. For these materials the superconducting electronic density of states is no longer given by Eqn.(5), but rather by (25):

$$N(0)\,\mathrm{Real}\left\{\frac{|E|}{\sqrt{|E|^2-\Delta^2(E)}}\right\} \qquad (12)$$

where the energy gap parameter $\Delta(E)$ is now a complex quantity:

$$\Delta(E) = \Delta_R(E) + i\Delta_I(E) \qquad (13)$$

and the solution of the transcendental equation $\Delta(E=\Delta_0) = \Delta_0$ corresponds to the simple BCS energy gap.

In order to obtain phonon spectra for the materials composing the tunnel junction, it is necessary first to obtain their superconducting densities of states. This can be done quite simply for a normal-superconducting junction using Eqn.(8) and for a superconducting-superconducting junction where one electrode is a BCS-like material using Eqn.(11).*

* In either of these cases, if the "unknown" is a strong coupling material the appropriate superconducting density of states is replaced by Eqn.(12).

In the latter case the normalized experimental conductance is used along with the BCS density of states with Δ_0 known, to "deconvolute" the integral expression implicit in Eqn.(11) and obtain the normalized "unknown" density of states. The deconvolution process is not an easy one, but the main procedure has previously been outlined by McMillan and others (13,15,20).

Although, in essence, we follow this outline, a different procedure for the deconvolution has been developed in this thesis. And in particular, it can also be used when neither of the junction electrodes is a BCS-like superconductor. This modification has been necessary for a number of reasons. First, the "inversion program" as received (13) required a rather large "density of states-deviation" from the BCS value (certainly well above 1%) in order to be able to accurately determine a realistic phonon spectrum for the "unknown" material. And second, many strong-coupling superconductors with small deviations from BCS-behavior make the best tunnel junctions with other non-BCS superconductors. An example of a material where both these problems arise is Niobium. It has been shown that the

cleanest possible single crystal Nb junctions are made with strong-coupling materials Indium (2,9) and the lead-bismuth alloy $Pb_{.7}Bi_{.3}$ (8). The expected deviations in the Nb density of states are less than 1%.*

The remainder of this thesis will concentrate on the mechanics of the Inversion Program and discussions of problem-areas in using the programs with experimental data.

* M. A. MacVicar, private communication.

Fig.1*

Energy diagram for a metal-insulator-metal junction

(a) atthermal equilibrium

(b) at potential difference V.

*reproduced from Ref.(31)

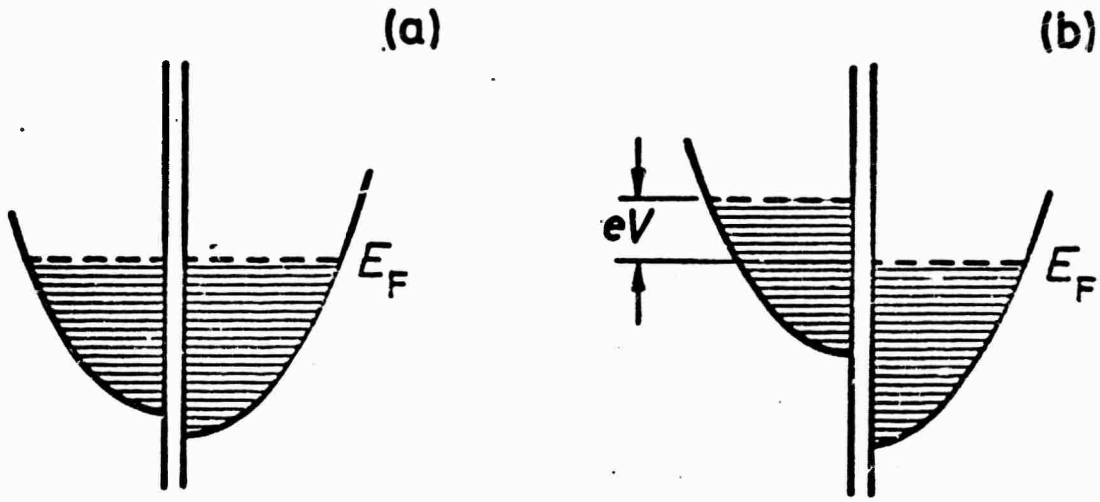
(a)
E_F
(b)
eV
E_F

Fig. 2.*

The energy diagram for an NS junction. (a) $V = 0$, (b) $V > \Delta/e$, (c) $I - V$ characteristic at $T = 0$.

---

*Reprinted from Ref. (31).

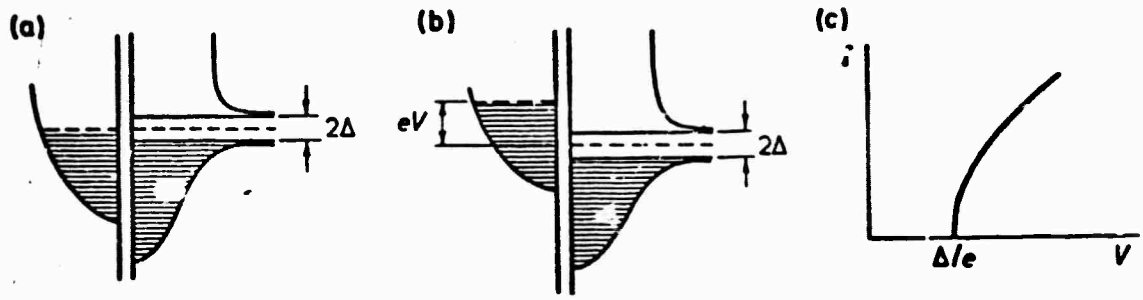
(a)
2Δ
(b)
eV
2Δ
(c)
i
Δ/e
V

Fig. 3.

The energy diagram for a SS junction at (a) $eV = \Delta_b - \Delta_a$, and (b) $eV = \Delta_b + \Delta_a$.

(c) The energy diagram for an NS junction at $eV = \Delta$.

The I - V characteristics of (a) an SS junction

(b) NS junction.

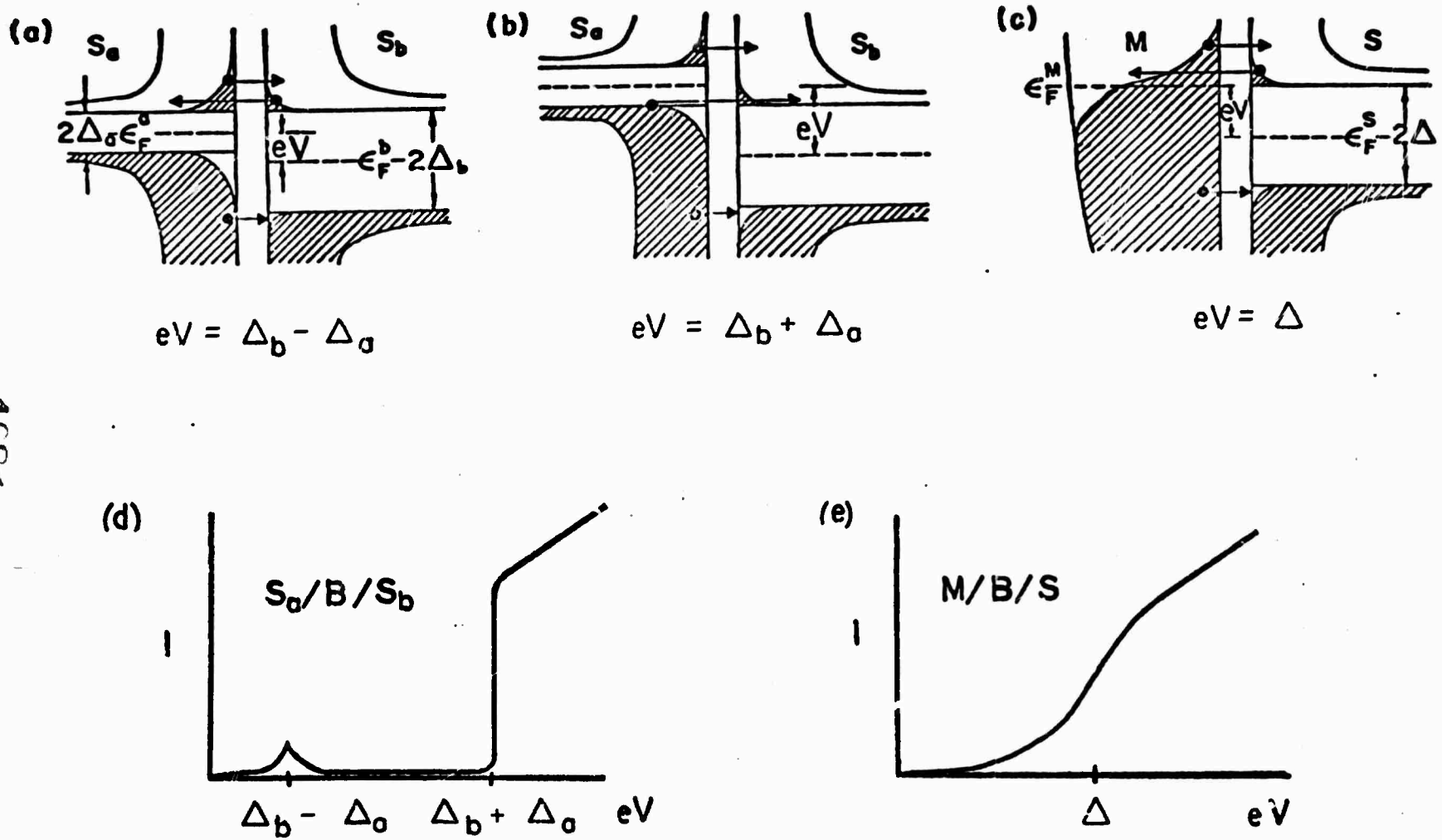
(a)
S_a
S_b
$2\Delta_a \epsilon_F^a$
eV
$\epsilon_F^b - 2\Delta_b$
$eV = \Delta_b - \Delta_a$
(b)
S_a
S_b
eV
$eV = \Delta_b + \Delta_a$
(c)
M
S
ϵ_F^M
eV
$\epsilon_F^S - 2\Delta$
$eV = \Delta$
(d)
$S_a/B/S_b$
I
$\Delta_b - \Delta_a$
$\Delta_b + \Delta_a$
eV
(e)
M/B/S
I
Δ
eV

CHAPTER II

A. Strong Coupling Theory

The BCS theory is based on an interaction between pairs of conduction electrons which is transmitted by the ionic lattice. The effective potential associated with this process is called the electron-phonon interaction, V. In the BCS treatment, it is assumed that the interactions between electrons are instantaneous and affect only those electrons within an energy E_D of the Fermi surface (E_D is the Debye energy). Thus, V is taken to be a constant for electron energies less than E_D and zero for larger electron energies. The weak coupling condition is also assumed in this treatment; i.e., that $N(0)V \ll 1$ where N(0) is the density of states at the Fermi surface. These assumptions resulted in a set of universal laws which all superconductors obey (3). The most important of these is an equation for the critical temperature where superconductivity occurs:

$$kT_c \simeq E_D e^{-\frac{1}{N(0)V}} \qquad (13a)$$

Most real superconductors, however, are observed to have properties which deviate, at least slightly, from these laws (27,28). In particular, it was observed

in tunneling experiments that the BCS density of states was not adequate to explain the experimental conductance. Hence, a more accurate treatment of the electron-phonon interaction was sought which would take into account both the non-instantaneous nature of this interaction (phonons have finite velocities) and the fact that the electronic energy states at energies of the order of E_D, are no longer well defined (electrons have short lifetimes which in turn give rise to damping effects in their transport properties). Using the thermodynamic Green's function approach Eliashberg (7) included both of these effects into a more general theory of superconductivity. While this approach is still based on the pairing concept introduced by BCS, it is more general in that it relates the superconducting state directly to details of the normal state such as the phonon spectrum of the material and the electron-phonon coupling constant (15,24).

Scalapino, Schrieffer, and Wilkins (SSW)* added the residual Coulomb interaction effects that screen the electron-phonon interaction which were also neglected in the BCS theory (23) to the Eliashberg treatment and found the following equations properly describe the superconducting state for a one-band isotropic model at zero temperature:

* Ref. (23) by SSW contains most of the following discussion; also helpful is Ref. (17).

$$\phi(E) = \int dE' \mathrm{Re}\left\{\frac{\phi(E')}{Z(E')}\left[E'^2 - \frac{\phi(E')^2}{Z(E')^2}\right]^{-1/2}\left\{K_+(E',E) - \mu^*\right\}\right. \tag{14}$$

$$\left[1 - Z(E)\right]E = \int_{\Delta_0}^{\infty} dE' \mathrm{Re}E'\left\{E'^2 - \left(\frac{\phi(E')}{Z(E')}\right)^2\right\}^{-1/2}\left[K_-(E',E)\right] \tag{15}$$

where

$$K_\pm(E,E') = \sum_{\wp}\int_0^{\infty} dE_q \alpha_{\wp}^2(E_q) F_{\wp}(E_q) \times \left[(E' + E + E_q + i\delta)^{-1} \pm (E' - E + E_q - i\delta)^{-1}\right] \tag{16}$$

and $\Delta(E) = \dfrac{\phi(E)}{Z(E)} = \Delta_R(E) + i\Delta_I(E)$. (17)

Here E is the electron energy measured from the Fermi surface, E_q is the phonon energy, F is the phonon density of states function, $\wp$ labels the phonon polarization and $\alpha^2(Eq)$ is an effective phonon coupling function. ϕ is the superconducting electron pairing function; Z is the electron-phonon renormalization function; and Δ is the energy gap function analogous to the simple BCS energy gap value Δ_0.

Now $\phi(E)$ is a measure of the pairing self-energy of the Cooper pairs, it gives a measure of how much the energy of the quasi-particles (or excited single particle states) is changed because pairing exists in the system. $Z(E)$ is a measure of how much the mass of the quasi-particle differs from the electronic mass because of the electron-phonon interactions in the system (i.e., a quasi-particle is a "dressed electron"). It is taken to be the same in the conducting state as it is in the normal state. The gap function $\Delta(E)$ has two parts. The real part gives the amount of energy needed to break a Cooper pair; i.e., the pair binding energy as a function of energy. The imaginary part corresponds to the shortening of the lifetimes of the excited quasi-particles; i.e., it is proportional to the probability that a virtual excited quasi-particle will decay from an energy E to the gap edge Δ_0 with the emission of a phonon.

Roughly, the physics of the pairing process is that a spin-up electron at the Fermi surface exchanges a phonon with a spin-down electron also at the Fermi-surface with a momentum transfer "q". $\alpha(E)$ is a measure of the "strength of the interaction" or probability that this exchange will be made. $F(E)$ indicates the kind of "particle" (a phonon)

that will be exchanged.*

Instead of using an additional self-consistent equation which would take care of the Coulomb repulsion between electrons, SSW used a Coulomb pseudo-potential method that accounts for higher energy excitations ($E>E_C$) by cutting off their integrals at $E=E_C$ where $E_C \approx 10E_D$ and inserting a dimensionless parameter $\mu^* = N(0)U_C$ into their equations. This factor is a number and not a function of energy because the effective Coulomb potential varies on a scale of the order of 1 eV while the pairing potential varies only in an energy interval of meV's about the Fermi energy. The effect of the Coulomb term on the superconducting system is, basically, to reduce the ability of the phonons to respond to the electrons; and thus to reduce the contribution of the phonons to the electron's self energy.

SSW were also able to show that the density of states of a superconductor is (23,25):

$$N_s(E) = N(0)\,\mathrm{Re}\left\{\frac{|E|}{\sqrt{E^2-[\Delta(E)]^2}}\right\} \qquad (18)$$

* If the phonon is emitted when the first electron goes from state $\vec{k}'\uparrow \rightarrow \vec{k}\uparrow$, then it must be absorbed by the other partner of the pair which will scatter from $-\vec{k}'\downarrow$ to $-\vec{k}\downarrow$; and $\vec{q}$ is $(\vec{k}'-\vec{k})$. We shall refer to either of the two electrons mentioned as the virtual excited quasi-particles or electrons.

which agrees with the BCS expression for the density of states (Eqn.(5)) in the limit of an energy independent gap function. Although this expression for the normalized density of states (NDS) makes clear that structure in $\Delta(E)$ will be reflected in the NDS, this fact is more clearly brought out by expanding $N_S(E)$ in powers of (Δ/E):

$$N_s(E) \underset{E \gg \Delta(E)}{\approx} 1 + \left\{ \frac{\mathrm{Re}\,\Delta^2(E) - \mathrm{Im}\,\Delta^2(E)}{2E^2} \right\}. \quad (19)$$

There exists a simple model (23,24) for describing how the solution of Eqns.(14)-(17) relate to the "picture" we have used. Consider the case where the material has a phonon density of states with a single particle peak at E_o (See Fig. 4.). At excitation energies less than E_o, since most of the phonons which can be exchanged by the electrons have a higher natural frequency than E_o they tend to over-respond to the "driving frequency" causing an attractive electron-electron interaction while at energies greater than E_o the phonons are driven above the natural frequencies and tend to respond out of phase with the driving field. This corresponds to a repulsive electron-electron interaction. For excitation energies near E_o, the real part of Δ peaks, or, the pair binding energy increases strongly because of

Fig. 4.*

(a) A phonon peak at ($\omega = \omega_0$) causes $\Delta(\omega)$ to look as (b) and produces density of states (c).

*reprinted from Ref. (11).

(a)

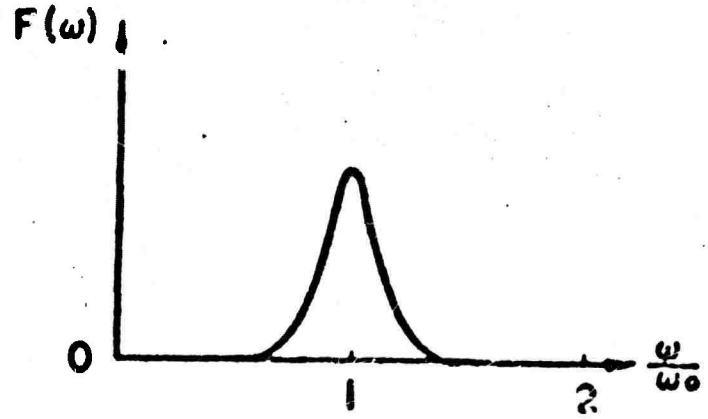

(b)

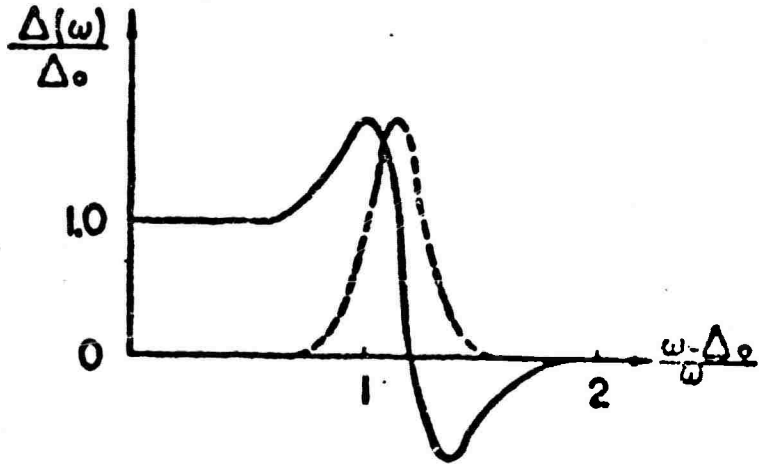

(c)

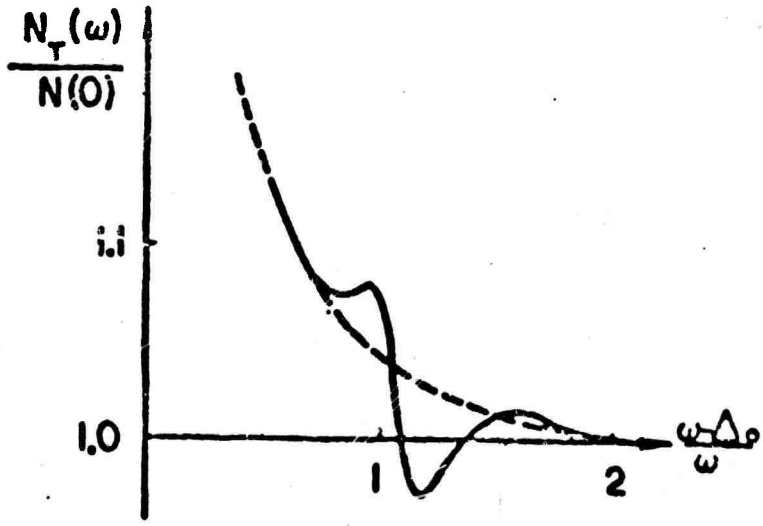

the resonant exchange of phonons that have the same response frequency as that of the real lattice. The $Re\Delta(E)$ decreases to negative values for $E>E_0$ since the electron-electron interaction is repulsive. The $Im\Delta(E)$ which is a measure of the damping effects will be zero at very low energies since the quasi-particles are well defined there; rise to a peak near the resonance because of the increase in phonon emission; and finally it will vanish because the excited electrons can no longer fall to the gap edge by emitting a phonon.

By considering Eqn.(19) for the density of states it is clear how the phonon structure is indirectly mirrored in $N_S(E)$ through the gap function and why there are shoulders and drops in $N_S(E)$ with respect to the BCS-NDS. Adding a Coulomb term to this picture would only change, qualitatively, the $Re\Delta(E)$ after resonance. In this case, it would remain negative instead of going to zero, indicating the net Coulomb repulsion of the virtual unbound electrons (23,24).

Another important quantity of interest is the effective electron-phonon coupling constant, λ, which equals (16,23)

$$\lambda = 2\int_0^\infty \frac{\alpha^2(E)F(E)}{E}\,dE \qquad (20)$$

and represents some "averaged" electron-phonon parameter for the whole system. In fact, the renormalization function, Z(E), near the gap edge can be shown to be equal to:

$$Z = 1 + \lambda = \frac{m^*}{M} \qquad (21)$$

where m* is the effective electron mass. This expression makes sense since λ is a measure of the phonon screening of electrons.

McMillan (16) has given a very clear discussion on how, once λ, Z(E), and α^2F are known, many other electronic properties of the normal state of metals can be determined such as the Fermi velocity, the electronic coefficient of the specific heat, the electronic band structure, and the normal metal density of states. It is through a knowledge of such properties that new uses for these materials can be found. These normal state properties can also be used to predict what the critical temperature for the superconducting state will be. McMillan (16) has derived the formula:

$$kT_c \approx E_D e^{\frac{-1.04(1+\lambda)}{\lambda-\mu^*-.62\lambda\mu}} \qquad (22)$$

When compared with the BCS Eqn.(13a) it is clear that the "effective interaction" for superconductivity becomes: $N(0)V \approx \lambda - \mu^*$, (23)

just as our crude picture would predict.

Using the fact that $\Delta(E)$ is reflected in the density of states of superconductor and that $\alpha^2(E)F(E)$ is related through the gap equations to $N_S(E)$ McMillan and Rowell (17,13) developed a program to determine the α^2F of a metal from the experimental first derivative curve of a tunnel junction. The method by which this "inversion" is accomplished is described in Chapter 3.

B. Practical Details

It would be instructive to point out several properties about dI/dV and d^2I/dV^2 curves and the junction samples which influences the correctness of the input data and, thus, the correctness of the output of this program.

First, the junctions used must be good ones. Rowell (17,20) has laid down, in several places, the basic criteria for determining the perfection of junctions. Rowell and MacVicar, et al., have laid down rules for determining if the dI/dV curves of a given junction do reflect bulk material characteristics (17,9).

From the BCS-NDS given in Eqn.(5) we see that as E approaches infinity the BCS-NDS approaches 'one'. Even for non-BCS superconductors for larger bias the NDS equals the BCS-NDS. Therefore, for higher voltages the value of the normal first derivative should equal the

value of the superconducting first derivative. It has been found, however, that this does not always happen (12,11). A possible explanation of this phenomenon is that in the normal state the resistance of the metal films of the junction is significant in comparison with the junction resistance (12). To compensate for errors of this type, in the past, a constant has been added to all values of the normal first derivative data such that this data is made equal to the superconducting data at high biases. The phonon curves generated from this data have been unlike the phonon curves for other metals (17). The effect of such a procedure on the generated α^2F spectrum is unknown.

McMillan's program requires only that the NDS of a metal be known in order to determine its phonon spectrum. Still, it is preferable to modify the first derivative data by the second derivative data. The reason for this is that critical points in the phonon spectrum of a metal (the places where $(dF(E)/dE)$ equals infinity) are reflected as square root singularities and logarithmic singularities in the d^2I/dV^2 curve (21). However, due to thermal smearing and phonon broadening, singularities appear as peaks and valleys rather than mathematically sharp singularities. The point is that while the conductance curve contains very accurate data, the second derivative curve itself resolves the "small" structure in the first derivative data.

Finally, it should be pointed out that the McMillan inversion gives α^2F, the phonon spectrum multiplied by the electron-phonon coupling function. α^2F should, nevertheless, be a good reflection of $F(E)$ since $\alpha^2(E)$ is thought to be a slowly changing continuous function with no critical points.[21] Thus one expects the "general shape" of $\alpha^2F(E)$ to be that of $F(E)$, and the critical points of $\alpha^2F(E)$ to be those of $F(E)$.

Neutron scattering is an alternative way of determining a phonon spectrum of a metal. Comparisons of the two methods for various metals have shown that the critical points of the phonon spectrums are in general agreement (17). The discrepencies in the magnitude of the peaks can be accounted for by the fact that tunneling inversion generates $\alpha^2(E)F(E)$ while neutron scattering is thought to generate $F(E)$.

C. Temperature Dependence(23)

Finite temperature dependence has also been introduced into the strong coupling theory of superconductivity [Eqns.(14)-(17) become very much more complicated.]. Here we merely want to point out that qualitative changes that temperature brings into our crude picture of the superconducting state. Increasing T is equivalent to

putting thermal energy into our system. This thermal energy will tend to weaken or break pairs which are not tightly bound. Thus, just as in theBCS theory, the gap edge function Δ_0 becomes a function of temperature, decreasing as T increases. In an analogous way we expect the entire real part of $\Delta(E)$ to be reduced from the T=0 value of $\Delta(E)$. In addition the virtual excited quasi-particles in this state can now recombine with the thermally generated quasi-particles, so we expect more structure (or resonances) in both real and imaginary parts of the gap functions. Clearly, the damping effects, reflected in the $\mathrm{Im}\Delta(E)$ will also be decreased, energy for energy, over the zero temperature case. Finally, it has been shown that (24)

$$\Delta(E,T) \approx \left[\frac{\Delta_0(T)}{\Delta_0}\right] \Delta(E,0) \qquad (24)$$

that is, the temperature dependent gap function is, roughly, a scaled down version of the $\Delta(E)$ curve where the scale factor is the BCS temperature dependent gap edge.

Chapter III

"The Programs"

Three programs are required to produce a phonon spectrum from the raw tunneling data. Stage I smoothes and interpolates the experimental input. Stage II removes the influence of the counter-electrode and produces data characteristic only of the unknown metal. Stage III manipulates theoretical functions which should reproduce the output of Stage II. A detailed discussion of each stage is given below.

Stage I

The goal of the first program, Stage I, is to take the raw data and compute the deviation of the experimental conductance values of the junction from that predicted by the BCS tunneling model [Given in Eqn.(11)]. The quantity $\sigma(V)$ determined at all applied voltages, V, where

$$\sigma = \frac{\text{(normalized experimental data)}}{\text{(BCS predicted normalized function)}} - 1$$

is used as the measure of that deviation. (One is subtracted from the quotient to emphasize the deviations which are of the order of 6%, at most (17, 24)).

Stage I proceeds in the following steps. dI/dV with both metals superconducting, dI/dV with both metals normal, and d^2I/dV^2 with both metals superconducting are computed from the input data which is taken directly from the xy-recorder. Then the normalized density of states, $(dI/dV)_{SUPER}/(dI/dV)_{NORMAL}$ is computed. If second derivative data is available, the integral of the second derivative data is least square fitted to the normalized first derivative data, and this fitted normalized first derivative is smoothed. Then, the deviation of this experimental normalized first derivative from the BCS predicted normalized first derivative is computed.

Several steps are required to compute $(dI/dV)_{SUPER}$ and $(dI/dV)_{NORMAL}$ from the laboratory input:

The input is given in pairs, an X value and a corresponding Y value. It would be preferable if X equalled a voltage value, V, and Y equalled dI/dV at V; instead, X=aV+b and Y=c(dI/dV)+d. Therefore the actual values of V and dI/dV must be computed. To do this several parameters must be supplied to the program to compute a,b, c, and d.

Secondly, there may exist in the input stream several anomalous points which repeat previously recorded input pairs; that is, the X values of these points is less than a previous X value of the input stream. The program

assumes a monotonically increasing X value; hence, these anomalous points are removed.

Thirdly, the values of dI/dV will not usually be recorded experimentally at a specific voltage interval, i.e. at V=0,H,2H,...,nH with H being the interval. However, the programs Stage II and Stage III require that $\sigma(V)$, and therefore dI/dV values, be taken at constant intervals. Therefore, the values of dI/dV for specified increments of the bias voltage, V must be computed. This is done either by polynomial interpolation using the points whose voltage values are in the vicinity of the voltage at which the values of dI/dV are required, or by linear or quadratic least square fitting. The least square fitting determines either a first or second degree polynomial to represent the input data. Polynomial interpolation then is used to determine dI/dV at $V_1, V_2, V_3, \ldots$, etc. The advantage of the linear or quadratic fitting option is that it tends to eliminate the random noise found in the input.

Stage I was designed modularly so that it can be easily changed if different experimenters should have slightly different requirements. In addition to this, an effort was made to put in a variety of features for extra flexibility. Among the features included are a choice of either polynomial interpolation using from 1

to 10 points or linear or quadratic fitting using from 1 to 100 points; the ability to measure dI/dV with V positive or negative [(dI/dV) is symmetric around V=0]; and the ability to find the normalized first derivative even though the second derivative curve is unavailable.

Stage II

Stage II is a generalized deconvolution routine. As mentioned in Chapter I if both metals are superconducting the normalized first derivative equals

$$\left.\frac{\left(\frac{dI}{dV}\right)_S}{\left(\frac{dI}{dV}\right)_N}\right|_{EXP} = \frac{d}{dV}\int_{\Delta_{01}}^{V-\Delta_{02}} D_1(E)\, D_2(V-E)\, dE$$

where D_1 is the normalized density of states of metal I and Δ_{01} is its energy gap value and D_2 and Δ_{02} are the analogous quantities for metal II.

When the phonon spectrum of some material is desired, it is not always possible to fabricate a tunnel junction where the counter-electrode remains normal at the temperature where the experiment must be done. Instead, the counter-electrode becomes superconducting; if it is a BCS-like superconductor then Eqn.(11) can be used, with little difficulty, to obtain the unknown electronic density of states. If, on the other hand, the counter-electrode is non-BCS, it introduces its own deviations into the normalized experimental conductance data. Therefore, the effect of the counter-electrode must be eliminated from the experimental data

at the same time that the deconvolution of Eqn.(11) is being accomplished. To deconvolute the experimental data Stage II requires two sets of inputs: the smoothed experimental data from Stage I and the normalized first derivative of the "given" counter-electrode.

The exact workings of the program are explained in the appendix. Only one problem involved in handling the input data will be discussed here: the problem revolves about the experimental fact that it is difficult to determine accurately junction conductances very close to the gap edge (13). It is usual to assume that the junction conductance equals the value predicted by the BCS theory at these biases. This is not really too gross an assumption since the BCS function is rising rapidly towards its singularity for $V=\Delta_0$, and the deviations due to strong-coupling effects are far smaller than those due to the finite rounding off of the BCS function. This means, however, that the first non-zero experimental value in the input data suddenly has a deviation from the BCS value while the preceding point does not. Theoretically the deviation from BCS should start at zero and continuously increase for very low offset voltages.

The lack of experimental information at low offset voltages introduces a large error into the deconvolution routine especially for the first data points. The computer

sub-routine is written so that the first few "input" data slots are zero. The deviation of the first non-trivial experimental input should be looked at by the program operator and "data" inserted in the "empty slots" which takes the deviations from 0 to the first experimental deviation in a smooth way. So, for example, if the first deviation is .0035, the "data points" .001, .002, .003 might be inserted.

The normalized density of states (NDS) for the known counter-electrode ("given") can be determined in one of two ways. The first method is to make two tunneling junctions simultaneously with films of the "given": one with the metal of interest and the second with a BCS or normal metal. The NDS of the given material can then be determined using Stages I and II with tunneling data from the BCS or normal metal junction. This computed NDS of the given is then simply "read-in" Stage II when the tunneling data from the junction containing the material of interest is processed by the inversion program. Since the two junctions were processed simultaneously, and thus under the exact same conditions, one would hope that the NDS is the same for both junctions. Needless to say, this may not be true. However, by running several different samples, or junctions, with the material of interest (all either processed at the same time as the "reference

junction" with the non-BCS counter-electrode, or each made separately and each having its own "reference junction") a close check can be made on the validity of the procedure by comparing the NDS for the "unknown" from the different runs.

For the case where it is not possible to prepare simultaneous "reference junctions" another option is provided in the program. It consists of reading in a phonon spectrum for the given material and from that phonon spectrum computing the NDS of the given. This routine has been taken directly from Stage III and presumes that the "given" material is sufficiently well-characterized that its phonon spectrum is easily obtained and is not sensitive to material changes inherent in the present method of making the tunnel junction. The only check on the accuracy of the unknown's NDS and phonon spectrum (calculated in Stage III) is the ability to reproduce the results from sample to sample. This can, of course, be made quite rigorous by using different counter-electrodes for the given material. Agreement of the calculated NDS and phonon spectrum for the unknown material under such circumstances, makes it almost certain that the basic material properties <u>have</u> been calculated.

Stage III

Stage III is the original McMillan-Rowell Inversion Program Stage III (13). The main idea in this program is to calculate the normalized electronic density of states for the unknown and compare these values with those determined in Stage II. If these two data arrays agree, then it is assumed that the phonon spectrum used to calculate the data of Stage III is that characterizing the unknown. Although this may seem like a simple enough procedure, it is not...it hinges on knowing the approximate phonon spectrum and/or knowing "how" to change the assumed phonon spectrum to bring the calculated electronic NDS of Stage III into agreement with that derived from the raw tunneling data; i.e., the output of Stage II.

The functions that are calculated and plotted in this stage were described previously in Chapter II. In this section, only the general mechanics of this stage will be discussed. The program is written to operate in either of two modes: (a) the approximate form of the phonon spectrum is known and (b) it is not known. Only mode (b) will be described, since during the iterations of the program, in this instance, the phonon spectrum that is directly "read-into" the program in mode (a) is calculated and subsequently "improved" or iterated to obtain the final phonon spectrum. Clearly, if a good

approximation to the phonon spectrum is already known, the cost of running this program is substantially reduced. It should be noted, therefore, that in an experimental investigation once an $\alpha^2(E)F(E)$ spectrum is obtained for one sample (using mode (b), say) then this spectrum should be used in Stage III operated in mode (a) for other samples. If, in fact, the α^2F spectrum calculated for a single sample is characteristic of the material, then the changes of spectrum from sample to sample should be within the "error-bars" of the experimental data set, itself. Given that this occurs, the investigation is completed.

Mode (b) of Stage III operates in the following way.* An iteration process is used by McMillan's inversion program to solve the gap equations. Starting zeroth order values must be chosen for μ^*, $\Delta(E)$, and $\alpha^2F(E)$. $\mu^{*(0)}$ the first value chosen for μ^* is usually set equal to .11 and $\alpha^2F(E)^{(0)}$ can be an almost arbitrary function defined up to $E=E_0$, the maximum energy of the phonon spectrum. $\Delta^{(0)}(E)$, the zeroth order value, is taken to be equal to Δ_0 for $E< E_C$, and equal to zero for $E > E_C$, where $E_C=3E_0$ and $\Delta_0=\Delta(E=\Delta_0)$, the BCS gap value.

---

*The following discussion has been adapted from Ref. (13).

Inserting these starting values in the right hand side of Eqn.(14) and Eqn.(16) will then give a calculated value for the gap function, $\Delta^{(1)}(E)$. Reinserting $\Delta^{(1)}(E)$ in the equations, with the same μ^* and α^2F, will give a second calculated value $\Delta^{(2)}(E)$. This process is continued until $\Delta^{(n)}(E)$ converges. Then the density of states, $N_C(E)$, can be calculated using Eqn.(12).

It is now necessary to correct the starting α^2F and μ^* based on the difference between N_C, the calculated density of states, and the input data from Stage II, N_e the experimental density of states. We use linear feedback techniques (17) to correct α^2F for the error $[N_e(E)-N_C(E)]$. This is done by first calculating the effect on N(E), for all data points, of a small change in α^2F; i.e.,

$$\delta[N(E')]/\delta[\alpha^2F(E)].$$

Then

$$\alpha^2F^{(n+1)}(E_q)=\alpha^2F^{(n)}(E_q)+\delta[\alpha^2F(E_q)],$$

where

$$\delta[\alpha^2F(E_q)]=\int\frac{dE_q'[N_e(E_q')-N_C^{(0)}(E_q')]}{(\delta N(E_q')/\delta[\alpha^2F(E_q)])}$$

where $N_C^{(0)}$ is the first value calculated for N_C and the functional derivative is calculated from the analytic form of the gap equation. The iteration of α^2F, namely, solving for $\Delta(E)$ and NDS from α^2F and changing α^2F depending on how the calculated NDS compares to the experimental NDS is continued until α^2F converges. That is, since the gap equation is non-linear the total process must be iterated until α^2F converges. $\mu^*(n)$ is determined by the requirement that $\Delta(E=\Delta_0)$ always equals the BCS value, Δ_0.

Note, however, that because the data does not extend to the gap edge, it is necessary to make an assumption regarding the energy dependence of α^2F at low energies. The program assumes that α^2F is proportional to the square of the energy up to some prespecified value of energy.

It is appropriate here to give a few guidelines on the operation of this stage of the inversion program. A "normal" convergence run will have Δ iterated approximately 5 times and α^2F approximately 8 times. If the form of α^2F is known from previous samples, the "new-sample" might need to iterate as many as 4 times. Notice that it is impossible for α^2F to converge while the experimental density of states in <u>not</u> close to the

calculated density of states. This is because it is the difference between the two that determines how much α^2F will change; a big difference, N_e-N_c, implies a large, or significant change in α^2F.

(d^2I/dV^2) data is used to resolve the (dI/dV) data because the critical points in α^2F should appear as singularities in (d^2I/dV^2). On the other hand, the singularities in this curve are smeared due to thermal excitations and the most sensitive way to determine if the critical points of α^2F agree with those in (d^2I/dV^2) is the human eye. Although the computer could be used for this cross-checking procedure, it would not be very efficient.

It is also important to know if changes in $\alpha^2F(E)$ correspond to experimental uncertainty or to real differences in the experimental density of states. A measure of precision of α^2F can be obtained by running the inversion program with the experimental density of states at their greatest and least values within the experimental error and thus determining the maximum change in $\alpha^2F(E)$. Any change less than this is certainly inherent in the experiment, itself. (This assumes, of course, that both sets of data are such as to produce a converging α^2F).

COSTS

The three stages were run on the IBM 170-155 at the MIT Information Processing Center. The costs of running each of the three programs can be kept low by running them under low priority and by using object decks. The range of costs are:

Stage I	$ 6 - $10
Stage II	$ 2 - $ 4
Stage III (McMillan program alone)	$ 8 - $12

CHAPTER IV

"Future Work"

The previously mentioned programs can certainly be improved. The first improvement is to put temperature dependence into the convolution program. The theory of strong-coupling superconductivity at finite temperatures has been completely worked out and equations analogous to those used in the zero temperature case are available (22). With these equations in hand, it does not seem as if in principle, there will be problems in addition to those already treated, to be solved. However, until such a project is undertaken it is impossible to estimate what difficulties could be encountered.

Secondly, it would be interesting to consider the effects of various choices of the parameter μ^* on the final $\alpha^2(E)F(E)$ spectrum selected. In some recent tunneling studies (29,14) it has been found that once μ^* is chosen to give a phonon spectrum which duplicates the experimental input data, just by scaling up (in amplitude) α^2F, a different μ^* which is in better agreement with the "expected" μ^* can be chosen that will also duplicate the experimental input data. This behavior is NOT understood and the reason for this

behavior should be determined. Understanding the mechanism behind it might enable the theoretician to determine if, in these cases, it really is totally the electron-phonon mechanism which produces superconductivity (30). Or, more pessimistically, if the parameter μ^* really is a sensitive superconducting parameter (6).

Another improvement would be to arrange Stage II and Stage III in such a way that a phonon spectrum for the "given" electrode would be used to calculate its superconducting electronic density of states (this is fed into Stage II). Then Stage III would iterate the phonon spectrum of the "unknown" until the "best possible value" for its calculated density of states is obtained. If total convergence with experimental data has not been achieved with this "best possible value", small changes would be made in the phonon spectrum of the given, and a new iteration on the "unknown" phonon spectrum carried out. This is done repetitively until McMillan's program converges. Unless the "given" counter-electrode is a well-characterized material, however, such a procedure might be prohibitive from a cost-efficiency point of view. In addition, the problem of the

accuracy of the given's normalized density of states (NDS) remains. That is, if this parameter does NOT truly reflect the density of states of the counter-electrode, even though the inversion program converges, there is no assurance that the phonon spectrum or electron-phonon coupling constant obtained for the "unknown" material accurately reflect its basic properties.

This brings us to the final recommendation of this thesis. A careful and quantitative study of the effects of errors in the "given" NDS on the final phonon spectrum for the "unknown" material should be carried out. In particular, it should be determined if Stage III will converge when this NDS in not accurate. In the event that it would, such that several tunnel junctions composed of the same two materials all give identically the same "unknown" $\alpha^2(E)F(E)$ (with the wrong given), the present method of deconvoluting the tunneling data could not be used in the case that both junction electrodes are strong-couplers. The best theoretical estimates*

* J. Bostock, private communication

at the present time indicate that this will not be true. Hence, we expect that implementing a "double deconvolution" is, in principal, quite possible and should be done in the near future.

APPENDIX

Computer Programs and Comments

STAGE I

STAGE I takes experimental data from the laboratory setup and converts it to the following form:

$$\frac{\left[\frac{dI}{dV_S} \Big/ \frac{dI}{dV_N}\right]_{\text{Experimental}}}{\left[\frac{dI}{dV_S} \Big/ \frac{dI}{dV_N}\right]_{\text{BCS Predicted}}} - 1 = \sigma$$

Details will be given in comment cards within the program and in the introductions to the various subroutines.

INPUT

TITLE an array of 80 characters to be printed which gives a title or contains information such as date, metals, junction number, and any comments on the data set.

H is the interval in millivolts at which values for the normalized density of states is output. The default value for H = .2 millivolts.

MAXX the maximum desired energy at which the normalized density of states (NDS) and σ is to be computed. If MAXX is greater than the maximum energy, E, for which there exists input, MAXX will be set equal to E.

IROUT — If IROUT = 1 the data will be interpolated. If IROUT = 2 the data will be linearly fitted. Default value for IROUT = 1. A further explanation of the fitting and interpolation routines will be given within the program.

GAP 1 — the gap value for the metal whose phonon spectrum is desired.

GAP 2 — the gap value for the counter-electrode.

IPLT — If IPLT = 1 the original graphical input will be plotted as it appears on the laboratory X-Y recorder. If IPLT = 0 no plotting will occur. Default value for IPLT = 0.

IFIX — The value of IFIX will determine the routines used to convert the input values to dI/dV values. In the present program only one routine exists and IFIX = 1 as the default.

ISS — If ISS = 0 the first derivative data is not fitted to the second derivative data but the NDS and σ are found. If ISS is not specified, second derivative data is used.

ISKIP — If ISKIP = 0 then only the NDS is found. Again, the first derivative data is not fitted to the second derivative data.

M	M is the number of points around the point of interest used in both the interpolation and fitting routines.
INEG1 INEG2 INEG3	If INEG = 1 the junction was reversed biased when taking dI/dV data. If INEG = 0 the junction was forward biased. INEG1 is for the superconducting data; INEG2, the normal data; INEG3, the second derivative data. Default: INEG1 = 1; INEG2 and INEG3 equal by default the value read in or assigned by default to INEG1.
IPLT1	If IPLT1 = 0 the NDS will not be plotted. Default value, IPLT1 = 1.
IPLT2	If IPLT2 = 0 σ will not be plotted. Default, IPLT2 = 1.
IDEBG	If IDEBG = 1 the input data points with anomalous points removed is printed. Default, IDEBG = 0, means nothing is printed.
ISM	the number of points greater than the first relevant point at which smoothing occurs.
ISMAX	the number of points less than the last relevant point at which smoothing occurs.
ESM	a smoothing parameter to be explained within the program. Default, ESM = .25H.

IFLAG If fitting is used: If IFLAG = 1, linear fitting is used; If IFLAG = 2, quadratic fitting is used.

XSCLE1, XSCLE2, XSCLE3, DX1, DX2, DX3, EX1, EX2, EX3, DY1, DY2, DY3, EY1, EY2, EY3, X1, X2, X3, AX1, AX2, AX3, Y1, Y2, Y3, AY1, AY2, AY3, ZERO1, ZERO2, ZERO3, DXO1, DXO2, DXO3, DYO1, DYO2, DYO3, BERO1, BERO2, BERO3, are parameters for subroutine IFIX. If the parameter name ends with a 'one' it is associated with the superconducting data. If its name ends with a 'two', the normal data; if its name ends with a 'three', the second derivative data. The superconducting parameters have no default values. Each parameter of the normal and second derivative data is defaulted to be equal to the value of the same parameter for the superconducting data. For example, X2 = X1 and X3 = X1 are the default values for X2 and X3.

XFS,YFS the experimental superconducting "first derivative" data.

XFN,YFN the experimental normal "first derivative" data.

XSS,YSS the experimental superconducting "second derivative" data.

FORMATS FOR INPUT PARAMETERS

INPUT	FORMAT
TITLE	20A4

The elements of the PAREM NAMELIST are: H, MAXX, IROUT, GAP1, GAP2, IPLT, IFIX, ISS, M, INEG1, IPLT1, IPLT2, ISKIP, N1, XSCLE1, YSCLE1, DX1, EX1, DY1, EY1, X1, AX1, Y1, AY1, ZERO1, DXO1, IDEBG, DYO1, BERO1, IFLAG.

The elements of the INPUT NAMELIST are: ISM, ISMAX, ESM, DX2, DX3, EX2, EX3, DY2, DY3, EY2, EY3, X2, X3, INEG2, INEG3, AX2, AX3, Y2, Y3, AY2, AY3, ZERO2, ZERO3, BERO2, BERO3, DXO2, DXO3, DYO2, DYO3, N2, N3, XSCLE2, XSCLE3, YSCLE2, YSCLE3.

INPUT	FORMAT
XFS,YFS	10(1X,I1, F6.0)
XFN,YFN	10(1X,I1, F6.0)
XSS,YSS	10(1X,I1, F6.0)

OUTPUT PARAMETERS

TITLE, NAMELIST PAREM, and NAMELIST INPUT are the same as their definition in the input parameters list.

XFS,YFS arrays of the superconducting dI/dV x and y values, respectively.

XFS,YFS If IDEBG = 1 then the previously mentioned arrays with anomalous points removed are printed.

XFS,YFS arrays containing the x and y coordinates, respectively, of the input points as they appeared on the xy-recorder expressed in terms of inches away from the xy-recorders midpoint.

XFS,YFS arrays containing the voltage and corresponding $\left.\frac{dI}{dV}\right|_{SUPER}$ values.

The exact same information is printed for dI/dV_{NORMAL} data and the d^2I/dV^2 data.

FSI the normalized first derivative.

Information to track the fitting and smoothing section is printed out. The titles printed are self-explanatory.

BCS the values of

$$\frac{d}{dV}\int_{\Delta_{01}}^{V-\Delta_{02}} \frac{E}{\sqrt{E^2-\Delta_{01}^2}}\,\frac{(V-E)}{\sqrt{(V-E)^2-\Delta_{02}^2}}\,dE$$

FRAT σ.

PUNCHED OUTPUT

TITLE	same as input	
IMAX	number of output σ.	FORMAT - (6X,I4)
FRAT	σ	FORMAT - 7F10.6

* Notice that all plotting routines listed in these programs are peculiar to the MIT Computation Center. They must be replaced by equivalent programs.

** A description of the second derivative fitting routine can be found in Ref. 11 and Ref. 13.

```
C*****************************************************************************
C*****************************************************************************
C*****************************************************************************
C                                                                            *
C                                                                            *
C       STAGE  NE:   THE NORMALIZED DENSITY OF STATES AND ITS DEVIATION FROM THE
C                    BCS PREDICTED DENSITY OF STATES IS COMPUTED
C                                                                            *
C                                                                            *
C*****************************************************************************
C
C
      DIMENSION  XFN(920),YFN(920),XFS(920), YFS(920), XSS(920),
     CYSS(920), A(10,10),V(10)
      DIMENSION TITLE(20), FS(920),FN(920),SS(920), EI(920), FSI(920),
     C DFSI(920), FRAT (920),FSII(920), BCS(920), AMAT (4,4),V(4),
     CDC(920), SM(19), DCSM(920)
      EQUIVALENCE    (XFN,XFS,XSS),(YFN,YFS,YSS,FSII),(DFSI,FRAT),
     C (FN,DCSM),(FS,BCS)
      REAL MAXX
      NAMELIST /PAREM/ H,MAXX,IROUT,GAP1,GAP2,IPLT,IFIX,ISS,  M,
     C INEG1,
     C IPLT1,IPLT2,
     C ISKIP,
     C N1,XSCLE1,YSCLE1   ,DX1,FX1,DY1,EY1,X1,AX1,Y1,AY1,ZERO1,DXO1,
     C     IDEBG,
     C     DYO1,BERO1 ,IFLAG
     C /INPUT/ ISM,ISMAX,ESM, DX2,DX3,FX2,FX3,DY2,DY3,EY2,EY3,X2,X3,
     C  INEG2,INEG3,
     C  AX2,AX3,Y2,Y3, AY2,AY3,ZERO2,ZERO3, BERO2,BERO3,DXO2,DXO3,
     C DYO2,DYO3          ,N2,N3, XSCLE2,XSCLE3,YSCLE2,YSCLE3
C
C
C*****************************************************************************
C                                                                            *
C                                                                            *
```

```
C    TITLE, INFORMATION ABOUT THE JUNCTION, IS READ IN AND PRINTED OUT
C                                                                       *
      READ (5,10) TITLE
      WRITE (6,10) TITLE
10    FORMAT (20A4)
C                                                                       *
C                                                                       *
C***********************************************************************
C
C
      CALL NEWPLT ('M10763','10741')
C
C
C***********************************************************************
C                                                                       *
C                                                                       *
C    PARAMETERS IN THE PARAM NAMELIST ARE SET EQUAL TO THEIR DEFAULT VALUES
C                                                                       *
      INFGL=1
      IPLT1=1
             IDEBG=0
      IPLT2=1
      ISKIP=1
      IFLAG =1
      ISS=1
       MAXX =500.
                   H=.2
      IFIX=1
      IPLT=1
      M=2
      IROUT=1
      ISM=10
      ISMAX=10
C                                                                       *
C                                                                       *
C***********************************************************************
```

```
C
C
C
C
C*****************************************************************************
C                                                                            *
C                                                                            *
C    THE PAREM NAMELIST IS NOW READ IN.  ALL PARAMETERS WITHOUT DEFAULT VALUES
C    AND ALL PARAMETERS WITH DEFAULT VALUES WHOSE DEFAULT VALUE IS TO BE
C    OVERRIDDEN MUST BE INCLUDED IN THE PAREM NAMELIST
C
      READ (5,PAREM)                                                         *
      WRITE (6,PAREM)
C
C                                                                            *
C*****************************************************************************
C
C
C
C
C*****************************************************************************
C                                                                            *
C                                                                            *
C    PARAMETERS IN THE INPUT NAMELIST ARE SET EQUAL TO THEIR DEFAULT VALUES
C
      ESM=.25*H                                                              *
       INEG2=INEG1
      INEG3=INEG1
      DXO2=DXO1
      DXO3=DXO1
      DYO2=DYO1
      DYO3=DYO1
      N2=N1
      N3=N1
      XSCLE2=XSCLE1
      XSCLE3=XSCLE1
```

```
      YSCLE2=YSCLE1
      YSCLE3=YSCLE1
      DX2=DX1
      DX3=DX1
      EX2=EX1
      EX3=EX1
      DY2=DY1
      DY3=DY1
      EY2=EY1
      EY3=EY1
      X2=X1
      X3=X1
      AX2=AX1
      AX3=AX1
      Y2=Y1
      Y3=Y1
      AY2=AY1
      AY3=AY1
      ZERO3=ZERO1
      ZERO2=ZERO1
      BERO2=BERO1
      BERO3=BERO1
C                                                                       *
C                                                                       *
C***********************************************************************
C
C
C
C
C***********************************************************************
C                                                                       *
C                                                                       *
C   THE INPUT NAMELIST IS NOW READ IN.  ALL PARAMETERS WITHOUT DEFAULT VALUES
C   AND ALL PARAMETERS WITH DEFAULT VALUES WHOSE DEFAULT VALUE IS TO BE
C   OVERRIDDEN MUST BE INCLUDED IN THE INPUT NAMELIST
C                                                                       *
```

```
      READ (5,INPUT)
      WRITE (6,INPUT)
C                                                                       *
C                                                                       *
C***********************************************************************
C
C
C
C
C***********************************************************************
C                                                                       *
C                                                                       *
C     MAXX,THE MAXIMUM ENERGY FOR WHICH OUTPUT IS DESIRED IS CONVERTED INTO
C    MAXA, THE DESIRED NUMBER OF OUTPUT POINTS.
C                                                                       *
      MAXA=MAXX/H+2
C                                                                       *
C                                                                       *
C***********************************************************************
C
C
C
C
C***********************************************************************
C                                                                       *
C                                                                       *
C    THE SUPERCONDUCTING FIRST DERIVATIVE IS NOW COMPUTED FROM THE EXPERIMENTAL
C    DATA IN THE FOLLOWING MANNER:
C      1) THE INPUT IS READ IN BY SUBROUTINE READR
C      2) THE X VALUES, THE VOLTAGE, SHOULD BE MONOTONICALLY INCREASING BUT
C      DUE TO EXTERNAL DISTURBANCES (SUCH AS SLAMMING DOORS) THE LABORATORY
C      APPARATUS MAY PRODUCE CERTAIN POINTS WHOSE VOLTAGE VALUES ARE LESS THAN
C      THE VOLTAGE VALUES OF PRECEEDING POINTS.  THESE POINTS MUST BE DROPPED,
C      THUS, SUBROUTINE EVEND MUST BE CALLED
C      3) THE X AND Y INPUT VALUES ARE NOT V AND DI/DV RESPECTIVELY, INSTEAD,
C      V=A*X+B AND DI/DV=C*Y+D WHERE A, B, C, AND D ARE CONSTANTS TO BE
```

```
C      DETERMINED BY INPUT PARAMETERS,THEREFORE IFIX MUST BE CALLED TO COMPUTE
C      (V,DI/DV) PAIRS FROM (X,Y) PAIRS.
C      4) THE VALUES OF DI/DV ARE DESIRED AT V=I*H,I=1,2,...,MAXA.
C      DI/DV AT THESE VALUES MUST BE INTERPOLATED FROM THE GIVEN VALUES
C       OF DI/DV.  TO DO THIS EITHER SUBROUTINE INTER OR SUBROUTINE LINFIT,
C      WHICH SMOOTHES THE DATA AS WELL, IS CALLED
C
C    THE NORMAL FIRST DERIVATIVE AND THE SECOND DERIVATIVE ARE COMPUTED
C    IN A LIKE MANNER
C                                                                          *
       CALL READR(XFS,YFS,N1)
       WRITE (6,36) (XFS(I),YFS(I),I=1,N1)
36     FORMAT ('1THE FOLLOWING IS THE INPUT DV/DI SUPER'/
      C     5 (1X,F8.5,2X,F8.5,5X))
       CALL EVENC(XFS,YFS,N1,N1)
            IF (IDEBG .EQ. 0) GO TO 797
       WRITE (6,136) N1,(XFS(I),YFS(I),I=1,N1)
797          CONTINUE
136    FORMAT ('1 THE FOLLOWING IS THE AVERAGED AND ANOMOLY REMOVED DATA
      C,THERE ARE',1X,I4,1X,'POINTS REMAINING'/
      C     5 (1X,F8.5,2X,F8.5,5X))
       IF (IFIX .EQ.1) CALL IFIX1( IPLT,YSCLE1,XSCLE1  ,X1,AX1,Y1,AY1,
      C DX1,EX1,DY1,EY1,ZERO1,BERO1,XFS,YFS,DXO1,DYO1,N1,INEG1)
C       IF (IFIX .EQ.2) CONTINUE
       IF (IROUT .EQ.1) CALL INTER (XFS,YFS,EI,FS,N1,MAXA,H,M,A,B,MAXI)
       IF (IROUT .EQ. 2) CALL LINFIT (MAXA,N1,H,M,XFS,YFS,EI,FS,IFLAG,
      C MAXI)
       N1=MAXA
C                                                                          *
C                                                                          *
C*************************************************************************
C
C
C
C
C*************************************************************************
```

```
C                                                                       *
C                                                                       *
C    THE NORMAL FIRST DERIVATIVE IS NOW COMPUTED
C                                                                       *
      CALL READR(XFN,YFN,N2)
      WRITE (6,379)(XFN(I),YFN(I),I=1,N2)
379   FORMAT ('1THE FOLLOWING IS THE INPUT DV/DI NORMAL'/
     C     5 (1X,F8.5,2X,F8.5,5X))
      CALL EVENC(XFN,YFN,N2,N2)
          IF  (IDERG .EQ. 0)  GO TO 799
      WRITE (6,136) N2, (XFN(I),YFN(I),I=1,N2)
799          CONTINUE
      IF (IFIX .EQ.1) CALL  IFIX1(IPLT,YSCLE2,XSCLE2,  X2,AX2,Y2,AY2,
     CDX2,EX2,DY2,EY2,ZERO2,BERO2,XFN,YFN,DXO2,DYO2,N2,INFG2)
C     IF (IFIX .EQ. 2) CONTINUE
      MAXA=MAXX/H+2
      IF (IROUT .EQ. 1) CALL INTER (XFN,YFN,EI,FN,N2,MAXA,H,M,A,B,MAX2)
      IF(IROUT.EQ.2) CALL LINFIT (MAXA,N2,H,M,XFN,YFN,FI,FN,IFLAG,MAX2)
      N2=MAXA
C                                                                       *
C                                                                       *
C***********************************************************************
C
C
      NC=MAXO(MAXI,MAX2)
      J1=NC-1
      NS=MINO(N1,N2)
      ISM=NC+ISM
      ISMAX=NS-ISMAX
      DO 17 I=1,J1
      DFSI(I)=0
17    FSI(I)=0
      DO 37 I=1,NS
      AI=I-1
37    FI(I)=AI*H
C
```

```
C
C*****************************************************************************
C                                                                            *
C                                                                            *
C     COMPUTE NORMALIZED FIRST DERIVATIVE
C                                                                            *
      DO 38 I= NO,NS
30    FSI(I)= FN(I)/FS(I)-1
C                                                                            *
C                                                                            *
C*****************************************************************************
C
C
C
C
C*****************************************************************************
C                                                                            *
C                                                                            *
C    COMPUTE DERIVATIVE OF NORMALIZED FIRST DERIVATIVE
C                                                                            *
      K1= NO + 1
      DO 124 I=        K1,NS
124   DFSI(I)=(FSI(I)-FSI(I-1))/H
      DFSI(NO)=0
      WRITE (6,30) (EI(I),FSI(I),DFSI(I),I=1,NS)
30    FORMAT  ('1 THE FOLLOWING IS THE NORMALIZED DI/DV AND ITS DERIVATI
     CVE,RESPECTIVELY   '  /    3(F10.6 ,2X,F10.6,2X,F10.6,6X))
      IF (IPLT1 .EQ. 0) GO TO 68686
C                                                                            *
C   PICTUR IS A PLOTTING SUBROUTINE
C                                                                            *
      CALL PICTUR (11.0,8.2,' ',1,'SUPER/NORMAL',12,FI,FSI,NS,0.0,0)
68686  CONTINUE
C                                                                            *
C                                                                            *
C*****************************************************************************
```

```
C
C
       IF (ISKIP    .EQ. 0) GO TO 59595
      IF (ISS .EQ.0) GO TO 91919
C
C
C*****************************************************************************
C                                                                            *
C                                                                            *
C   THE SUPERCONDUCTING SECOND DERIVATIVE IS COMPUTED
C                                                                            *
      CALL READR (XSS,YSS,N3)
      WRITE (6,1654) (XSS(I),YSS(I),I=1,N3)
1654  FORMAT ('1 THE FOLLOWING IS THE INPUT D2I/DV2 SUPER'/
     C    5 (1X,F8.5,2X,F8.5,5X))
      CALL EVENO (XSS,YSS,N3,N3)
                IF  (IDEBG .EQ. 0)   GO TO 2356
      WRITE (6,136) N3, (XSS(I),YSS(I),I=1,N3)
2356                CONTINUE
      IF (IFIX .EQ. 1) CALL IFIX1(IPLT,YSCLE3,XSCLE3   ,X3,AX3,Y3,AY3,
     CDX3,EX3,DY3,EY3,ZERO3,BERO3,XSS,YSS,DXC3,DYC3,N3,INEG3)
C     IF (IFIX .EQ. 2) CONTINUE
      MAXA=MAXX/H+2
      IF (IROUT .EQ. 1) CALL INTER (XSS,YSS,EI,SS,N3,MAXA,H,M,A,B,MAX3)
      IF (IROUT .EQ. 2) CALL LINFIT (MAXA,N,H,M,XSS,YSS,EI,SS,IFLAG,
     CMAX3)
C                                                                            *
C                                                                            *
C*****************************************************************************
C
C
        N3=MAXA
      NS= MINO(N1,N2,N3)
      NO=MAXO(MAXI,MAX2,MAX3)
      ISM=NO+ISM
      ISMAX=NS-ISMAX
```

```
C
C
C*****************************************************************************
C                                                                            *
C                                                                            *
C    THIS SECTION FITS THE INTEGRATED SECOND DERIVATIVE DATA TO THE
C    FIRST DERIVATIVE DATA USING A LEAST SQUARES METHOD
C                                                                            *
      DO 39 I=1,920
      FRAT(I)=0
      FSII(I)=0
      DC(I)=0
      BCS(I)=0
39    BCSM(I)=0
      DO 12 I= NO,NS
      FSII(I)= FSII(I-1) + SS(I) *H
12    BCS(I)= BCS(I-1) +SS(I) * FSI(I) *H
      DO 170 I=ISM,ISMAX
      SM(1) = FSII(I)
      SM(2) = 1.
      SM(3)=FI(I)
      SM(4) =BCS(I)
      SM(5) = FSI(I)
      DO 170 J=1,4
      V(J)= V(J) + SM(J) *SM(5)
      DO 170 K=1,4
170   AMAT(J,K) =AMAT(J,K) + SM(J) *SM(K)
      CALL SIMO (AMAT,V,4,KI)
      WRITE(6,100) (V(I),I=1,4)
100   FORMAT(' V(I)=',4E13.6)
      DO 20 I=1,NS
      SS(I)=V(1) *SS(I) + V(3) + V(4)*SS(I)*FSI(I)
      IF(FSII(I)) 21,20,21
21    FSII(I)=V(1)*FSII(I)+V(2)+V(3)*FI(I)+V(4)*BCS(I)
20    CONTINUE
      WRITE(6,32) (SS(I),I=1,NS          )
```

```
32    FORMAT('1FITTED SECOND DERIVATIVE'/(1X,10E13.6))
      WRITE(6,33) (FSII(I),I=1,NS)
33    FORMAT('1FITTED INTEGRAL OF 2ND DERIVATIVE'/(1X,10E13.6))
      DO 60 I=NC,NS
60    DC(I)=FSI(I)-FSII(I)
      WRITE(6,63) (DC(I),I=1,NS)
63    FORMAT('1DIFF,NORM 1ST DER AND INT OF 2ND DER'/ (1X,10E13.6))
      DO 40 I=K1,NS
      V2=FI(I)
      BCS(I)=FBCS(GAP1,GAP2,V2,40)-1
40    FRAT(I)=(FSI(I)-BCS(I))/(1.+BCS(I))
      WRITE(6,34) (BCS(I),I=1,NS)
34    FORMAT('1BCS FIRST DERIVATIVE'/(1X,10E13.6))
      WRITE(6,35) (FRAT(I),I=1,NS)
35    FORMAT('1NORM 1ST DER/BCS'/(1X,10E13.6))
C
C     THE NORMALIZED DV/DI IS NOW SMOOTHED,USING THE INTEGRATED,
C     FITTED SECOND DERIVATIVE
C
      SUM=0
      DO 64 I=1,19
      AI=I-10
      SM(I)=EXP(-(AI*H /ESM)**2)
64    SUM=SUM+SM(I)
      DO 67 I=1,19
67    SM(I)=SM(I)/SUM
      DO 65 I=10,ISMAX
      DO 65 J=1,19
      IJ=I+J-10
65    DCSM(I)=DCSM(I)+DC(IJ)*SM(J)
      DO 66 I=ISM,ISMAX
66    FSI(I)=FSII(I)+DCSM(I)
      DO 69 I=2,ISMAX
69    DC(I)=(FSI(I)-FSI(I-1))/H
      WRITE(6,70) (FSI(I),I=1,ISMAX)
70    FORMAT('1SMOOTHED FIRST DERIVATIVE'/(1X,10E13.6))
```

```
      WRITE(6,71) (DC(I),I=1,ISMAX)
71    FORMAT('1DER OF SMOOTHED 1ST DER'/(1X,10E13.6))
91919   CONTINUE
C                                                                       *
C                                                                       *
C***********************************************************************
C
C
C
C
C***********************************************************************
C                                                                       *
C                                                                       *
C   THE BCS PREDICTED NORMALIZED DENSITY OF STATES IS COMPUTED FOR ALL V FOR
C   WHICH THERE EXISTS EXPERIMENTAL DENSITY OF STATES DATA.  IF SECOND
C   DERIVATIVE SMOOTHING WAS USED THE BCS VALUES WERE ALREADY COMPUTED AND THIS
C   SECTION IS SKIPPED
C                                                                       *
        IF (ISS .EQ. 1) GO TO 96336
           DO 74114   K23=1,J1
74114      BCS(K23)  =0.0
          DO 85225    K12=NC,NS
              V2=EI(K12)
85225     BCS(K12)=FBCS(GAP1,CAP2,V2,60)-1
96336     CONTINUE
              WRITE (6,523)  (EI(KT),BCS(KT),KT=1,NS)
523          FORMAT ('1THE VALUES OF (D/DV(BCS INT.)-1)  ARE'/
     C    5 (1X,F8.5,2X,F8.5,5X))
C                                                                       *
C                                                                       *
C***********************************************************************
C
C
C
C
C***********************************************************************
```

```
C                                                                       *
C                                                                       *
C   THE ZERO OF ENERGY IS NOW SHIFTED SO THAT ENERGIES ARE HENCEFORTH
C   MEASURED FROM THE SUM OF THE GAPS
      DO 72 I=1,ISMAX
72    FRAT(I)=(FSI(I)-BCS(I))/(1.+BCS(I))
      EMAX=EI(ISMAX)
      IMAX=(EMAX-GAP1-GAP2)/H+1.
      J=1
      DO 134 I=1,IMAX
      AI=I-1
      E=AI*H+GAP1 +GAP2
      DO 133 K=1,100
      IF(E-EI(J)) 131,131,132
132   J=J+1
133   CONTINUE
131   EM=EI(J-1)
      EP=EI(J)
      FM=FRAT(J-1)
      FP=FRAT(J)
134   BCS(I)=FM+ (FP-FM)*(E-FM)/(EP-EM)
            ILA=((NC-1)*H-GAP1)/H
            ILA=ILA+1
                  BCS(ILA)=0.0
C                                                                       *
C                                                                       *
C***********************************************************************
C
C
      DO 135 I=1,IMAX
135   FRAT(I)=BCS(I)
      IF (IPLT2 .EQ. 0) GO TO 69696
      CALL PLOT (13.0,0.0,-3)
      CALL PICTUR(11.0,8.5,' ',1,'DEVIATION',9,EI,FRAT,IMAX,0.0,0)
                CALL ENDPLT
69696   CONTINUE
```

```
                WRITE (6,73) (EI(I),FRAT(I),I=1,IMAX)
73          FORMAT ('1SMOOTHED NORM DER/D/DV(BCS INT)-1  FROM GAP EDGE'/
     C     5 (1X,F8.5,2X,F8.5,5X,))
      WRITE(7,93) GAP1,GAP2,H
93    FORMAT(' GAP1=',4X,F10.5,' GAP2=',4X,F10.5,' H=',7X,F10.5)
      WRITE(7,10)(TITLE (I),I=1,20)
      WRITE(7,94) IMAX
94    FORMAT(' IMAX=',I4)
      WRITE(7,74)(FRAT(I),I=1,,MAX)
74    FORMAT(7F10.6)
59595    CONTINUE
      STOP
      END

C*********************************************************************
C*********************************************************************
C*********************************************************************
```

SUBROUTINE READR

Subroutine READR reads in raw input data and puts the x values sequentially into array X, and the corresponding y values sequentially into array Y. The input of a x value is of the form Xa±nnnnn and its numerical values is $(\pm .nnnnn)10^{-a}$. The input of a y value is of the form Ya±nnnnn and its numerical value is computed in an analogous manner. As an example, if the first input card is as follows:

X4+01299Y4+03298X4+01302Y4+03320X4+01308Y4+03332X4+01312Y4
+03348X4+01318Y4+03356

then	X(1) = .1299	Y(1) = .3298
	X(2) = .1302	Y(2) = .3320
	X(3) = .1308	Y(3) = .3332
	X(4) = .1312	Y(4) = .3348
	X(5) = .1318	Y(5) = .3356

<u>INPUT PARAMETERS</u> (passed)

N = the number of x(y) values to be read.

INPUT PARAMETERS (from I/O device)

X = the input x values in untranslated form.

Y = the input y values in untranslated form.

OUTPUT PARAMETERS

X = an array of the translated input x values.

Y = an array of the translated input y values.

THE INPUT RECORDS ARE OF THE FOLLOWING FORM

5(Xa±nnnnn,Ya±nnnnn).

```
C*****************************************************************************
C*****************************************************************************
C*****************************************************************************
C
C
      SUBROUTINE READR (X,Y,N)
      DIMENSION X(920),Y(920), ILX(920),ILY(920)
C
C
C*****************************************************************************
C                                                                            *
C                                                                            *
C   THE INPUT RECORDS ARE READ.  THE A'S ARE PUT INTO ILX AND ILY,
C   THE NNNNN'S ARE PUT INTO X AND Y.
C                                                                            *
      READ(5,11,END=9000) (ILX(I),X(I),ILY(I),Y(I),I=1,N)
11    FORMAT (10(1X,I1,F6.0))
      GO TO 30
C                                                                            *
C                                                                            *
C*****************************************************************************
C
C
C
C
C*****************************************************************************
C                                                                            *
C                                                                            *
C   THE VALUE OF N IS RESET TO THE ACTUAL NUMBER OF RECORDS READ AND THE NEW
C   VALUE OF N IS PRINTED OUT.  A WARNING IS PRINTED IF AN INCORRECT VALUE
C   FOR N IS GIVEN FOR THE SECOND DERIVATIVE DATA.
C                                                                            *
9000  N=I-1
      WRITE (6,99)  N
99    FORMAT (' YOUR N WAS TOO BIG N''S NEW VALUE IS',I5,1X,
     C '**BEWATE THAT THIS APPEARS ONLY FOR SS')
```

```
30      CONTINUE
C                                                                       *
C                                                                       *
C***********************************************************************
C
C
C
C
C***********************************************************************
C                                                                       *
C                                                                       *
C    THE NUMERICAL VALUES OF THE INPUT RECORDS ARE COMPUTED
C                                                                       *
        DO 1 I=1,N
        X(I)=X(I)*(10.)**(-ILX(I))
        Y(I)=Y(I)*(10.)**(-ILY(I))
1       CONTINUE
C                                                                       *
C                                                                       *
C***********************************************************************
        RETURN
        END
C
C
C***********************************************************************
C***********************************************************************
C***********************************************************************
```

SUBROUTINE EVENO

If a routine requires argument and function arrays as input, but the given input data has certain anomalies where the argument values are not monotonically increasing, EVENO when called will drop all argument and their corresponding function values from the input arrays that cause the input argument array to be non-monotonically increasing. If several arguments which follow successively are equal, one argument-function-value-pair is generated whose function value equals the average of the function values; e.g., if X is an array of argument values, and Y is an array of function values if

X = 1,1,1,1,2,3,4,2,3,1,5,5,4,6,6

and

Y = 0,1,2,3,4,5,6,7,8,9,10,11,12,13,14

and X and Y are input to EVENO, they will be output as follows:

X = 1,2,3,4,5,6

Y = 3/2,4,5,6,10 1/2, 13 1/2

(referring to the original arrays the pairs with y = 0.1,2,

and 3 are averaged, y = 7,8,9, and 12 are dropped, y = 10 and 11 are averaged, and y = 13 and 14 are averaged).

INPUT PARAMETERS

X - an array of argument values.

Y - an array of corresponding function values.

N - the first N points of X and Y are argument and function values respectively.

OUTPUT PARAMETERS

X - an array of monotonically increasing argument values.

Y - an array of their corresponding function values.

ITC - the first ITC points of X and Y are argument and function values respectively.

```
C*****************************************************************************
C*****************************************************************************
C*****************************************************************************
C
C
      SUBROUTINE EVENO (X,Y,N,ITC)
      DIMENSION X(920),Y(920)
      XMUL=1.0
      ITC=2
      DO 7 I=2,N
C
C
C*****************************************************************************
C                                                                            *
C                                                                            *
C   TEST TO DETERMINE IF TWO SUCCESSIVE ARGUMENT VALUES ARE EQUAL
C                                                                            *
      IF (ABS(X(I)-X(I-1)) .LT. .00001)GO TO 13
C                                                                            *
C                                                                            *
C*****************************************************************************
C
C
      GO TO 18
C
C
C*****************************************************************************
C                                                                            *
C                                                                            *
C   AVERAGE FUNCTION VALUES
C                                                                            *
13          IF  (XMUL  .LT. 1.1)  ITC=ITC-1
      XMUL = XMUL+1.
       Y(ITC)=((XMUL-1.)*Y(I-1)+Y(I))/XMUL
      Y(I)= Y(ITC)
C                                                                            *
```

```
C                                                                       *
C***********************************************************************
C
C
      GO TO 7
18      IF (XMUL .GT.1.0) ITC=ITC+1
      XMUL=1.0
      IF (X(I) .GT. X(I-1)) GO TO 10
19    X(I)=X(I-1)
      GO TO 7
10     X(ITC)=X(I)
        Y(ITC)=Y(I)
      ITC =ITC+1
7     CONTINUE
      ITC=ITC-1
      RETURN
      END
C
C
C***********************************************************************
C***********************************************************************
C***********************************************************************
```

IFIX*

This subroutine was written for a particular experimental investigation. In these experiments it became convenient (as it usually is) to off-set the absolute magnitude of the conductance signal so that a small portion of the curve could be centered on the xy-recorder and measured on a highly magnified scale. Hence, the purpose of the subroutine is to convert the xy-recorder data to its absolute values.

Schematically one could say, we seek the normalized conductance ratio:

$$\frac{FS}{FN} \qquad \frac{R_o + (\text{data point})_s}{R_o + (\text{data point})_n}$$

where "(data point)" values are read into the program and R_o is a constant determined from the dial settings of the xy-recorder and the Doric voltmeter. In a crude way we may also represent the xy-recorder traces as:

* Only the general features of this subroutines will be considered.

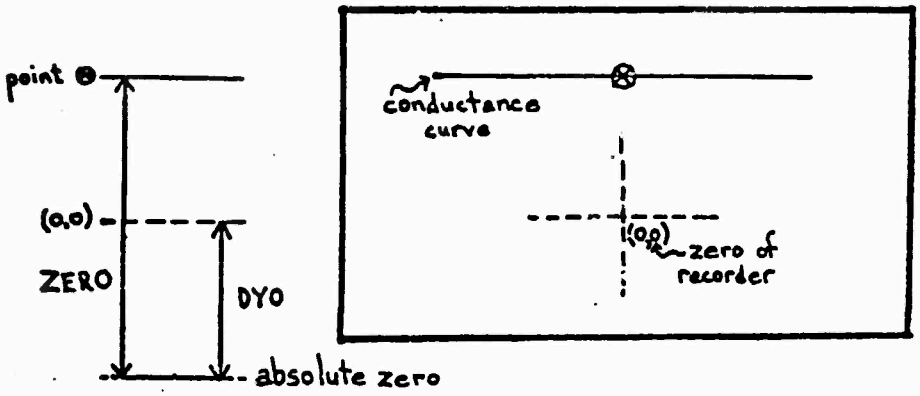
point ⊗
(0,0)
ZERO
DYO
absolute zero
conductance curve
(0,0)
zero of recorder

and

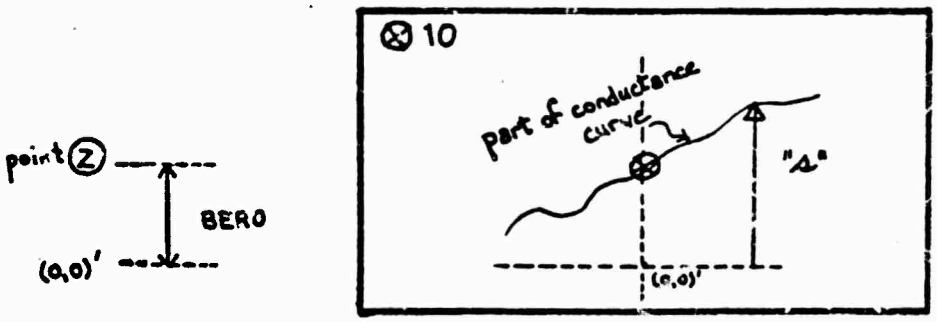
point Z
BERO
(0,0)'
⊗ 10
part of conductance curve
"s"
(0,0)'

Physically, the signal on the xy-recorder as measured from ground is too "flat" to observe fine structure, so the conductance curve is shifted down to a new xy-recorder zero and magnified by a factor M (in this case 10) for sensitivity. With respect to the new axis the point Ⓩ becomes BERO with an amplitude 10 times the original Ⓩ signal on the xy-recorder. Thus, the shift/point from the (0,0) ⟶ (0,0)′ recorder zero would be:

$$A=(ZERO-DYO) - \frac{BERO}{10}$$

This gives an absolute signal magnitude of*

$$S= \frac{10(ZERO-DYO)-BERO}{10} + \frac{1}{10}\, s(I)$$

for any arbitrary point s(I), measured with respect to the recorder zero (0,0).

* All values for this experiment are multiplied by the factor M. Since we desire a ratio of super conducting to normal state conductances, this causes no problem.

```
C*****************************************************************************
C*****************************************************************************
C*****************************************************************************
      SUBROUTINE IFIX1    (IPLT,YSCALE,XSCALE,X1,X2,Y1,Y2,DX1,DX2,DY1,
     C  DY2,ZERO,BERO,X,Y,DXC,DYC,N,INEG)
      DIMENSION X (920), Y (920)
          DIMENSION Z(920)    ,W(920)
       XFCTR =(DX2-DX1)/(X2-X1)
      YFCTR=(DY2-DY1)/(Y2-Y1)
C
C
C*****************************************************************************
C                                                                            *
C                                                                            *
C   THE COORDINATES OF THE INPUT POINTS AS SEEN ON THE X-Y RECORDER ARE
C   COMPUTED.  THE VALUES OF THE COORDINATES ARE EXPRESSED IN INCHES AWAY
C   FROM THE MIDPOINT OF THE RECORDER PLOT.
C                                                                            *
      DO 1 I=1,N
      Y(I)= (Y(I)-DYO)/YFCTR
      X(I)=(            X(I)-DXC)/XFCTR
1      CONTINUE
            WRITE (6,10)(X(I),Y(I),I=1,N)
10    FORMAT ('1 THE FOLLOWING ARE VALUES OF THE POINTS OF THE PLOT IN I
     CNCHES AWAY FROM THE ORIGIN AT CENTER OF THE GRAPH'/
     C    5 (1X,F8.5,2X,F8.5,5X))
      IF (IPLT  .EQ.  0) GO TO 30
      CONTINUE
                                                                            *
                                                                            *
C*****************************************************************************
C
C
C
C
C*****************************************************************************
```

```
C
C                                                                       *
C    THE NUMERICAL VALUES OF V AND DI/DV ARE COMPUTED                   *
       DO 2 I=1,N
       Z(I)=X(I)*XSCALE
           W(I)=Y(I)*YFCTR+DYO-BERO+ (ZERO-DYO)*10
2      CONTINUE
C
C                                                                       *
C***********************************************************************
C
C
C
C
C***********************************************************************
C
C                                                                       *
C    LOAD THE NUMERICAL VALUES OF V AND DI/DV INTO ARRAYS X AND Y RESPECTIVELY
C    IN SUCH A WAY THAT V IS MONOTONICALLY INCREASING
C
       IF (INFG .EQ. 1) GO TO 3                                         *
       IF (INFG .EQ.0) GO TO 4
3      DO 23 I=1,N
           Y(N-I+1)=W(I)
23     X (N-I+1)=-Z(I)
       GO TO 7
4        DO 24 I=1,N
           Y(I)=W(I)
24     X(I)=Z(I)
7       CONTINUE
C
C                                                                       *
C***********************************************************************
C
C
              WRITE (6,44444    )  (X(I),Y(I),I=1,N)
```

```
44444     FORMAT ('1THE ABSOLUTE INPUT VALUES ARE AS FOLLOWS'/
     C    5 (1X,F8.5,2X,F8.5,5X))
      RETURN
      END
C
C
C*****************************************************************************
C*****************************************************************************
C*****************************************************************************
```

SUBROUTINE LINFIT

Subroutine LINFIT finds the values of a function F at an equally spaced interval h. The inputs are (x,y) pairs such that y=f(x). f contains random noise and F is to be a smoothed f. To determine $F(x_0)$ the points in the vicinity of x_0 are least square fitted to either a straight line, P(x), or to a parabola, P(x), and $F(x_0) = P(x_0)$.

INPUT PARAMETERS

H - the values of F(x) are generated at 0,H,2H,...

X - an array of input argument values, this array must be monotonically increasing.

N - only the first N points of arrays X and Y are valid argument and function values respectively.

M - the number of points around x_0 which are used to determine P(x) by fitting. If M is even, M/2 points whose arguments is less than x_0 and M/2 points whose argument is greater than x_0 are used. If M is odd, M/2 - 1/2 points whose argument is less than x_0 and M/2 + 1/2 points whose argument is greater than x_0 are used.

IFLAG - if IFLAG = 1, linear least square fitting is used.
If IFLAG = 2, quadratic least square fitting is used.

MAXA - values of F(x) are generated for values up to (MAXA-1)H. If the greatest input argument, c, is less than (MAXA-1)H, the values of F(x) are generated only for x < c.

OUTPUT PARAMETERS

XT - an array of output arguments, namely 0,H,2H,...

YT - an array of output function values, namely, F(0), F(H),...

MAXO - the index in arrays XT and YT of the first meaningful argument and function value respectively. [F(x) = 0 for all x which are less than the minimum input argument.]

MAXA - the index in arrays XT and YT of the last meaningful argument and value of F(x) respectively.

```
C*****************************************************************************
C*****************************************************************************
C*****************************************************************************
      SUBROUTINE LINFIT(MAXA,N,H,M,X,Y,XT,YT,IFLAG,MAXO)
      DIMENSION X(920),Y(920),XT(920),YT(920)
      DIMENSION A(3,3),B(3)
            DIMENSION V(100),W(100)
      MAXO=0
C
C
C*****************************************************************************
C                                                                            *
C                                                                            *
C    SUBROUTINE LINFIT WORKS AS FOLLOWS:
C    THE VALUES OF FUNCTION F ARE DESIRED AT XINT=I*H WHERE
C    I=1,2,3,...MAXA.  DEPENDING ON THE VALUE OF XINT, ONE OF THE FOLLOWING
C    THINGS IS DONE.
C      IF XINT IS LESS THAN THE MINIMUN INPUT ARGUMENT THEN F(XINT) IS UNDEFINED
C      AND IS ARBITRARILY SET EQUAL TO ZERO.  MAXO IS INCREASED BY ONE.
C      (MAXO IS THE INDEX OF THE FIRST SIGNIFICANT F(XINT) AND IS DETERMINED BY
C      COUNTING THE NUMBER OF TIMES F(XINT) IS ARBITRARILYSET TO ZERO.)
C      IF XINT IS GREATER THAN THE MAXIMUM INPUT ARGUMENT F(XINT) IS UNDEFINED
C      IF SUCH A VALUE FOR XINT IS GENERATED IT MEANS THAT THE INPUT VALUE FOR
C      MAXA WAS TOO BIG, THEREFORE MAXA IS REDEFINED TO EQUAL THE INDEX IN THE
C      OUTPUT ARRAYS, XT AND YT, OF THE LAST DEFINED VALUE OF F(XINT).  EXECUTION
C      OF THE SUBROUTINE TERMINATES.
C      IF XINT FALLS BETWEEN THE MAXIMUM AND MINIMUM INPUT ARGUMENTS THEN
C      F(XINT) IS FOUND BY EITHER QUADRATIC OR LINEAR FITTNG OF THE NEIGHBORING
C      POINTS TO DETERMINE A POLYNOMIAL H AND F(XINT)=H(XINT)
C      FOR SOME VALUES OF XINT LESS THAN THE MAXIMUM INPUT ARGUMENT AND GREATER
C      THAN THE MINIMUM INPUT ARGUMENT THERE MIGHT NOT EXIST K INPUT POINTS
C      WITH ARGUMENT VALUES LESS THAN XINT OR L INPUT POINTS WITH ARGUMENT VALUES
C      GREATER THAN XINT.  IN THE FORMER CASE THE FIRST M INPUT POINTS ARE
C      USED TO DETERMINE H AND IN THE LATTER CASE THE LAST M INPUT POINTS
C      ARE USED TO DETERMINE H.
C
                                                                            *
```

```
      DO 10 I=1,M
      X(I)=X(I)
10    V(I)=Y(I)
      GO TO(20,22),IFLAG
21    CONTINUE
C                                                                       *
C                                                                       *
C***********************************************************************
C
C
C
C
C***********************************************************************
C                                                                       *
C                                                                       *
C   THIS DO LOOP STEPS THE VALUE OF XINT AND COMPUTES F(XINT)
C                                                                       *
      DO 1 I=1,MAXA
      XINT =(I-1)*H
      XT(I)=XINT
C                                                                       *
C                                                                       *
C***********************************************************************
C
C
C
C
C***********************************************************************
C                                                                       *
C                                                                       *
C   TEST IF XINT IS < MINIMUM INPUT ARGUMENT
C                                                                       *
      IF (XINT.LT. X(1)) GO TO 30
C                                                                       *
C                                                                       *
C   TEST IS XINT IS > MAXIMUM INPUT ARGUMENT
```

```
C                                                                       *
      IF (XINT.GT. X(N)) GO TC 90
C                                                                       *
C                                                                       *
C   TEST IF THERE EXISTS K POINTS WHOSE INPUT ARGUMENTS ARE < XINT
C                                                                       *
      IF (XINT .LE. X(K+1)) GO TO(40,41),IFLAG
C                                                                       *
C                                                                       *
C   TEST IF THERE EXISTS L POINTS WHOSE INPUT ARGUMENTS ARE > XINT
C                                                                       *
      IF (XINT .GT. X(N-L   ))GO TO 50
C                                                                       *
C                                                                       *
C   DETERMINE THE NEIGHBORING POINTS OF XINT.
C                                                                       *
      DO 60 J=ITRAC,N
      IF (XINT .GE. X(J) .AND. XINT .LE. X(J+1)) GO TO 70
60    CONTINUE
C                                                                       *
C                                                                       *
C***********************************************************************
C
C
C
C
C***********************************************************************
C                                                                       *
C                                                                       *
C   IF XINT < THE MINIMUM INPUT ARGUMENT THE FOLLOWING IS DONE:
C                                                                       *
30        YT(I)=0.0
      MAXO=MAXC+1
      GO TO 1
C                                                                       *
C                                                                       *
```

```
C*****************************************************************************
C
50      IF (ITE .EQ. 1) GO TO 100
        IF (IFLAG .EQ.2) GO TO 41
C
C*****************************************************************************
C
C                                                                            *
C    IF LINEAR LEAST SQUARE FITTING IS USED F(XINT)=YT(I)                    *
C
40      YT(I)=SL*XT(I)+B1                                                    *
        GO TO 1
C
C                                                                            *
C*****************************************************************************
C
C
C
C
C*****************************************************************************
C
C                                                                            *
C    IF QUADRATIC LEAST SQUARE FITTING IS USED F(XINT)=YT(I)                 *
C
41      YT(I)= AA*XT(I)*XT(I)+BB*XT(I)+CC                                    *
        GO TO 1
C
C                                                                            *
C*****************************************************************************
C
C
C
C
C*****************************************************************************
C
C                                                                            *
```

```
C    W AND V ARE LOADED WITH THE LAST M INPUT POINTS
C                                                                        *
100    DO 200 ID=1,M
       W(M-ID+1)=X(N-ID+1)
200    V(M-ID+1)=Y(N-ID+1)
C                                                                        *
C                                                                        *
C*************************************************************************
C
       ITE=2
       ITE=2
       ISET=2
       GO TO(20,22),IFLAG
70     IB=J
       ITPAC=J
82     CONTINUE
C
C*************************************************************************
C                                                                        *
C                                                                        *
C    W AND V ARE LOADED WITH THE POINTS TO BE LEAST SQUARE FITTED
C                                                                        *
       DO 300 JB=1,M
       W(JB)=X(IB-K+JB)
300    V(JB)=Y(IB-K+JB)
C                                                                        *
C                                                                        *
C*************************************************************************
C
       ISET=2
       GO TO(20,22),IFLAG
1      CONTINUE
       GO TO 500
C
C*************************************************************************
C                                                                        *
```

```
C                                                                       *
C    IF XINT > THE MAXIMUM INPUT ARGUMENT THE FOLLOWING IS DONE:
C                                                                       *
90     MAXA=I-1
       WRITE (6,1000) MAXA
1000   FORMAT (     ' MAXA VALUE WAS TOO HIGH:MAXA= ',I4)
       GO TO 500
C                                                                       *
C                                                                       *
C***********************************************************************
C
C
C
C
C***********************************************************************
C                                                                       *
C                                                                       *
C    IF LINEAR LEAST SQUARE FITTING IS USED H(X)=SL*X+B; HERE SL AND B ARE
C    DETERMINED
C    FOR MATHEMATICAL BACKGROUND SEE HILDERBRAND, F.P., INTRODUCTION TO
C    NUMERICAL ANALYSIS, MC GRAW HILL, NEWYORK/TORONTO/LONDON, 1956, PP. 258-311.
C                                                                       *
20     TX=0.0
       TY=0.0
       TX2=0.0
       TXY=0.0
       DO 700 IP=1,M
       TX=TX+W(IP)
       TY=TY+V(IP)
       TXY= TXY+W(IP)*V(IP)
700    TX2=TX2+ W(IP)*W(IP)
       SL=(M*TXY-TX*TY)/(M*TX2-TX*TX)
       B1=(TY-SL*TX)/M
       GO TO (21,40),ISET
C
C
                                                                        *
                                                                        *
```

```
C*****************************************************************************
C
C
C
C
C*****************************************************************************
C                                                                            *
C                                                                            *
C    IF QUADRATIC LEAST SQUARE FITTING IS USED H(X)=AA*X**2+BB*X+CC; HERE
C    AA, BB, AND CC ARE DETERMINED
C                                                                            *
22      TYX2=0.0
      TYX1=0.0
      TY=0.0
      TX4=0.0
      TX3=0.0
      TX2=0.0
      TX=0.0
      DO 56 IY=1,M
      TYX2 =TYX2+ V(IY)*W(IY)*W(IY)
      TYX1 =TYX1+ W(IY)*V(IY)
      TY=TY+V(IY)
      TX4 = TX4+W(IY)*W(IY)*W(IY)*W(IY)
      TX3= TX3+ W(IY)*W(IY)*W(IY)
      TX2=TX2+W(IY)*W(IY)
      TX=TX+W(IY)
56     CONTINUE
      A(1,1)=TX4
      A(2,1)= TX3
      A(3,1)=TX2
      A(1,2)=TX3
      A(2,2)=TX2
      A(3,2)=TX
      A(1,3)=TX2
      A(2,3)=TX
      A(3,3)=M
```

```
      B(1)=TYX2
      B(2)=TYX1
      B(3)=TY
      CALL THREE (A,B, AA,BB,CC)
      GO TO (21,41),ISET
C                                                                       *
C                                                                       *
C***********************************************************************
500       CONTINUE
      WRITE (6,2000) M, (XT(I),YT(I),I=1,MAXA    )
2000  FORMAT (     'OTHE FOLLOWING IS THE LEAST SQUARE FITTED DATA'/
     C ' USING',1X,I2,'POINTS AROUNG THE GIVEN POINT'   /
     C     5 (1X,F8.5,2X,F8.5,5X))
      MAXO=MAXO+1
      WRITE (6,23123)    MAXO
23123 FORMAT   (' MAXO =',I5)
      RETURN
      END
C
C
C***********************************************************************
C***********************************************************************
C***********************************************************************
```

SUBROUTINE INTER

Subroutine INTER finds the values of a function F at an equally spaced interval h. The inputs are (x,y) pairs such that $y = F(x)$. To determine $F(x_0)$ the n points in the vicinity of x_0 are fitted to a n-1 degree polynomial, P(x), and $F(x_0) = P(x_0)$.

INPUT PARAMETERS

M,H,X,Y,N, and MAXA are the same as in LINFIT. A and B are dynamic storage arrays which are used in subprograms but are not declared in the input lists.

OUTPUT PARAMETERS

XT, YT, MAXO, and MAXA are the same as in LINFIT.

```
C*****************************************************************************
C*****************************************************************************
C*****************************************************************************
      SUBROUTINE INTER (X,Y,XT,YT,N,MAXA,H,M,A,B,MAXO)
      DIMENSION X(920),Y(920),XT(920),YT(920)
      DIMENSION A(M ,M ),B(M )
C
C
C*****************************************************************************
C                                                                            *
C                                                                            *
C   SUBROUTINE INTER WORKS AS FOLLOWS:
C   THE VALUES OF FUNCTION F ARE DESIRED AT XINT=I*H WHERE
C   I=1,2,3,...MAXA.  DEPENDING ON THE VALUE OF XINT, ONE OF THE FOLLOWING
C   THINGS IS DONE.
C     IF XINT IS LESS THAN THE MINIMUN INPUT ARGUMENT THEN F(XINT) IS UNDEFINED
C     AND IS ARBITRARILY SET EQUAL TO ZERO.  MAXO IS INCREASED BY ONE.
C     (MAXO IS THE INDEX OF THE FIRST SIGNIFICANT F(XINT) AND IS DETERMINED BY
C     COUNTING THE NUMBER OF TIMES F(XINT) IS ARBITRARILYSET TO ZERO.)
C     IF XINT IS GREATER THAN THE MAXIMUM INPUT ARGUMENT F(XINT) IS UNDEFINED
C     IF SUCH A VALUE FOR XINT IS GENERATED IT MEANS THAT THE INPUT VALUE FOR
C     MAXA WAS TOO BIG, THEREFORE MAXA IS REDEFINED TO EQUAL THE INDEX IN THE
C     OUTPUT ARRAYS, XT AND YT, OF THE LAST DEFINED VALUE OF F(XINT).  EXECUTION
C     OF THE SUBROUTINE TERMINATES.
C     IF XINT FALLS BETWEEN THE MAXIMUM AND MINIMUM INPUT ARGUMENTS THEN
C     F(XINT) IS FOUND BY DETERMINING A M DEGREE POLYNOMIAL H FROM M
C     NEIGHBORING INPUT POINTS AND F(XINT)=H(XINT)
C     FOR SOME VALUES OF XINT LESS THAN THE MAXIMUM INPUT ARGUMENT AND GREATER
C     THAN THE MINIMUM INPUT ARGUMENT THERE MIGHT NOT EXIST K INPUT POINTS
C     WITH ARGUMENT VALUES LESS THAN XINT OR L INPUT POINTS WITH ARGUMENT VALUES
C     GREATER THAN XINT.  IN THE FORMER CASE THE FIRST M INPUT POINTS ARE
C     USED TO DETERMINE H AND IN THE LATTER CASE THE LAST M INPUT POINTS
C     ARE USED TO DETERMINE H.
C     IF THERE SHOULD EXIST AN INPUT ARGUMENT VALUE, XX, SUCH THAT XX=XINT
C     THE F(XINT) IS SET EQUAL TO THE INPUT FUNCTION VALUE FOR THAT ARGUMENT
C
```

```
C                                                                       *
C***********************************************************************
C
C
      MAXO=0
      WRITE (6,424) M
424    FORMAT ('1THIS PROGRAM INTEPPOLATES USING AN ',I2,1X,'POLYNOMAL')
      ITRAC=2
      K1=M/2
      L1=M-K1
C
C
C***********************************************************************
C                                                                       *
C                                                                       *
C   THIS DO LOOP STEPS THE VALUE OF XINT AND COMPUTES F(XINT)
C                                                                       *
      DO 10011 I=1,MAXA
      XINT= (I-1)*H
      XT(I)=XINT
C                                                                       *
C                                                                       *
C***********************************************************************
C
C
C
C
C***********************************************************************
C                                                                       *
C                                                                       *
C   TEST IF XINT IS < MINIMUM INPUT ARGUMENT
C                                                                       *
      IF (XINT .LT. X(1)) GO TO 13
C                                                                       *
C                                                                       *
C***********************************************************************
```

```
C
C
C
C
C*****************************************************************************
C                                                                            *
C                                                                            *
C   TEST IF XINT IS > MAXIMUM INPUT ARGUMENT
C                                                                            *
      IF (XINT  .GT. X(N)) GO TO 3833
C                                                                            *
C                                                                            *
C*****************************************************************************
C
C
C
C
C*****************************************************************************
C                                                                            *
C                                                                            *
      DO 3891 J=ITRAC,N
C                                                                            *
C                                                                            *
C   TEST TO SEE IF THERE EXISTS AN INPUT ARGUMENT VALUE, XX, SUCH THAT XINT=XX
C                                                                            *
      IF (ABS(XINT-X(J-1)) .LT. .00001) GO TO 191
C                                                                            *
C                                                                            *
C   DETERMINE THE NEIGHBORING POINTS OF XINT.
C                                                                            *
      IF (XINT .LT.(X(J)-.00001) )  GO TO 700
C                                                                            *
C                                                                            *
3891  CONTINUE
C                                                                            *
C                                                                            *
```

```
C*****************************************************************************
C
C
C
C
C*****************************************************************************
C                                                                            *
C                                                                            *
C    IF THERE EXISTS AN INPUT ARGUMENT VALUE, XX, SUCH THAT XX=XINT
C    THE F(XINT) IS SET EQUAL TO THE INPUT FUNCTION VALUE FOR THAT ARGUMENT
C                                                                            *
191    YT(I)=Y(J-1)
       ITRAC=J
       GO TO 10011
C                                                                            *
C                                                                            *
C*****************************************************************************
C
C
C
C
C*****************************************************************************
C                                                                            *
C                                                                            *
C    IF XINT < THE MINIMUM INPUT ARGUMENT THE FOLLOWING IS DONE:
C                                                                            *
13     YT(I)=0.0
       MAXO=MAXO+1
       GO TO 10011
C                                                                            *
C                                                                            *
C*****************************************************************************
C
C
C
C
```

```
C*****************************************************************************
C                                                                            *
C                                                                            *
C   TEST IF THERE EXISTS K POINTS WHOSE INPUT ARGUMENTS ARE < XINT
C                                                                            *
700    CONTINUE
       IF (XINT .LT. X(K1))GO TO 87878
C                                                                            *
C                                                                            *
C*****************************************************************************
C
C
C
C
C*****************************************************************************
C                                                                            *
C                                                                            *
C   TEST IF THERE EXISTS L POINTS WHOSE INPUT ARGUMENTS ARE > XINT
C                                                                            *
       IF (XINT .GT. X(N-L1)) GO TO 22222
C                                                                            *
C                                                                            *
C*****************************************************************************
C
C
C
C
C*****************************************************************************
C                                                                            *
C                                                                            *
C   SET UP AND SOLVE SIMULTANEOUS EQUATIONS TO DETERMINE H
C   IF M=2 THIS SECTION IS SKIPED AND F(XINT) IS COMPUTED DIRECTLY
C                                                                            *
       II=J
       GO TO 38
87878  II=K1+1
```

```
      GC TO 38
22222 II=N-M+1+K1
38    IF (M .FQ. 2)GO TO 2
      DO 222 K=1,M
      B(K)=Y(II-K'-1+K)
      DC 222 L=1,M
222   A(K,L)=X(II-K1-1  +K)          ** (M-L)
      IF (M .EQ. 3) CALL THREE (A,B,B(1),B(2),B(3)    )
      IF (M .NE. 3) CALL SIMQ (A,B,      M,KS)
C                                                                       *
C                                                                       *
C***********************************************************************
C
C
C
C
C***********************************************************************
C                                                                       *
C                                                                       *
C   F(XINT)=YT(I)
C                                                                       *
      YT(I)=0.0
      DO 99 IC=1,M
99    YT(I)=B(M-IC+1)*XINT**(IC-1)+YT(I)
      GC TO 1CC11
C                                                                       *
C                                                                       *
C***********************************************************************
C
C
C
C
C***********************************************************************
C                                                                       *
C                                                                       *
C   IF M=2 THE FOLLOWING FORMULA IS USED TO COMPUTE F(XINT)
```

```
C
2       YT(I)=((Y(J-1)-Y(J))/(X(J-1)-X(J)))*(XINT-X(J-1))        +Y(J-1)
C                                                                                  *
C                                                                                  *
C*****************************************************************************
C
C
10011  CONTINUE
       GO TO 888
C
C
C*****************************************************************************
C
C                                                                                  *
C    IF XINT > THE MAXIMUM INPUT ARGUMENT THE FOLLOWING IS DONE:                   *
C
3883   WRITE (6,3113)                                                              *
3113      FORMAT (' THE INPUT DATA DOESNT GO THAT HIGH  ')
       MAXA =I-1
C
C                                                                                  *
C*****************************************************************************
C
C
888       CONTINUE
       WRITE (6,224)  MAXA, (XT(I),YT(I),I=1,MAXA)
224    FORMAT (' MAXA=',I5/      '     INTERPOLATED DATA IS AS FOLLOWS'/
     C     5 (1X,F8.5,2X,F8.5,5X))
       MAXO=MAXO+1
       WRITE (6,23123)   MAXO
23123  FORMAT   (' MAXO =',I5)
       RETURN
       END
C*****************************************************************************
C*****************************************************************************
C*****************************************************************************
```

SUBROUTINE THREE

Subroutine THREE solves a system of simultaneous linear equations by computing the solution in terms of the coefficients of the variables and the constant terms in the equations.

INPUT PARAMETERS

If the equations are of the following form

$$a_{11}x + a_{12}y + a_{13}z = b_1$$

$$a_{21}x + a_{22}y + a_{23}z = b_2$$

$$a_{31}x + a_{32}y + a_{33}z = b_3.$$

A is the array of the input coefficients of the variables.

B is an array such that $B(1) = b_1$, $B(2) = b_2$, $B(3) = b_3$.

OUTPUT PARAMETERS

X - the value of x.

Y - the value of y.

Z - the value of z.

```
C*****************************************************************************
C*****************************************************************************
C*****************************************************************************
C
C
      SUBROUTINE THREE (A,B,X,Y,Z)
      DIMENSION A(3,3),B(3)
       C=A(1,1)*A(2,2)*A(3,3)+A(2,1)*A(3,2)*A(1,3)+A(3,1)*A(1,2)*A(2,3)
     1 -A(1,3)*A(2,2)*A(3,1)-A(2,3)*A(3,2)*A(1,1)-A(3,3)*A(1,2)*A(2,1)
       CA=B(1)*A(2,2)*A(3,3)+B(2)*A(3,2)*A(1,3)+B(3)*A(1,2)*A(2,3)
     1 -A(1,3)*A(2,2)*B(3)-A(2,3)*A(3,2)*B(1)-A(3,3)*A(1,2)*B(2)
       CB=A(1,1)*B(2)*A(3,3)+A(2,1)*B(3)*A(1,3)+A(3,1)*B(1)*A(2,3)
     1 -A(1,3)*B(2)*A(3,1)-A(2,3)*B(3)*A(1,1)-A(3,3)*B(1)*A(2,1)
       CC=A(1,1)*A(2,2)*B(3)+A(2,1)*A(3,2)*B(1)+A(3,1)*A(1,2)*B(2)-
     -B(1)*A(2,2)*A(3,1)-B(2)*A(3,2)*A(1,1)-B(3)*A(1,2)*A(2,1)
      X=CA/C
      Y=CB/C
      Z=CC/C
      RETURN
      END
C
C
C*****************************************************************************
C*****************************************************************************
C*****************************************************************************
```

195<

SUBROUTINE FBCS*

The BCS theory predicts that the tunneling current for two weak-coupling superconductors is:

$$I_{SS} = D \int_{\Delta_{01}}^{V-\Delta_{02}} \frac{E}{\sqrt{E^2-\Delta_{01}^2}} \frac{E-eV}{\sqrt{(E-eV)^2-\Delta_{02}^2}} \, dE \qquad (1)$$

Therefore, the normalized tunneling conductance is

$$\frac{\left(\frac{dI}{dV}\right)_{SS}}{\left(\frac{dI}{dV}\right)_{NN}} = \frac{d}{dV} \int_{\Delta_{01}}^{V-\Delta_{02}} \frac{E}{\sqrt{E^2-\Delta_{01}^2}} \frac{E-eV}{\sqrt{(E-eV)^2-\Delta_{02}^2}} \, dE \qquad (2)$$

Now in general,

$$\frac{d}{dx} \int_{a(x)}^{b(x)} f(x)dx = f(x) \frac{d}{dx} b(x) \Big|_{x=b(x)} - f(x) \frac{d}{dx} a(x) \Big|_{x=a(x)}$$

$$+ \int_{a(x)}^{b(x)} \frac{d}{dx} f(x)dx \qquad (3)$$

* This section was kindly provided by J. Bostock.

Because of the singularities in the two densities of states in Eqn.(2), the term analogous to the first two terms in Eqn.(3) will be non-analytic. Hence, the general form of Eqn.(3) applied to Eqn.(1) is not suitable for programming. To avoid this difficulty a different form of Eqn.(1) must be used. The current I_{SS} can also be written as

$$\int_{V-\Delta_{01}}^{\Delta_{02}} \frac{E}{\sqrt{E^2-\Delta_{02}^2}} \frac{E-eV}{\sqrt{(E-eV)^2-\Delta_{01}^2}} \, dE \qquad (4)$$

This is most easily seen by writing

$$I_{SS} = \int_{\Delta_{01}}^{V-\Delta_{02}} \mathcal{d}(E, V, \Delta_{01}, \Delta_{02}) \, dE = \int_{V-\Delta_{01}}^{\Delta_{02}} \mathcal{d}'(E, V, \Delta_{01}, \Delta_{02}) \, dE \qquad (5)$$

and evaluating the integrands $\mathcal{d}$ and $\mathcal{d}'$ at equivalent points in their ranges of integration, that is evaluating $\mathcal{d}$ at the lower limit, Δ_{01}, then at $\Delta_{01} + H, \ldots, (V - \Delta_{02}) - H, \approx (V - \Delta_{02})$; and $\mathcal{d}'$ at $\approx (V - \Delta_{01})$, $(V - \Delta_{01}) + H, \ldots, \Delta_{02} - H, \approx \Delta_{02}$. It is easily seen then that:

$$\lim_{E \to UL} \left\{ \mathcal{d}\,(\text{upper limit}) = \mathcal{d}'\,(\text{upper limit}) \right\}$$

$$\mathcal{d}\,(\text{mid-point}) = \mathcal{d}'\,(\text{mid-point})$$

$$\lim_{LL \leftarrow E} \left\{ \mathcal{d}\,(\text{lower limit}) = \mathcal{d}'\,(\text{lower limit}) \right\}$$

for example; and this is true for all "H-intervals".

Thus,

$$I_{SS} = \int_{\Delta_{01}}^{V1} \mathcal{J}(E,V,\Delta_{01},\Delta_{02})dE + \int_{V2}^{\Delta_{02}} \mathcal{J}'(E,V,\Delta_{01},\Delta_{02})dE \qquad (6)$$

where V1 is the mid-point of the first integral:

$$V1 = \Delta_0 + \tfrac{1}{2}([V-\Delta_{02}]-\Delta_{01}) = (V-\Delta_{02}) - \tfrac{1}{2}([V-\Delta_{02}]-\Delta_{01})$$

and V2 is the mid-point of the second integral:

$$V2 = (V-\Delta_{01}) + \tfrac{1}{2}(\Delta_{02}-[V-\Delta_{01}]) = \Delta_{02} - \tfrac{1}{2}(\Delta_{02}-[V-\Delta_{01}]) .$$

Thus, the analogous equation to Eqn.(3) is the derivative of the Eqn.(6):

$$\mathcal{J}\,\frac{d}{dV}V1\Big|_{E=V1} - \mathcal{J}'\,\frac{d}{dV}V2\Big|_{E=V2}$$
$$+\int_{\Delta_{01}}^{V1}\left(\frac{d}{dV}\mathcal{J}\right)dE + \int_{V2}^{\Delta_{02}}\left(\frac{d}{dV}\mathcal{J}'\right)dE \qquad (7)$$

The final form of Eqn.(7) then becomes (realizing that $\frac{EdE}{\sqrt{E^2-a^2}} = d\sqrt{E^2-a^2}$):

$$\frac{\left(\frac{dI}{dV}\right)_{SS}}{\left(\frac{dI}{dV}\right)_{NN}} = \frac{1}{\sqrt{1-\left(\frac{\Delta_{01}}{V1}\right)^2}} \times \frac{1}{\sqrt{1-\left(\frac{\Delta_{02}}{V2}\right)^2}}$$

$$-\Delta_{02}^2\int_{\Delta_{01}}^{V1}\frac{d\sqrt{E^2-\Delta_{01}^2}}{[(E-V)^2-\Delta_{02}^2]^{3/2}}$$

$$-\Delta_{01}^2\int_{\Delta_{02}}^{V2}\frac{d\sqrt{E^2-\Delta_{02}^2}}{[(E-V)^2-\Delta_{01}^2]^{3/2}}$$

where $V1 = 1/2\ (V - \Delta_{02} + \Delta_{01})$

and $V2 = 1/2\ (V - \Delta_{01} + \Delta_{02})$.

This function was not that used in the original inversion program. The accuracy with which it evaluates the normalized conductance can, however, be seen by using it to calculate the BCS density of states for a normal-superconductor tunnel junction. That is, the calculated values from this function should be compared, in this case, to ($\Delta_{02} = 0$):

$$\frac{E}{\sqrt{E^2-\Delta_{01}^2}}$$

The comparison shows that FBCS is correct to 5 significant figures.

```
C*****************************************************************************
C*****************************************************************************
C*****************************************************************************
      FUNCTICN FBCS(D1,D2,V,N)
      DIMENSICN D(3)
      D(1)=D1
      D(2)=D2
      D(3)=D1
      V1=(V+D1-D2)/2.
      V2=(V+D2-D1)/2.
      X=(1./SQRT(1.-(D1/V1)**2))*(1./SQRT(1.-(D2/V2)**2))
      AN=N
      H=.5*(V-D1-D2)/AN
      AMP=1.
      JMAX=2
      IF(ABS (D1-D2)/(D1+D2)-.001) 1,1,2
1     AMP=2.
      JMAX=1
2     DC 3 J=1,JMAX
      G1=D(J)
      G2=D(J+1)
      BC=0.0
      DC 3 I=1,N
      AI=I
      EH=G1+AI*H
      EM=EH-.5*H
      BN=SQRT (EH**2-G1**2)
      X=X-AMP*G2**2*(BN-BO)*((V-EM)**2-G2**2)**(-1.5)
3     BC=BN
      FBCS=X
      RETURN
      END
C
C*****************************************************************************
C*****************************************************************************
C*****************************************************************************
```

```
C***********************************************************************
C***********************************************************************
C***********************************************************************
C
C
C    SUBROUTINE SIMQ IS THE IBM SSP ROUTINE FOR SOVING SIMULTANEOUS EQUATIONS
C
C                                                                      SIMQ  10
C     ..................................................................SIMQ  20
C                                                                      SIMQ  30
C        SUBROUTINE SIMQ                                               SIMQ  40
C                                                                      SIMQ  50
C        PURPOSE                                                       SIMQ  60
C           OBTAIN SOLUTION OF A SET OF SIMULTANEOUS LINEAR EQUATIONS, SIMQ  70
C           AX=B                                                       SIMQ  80
C                                                                      SIMQ  90
C        USAGE                                                         SIMQ 100
C           CALL SIMQ(A,B,N,KS)                                        SIMQ 110
C                                                                      SIMQ 120
C        DESCRIPTION OF PARAMETERS                                     SIMQ 130
C           A - MATRIX OF COEFFICIENTS STORED COLUMNWISE.  THESE ARE   SIMQ 140
C               DESTROYED IN THE COMPUTATION.  THE SIZE OF MATRIX A IS SIMQ 150
C               N BY N                                                 SIMQ 160
C           B - VECTOR OF ORIGINAL CONSTANTS (LENGTH N). THESE ARE     SIMQ 170
C               REPLACED BY FINAL SOLUTION VALUES, VECTOR X.           SIMQ 180
C           N - NUMBER OF EQUATIONS AND VARIABLES. N MUST BE .GT. ONE. SIMQ 190
C           KS - OUTPUT DIGIT                                          SIMQ 200
C                0 FOR A NORMAL SOLUTION                               SIMQ 210
C                1 FOR A SINGULAR SET OF EQUATIONS                     SIMQ 220
C                                                                      SIMQ 230
C        REMARKS                                                       SIMQ 240
C           MATRIX A MUST BE GENERAL.                                  SIMQ 250
C           IF MATRIX IS SINGULAR , SOLUTION VALUES ARE MEANINGLESS.   SIMQ 260
C           AN ALTERNATIVE SOLUTION MAY BE OBTAINED BY USING MATRIX    SIMQ 270
C           INVERSION (MINV) AND MATRIX PRODUCT (GMPRD)                SIMQ 280
C                                                                      SIMQ 290
```

```
C        SUBROUTINES AND FUNCTION SUBPROGRAMS REQUIRED                  SIMQ 300
C           NONE                                                        SIMQ 310
C                                                                       SIMQ 320
C        METHOD                                                         SIMQ 330
C           METHOD OF SOLUTION IS BY ELIMINATION USING LARGEST PIVOTAL  SIMQ 340
C           DIVISOR. EACH STAGE OF ELIMINATION CONSISTS OF INTERCHANGINGSIMQ 350
C           ROWS WHEN NECESSARY TO AVOID DIVISION BY ZERO OR SMALL      SIMQ 360
C           ELEMENTS.                                                   SIMQ 370
C           THE FORWARD SOLUTION TO OBTAIN VARIABLE N IS DONE IN        SIMQ 380
C           N STAGES. THE BACK SOLUTION FOR THE OTHER VARIABLES IS      SIMQ 390
C           CALCULATED BY SUCCESSIVE SUBSTITUTIONS. FINAL SOLUTION      SIMQ 400
C           VALUES ARE DEVELOPED IN VECTOR B, WITH VARIABLE 1 IN B(1),  SIMQ 410
C           VARIABLE 2 IN B(2),........, VARIABLE N IN B(N).            SIMQ 420
C           IF NO PIVOT CAN BE FOUND EXCEEDING A TOLERANCE OF 0.0,      SIMQ 430
C           THE MATRIX IS CONSIDERED SINGULAR AND KS IS SET TO 1. THIS  SIMQ 440
C           TOLERANCE CAN BE MODIFIED BY REPLACING THE FIRST STATEMENT. SIMQ 450
C                                                                       SIMQ 460
C     ..................................... ......................SIMQ 470
C                                                                       SIMQ 480
      SUBROUTINE SIMQ(A,B,N,KS)                                         SIMQ 490
      DIMENSION A(1),B(1)                                               SIMQ 500
C                                                                       SIMQ 510
C        FORWARD SOLUTION                                               SIMQ 520
C                                                                       SIMQ 530
      TOL=0.0                                                           SIMQ 540
      KS=0                                                              SIMQ 550
      JJ=-N                                                             SIMQ 560
      DO 65 J=1,N                                                       SIMQ 570
      JY=J+1                                                            SIMQ 580
      JJ=JJ+N+1                                                         SIMQ 590
      BIGA=0                                                            SIMQ 600
      IT=JJ-J                                                           SIMQ 610
      DO 30 I=J,N                                                       SIMQ 620
C                                                                       SIMQ 630
C        SEARCH FOR MAXIMUM COEFFICIENT IN COLUMN                       SIMQ 640
C                                                                       SIMQ 650
```

```
      IJ=IT+I                                                           SIMQ 660
      IF(ABS(BIGA)-ABS(A(IJ))) 20,30,30                                 SIMQ 670
   20 BIGA=A(IJ)                                                        SIMQ 680
      IMAX=I                                                            SIMQ 690
   30 CONTINUE                                                          SIMQ 700
C                                                                       SIMQ 710
C        TEST FOR PIVOT LESS THAN TOLERANCE (SINGULAR MATRIX)           SIMQ 720
C                                                                       SIMQ 730
      IF(ABS(BIGA)-TOL) 35,35,40                                        SIMQ 740
   35 KS=1                                                              SIMQ 750
      RETURN                                                            SIMQ 760
C                                                                       SIMQ 770
C        INTERCHANGE ROWS IF NECESSARY                                  SIMQ 780
C                                                                       SIMQ 790
   40 I1=J+N*(J-2)                                                      SIMQ 800
      IT=IMAX-J                                                         SIMQ 810
      DO 50 K=J,N                                                       SIMQ 820
      I1=I1+N                                                           SIMQ 830
      I2=I1+IT                                                          SIMQ 840
      SAVE=A(I1)                                                        SIMQ 850
      A(I1)=A(I2)                                                       SIMQ 860
      A(I2)=SAVE                                                        SIMQ 870
C                                                                       SIMQ 880
C        DIVIDE EQUATION BY LEADING COEFFICIENT                         SIMQ 890
C                                                                       SIMQ 900
   50 A(I1)=A(I1)/BIGA                                                  SIMQ 910
      SAVE=B(IMAX)                                                      SIMQ 920
      B(IMAX)=B(J)                                                      SIMQ 930
      B(J)=SAVE/BIGA                                                    SIMQ 940
C                                                                       SIMQ 950
C        ELIMINATE NEXT VARIABLE                                        SIMQ 960
C                                                                       SIMQ 970
      IF(J-N) 55,70,55                                                  SIMQ 980
   55 IQS=N*(J-1)                                                       SIMQ 990
      DO 65 IX=JY,N                                                     SIMQ1000
      IXJ=IQS+IX                                                        SIMQ1010
```

```
      IT=J-IX                                                           SIMQ1020
      DO 60 JX=JY,N                                                     SIMQ1030
      IXJX=N*(JX-1)+IX                                                  SIMQ1040
      JJX=IXJX+IT                                                       SIMQ1050
   60 A(IXJX)=A(IXJX)-(A(IXJ)*A(JJX))                                   SIMQ1060
   65 B(IX)=B(IX)-(B(J)*A(IXJ))                                         SIMQ1070
C                                                                       SIMQ1080
C        BACK SOLUTION                                                  SIMQ1090
C                                                                       SIMQ1100
   70 NY=N-1                                                            SIMQ1110
      IT=N*N                                                            SIMQ1120
      DO 80 J=1,NY                                                      SIMQ1130
      IA=IT-J                                                           SIMQ1140
      IB=N-J                                                            SIMQ1150
      IC=N                                                              SIMQ1160
      DO 80 K=1,J                                                       SIMQ1170
      B(IB)=B(IB)-A(IA)*B(IC)                                           SIMQ1180
      IA=IA-N                                                           SIMQ1190
   80 IC=IC-1                                                           SIMQ1200
      RETURN                                                            SIMQ1210
      END                                                               SIMQ1220
$ENTRY
C*****************************************************************************
C*****************************************************************************
C*****************************************************************************
```

STAGE II

Eqn.(11) gives the expression for the normalized first derivative of a tunnel junction assuming that both metals of the junction have BCS NDS's. If the metals don't have BCS NDS's the analysis of Chapter I in deriving Eqn.(11) still applies and

$$\frac{\left(\frac{dI}{dV}\right)_S}{\left(\frac{dI}{dV}\right)_N} = C(V) = \frac{d}{dV}\int_{\Delta_{01}}^{V-\Delta_{02}} D_1(E)\, D_2(V-E)\, dE$$

where D_1 is the NDS of one electrode, D_2 the NDS of the other, and C the experimental normalized first derivative. Δ_{01} and Δ_{02} are the BCS energy gap values of the respective metals. D_2, Δ_{01}, Δ_{02}, and C are assumed to be known so that STAGE II solves for D_1.

INPUT PARAMETERS

TITLE	same as in STAGE I
GAP1	Δ_{01}
GAP2	Δ_{02}
H	the interval at which values of C and D_2 are known and at which the values of D_1 are desired.

The following 6 integer variables are indexing parameters.

IEXPF (IEXPF)H + GAP1 + GAP2 is the first value of V for which C is known. For V < (IEXPF)H + GAP1 + GAP2 C is assumed to be equal to

$$\frac{d}{dV}\int_{\Delta_{01}}^{V-\Delta_{02}} \frac{E}{\sqrt{E^2-\Delta_{01}^2}}\,\frac{(V-E)}{\sqrt{(V-E)^2-\Delta_{02}^2}}\,dE$$

IEXPL (IEXPL)H + GAP1 + GAP2 is the last value of V for which C is known.

IGIVF (IGIVF-1)H + GAP2 is the first value of ω for which D_2 is known. For E < (IEXPF)H + GAP2 D_2 is assumed to be equal to

$$\frac{E}{\sqrt{E^2-\Delta_{02}^2}}$$

IGIVL (IGIVL-1)H + GAP2 is the last value for which D_2 is known.

LF (LF)H + GAP1 is the first value of V at which D_1 is desired. For E < (LF)H + GAP1

$$\frac{E}{\sqrt{E^2-\Delta_{01}^2}}$$

LL	(LL)H + GAP1 is the last value of V at which D_2 is desired.
EXP	C in σ form; namely, divided by the BCS predicted values and decreased by one.
GIVEN	D_1 in σ form.

INPUT FORMATS

INPUT	FORMAT
TITLE	20A4

The elements of the INPUT NAMELIST are LF,LL,IEXPF, IEXPL, IGIVF, and IGIVL.

GAP1, GAP2,H	3(10X,F10.5)
GIVEN(I), I=1, IGIVL	7F10.6
EXP(I), I=1, IEXPL	7F10.6

OUTPUT PARAMETERS

TITLE, NAMELIST INPUT, GAP1, GAP2, and H are the same as their definition in the input list.

EXP

$$\frac{d}{dV}\int_{\Delta_{01}}^{V-\Delta_{02}} \frac{E}{\sqrt{E^2-\Delta_{01}^2}}\,\frac{V-E}{\sqrt{(V-E)^2-\Delta_{02}^2}}\,dE$$

the input from STAGE I, the first time EXP is printed out.

GIVEN

$$\frac{E}{\sqrt{E^2 - \Delta_{02}^2}}$$

the BCS density of states, the first time GIVEN is printed out.

UNKWN

$$\frac{E}{\sqrt{E^2 - \Delta_{01}^2}}$$

the first time UNKWN is printed out.

ERR is the change in value for the equivalent BCS density of states in the interval H.

EXP the convoluted input in σ form.

GIVEN the values of D_2 in σ form.

UNKWN the values of D_1 which are assumed equal to the BCS predicted values

UNKWN the values of D_1.

UNKWN the values of D_1 in σ form.

FUNCTIONS

DINT(GAP,H) = $$\int_{GAP}^{GAP+H} \frac{E}{\sqrt{E^2-GAP^2}}\, dE$$

SQ(X,A) = $$\int \frac{E^2}{\sqrt{E^2-A^2}}\, dE,$$

END = $$\int_{H}^{GAP2+H} \frac{E^2}{\sqrt{E^2-GAP2^2}}\, dE$$

ENC = $$\int_{H}^{GAP1+H} \frac{E^2}{\sqrt{E^2+GAP1^2}}\, dE$$

```
C*****************************************************************************
C*****************************************************************************
C*****************************************************************************
C
C
      IMPLICIT REAL*8 (A,B,C,D,E,F,G,H,O,P,Q,R,S,T,U,V,W,X,Y,Z)
        DIMENSION EXP(300),GIVEN(300),UNKWN(300),EI(300),ZMUL(300),
     C   SINT(300) ,TITLE(20)
            DIMENSION E(300),FRR(300)
          EQUIVALENCE    (E(1),EI(1))
        NAMELIST/INPUT/LF,LL,IEXPF,IEXPL,IGIVF,IGIVL
          SQRT(X)=DSQRT(X)
        DINT (GAP,H) = DSQRT ((GAP+H)**2-GAP**2)
         READ (5,37) TITLE
            WRITE (6,37) TITLE
        READ (5,INPUT)
        WRITE (6,INPUT)
        READ (5,3) GAP1,GAP2,H
3       FORMAT (3(10X,F10.5))
        WRITE (6,7) H,GAP1,GAP2
7       FORMAT (' H=',F6.3,' GAP1=',F6.3,' GAP2=',F6.3)
         HH= GAP2+H
           ENC= SQ(HH,GAP2)-SQ(GAP2,GAP2)
        HHHH= GAP1+H
          ENC=SQ(HHHH,GAP1)-SQ(GAP1,GAP1)
        GRAL = DINT (GAP2,H)
        TEGRAL=DINT(GAP1,H)
        DO 4 I=1,300
4       EI(I) =(I-1)*H
           DO 777 MMM=1,300
                EXP(MMM)=0.0
777           GIVEN(MMM)=0.0
C
C
C*****************************************M*****************************
C                                                                      *
```

```
C                                                                       *
C   THE FIRST TIME THROUGH THIS LOOP BCS VALUES ARE PRINTED OUT FOR BOTH METALS,
C   AS WELL AS THEIR BCS CONVOLUTION.
C   THE SECOND TIME THROUGH, THE ACTUAL NORMALIZED
C   CONDUCTANCE FOR THE JUNCTION IS PRINTED OUT, AS WELL AS THE DENSITY OF
C   STATES FOR THE KNOWN (OR GIVEN) METAL.
C                                                                       *
            DO 4444     KKK=1,2
C                                                                       *
C                                                                       *
C***********************************************-*****************************
C
C
             IF (KKK .EQ.1) GO TO 224
          READ (5,1) (GIVEN(I),I=1,IGIVL)
1        FORMAT (7F10.6)
         READ(5,5) (EXP(I),I=1,IEXPL)  .
5        FORMAT  (7F10.6)
         WRITE (6,74) (EI(I),EXP(I),I=1,IEXPL)
74       FORMAT ('1 THE FOLLOWING IS THE CONVOLUTED INPUT FROM PART ONE
     C'/
     C  (1X,5(F9.6,2X,F9.6,4X)))
         WRITE (6,79) (EI(I),GIVEN(I),I=1,IGIVL)
79       FORMAT ('OTHE GIVEN DI/DV IS AS FOLLOWS'/
     C  (1X,5(F9.6,2X,F9.6,4X)))
224        CONTINUE
         DO 11 I=2,IEXPL
        ZE=(I-1)*H+GAP1+GAP2
        ZBCS=FBCS(GAP1,GAP2,ZE,40)
11       EXP(I)=(EXP(I)+1.)*ZBCS
         WRITE (6,92)       (EI(I),EXP(I),I=2,IEXPL)
92       FORMAT ('OTHE FIXED UP EXP IS AS FOLLOWS'/
     C  (1X,5(F9.6,2X,F9.6,4X)))
         DO 12 I=2,IGIVL
        ZE=(I-1)*H+GAP2
         ZBCS=ZE/SQRT(   ZE**2-GAP2**2)
```

```
12          GIVEN(I) =(GIVEN(I)+1.)*ZBCS
            WRITE (6,95)   (EI(I),GIVEN(I),I=1,IGIVL)
95          FORMAT ('OTHE FIXED UP GIVEN ARE AS FOLLOWS '/
     C     (1X,5(F9.6,2X,F9.6,4X)))
                 LL1=LL+1
             LF1=LF
             IF (KKK .EQ. 1) LF=LL+1
            DO 18  I=2,LF
           ZF=(I-1)*H+GAP1
            UNKWN(I)=ZF/SQRT(ZF**2-GAP1**2)
18            CONTINUE
C
C
C*****************************************************************************
C                                                                            *
C                                                                            *
C   THE CHANGE IN VALUE OF THE BCS-DOS BETWEEN V-COORDINATES I AND I+1 IS
C   DETERMINED.  THIS IS CALLED B IN THE FOLLOWING COMMENT CARD
C                                                                            *
                IF (KKK.EQ.2) GO TO 8989
            DO 5151     LK=1,LL1
            ERR(LK)=UNKWN(LK)-UNKWN(LK+1)
5151        CONTINUE
8989              CONTINUE
C                                                                            *
C                                                                            *
C*****************************************************************************
C
C
            WRITE (6,96) (EI(I),UNKWN(I)       ,I=2,LF       )
96          FORMAT ('OTHE BEGINNING UNKOWN VALUES ARE'/
     C     (1X,5(F9.6,2X,F9.6,4X)))
        IF (KKK .EQ.1) WRITE (6,74574) (EI(JKL),ERR(JKL),JKL=2,LL1)
74574     FORMAT ('OTHE FOLLOWING IS THE DIFFERENCE IN THE BCS VALUES'/
     C     (1X,5(F9.6,2X,F9.6,4X)))
                 LF=LF1
```

```
4444      CONTINUE
          NOT=LL-LF+2
          IC=LF+1
C
C
C*************************************************************************
C                                                                        *
C                                                                        *
C   THIS DO-LOOP CALCULATES THE ACTUAL VALUES EXP CONDUCT.=(D/DV) (INTEGRAL
C   FROM GAP1 TO  V-GAP2) BY USING (1/H) TIMES (INTEGRAL(V+H)-INTEGRAL(V)).
C   HERE THE INTEGRANDS ARE A PRODUCT OF THE GIVEN DOS AND PREVIOUSLY CALCULATED
C   VALUES FOR THE UNKNOWN'S DOS--EXCEPT FOR THE NEXT TO THE LAST INTEGRAND
C   VALUE OF THE HIGHER BIAS INTEGRAL.  THIS LAST 'PIECE' CONTAINS THE UNKNOWN
C   DOS FOR THE BIAS OF INTREST.  NOTICE THAT THE UNKNOWN DOS FOR BIAS
C   (V-GAP2) IS ASSUMED TO BE EQUAL TO (A+B*ENERGY) WHERE 'A' IS THE VALUE OF
C   THE UNKNOWN DOS FOR BIAS (V-GAP2-H).   THE INTEGRAL BETWEEN (V-GAP2-H). AND
C   (V-GAP2) IS THEN DONE ANALYTICALLY SO THAT THE TOTAL EXPRESSION FOR EXP.
C   CONDUCTANCE (ABOVE) CONTAINS ONLY ONE 'UNKNOWN' UNKNOWN DOS...
C   FINALLY, THE VALUES OF UNKNOWN FROM THE GAP EDGE (GAP1) TO THE FIRST
C   NON-TRIVIAL EXP. POINT ARE ASSUMED TO BE THE BCS VALUES (JUST AS GIVEN IS
C   ASSUMED TO BE BCS FROM GAP1 TO THAT POINT).
C                                                                        *
          DO 100 I=1,NOT
          V=(LF-2+I)*H+GAP1+H+GAP2
             DO 13 KK=1,300
                   K=KK-1
          IF ( K .EQ. LF-1+I) GO TO 14
          VPLH=V-GAP1-K*H
          DO 132 IJ=1,300
          IF (VPLH-E(IJ)-GAP2) 131,131,133
132       CONTINUE
131       IF ((IJ-1) .LT. IGIVE) GO TO 135
          EM=EI(IJ-1)+GAP2
          EP=EI(IJ) + GAP2
          FM= GIVEN(IJ-1)
          FP = GIVEN (IJ)
```

```
          IF (K .EQ. 0) GO TO 142
          ZMUL(K)=FM+(FP-FM)*(VPLH-EM)/(EP-EM)
          GO TO 13
135       IF (K .EQ. 0) GO TO 143
          ZMUL(K)=VPLH/SQRT(VPLH**2-GAP2**2)
          GO TO 13
142           Z= FM+ (FP-FM)*(VPLH-FM)/(EP-EM)
          GO TO 13
143        Z=VPLH/SQRT (VPLH**2-GAP2**2)
13        CONTINUE
14        CONTINUE
           ZZ=ZMUL(I)-Z
          KITE=LF-3+I
          DO 73 IT=1,KITE
73          SINT(IT)=UNKWN(IT+1) * ZMUL(IT)
                KITE1=KITE+1
            A=SINT(KITE)
          I1=KITE+2
          CALL DCSF(H,SINT,SINT,KITE )
          SUM =SINT(KITE )
             SUM= SUM +ZMUL(1)*TEGRAL+A*.5*H
C            + FRP(I1)* (FND/H-(1+GAP2/H)*GRAL)
C   +      ZZ* (FNC/H-(1+GAP1/H)*TEGRAL)
          CCC= GRAL +ZMUL(KITE1)*H*.5
          IF (I .EQ. 1)     GO TO 137
             IC=IC+1
          VM=(EXP(IC)+EXP(IC-1))/2.
        UNKWN(I1)=(VM*H-SUM+PREVOS)/CCC
         PREVOS=CCC*UNKWN(I1)+SUM
          GO TO 100
137         CONTINUE
          SUC=CCC*UNKWN (KITE+2     )
          PREVOS =SCO+SUM
100     CONTINUE
C
C
```

```
C*****************************************************************************
C
C
      UNKWN(LLD)=0.0
      WRITE(6,120)(EI(LLD),UNKWN(LLD),LLL=1,LLD)
120      FORMAT(1'0UNKOWN EQUALS AS FOLLOWS'/
     C   (1X,5(F9.6,2X,F9.6,4X)))
            WRITE(7,37) TITLE
37       FORMAT (20A4)
C
C
C*****************************************************************************
C                                                                            *
C                                                                            *
C   THE UNKNOWN DOS DATA IS DIVIDED BY THE BCS DOS AND PUT INTO SIGMA FORM.
C                                                                            *
         DO 69 J=2,LL1
         EJ=GAP1+(J-1)*H
         FEJ=EJ/SQRT(EJ**2-GAP1**2)
69     UNKWN(J)=UNKWN(J)/FEJ-1
         WRITE (6,43)        (EI(I),UNKWN(I),I=1,LL1)
43       FORMAT        ('1THE DEVIATIONS OF THE UNKNOWN METAL FROM THE
     OF VALUES PREDICTED BY BCS ARE AS FOLLOWS:'       /
     C   (1X,5(F9.6,2X,F9.6,4X)))
            WRITE (7,44)      (UNKWN(I),I=1,LL1)
44       FORMAT   (7F10.6)
C                                                                            *
C                                                                            *
C*****************************************************************************
C
C
     WRITE (7,112) GAP1,H,LL1
112  FORMAT (' GAP1=', F10.6,' H=',F10.6,' NF=',I5)
        STOP
        END
        FUNCTION SQ(X,A)
```

```
      IMPLICIT REAL*8 (A,B,C,D,E,F,G,H,O,P,Q,R,S,T,U,V,W,X,Y,Z)
       IF ( A .EQ. 0) SQ= X*X* .5
           IF (A .NE. 0)
C          SQ=X*.5*DSQRT(X*X-A*A)+A*A*.5*DLOG(X+DSQRT(X*X-A*A))
           RETURN
       END
C
C
C*****************************************************************************
C*****************************************************************************
C*****************************************************************************
```

```
C     ..................................................................DQSF  20
C                                                                       DQSF  30
C        SUBROUTINE DQSF                                                DQSF  40
C                                                                       DQSF  50
C        PURPOSE                                                        DQSF  60
C           TO COMPUTE THE VECTOR OF INTEGRAL VALUES FOR A GIVEN        DQSF  70
C           EQUIDISTANT TABLE OF FUNCTION VALUES.                       DQSF  80
C                                                                       DQSF  90
C        USAGE                                                          DQSF 100
C           CALL DQSF (H,Y,Z,NDIM)                                      DQSF 110
C                                                                       DQSF 120
C        DESCRIPTION OF PARAMETERS                                      DQSF 130
C           H       - DOUBLE PRECISION INCREMENT OF ARGUMENT VALUES.    DQSF 140
C           Y       - DOUBLE PRECISION INPUT VECTOR OF FUNCTION VALUES. DQSF 150
C           Z       - RESULTING DOUBLE PRECISION VECTOR OF INTEGRAL     DQSF 160
C                     VALUES. Z MAY BE IDENTICAL WITH Y.                DQSF 170
C           NDIM    - THE DIMENSION OF VECTORS Y AND Z.                 DQSF 180
C                                                                       DQSF 190
C        REMARKS                                                        DQSF 200
C           NO ACTION IN CASE NDIM LESS THAN 3.                         DQSF 210
C                                                                       DQSF 220
C        SUBROUTINES AND FUNCTION SUBPROGRAMS REQUIRED                  DQSF 230
C           NONE                                                        DQSF 240
C                                                                       DQSF 250
C        METHOD                                                         DQSF 260
C           BEGINNING WITH Z(1)=0, EVALUATION OF VECTOR Z IS DONE BY    DQSF 270
C           MEANS OF SIMPSONS RULE TOGETHER WITH NEWTONS 3/8 RULE OR A  DQSF 280
C           COMBINATION OF THESE TWO RULES. TRUNCATION ERROR IS OF      DQSF 290
C           ORDER H**5 (I.E. FOURTH ORDER METHOD). ONLY IN CASE NDIM=3  DQSF 300
C           TRUNCATION ERROR OF Z(2) IS OF ORDER H**4.                  DQSF 310
C           FOR REFERENCE, SEE                                          DQSF 320
C           (1) F.B.HILDEBRAND, INTRODUCTION TO NUMERICAL ANALYSIS,     DQSF 330
C               MCGRAW-HILL, NEW YORK/TORONTO/LONDON, 1956, PP.71-76.   DQSF 340
C           (2) R.ZURMUEHL, PRAKTISCHE MATHEMATIK FUER INGENIEURE UND   DQSF 350
C               PHYSIKER, SPRINGER, BERLIN/GOETTINGEN/HEIDELBERG, 1963, DQSF 360
C               PP.214-221.                                             DQSF 370
```

```
C                                                                       DQSF 380
C     ..................................................................DQSF 390
C                                                                       DQSF 400
      SUBROUTINE DQSF(H,Y,Z,NDIM)                                       DQSF 410
C                                                                       DQSF 420
C                                                                       DQSF 430
      DIMENSION Y(1),Z(1)                                               DQSF 440
      DOUBLE PRECISION Y,Z,H,HT,SUM1,SUM2,AUX,AUX1,AUX2                 DQSF 450
C                                                                       DQSF 460
      HT=.33333333333333333D0*H                                         DQSF 470
      IF(NDIM-5)7,8,1                                                   DQSF 480
C                                                                       DQSF 490
C     NDIM IS GREATER THAN 5. PREPARATIONS OF INTEGRATION LOOP          DQSF 500
    1 SUM1=Y(2)+Y(2)                                                    DQSF 510
      SUM1=SUM1+SUM1                                                    DQSF 520
      SUM1=HT*(Y(1)+SUM1+Y(3))                                          DQSF 530
      AUX1=Y(4)+Y(4)                                                    DQSF 540
      AUX1=AUX1+AUX1                                                    DQSF 550
      AUX1=SUM1+HT*(Y(3)+AUX1+Y(5))                                     DQSF 560
      AUX2=HT*(Y(1)+3.875D0*(Y(2)+Y(5))+2.625D0*(Y(3)+Y(4))+Y(6))       DQSF 570
      SUM2=Y(5)+Y(5)                                                    DQSF 580
      SUM2=SUM2+SUM2                                                    DQSF 590
      SUM2=AUX2-HT*(Y(4)+SUM2+Y(6))                                     DQSF 600
      Z(1)=0.D0                                                         DQSF 610
      AUX=Y(3)+Y(3)                                                     DQSF 620
      AUX=AUX+AUX                                                       DQSF 630
      Z(2)=SUM2-HT*(Y(2)+AUX+Y(4))                                      DQSF 640
      Z(3)=SUM1                                                         DQSF 650
      Z(4)=SUM2                                                         DQSF 660
      IF(NDIM-6)5,5,2                                                   DQSF 670
C                                                                       DQSF 680
C     INTEGRATION LOOP                                                  DQSF 690
    2 DO 4 I=7,NDIM,2                                                   DQSF 700
      SUM1=AUX1                                                         DQSF 710
      SUM2=AUX2                                                         DQSF 720
      AUX1=Y(I-1)+Y(I-1)                                                DQSF 730
```

```
      AUX1=AUX1+AUX1                                                    DQSF 740
      AUX1=SUM1+HT*(Y(I-2)+AUX1+Y(I))                                   DQSF 750
      Z(I-2)=SUM1                                                       DQSF 760
      IF(I-NDIM)3,6,6                                                   DQSF 770
    3 AUX2=Y(I)+Y(I)                                                    DQSF 780
      AUX2=AUX2+AUX2                                                    DQSF 790
      AUX2=SUM2+HT*(Y(I-1)+AUX2+Y(I+1))                                 DQSF 800
    4 Z(I-1)=SUM2                                                       DQSF 810
    5 Z(NDIM-1)=AUX1                                                    DQSF 820
      Z(NDIM)=AUX2                                                      DQSF 830
      RETURN                                                            DQSF 840
    6 Z(NDIM-1)=SUM2                                                    DQSF 850
      Z(NDIM)=AUX1                                                      DQSF 860
      RETURN                                                            DQSF 870
C     END OF INTEGRATION LOOP                                           DQSF 880
C                                                                       DQSF 890
    7 IF(NDIM-3)12,11,8                                                 DQSF 900
C                                                                       DQSF 910
C     NDIM IS EQUAL TO 4 OR 5                                           DQSF 920
    8 SUM2=1.125D0*HT*(Y(1)+Y(2)+Y(2)+Y(2)+Y(3)+Y(3)+Y(3)+Y(4))         DQSF 930
      SUM1=Y(2)+Y(2)                                                    DQSF 940
      SUM1=SUM1+SUM1                                                    DQSF 950
      SUM1=HT*(Y(1)+SUM1+Y(3))                                          DQSF 960
      Z(1)=0.D0                                                         DQSF 970
      AUX1=Y(3)+Y(3)                                                    DQSF 980
      AUX1=AUX1+AUX1                                                    DQSF 990
      Z(2)=SUM2-HT*(Y(2)+AUX1+Y(4))                                     DQSF1000
      IF(NDIM-5)10,9,9                                                  DQSF1010
    9 AUX1=Y(4)+Y(4)                                                    DQSF1020
      AUX1=AUX1+AUX1                                                    DQSF1030
      Z(5)=SUM1+HT*(Y(3)+AUX1+Y(5))                                     DQSF1040
   10 Z(3)=SUM1                                                         DQSF1050
      Z(4)=SUM2                                                         DQSF1060
      RETURN                                                            DQSF1070
C                                                                       DQSF1080
C     NDIM IS EQUAL TO 3                                                DQSF1090
```

```
   11 SUM1=HT*(1.25D0*Y(1)+Y(2)+Y(2)-.25D0*Y(3))                    DQSF1100
      SUM2=Y(2)+Y(2)                                                DQSF1110
      SUM2=SUM2+SUM2                                                DQSF1120
      Z(3)=HT*(Y(1)+SUM2+Y(3))                                      DQSF1130
      Z(1)=0.D0                                                     DQSF1140
      Z(2)=SUM1                                                     DQSF1150
   12 RETURN                                                        DQSF1160
      END                                                           DQSF1170
$ENTRY
```

STAGE III*

The object of this stage is to find a complex energy gap function $\Delta(E)$, a complex renormalization function $Z(E)$, an effective phonon spectrum $\alpha^2(E)F(E)$, and a Coulomb pseudopotential μ^* which will reproduce the tunneling electron density of states and also gives the measured value for the gap function at the gap edge, $\Delta_0 = \Delta(E=\Delta_0)$. The theory behind these calculations has been discussed in Chapters 2 and 3.

FUNCTION NAMES AND INPUT PARAMETERS

Function Name

SAMPLE	Identifies the input data
DM	Initially is used to label the input data
TZPE	Numerically computed derivative of the input data
TZ	Calculated density of states, $N_c(E)$
EI	Energy in 10^{-3} electron volts
G	(a) $\alpha^2F(Eq)$
	(b) The above divided by a sort of average value of α^2; equal to $[\alpha^2F(Eq) \div \int\alpha^2F(Eq)dEq]$.
DG	The incremental correction to $\alpha^2F(Eq)$.
DR	$\Delta_1(E)$, the real part of the gap function
DI	$\Delta_2(E)$, The imaginary part of the gap function
ZR	$Z_1(E)$, the real part of the renormalization function

* The following has been adapted from Ref. (13).

ZI	$Z_2(E)$, the imaginary part of the renormalization function
FR	Real $\{[1 - Z(E)]E\}$
FI	Imag $\{[1 - Z(E)]E\}$
PAR	Real $\{\Delta(E)Z(E)\}$
PAI	Imag $\{\Delta(E)Z(E)\}$

Input Parameters

JO	The index specifying the maximum phonon energy, E_o. For an energy spacing of $H=.1x10^{-3}$ electron volts, for example, JO=161 corresponds to $E_o=16.0x10^{-3}$ electron volts.
JC	The index specifying E_c. JC=451 corresponds to $E_c=45.0x10^{-3}$ electron volts for $H=.1x10^{-3}$ electron volts, for example.
MAXG	The index specifying the maximum energy to which corrections to α^2F will be made in the iteration procedure. Usually MAXG is set equal to JO, but lower values may be useful in refinements of a previously calculated spectrum.
NITER	Number of iterations of the gap equation.
NREF	Number of iterations in which $\alpha^2F(Eq)$ is refined.

NG This is the ratio of the energy spacing of the input $\alpha^2F(Eq)$ to the energy spacing given by the parameter H. For example, if the input $\alpha^2F(Eq)$ has an energy interval of 0.1×10^{-3}eV while H=.05, then NG=2. The program will interpolate to obtain the same energy interval for all the functions. However, if NG $\leq$ 0, no data will be read in and the program will use a starting $\alpha^2F(Eq)$ of $\alpha^2F(Eq) = (Eq/H)^2(E_o-Eq/H)^2$.

ND This is the ratio of the energy spacing of the input $\Delta_1(E)$ and $\Delta_2(E)$ to the energy spacing given by the parameter H, in the same manner as NG served for the input $\alpha^2F(Eq)$ data. For ND $\geq$ 1, the program will interpolate to obtain the same energy interval as for the other functions. For ND $\leq$ 0, no data will be read in and the program will use a starting function of $\Delta_1=\Delta_0$ for $E \leq E_c$, $\Delta_1=0$ for $E > E_c$, and $\Delta_2 = 0$.

NH This is the ratio of the energy spacing given by the parameter H to the energy spacing of the input density of states data, DM. If NH=2, for example, then the program will use only every other data point.

MING — The index specifying the energy up to which $\alpha^2F(Eq)$ is to be taken as proportional to Eq^2. MING=9, NH=1, and H=.1 mean that $\alpha^2F(Eq)$ is taken to be proportional to Eq^2 up to [(MING/NH) + 1] x H, or 1×10^{-3} eV.

W — The starting value for the Coulomb pseudo-potential μ^*. Usually set equal to 0.11.

DO — This is the GAP1=Δ_1 of the two earlier stages.

H — The energy spacing, in eV x 10^{-3}, for the calculations.

NR — The number of data points in the input density of states. If the second stage is used, these last three parameters will be part of the punched output of that stage.

INPUT DATA FORMAT

Data Card Number	Information on Card	Format
1	JO,JC,MAXG,NITER,NREF, NG,ND	7(6X,I4)
2	NH,MING,W	2(7X,I3),10X, F10.2
3	SAMPLE	20A4
4	DO,H,NR	(6X,F10.6,3X, F10.6,4X,I5)

5ff	DM	7F10.6
6ff(only if NG≥1)	G	1P7E11.3
7ff(only if ND≥1)	DR	7E11.3
8ff(only if ND≥1)	DI	7E11.3

```
C*****************************************************************************
C*****************************************************************************
C*****************************************************************************
C
C
C    IF PROGRAM IS BEING USED TO CALCULATE (DI/DV) GIVEN, FOR STAGE 2
C    INSERT INSTRUCTION N(EXP)=N(CALCULATED).
C                                                                            *
C                                                                            *
C*****************************************************************************
      DIMENSION F(450),G(220),TP(611),TZ(450),PAR(450),PAI(450),
     1  FR(450), FI(450),ZR (450),ZI(450),DR(450),DI(450),TZP(450),
     2 CP(450),CZ(500),DM(2061),DP(2061),DRD(261),DID(261)   ,
     3 FI(2061),DPAI(20),DPAR(20),DTZP(261,10),DDR(20),DDI(20),
     4  DTZ(20),DT(261),TZPE(280),DIFT(261),DG(262),SAMPLE(20)
      DIMENSION Z(4)
      DIMENSION TX(2),TY(2)
          EQUIVALENCE  (PAR(1),DR(1)),(PAI(1),DI(1)),(FR(1),ZR(1)),
     C    (FI(1),DP(1)), (FI(1),ZI(1))
      COMPLEX UIV
      CALL NEWPLT  (M9904,10741)
      LCONV=2.
      ACONV=1.35
40    READ(5,41) JO,JC,MAXG,NITER,NREF,NG,ND
      J1=MAXG
41    FORMAT (7(6X,I4))
      READ(5,411) NH,MING,W
411   FORMAT (2(7X,I3),10X,F10.0)
      READ (5,410) SAMPLE
410   FORMAT (20A4)
      READ (5,42) DO,H,NR
42    FORMAT (6X,F10.6,3X,F10.6,4X,I5)
      MING=MING/NH+2
      READ (5,43) (DM(I),I=1,NR)
43    FORMAT (7F10.0)
      NMAX=NR/NH
```

226A

```
      DO 250 I=1,NMAX
      J=1+NH*(I-1)
250   DM(I)=DM(J)
      RO=DM(1)
      WRITE (6,412) SAMPLE,DO,H,W
412   FORMAT (20A4/' GAP=',E13.6,' H=', E13.6,
     1  ' SATARTING PSEUDOPOTENTIAL =',E13.6)
      WRITE (6,413) JO,JC,MING,MAXG,NITER,NREF,NG,NR,NH,ND
413   FORMAT (' JO=',I4,' JC=',I4,' MING=',I4,' MAXG=',I4,
     1  ' NITER=',I4, ' NREF=', I4,' NG=',I4,' NR=',I4,
     2  ' NH=',I4,' ND=',I4)
      WRITE (6,251) (DM(I),I=1,NMAX )
251   FORMAT (' INPUT REDUCED DENSITY OF STATES'/ (1X,10F10.6))
      IMAX=NMAX
      DO 252 I=2,IMAX
252   TZPE(I)=(DM(I)-DM(I-1))/H
      TZPE(1)=0
      WRITE (6,181) (TZPE(I),I=1,IMAX           )
181   FORMAT ( ' DERIVATIVE OF INPUT'/(1X,10F10.6))
      DO 310 I=1,JC
      AI=I-1
310   E(I)=DO+AI*H
      CALL PICTUR(8.5,10.,'ENERGY IN MV',12,'EXPERIMENTAL/BCS',16,
     1 E,DM,NMAX,0,0)
      IF(NG) 510,510,511
511   READ(5,512) (G(I),I=1,JC,NG     )
512   FORMAT (1X,7E11.3)
      WRITE (6,4000) (G(I),I=1,JO,NG  )
4000  FORMAT (' STARTING PHONON SPECTRUM'/ (1X,1P10E11.3))
      IF (NG-1) 514,514,513
513   ANG=NG
      DO 515 I=NG,JO,NG
      IM=I-NG
      DO 515 J=2,NG
      IJ=IM+J
      AJ=J-1
```

```
      AJ=AJ/ANG
515   G(IJ)=G(IM+1)+AJ*(G(I+1)-G(IM+1))
      GO TO 514
510       AN=MAXG-1
      DO 516 I=2,MAXG
      AI=I-1
516   G(I)=AI**2*(AN-AI)**2
514   CONTINUE
      IF(ND) 520,520,521
521   READ (5,522) (DR(I),I=1,JC,ND     )
      READ(5,522) (DI(I),I=1,JC,ND)
522   FORMAT (1X,7E11.3)
      IF (ND-1) 526,526,523
523   AND=ND
      DO 525 I=ND,JC,ND
      IM=I-ND
      DO  525 J=2,ND
      IJ=IM+J
      AJ=J-1
      AJ=AJ/AND
      DR(IJ)=DR(IM+1)+AJ*(DR(I+1)-DR(IM+1))
525   DI(IJ)=DI(IM+1)+AJ*(DI(I+1)-DI(IM+1))
526   CONTINUE
      DO 336 I=2,JC
      X=ABS(E(I)**2+DI(I)**2-DR(I)**2)
      Y=-2.*DR(I)*DI(I)
      UIV=CSQRT(CMPLX(X,Y))
      U=REAL(UIV)
      V=AIMAG(UIV)
      IF(U) 337,338,338
337   U=-U
      V=-V
338   ANORM=U*U+V*V
      TP(I)=(U*DR(I)+V*DI(I))/ANORM
      TZ(I)= E(I)*U/ANORM
      SQ=SQRT(E(I)**2-DO**2)
```

```
      TP(I)=TP(I)*SQ/DO
336   TZ(I)=TZ(I)*SQ/E(I)
      TP(1)=2.*TP(2)-TP(3)
      TZ(1)=2.*TZ(2)-TZ(3)
      JX=JC+1
      DO 1008 I=JX,611
1008  TP(I)=0
      GO TO 524
520   DO 1006 I=1,JC
      DR(I)=0
      DI(I)=0
1006  TZ(I)=0
      DO 1007 I=1,611
1007        TP(I)=0
      DO 403 I=1,JC
      DR(I)=DO
403   TP(I)=1.
      DO 404 I=1,JC
404   TZ(I)=1.
524   CONTINUE
      GM=G(MING+1)
      AM=MING
      DO 530 I=1,MING
      AI=I-1
530   G(I)=(AI/AM)**2*GM
      SUMG=0.
      DO 44 I=1,JO
44    SUMG=SUMG+G(I)
      SUMG=AM*SUMG
      SUMGF=0.
      DO 45 I=2,JO
      AI=I-1
      G(I)=G(I)/SUMG
45    SUMGF=SUMGF+G(I)/AI
      IMAX=JC
      DO 141 I=1,IMAX
```

229<

```
      CP(I)=0
141   CZ(I)=0
      SQL=0
      IMAX=JC
      APOO=DO*ALOG(DO)
      AP1O=0
      AZOO=0
      AZ1O=.5*DO**2*ALOG(DO)
      DO 140 I=1,IMAX
      I1=I+1
      AI=I-1
      EL=F(I)
      EM=EL+.5*H
      EH=EL+H
      SQH=SQRT(EH**2-DO**2)
      ELN=ALOG(EH+SQH)
      APON=DO*ELN
      APIN=DO*SQH
      BPO=APON-APOO
      BP1=APIN-AP1O-EM*BPO
      CP(I)=CP(I)+BPO*.5-BP1/H
      CP(I1)=CP(I1)+BPO*.5+BP1/H
      APOO=APON
      AP1O=APIN
      IF (ABS(CP(I)*SQL/(DO*H)-1.1-.0001) 297,297,140
297   ICP=I
      WRITE (6,4003) ICP
4003  FORMAT (' ICP=',I5)
      GO TO 298
140   SQL=SQH
      ICP=IMAX
298   DO 299 I=ICP,IMAX
      SQL=SQRT(F(I)**2-DO**2)
299   CP(I)=H*DO/ SQL
      DO 300 I=1,IMAX
      I1=I+1
```

230A

```
      AI=I-1
      EL=E(I)
      EM=EL+.5*H
      EH=EL+H
      SQH=SQRT(EH**2-DO**2)
      ELN=ALOG(EH+SQH   )
      AZON=SQH
      AZIN=.5*EH*SQH+.5*DO**2*ELN
      BZO=AZON-AZOO
      BZ1=AZIN-AZIO-EM*BZO
      CZ(I)=CZ(I)+BZO*.5-BZ1/H
      CZ(I1)=CZ(I1)+BZO*.5+BZ1/H
      AZOO=AZON
      AZIO=AZIN
      IF(ABS(CZ(I)*SQL/(EL*H)-1.)-.0001) 301,301,300
301   ICZ=I
      GO TO 302
300   SQL=SQH
      ICZ=IMAX
302   DO 303 I=ICZ,IMAX
      SQL=SQRT(E(I)**2-DO**2)
303   CZ(I)=H*E(I)/SQL
      IMAX=2*JC+JO
      DO 142 I=1,IMAX
142   DP(I)=0
      DP(1)=.5*H/(2.*DO)
292   DO 293 I=2,IMAX
      AI=I-1
      EL=2.*DO+AI*H
293   DP(I)=H/EL
      IMAX=2*JC+JO
      IMIN=JC+1
      DO 144 I=1,2061
144   DM(I)=0
      DO 296 I=IMIN,IMAX
      AI=I-JC
```

```
      EL=H*AI
296   DM(I)=H/EL
      DM(IMIN)=1.5
      ICP=0
      IDM=0
      IMAX=JC-1
      DO 146 I=1,IMAX
      IP=JC+I
      IM=JC-I
146   DM(IM)=-DM(IP)
      IMAX=JC
      IMAX=2*JC+JO
      DO 420 IREF=1,NREF
      IF(IREF-1) 422,422,421
421   NITER=1
422   CONTINUE
      DO 7 K=1,NITER
202   WRITE (6,8) K
8     FORMAT (10H ITERATION, I4)
      DO 162 I=1,JC
      TP(I)=TP(I)*CP(I)
162   TZ(I)=TZ(I)*CZ(I)
      IMAX=JO+JC
      DO 1 I=1,JC
      JMIN=MAX0(I-JO+1,1)
      JMAX=MIN0(I,JC)
      PAI(I)=0.
      FI(I)=0.
      DO 1 J= JMIN, JMAX
      IJ=I-J+1
      PAI(I)=PAI(I)+TP(J)*G(IJ)
1     FI(I)=FI(I)-TZ(J)*G(IJ)
      AJC=JC
      EH=AJC*H+DO
      DO 2 I=1,JC
      PAR(I)=PAI(JC)*EH*ALOG((EH+E(I))/(EH-E(I)))/E(I)
```

```
      FR(I)=-ALOG ((EH+E(I))/(EH-E(I)))
      DO 2 J=1,JC
      IP=I+J-1
      IM=JC-I+J
      PAR(I)=PAR(I)+(DP(IP)+DM(IM))*PAI(J)
2     FR(I)=FR(I)-(DP(IP)-DM(IM))*FI(J)
      PU=0.
      DO 3 J=1,JC
3     PU=PU+TP(J)
      IF (IREF-1) 351,351,350
351   A2=(DO+W*PU)/(PAR(1)+FR(1))
      GO TO 275
350   CONTINUE
      D1=A2*PAR(1)/(1.-A2*FR(1)/DO)
274   DU=D1-DO
      W=DU*(1.-A2*FR(1)/DO)/PU
275   PU=-W*PU
      AR2=A2
      AI2=3.1415927*A2
      DO 430 I=1,JC
      PAR(I)=AR2*PAR(I)+PU
430   PAI(I)=AI2*PAI(I)
      IF (IREF-NREF) 431,432,431
432   DO 436 I=1,JC
      AI=I-1
436   EI(I)=AI*H
      WRITE (6,4601) (PAR(I), I=1,JC)
4601  FORMAT (' PHI-REAL PART'/(1X,1P10E11.3))
      WRITE (6,4602) (PAI(I),I=1,JC     )
4602  FORMAT (' PHI-IMAGINARY PART'/(1X,1P10E11.3))
431   CONTINUE
      DO 4  I=1,JC
      ZR(I)=1.-AR2*FR(I)/E(I)
      ZI(I)=-AI2*FI(I)/E(I)
      ANORM=ZR(I)**2+ZI(I)**2
      DRT=((PAR(I))*ZR(I)+PAI(I)*ZI(I))/ANORM
```

```
      DI(I)=(PAI(I)*ZR(I)-(PAR(I))*ZI(I))/ANORM
      DR(I)=DRT
      IF (I-1) 4,4,163
163   X=ABS(F(I)**2+DI(I)**2-DR(I)**2)
      Y=-2.*DR(I)*DI(I)
      UIV=CSQRT(CMPLX(X,Y))
      U=REAL(UIV)
      V=AIMAG(UIV)
      IF (U) 50,51,51
50    U=-U
      V=-V
51    ANORM=U*U+V*V
      TP(I)=(U*DR(I)+V*DI(I))/ANORM
      TZ(I)=F(I)*U/ANORM
4     CONTINUE
      TZ(1)=0.
      DO 5  I=2,JC
5     TZP(I)=(TZ(I)-TZ(I-1))/H
      TZP(1)=0.
      S1=0.
      S2=0.
C     THE FOLLOWING STATEMENTS WERE ADDED TO PREVENT AN UNDEFINED DRO
C     AND DIO.
      IF (K-1) 3100,3101,3100
3101  DO 3102 KIM=1,JO
      DRO(KIM)=0.
3102  DIO(KIM)=0.
3100  CONTINUE
      DO 60 I=1,J1
      S1=S1+(DR(I)-DRO(I))**2+(DI(I)-DIO(I))**2
60    S2=S2+DR(I)**2+DI(I)**2
      DEVD=SQRT(S1/S2)
      IF (IREF-NREF) 440,441,440
441   CONTINUE
      WRITE (6,4471) (DR(I),I=1,JC)
4471  FORMAT (30H DR(I)=GAP FUNCTION, REAL PART/(1X,10F13.6))
```

```
      WRITE (6,4472) (DI(I),I=1,JC)
4472  FORMAT (35H DI(I)=GAP FUNCTION, IMAGINARY PART/(1X,10F13.6))
      WRITE(6,4470) (G(I),I=1,JO)
4470  FORMAT(' PHONON DENSITY OF STATES USING AVERAGE VALUE OF COUPLING
     1 CONST'/(1X,10F13.6))
      WRITE (7,5000)  (G(I),I=1,JO)
      WRITE (7,5000)(DR(I),I=1,JC)
      WRITE (7,5000)(DI(I),I=1,JC)
5000  FORMAT (1X,1P7E11.3)
      CALL PICTUR (8.5,10.,'ENERGY IN MV',12,'PHONON SPECTRUM',15,
     1FI,G,JO,0,0)
      CALL PICTUR (8.5,10.,'ENERGY IN MV',12,'CALCULATED GAP FUNCTION',2
     13,EI,DR,JC,0,0,EI,DI,JC,0,0)
      CALL ENDPLT
      WRITE (6,4605) (ZR(I),I=1,JC )
4605  FORMAT (37H RENORMALIZATION FUNCTION,SUPERC,REAL/(1X,1P10E11.3))
      WRITE (6,4606) (ZI(I),I=1,JC)
4606  FORMAT (37H RENORMALIZATION FUNCTION,SUPERC,IMAG/(1X,1P10E11.3))
4487  CONTINUE
      SUMP=0.
      SUMM=0.
      DO 453 I=2,JO
      AI=I-1
      EN=AI*H
      G(I)=A2*G(I)
      SUMP=SUMP+EN*G(I)*H
453   SUMM=SUMM+G(I)*H/EN
      CC=2.*SUMM
      GAP=SUMP
      WRITE(6,4479)  (G(I),I=1,JO)
4479  FORMAT (' (ALPHA)**2*F'/(1X,10F13.6))
440   CONTINUE
      DO 164  I=2,JC
      SQ=SQRT(E(I)**2-DO**2          )
      TP(I)=TP(I)*SQ/DO
164   TZ(I)=TZ(I)*SQ/E(I)
```

235A

```
      TZ(1)=2.*TZ(2)-TZ(3)
      TP(1)=2.*TP(2)-TP(3)
      IF (K.LT.NITER)   GO TO  470
      IF (IREF-NREF) 470,471,470
471   NMAX=NB/NH-1
      DM(1)=RC
      DO 472 I=2,NMAX
472   DM(I)=DM(I-1)+TZPE(I)*H
      DO 473 I=1,NMAX
473   DM(I)=DM(I)-TZ(I)+1.
      DO 540 I=1,JC
540   TZ(I)=TZ(I)-1.
      WRITE (6,4600) (TZ(I),I=1,NMAX)
4600  FORMAT (' CALCULATED DI/DV='/(1X,1P10E11.3))
      PI=3.1415927
      DO 3000 I=1,JC
3001  FI(I)=0
3000  FR(I)=0
      DO 480 I=2,JO
480   FI(I)=FI(I-1)-.5*(G(I-1)+G(I))*H* PI
      DO 481 I=JO,JC
481   FI(I)=FI(JO)
      IMAX=JC+2*JO
      AJO=JO-1
      EO=(-AJO-.5)*H
      AO=EXP(ALOG(ABS(EO))-1.)
      DO 482 I=1,IMAX
      AI=I-JO
      EN=(AI+.5)*H
      AN=EXP(ALOG(ABS(EN))-1.)
      DM(I)=AN-AO
482   AO=AN
      DO 483 I=2,JC
      DO 483 J=2,JO
      IPJ=I+J+JC-2
      IMJ=I-J+JO
```

```
453    FR(I)=FR(I)-G(J)*(DM(IPJ)-DM(IMJ))
       DO 484 I=2,JC
       AI=I-1
       EO=AI*H
       ZR(I)=1.-FR(I)/EO
484    ZI(I)=-FI(I)/EO
       ZI(1)=0.
       ZR(1)=ZR(2)
       WRITE (6,4603) (ZR(I),I=1,JC)
4603   FORMAT (' RENORMALIZATION FUNCTION, NORMAL, REAL'/(1X,1P10E11.3))
       WRITE (6,4604) (ZI(I),I=1,JC      )
4604   FORMAT (' RENORMALIZATION FUNCTION,NORMAL,IMAG'/(1X,1P10E11.3))
       WRITE (6,490) A2,CC,FBAR,W,PU,DU,DEVD
490    FORMAT(4H A2=,E13.6,4H CC=,E13.6,6H FBAR=,E13.6,3H U=,E13.6,4H PU=
      1 , E13.6,4H DU=,E13.6,6H DEVD=,E13.6)
       GO TO 40
470    CONTINUE
       TZP(1)=0.
       DO 166 I=2,JC
166    TZP(I)=(TZ(I)-TZ(I-1))/H
61     DO 63 I=1,J1
       DRO(I)=DR(I)
63     DIO(I)=DI(I)
7      CONTINUE
184    DO 170 I=1,JC
170    TP(I)=TP(I)*CP(I)
230    DO 120 I=1,9
120    DPAI(I)=0.
       DO 121 I=10,20
       L=I-9
121    DPAI(I)=AI2*TP(L)
       DO 122 I=1,20
       CPAR(I)=0.
       JMAX=JC+JC
       DO 123 J=1,JMAX
       IM=JC-I+J+9
```

```
123   DPAR(I)=DPAR(I)+DM(IM)*TP(J)
122   DPAR(I)=AR2*DPAR(I)
      DO 132 I=1,J1
      DO 132 J=1,10
132   DTZP(I,J)=0.
      DO 133 I=2,J1
      IF(I-10) 240,240,241
240   IP=11-I
      DPARO=DPAR(IP)
      GO TO 242
241   AI=I
      DPARO=DPAR(1)*10./AI
242   CONTINUE
      JMIN=MAXO(I-5,2)
      JMAX=MINO(I+5,J1+1)
      DO 134 J=JMIN,JMAX
      L=J-I+6
      M=L+1
      ANORM=ZR(J)**2+ZI(J,**2
      IK=JMIN-I+5
      IF (IK) 4701,4701,4702
4702  DO 4703 IJ=1,IK
4703  DTZ(IJ)=0
4701  CONTINUE
      DDR(L)=((DPAR(M)-DPARO)*ZR(J)+DPAI(M)*ZI(J))/ANORM
      DDI(L)=(-(DPAR(M)-DPARO)*ZI(J)+DPAI(M)*ZR(J))/ANORM
134   DTZ(L)=(DR(J)*DDR(L)-DI(J)*DDI(L))/E(J)**2
      DO 135 J=1,10
135   DTZP(I,J)=(DTZ(J+1)-DTZ(J))/H
133   DT(I)=(DTZ(11)-DTZ(1))/H
      SUM1=0.
      SUM2=0.
      DO 2006 I=1,J0
2006  DIFT(I)=0
      IMIN=MING-3
      DO 190 I=IMIN,MAXG
```

```
      DIFT(I)=(TZPE(I)-TZP (I))*(1.-(DO/E(I))**2  )
      SUM1=SUM1+DIFT(I)**2
190   SUM2=SUM2+(TZPE(I)*(1.-(DO/E(I))**2))**2
      DEVT=SQRT(SUM1/SUM2)
      DO 215 I=6,J1
      AS=DTZP(I,1)
      BS=(DTZP( I,10)-DTZP(I,1))/9.
      DO 215 J=1,10
      AJ=J-1
215   DTZP(I,J)=DTZP(I,J)-AS-BS*AJ
      JNMAX=J1-1
      DO 210 JN=2,JNMAX
      J=J1+2-JN
      KMIN=MAXO(J-3,2)
      KMAX=J-1
      DO 210 K=KMIN,KMAX
      KM=K-J+5
      RAT=DTZP(J,KM)/DTZP(J,5)
      IMIN=MAXO(J-4,2)
      DO 212 I=IMIN,J
      JM=J-I+5
      KM=K-I+5
212   DTZP(I,KM)=DTZP(I,KM)-RAT*DTZP(I,JM)
210   DIFT(K)=DIFT(K)-RAT*DIFT(J)
      JMIN=J1-1
      DO 213 J=2,JMIN
      KMAX=MINO(J+4,J1)
      KMIN=J+1
      DO 213 K=KMIN,KMAX
      KM=K-J+5
      RAT=DTZP(J,KM)/DTZP(J,5)
      DTZP(J,KM)=DTZP(J,KM)-RAT*DTZP(J,5)
213   DIFT(K)=DIFT(K)-RAT*DIFT(J)
      DO 220 I=2,J1
220   DG(I)=DIFT(I)/DTZP(I,5)
      DG(1)=0.
```

```
      DG(J1+1)=C.
      DO 222 I=MING,MAXG
222   G(I)=G(I)+(.25*DG(I-1)+.5*DG(I)+.25*DG(I+1))*(1.-(DO/E(I))**2)*
     1ACONV
      CM=G(MING+1)
      AM=MING
      DO 531 I=1,MING
      AI=I-1
531   C(I)=(AI/AM)**2*GM
      SUMG=0.
      DO 223 I=2,JC
223   SUMG=SUMG+G(I)
      SUMG=H*SUMG
      WRITE(6,7071) G(MAXG)
7071  FORMAT (' G(MAXG)=',4X,F10.6)
      SUMGE=0.
      DO 224 I=2,JC
      AI=I-1
      G(I)=G(I)/SUMG
224   SUMGE=SUMGE+G(I)/AI
      A2=A2+A2*(SUMG-1.)*UCCNV
      DO 201 I=1,JC
201   TP(I)=TP(I)/CP(I)
      WRITE (6,500) A2,W,PU,DU,DEVD,DEVT
500   FORMAT (4H A2=,E13.6,3H U=, E13.6,4H PU=, E13.6,4H DU=, E13.6,
     1 6H DEVD=, E13.6/6H DEVT=, E13.6)
420   CONTINUE
      STOP
      END
C
C
C*****************************************************************************
C*****************************************************************************
C*****************************************************************************
```

240<

REFERENCES

1. J. Adler and J. S. Rogers, Phys. Rev. Letters 10, 217 (1963).

2. K. Agyeman, S.M. Thesis, M.I.T., 1973 (unpublished).

3. J. Bardeen, L. N. Cooper, and J. R. Schrieffer, Phys. Rev. 108, 1175 (1957).

4. J. Bardeen, Physics Today 26, 41 (July, 1973).

5. S. Bermon and D. M. Ginsberg, Phys. Rev. 188, 716 (1969).

6. J. Bostock, The Science and Technology of Superconductivity, edited by W. D. Gregory et al. (Plenum Press, New York, 1973), Vol. 2, p. 735.

7. G. M. Eliashberg, J. Exptl. Theort. Phys. (USSR) 38, 966 (1960) [English translation: Soviet Physics JETP 11, 696 (1960)].

8. M. H. Frommer, Ph.D. Thesis, M.I.T., 1973 (unpublished).

9. M. H. Frommer, J. Bostock, Kofi Agyeman, R. M. Rose, and M. L. A. MacVicar, Sol. St. Com. (to be published); J. Bostock, Kofi Agyeman, M. H. Frommer, and M. L. A. MacVicar (to be published).

10. I. Giaever, in Tunneling Phenomena in Solids, edited by E. Burstein and S. Lundquist (Plenum, New York, 1969), Chap. 19.

11. W. Hubin, Ph.D. Thesis, University of Illinois, 1969 (unpublished).

12. W. Hubin and D. M. Ginsberg, Phys. Rev. 188, 716 (1969).

13. W. Hubin, Technical Report No. 182, (Department of Physics, University of Illinois, Urbana, Illinois, 1970 (unpublished).

14. L. F. Lou and W. J. Tomasch, Phys. Rev. Letters 29, 858 (1972).

15. W. L. McMillan and J. M. Rowell, Phys. Rev. Letters 14, 108 (1965).

16. W. L. McMillan, Phys. Rev. 167, 331 (1968).

17. W. L. McMillan and J. M. Rowell, in Superconductivity, edited by R. D. Parks (Dekker, New York, 1969), Chap. 11.

18. J. M. Rowell and A. G. Chynoweth, Phys. Rev. Letters 9, 59 (1962).

19. J. M. Rowell and L. Kopf, Phys. Rev. 137, A907 (1965).

20. J. M. Rowell, W. L. McMillan, and W. L. Feldman, Phys. Rev. B 3, 4065 (1971).

21. D. J. Scalapino and P. W. Anderson, Phys. Rev. 133, A921 (1964).

22. D. J. Scalapino and Y. Wada, Phys. Rev. Letters 14, 102 (1968).

23. D. J. Scalapino, J. R. Schrieffer and J. W. Wilkins, Phys. Rev. 148, 263 (1966).

24. D. J. Scalapino, in Superconductivity, edited by R. D. Parks (Dekker, New York, 1969), Chap. 11.

25. J. R. Schrieffer, Rev. of Modern Physics 36, 200 (1964).

26. J. R. Schrieffer, in Tunneling Phenomena in Solids, edited by E. Burstein and S. Lundquist (Plenum, New York, 1969), Chap. 19.

27. T. P. Sheahen, Phys. Rev. 149, 368 (1966).

28. T. P. Sheahen, Phys. Rev. 149, 370 (1966).

29. L. Y. L. Shen, Phys. Rev. Letters 29, 1082 (1972).

30. L. Y. L. Shen, in Superconductivity in d- and f-Band Metals, edited by David H. Douglass (American Institute of Physics, New York, 1972).

31. L. Solymar, Superconductive Tunneling and Applications (John Wiley and Sons, New York, 1972).

VITA

The author was born in The Bronx, New York on May 28, 1952. After graduating from Yeshiva University High School, New York City, New York, he began attending the Massachusetts Institute of Technology in Cambridge, Massachusetts.

He is presently attending the Rabbi Isaac Elchanan Theological Seminary in New York City, New York.

SEMI-ANNUAL TECHNICAL REPORT #1

Period: July 1, 1973 - Dec. 31, 1973

Title: Research in Materials Sciences

Project Title: Chemical Synthesis Using High Temperature Lithium Vapor Species

Contract Number: DAHC 15-73-C-0316

ARPA Order Number: 2469

Program Code Number: 3D10

Name of Contractor: Massachusetts Institute of Technology
Cambridge, Mass. 02139

Principal Investigator: N. J. Grant (617) 253-5638

Project Scientists or Engineers: Prof. R. Lagow (617) 253-5617

Effective Date of Contract: June 1, 1973

Contract Expiration Date: May 31, 1974

Amount of Contract: $425,000

Amount of Project: $ 60,000

Sponsored By
Advanced Research Projects Agency
ARPA Order No. 2469

Chemical Synthesis Using High Temperature Lithium Vapor Species

Abstract and Objectives

Recent work in our laboratory has resulted in the discovery of several new routes to polylithiocarbons, perlithiocarbons, and inorganic polylithium species. Previously for these classes of compounds, there were very few known examples, and there were no general synthetic routes in the literature. The new synthetic methods are all in the early stages of development and all involve the reaction of high temperature lithium vapor in the range of 800 - 1000°C with various organic, inorganic and polymeric species. During the past year we have succeded in the synthesis of the first perlithioalkanes, tetralithiomethane, $C(Li)_4$ and hexalithioethane, C_2Li_6. We have also prepared hexalithiobenzene C_6Li_6. An intensive study of these species is now underway and efforts are underway to prepare other polylithiated species. Support for this work is urgently needed to expand the small effort in the exciting new area. It appears that polylithiocarbons will be very useful reagents in organic synthesis as well as important monomers and crosslinking agents in polymer synthesis. The synthesis of several types of three dimensional polymers and high temperature materials is proposed based on routes involving these new polylithium species. The preparation of a series of diamond-like polymeric materials is proposed and would result in a new class of high performance materials. Polylithium compounds may also be useful as catalysts and a new synthesis is proposed for diamond based on these compounds.

Summary of Research Progress in the Synthesis Characterization and Reactions of Polylithium Compounds

6/1/73 - 12/1/73

Initially a study of the reaction of carbon tetrachloride, CCl_4 and the reaction of hexachloroethane C_2Cl_6 was studied with lithium vapor at a 1000°C.[1] The products of the initial reaction were tetralithiomethane CLi_4 and tetralithioethylene $Li_2C\text{-}CLi_2$. These compounds were characterized (see the attached reprint) and it has been found that they react with various organic and inorganic substrates in the manner characteristic of other lithium compounds such as the conventionally prepared monolithium compounds. This experimental result provides evidence of the suitability of such polylithium compounds for reactions as monomers in the proposed diamond-like polymer systems. Subsequently, the reaction of hexachloroethane with lithium produced hexolithioethane in approximately 80% yield. Again this material has been shown to be a potentially reactive monomer.

A study of the reaction of carbon vapor generated from a carbon arc apparatus at 2500°C was undertaken to establish an alternative method for synthesizing polylithium compounds.[2] The principal product was C_3Li_4 which appears to have the allene structure and might be an attractive monomer. Varying amounts of tetralithiomethane and

tetralithioethylene were also produced in this study.

A third publication has resulted from the reaction of lithium vapor with benzene.[3] While for most of our systems the reactants are admitted to the reactor at room temperature and reacted with the high temperature lithium vapor, initial studies giving a small yield of hexalithio benzene prompted us to do a more extensive study based on the reaction of lithium vapor plus benzene at various temperatures. A new type of reactor was designed for this purpose. At room temperature one gets a distribution of lithiated benzene ranging from over the range of $C_6Li_{6-n}H_n$ where n = 1 to 6. At room temperature the species of highest yield is dilithiobenzene. As one raises the temperature progressively to 800°C a shift toward the higher benzene polylithium compounds is noted. The temperature of the benzene is raised to 900°C and a striking new result is attained. One begins to obtain polylithiated cyclohexanes from the benzene starting material. This results from a tendency for the lithium to add to the double bonds as well as replace the protons on the ring. Studies were made up to temperatures of 1200°C producing such striking compounds as perlithiocyclohexane and $C_6Li_6H_6$. It has been found subsequently that the reaction of hexachlorobenzene with lithium provides a much cleaner route to hexalithiobenzene.[4]

The reaction of methane gas with lithium has also been extensively investigated.[5] We predicted and found that lithium at 1000° will not react with methane gas at room temperature. The activation energy for

this reaction appears to be in the 30 kcal mole range. Lithium at 1000°C usually has about 3 kcal mole of translational or kinetic energy and only a very small percentage of lithium in the first excited electronic state. Therefore, the activation energy for the lithium-methane reaction is not likely to be available under these reaction conditions. The reaction between methane and lithium would be a very important one for the production of tetralithiomethane which we consider to be one of the important materials in subsequent polymer synthesis. We have used several approaches to provide the activation energy for this reaction. We nave found that if we either electronically excite the lithium or vibrationally excite the methane the reaction proceeds in a satisfactory manner. We have conducted an experiment in which the methane was heated to 900°C and obtained satisfactory results. Increased temperatures populate higher vibrational strates in the methane and thus allow a very significant decrease in the activation energy of the reaction. We also used a radio frequency source to excite the lithium vapor electronically and produced a successful reaction. Still another piece of work has been done using a methane plasma source which vibrationally excites the methane and allows the reaction to proceed.

In the study of tetralithiomethane, a fourth synthesis is being completed which involves intitial synthesis of dilithiomethane and

subsequent pyrolysis to give a substantial yield of tetralithiomethane.[6] Using this method we have obtained substantial quantities of tetralithiomethane. Extensive work has been done on solvent systems for tetralithiomethane so that one may do the polymer synthesis in solution. Several successful solvent systems are being developed and the concentrations of the polylithium compounds in solution are being determined by NMR studies and the preparation of derivatives.

An extensive study has been recently completed on the reactions of olefins with lithium vapor[7] A large number of new polylithium compounds such as tetralithio cyclohexadiene, 2,3 dilithio 2 butene, 2,3 tetralithio 2 butene, 1,2 dilithio isobutane, 1,4 dilithio 2 butene, and 1,2 trilithio isobutane have been prepared in this study. We have seen instances of both substitution for hydrogen on sites requiring a low activation energy for reaction and addition to double bonds. This study has established another general route to polylithium compounds.

Studies of reactions of inorganic species with lithium have also been undertaken. The reaction of silicon tetrachloride, $SiCl_4$, with lithium has been recently studied and the polylithium compound $SiLi_4$ was obtained in good yield. Hydrolysis and deuterolysis of the compound produced silanes and perdeutero silanes. A subsequent study of the reaction of tetralithiosilane with methyl chloride resulted in a

15% yield of tetramethyl silane indicating that the $SiLi_4$ is also a potential monomer. The reaction of BCl_3 and PCl_3 are currently under study. A fair yield of trimethylborane $B(CH_3)_3$ was obtained from the reaction of BLi_3 with methyl chloride. Additionally the synthesis of polylithiated carboranes has been attempted and a workup is now in progress. Isolation of a higher purity $SiLi_4$ is being undertaken. It should be pointed out that if the diamond syntheses from tetralithiomethane are successful, a synthesis of a silicon analog for a diamond will be attempted using the $SiLi_4$. Such a diamond-like silicon structure would have many unusual electrical and physical properties. This type of structure has been the object of numerous unsuccessful synthetic studies utilizing the phase diagram of silicon. This potentially valuable species has previously eluded all other synthetic approaches.

Recently structural studies have been initiated on several polylithium compounds. We have been interested in the lithium and carbon 13 NMR spectra and the laser-raman spectra of polylithium compounds both in solution and in the solid state. Very encouraging results have been obtained. Such studies will also lead to accurate methods for determination of concentration of reactive polylithium intermediates in solution and for identification of polylithium compounds.

The synthesis of diamonds which were proposed from the polylithium compounds is almost operational and a first attempt should be made within a month. A series of steel containers have been prepared for handling the polylithium compounds. These containers are cylindrical and have a length of about 3 inches and are 3 inches in diameter. Arrangements have been made to rent an ASEA high temperature - high pressure press from a local industrial firm. This press has reaction chamber dimensions of 6 inches in diameter by 20 inches in length, and is capable of pressures on the order of 35 kilobars at temperatures above 1200°C. The size of this high temperature reactor is indeed remarkable and results from a technological breakthrough within the last several years. Previously, high pressure chemistry had been limited to rather small volumes. These temperatures and pressures are not adequate for the synthesis of diamond by brute force methods involving graphite. We are very hopeful and thoroughly confident that our methods will generate diamonds at a much lower temperature and pressure. At this stage, of course, it would be impossible to predict the size of the diamonds. However, the reactors have been designed in such a manner that a successful experiment would result in many karats of diamonds. The fee for this press is about $650 per run and we are able to run approximately 10 reactions at once. This is done by placing a number of smaller steel containers

inside the large reaction container. Our laboratory has worked very hard in obtaining the samples for this work and we are awaiting results with great anticipation. Details of the proposed diamond syntheses are contained in the body of the original proposal.

1. C. Chung and R. J. Lagow, "The Reaction of Lithium Atoms at 1000°C with Chlorocarbons; A New Route to Polylithium Compounds", Chem. Comm. 1079 (1972).

2. L. A. Shimp and R. J. Lagow, "The Reaction of Carbon Vapor with Lithium Atoms; A Direct Synthesis of Polylithium Compounds". J. Amer. Chem. Soc. 95, 1343, (1973).

3. L. A. Shimp, C. Chung, J. A. Morrison and R. J. Lagow, "The Reaction of Lithium Vapor with Benzene." J. Am. Chem. Soc. (in press)

4. G. Lee and R. J. Lagow, "The Synthesis of Hexalithiobenzene" (to be published)

5. L. A. Shimp and R. J. Lagow, "The Reaction of High Temperature Lithium Vapor with Methane", (to be published).

6. J. A. Morrison and R. J. Lagow, "A New Synthesis for Tetralithiomethane," (to be published)

7. J. A. Morrison, C. Chung and R. J. Lagow, "The Reaction of High Temperature Lithium Vapor with Olefins; A Synthesis for Polylithium Compounds", J. Am. Chem. Soc. (in press).

SEMI-ANNUAL TECHNICAL REPORT #1

Period: July 1, 1973 - Dec. 31, 1973

Title: Research in Materials Sciences

Project Title: Fatigue and Fracture Properties of Austenitic Steels

Contract Number: DAHC 15-73-C-0316

ARPA Order Number: 2469

Program Code Number: 3D10

Name of Contractor: Massachusetts Institute of Technology
Cambridge, Mass. 02139

Principal Investigator: N.J. Grant (617) 253-5638

Project Scientists or Engineers: Prof. R. M. Pelloux (617) 253-3314

Effective Date of Contract: June 1, 1973

Contract Expiration Date: May 31, 1974

Amount of Contract: $425,000

Amount of Project: $ 33,500

Sponsored By
Advanced Research Projects Agency
ARPA Order No. 2469

TECHNICAL REPORT #1

July 1, 1973 - December 31, 1973

FATIGUE AND FRACTURE PROPERTIES OF AUSTENITIC STEELS

R.M. Pelloux
A.G. Pineau

255<

ABSTRACT

INFLUENCE OF STRAIN-INDUCED MARTENSITIC TRANSFORMATIONS ON FATIGUE CRACK GROWTH RATES IN STAINLESS STEELS

A.G. Pineau and R.M. Pelloux

The fatigue crack growth rates (FCGR) of two unstable austenitic stainless steels (Fe-16Cr-13Ni) and (Fe-18Cr-6.5Ni-0.19C) were determined in the M_s-M_d temperature range where a strain induced $\gamma \rightarrow \alpha'$ martensitic transformation occurs near the crack tip. These FCGR were compared to the rates measured in the stable austenitic phase of a Fe-31.5Ni and a Fe-34Ni alloy and in the martensitic phase obtained by quenching the Fe-31.5Ni alloy below M_s. In the Fe-31.5Ni alloy, the FCGR are an order of magnitude higher in the martensitic than in the austenitic structures for $\Delta K \leq 40$ ksi $\sqrt{in}$. The FCGR of the stainless steels decrease markedly when the test temperature approaches M_s in the M_s-M_d range. The FCGR for the alloy Fe-18Cr-6.5Ni-0.19C in a warm-worked condition are consistently higher than for the same alloy in the annealed condition for $\Delta K \leq 40$ ksi $\sqrt{in}$. The results are discussed in terms of the influence of phase structures, stacking fault energy and work hardening exponent on the FCGR.

INFLUENCE OF STRAIN-INDUCED MARTENSITIC TRANSFORMATIONS ON FATIGUE CRACK GROWTH RATES IN STAINLESS STEELS

A.G. Pineau and R.M. Pelloux*

INTRODUCTION

Martensitic transformations can be induced by plastic deformation in the temperature range M_s to M_d. M_s is the temperature for spontaneous transformation and M_d is the maximum temperature at which the transformation can be induced in a tensile test. A comparative study of these phase transformations in Fe-Ni-Cr-C alloys was recently completed by Lecroisey and Pineau (1). Depending upon the alloy composition, the M_s-M_d temperature range can vary from 30 to 200°C. The work hardening exponent and the UTS of an alloy undergoing strain-induced phase transformation increase markedly as the deformation temperature approaches M_s. The uniform elongation, which is also strongly dependent upon the test temperature, shows a well defined maximum in the M_s-M_d temperature range.

Following the results of Lecroisey and Pineau, it was decided to use some of those alloys for which the M_s and M_d temperatures and the tensile properties were well known, in order to study the influence of the strain induced martensitic transformation on the fatigue crack growth rate (FCGR). The aim of this investigation was to measure and compare the FCGR of the alloys in four different conditions:

a) Stable annealed austenite

b) Warm-worked austenite

c) Martensite formed by quenching below M_s

* A.G. Pineau is Maitre de Recherches at Centre des Materiaux de l'Ecole des Mines de Paris - 91 Corbeil Essonnes, France. R.M. Pelloux is Associate Professor, Massachusetts Institute of Technology, Cambridge, Mass. 02139

d) Strain-induced martensite at the fatigue crack tip in an austenitic matrix.

The alloys tested in condition (a) were Fe-Ni compositions and two stainless steels, a 16-Cr-13Ni and a type 301 steel with a high carbon content. This last alloy was also tested in condition (b), because it is representative of a new class of high strength, high toughness steels referred to as TRIP steels. The comparison between the FCGR in austenite and martensite (conditions a and c) was made on a Fe-31.5Ni alloy. The influence of the strain induced martensitic transformation on the FCGR (condition d) was determined for the two stainless steels which were tested at various temperatures in the M_s-M_d temperature range.

Most of the fatigue crack growth rate tests were performed in dry argon to minimize the effect of humidity. Microhardness measurements were used to determine the plastic zone sizes and to assess the degree of cyclic hardening or softening near the crack tip. The microscopic crack growth rates were measured by electron microscopy and compared to the overall growth rates.

The test results serve as a basis for the evaluation of the influence of austenite stacking fault energy, work hardening exponent and phase structure on fatigue crack growth rates.

EXPERIMENTAL PROCEDURE

1. Materials - Composition and Preparation

The chemical analysis of all the alloys are given in Table I. The Fe-Ni and 16-13 alloys were induction melted under vacuum and cast as 20 lb. ingots. These ingots were cut length-wise into two pieces, reduced 50% by hot rolling and homogenized for 70 hours at 1200°C under argon. They were finally hot rolled to plates of 9 mm in thickness.

Tensile specimens cut parallel to the rolling direction were sealed in

evacuated vycor capsules and given the austenitizing treatment reported in Table I, followed by water-quenching. The austenitizing conditions were selected to give a final grain size of approximately 100 microns.

A 200 lb. heat of a 301 type stainless steel was used to compare the tensile and fatigue properties of annealedand warm-worked austenite. The annealed 301 specimens were heat treated and prepared in the same manner as the Fe-Ni and 16-13 alloys. The warm-worked specimens were obtained by annealing 25 mm thick plates at 1120°C followed by water quenching and by rolling 65% at 450-500°C. The reduction of thickness from 25 to 9 mm was achieved in about 10 passes. Between each pass, the plates were reheated to 500°C in a salt bath furnace. The total warm-working operation took approximately 30 minutes. Tensile specimens parallel and perpendicular to the rolling direction were cut from these warm-worked plates.

Double cantilever beam fatigue specimens were cut from 9 mm thick plates, rough machined, annealed at the temperatures given in Table I and water - quenched. Cutting of the notch and final machining was always done after the final quench in order to minimize residual stresses. In the fatigue tests, the notch was perpendicular to the rolling direction. The phase transformation temperatures (M_s and M_d) were determined by the same methods which have been used previously (1,2).

2. Mechanical Properties

2:1 Tensile tests

Cylindrical tensile specimens of 3 mm diameter and 30 mm gage length were tested at a deformation rate of 2.8×10^{-3} sec^{-1}. The specimens were immersed in liquid baths (liquid nitrogen, alcohol + dry ice, oil) controlled to $\pm$ 2°C in the range -196°C to 150°C. In the two stainless steels and the Fe-31.5 alloy, the intensity of magnetization was measured continuously during

tensile tests. The magnetic measurements were carried out by using a double-coil device described elsewhere (2). These measurements give a good estimate of the volume fraction (f) of strain induced α' martensite.

2:2 Fatigue tests

Double cantilever beam specimens were used for the fatigue crack propagation tests. The specimens dimensions were 70 mm wide x 67.2 mm high x 7 mm thick. The original notch length was 32.5 mm. The tests were run at 20 Hz with sinusoidal tension stress waveform (R = 0.05) in a load controlled closed loop hydraulic fatigue machine. Crack lengths were measured to an absolute accuracy of 0.02 mm. The stress intensity range Δ K was measured from the following equation (3):

$$\Delta K = \frac{\Delta P}{BW^{1/2}} \left[29.6\left(\frac{a}{w}\right)^{1/2} - 185.5\left(\frac{a}{w}\right)^{3/2} + 655.7\left(\frac{a}{w}\right)^{5/2} - 1017\left(\frac{a}{w}\right)^{7/2} + 638.9\left(\frac{a}{w}\right)^{9/2}\right]$$

with Δ P the applied load range; a = crack length; w = 56 mm; B = 7 mm. The da/dN measurements were taken only after the initial fatigue crack length increment had reached a value between 0.5 and 1 mm.

Most of the tests were run in an inert argon environment (less than 200 ppm of water vapor). For tests run in air at 25°C, the humidity was between 20 and 60%. An air-tight temperature chamber was built for tests at various temperatures between -30°C and 100°C. The low temperatures were achieved by passing cold alcohol in a copper coil within the test chamber. Heating tapes were used for the experiments above 25°C. The temperature of the specimen was measured with a thermocouple and was controlled to ± 2°C.

2:3 Metallography and microhardness measurements

Microhardness measurements at mid-thickness of the fatigue specimens were used to determine the plastic zone sizes on each side of the fatigue fracture surfaces. The measurements were made at different crack lengths in

a direction perpendicular to the plane of fracture. The fracture edge was protected by an edge retainer made of a mixture of epoxiresin and silicon carbide and/or iron powders (600 mesh). Mechanical polishing was followed by electropolishing. The microhardness measurements were made with a micro - durimet Leitz with a hardness load of 25 g , except for the warm-worked 301 steel which required a 50 g load.

The fracture surfaces of fatigue specimens were studied both by scanning and transmission electron microscopy. The microscopic growth rates were obtained by measuring the average spacing of fatigue striations (i) in a direction parallel to the microscopic crack growth direction. For striation spacings lower than about 0.1 - 0.2 micron all the measurements were made on Cr-shadowed carbon replicas.

2:4 X-ray measurements

The amount of martensite on the fracture surface of 301 fatigue specimens tested at -30°C and 25°C was determined by X-ray diffraction. A comparison of the integrated intensity of the (311) austenite peak with the (220) martensite peak was made. CoKα radiation was used and the standard corrections were employed. (4)

RESULTS

1. Transformation Temperatures

The $M_s(\gamma \rightarrow \alpha')$ and $M_d(\gamma \rightarrow \alpha')$ temperatures are given in Table 1. The martensitic transformation $\gamma \rightarrow \varepsilon$ (hcp) also occurs in the two stainless steels. In alloy 16-13, the $M_s(\gamma \rightarrow \varepsilon)$ temperature coincides with $M_s(\gamma \rightarrow \alpha')$. On the other hand, in an alloy very similar to the 301 steel studied in this work, it was shown by Abrassart (5) that the $\gamma \rightarrow \varepsilon$ martensitic transformation does occur at a temperature above $M_s(\gamma \rightarrow \alpha')$. After quenching the 301 alloy to room temperature, only a few ε platelets were observed, while after quenching

to -196°C (below M_s ($\gamma \rightarrow \alpha'$)) , the structure of the 301 steel consists of α' martensite laths imbedded in bands containing ε platelets (Fig. 1).

2. Tensile Properties

Fe-Ni alloys

Tensile curves at 25°C are reported in Figure 2. The high yield strength of these austenitic alloys has been attributed to the ferromagnetic properties of these compositions (6). After quenching to -196°C, the amount of residual austenite in alloy Fe-31.5Ni is low and the tensile curve given in Figure 2 is comparable to that of a material which is nearly completely martensitic. The phase transformation $\gamma \rightarrow \alpha'$ leads to an increase in the yield strength and a decrease in the elongation.

Stainless steels

Tensile curves σ- ε and magnetization curves J-ε of 301 steel and 16-13 alloy are given respectively in Figures 3 and 4. In both alloys, the same qualitative behaviour is observed when the temperature is decreased within the M_s-M_d range. The following results should be kept in mind:

a) the elastic limit is not strongly temperature dependent as is usually the case for FCC materials tested near 25°C.

b) a strong increase in the hardening rate is observed as the deformation temperature approaches M_s. At 25°C, the monotonic strain hardening rate of 301 steel is higher than that of 16-13 alloy, mainly because the volume of strain-induced α' martensite at a given plastic strain is higher at this temperature in the 301 steel than in the 16-13 matrix.

c) At low temperatures, e.g. -45°C for 16-13 alloy and -30°C for 301 steel, for the same volume of transformed α' phase, the flow stress of 301 steel is higher than that of 16-13 alloy. This difference is mainly due to the difference in carbon content of the two alloys.

d) The rapid change in the work hardening exponent with decreasing temperatures in the M_d-M_s range results in large variations of the uniform elongation (Fig. 5). This behaviour is in agreement with results on stainless steels (1,7).

The tensile properties of 301 steel, in warm-worked condition, are reported in Table 2. At 25°C, the $\gamma \rightarrow \alpha'$ transformation results in a lower work hardening exponent for the warm-worked alloy than for the annealed alloy. At 25°C, the typical UTS/YS ratios are 1.23 for the warm-worked condition and 3.78 for the annealed alloy.

3. Fatigue Properties

3:1 Fatigue crack growth rates (FCGR)

FCGR in austenite compared with FCGR in martensite

The crack growth rates da/dN versus ΔK of the Fe-Ni alloys at 20°C are reported in Figure 6. The FCGR in Fe-34 alloy which has a higher yield strength than that of Fe-31.5 steel are slightly lower. In the Fe-31.5 alloy transformed to martensite by quenching to -196°C, the FCGR are an order of magnitude faster than for the austenite, for $\Delta K \leq 25$ ksi $\sqrt{in}$. Moreover, the slope of the da/dN - ΔK curve is lower for the martensite than for the austenite phase. The macroscopic crack growth rates measured in martensite and the slope of the da/dN - ΔK curve are in good agreement with those rates reported by Bathias (8) and van Swam(9) for Maraging steels which are also Fe-Ni martensites

FCGR and strain-induced martensitic transformations

The FCGR of the 16-13 alloy at three different temperatures in the M_s-M_d range are given in Figure 7. The propagation rates decrease with decreasing temperature. No significant change in the slope of the da/dN - ΔK curves are observed in the range of temperatures and ΔK which were studied.

In annealed and warm-worked 301 steel, the results of da/dN measurements are reported in Figure 8. A strong temperature dependence is observed between 95°C ($\approx M_d$) and -30°C for the annealed alloy. The FCGR and the slopes of the da/dN - ΔK curves decreased when the temperature approaches M_s. For $\Delta K \geq 35$ ksi $\sqrt{in}$, the FCGR at 30°C is an order of magnitude slower than at 95°C. Tests in air gave a propagation rate which was significantly higher than in dry argon. This difference could be due to the influence of humidity on crack growth rate in transformed α' martensite present at the crack tip. However, it is worthwhile to note that Shahinian et al (10) have also reported an increased growth rate due to humidity in air in a 304 stainless steel, tested at 25°C, although their alloy was more stable than the 301 alloy investigated here.

The fatigue behaviour of the 301 alloy in the warm-worked and in the annealed conditions is markedly different. Even without any large amount of α' strain-induced phase transformation (θ = 85°C), da/dN is significantly higher for low ΔK ($\Delta K \leq 40$ ksi $\sqrt{in}$) in the previously warm-worked structure. The results obtained with warm-worked 301 alloy are compared in Figure 8 with those results of Chanani et al (11) on another TRIP steel which was subjected to a thermomechanical treatment similar to that applied to the 301 steel. These authors performed all their tests in air on relatively thin sheet specimens (≈ 1.90 mm thick).

3:2 Plastic zone sizes measurements

Figure 9 shows two typical plots of hardness versus distance from the fracture surface, for the Fe-34Ni alloy. Each hardness curve shows two plateaus which clearly define the boundaries of the two plastic zones usually referred to as the monotonic (Rm) and the reversed (Rr) plastic zones.

Microhardness measurements were also used for the 301 steel both in

annealed and warm-worked conditions (Table 3). The annealed 301 steel shows a similar behaviour to that of the Fe-34Ni alloy. However, the heterogeneity of the phase transformations at the crack tip gives a large scatter of measurements. The high yield strength of the warm-worked steel leads to smaller plastic zone sizes and the reversed plastic zones could not be unambiguously identified for Rm $\leq$ 0.2 mm. Moreover, when there is no strain - induced $\gamma \rightarrow \alpha'$ transformation, the warm-worked alloy cyclically softens.

3:3 Metallography

Optical microscopy and X-ray observations

Optical metallography showed a qualitative agreement between the structures observed in tensile and fatigue specimens. Platelets present near the fracture surfaces at 95°C are twins and/or ε martensite (Fig. 10a). Testing with a strong magnet showed that the fracture surfaces of specimens tested at this temperature were not magnetic. On the other hand, at -30°C, the amount of phase transformation inside the plastic zone is significant (Fig. 10b). X-ray measurements showed that the amounts of α' martensite were respectively ≈100% at -30°C and ≈50% at 25°C.

Fractography

Fractographic investigation was limited to the stainless alloys. These steels exhibited flat transgranular fracture in all specimens tested. The fracture surfaces were much rougher at low ΔK than at high ΔK, while the fracture surface inside a given grain is flatter at high ΔK. Microscopic fracture features which could be associated with the martensitic transformations were observed (Fig. 11a, b).

The main difference between the two steels was the tendancy to form secondary cracks. In 301 alloy, secondary cracks were occasionally observed only at high ΔK. On the other hand, in 16-13 alloy, even for low ΔK

($\approx$ 25 ksi $\sqrt{in}$), a high density of secondary cracks was present (Fig. 12a, b). In the 301 steel, at high growth rates (e.g. at 95°C, $\Delta K \approx 40$ ksi $\sqrt{in}$), the fracture surfaces exhibited extensive tear dimples.

Striation spacings measurements for the two stainless steels are reported in figures 13 and 14. Each datum point corresponds to the mean value of the distance between at least 20 striations. Measurements were taken with the SEM for $i \geq 0.2$ micron and a good agreement between measurements made by SEM and electron microscopy of replicas was obtained in this range of growth rates.

In both alloys, it is observed that the microscopic crack growth rates decrease with the macroscopic rateswith decreasing temperatures. The slopes of the i - ΔK curves increase when the amount of strain induced α' martensite increases, and the slopes of these curves are quite high (≥ 5) even when there is no $\gamma \rightarrow \alpha'$ phase transformation.

DISCUSSION

1. Plastic Zone Sizes - Cyclic Hardening and Softening at the Crack Tip

Microhardness measurements at different depths below the fracture surfaces gave an excellent estimation of the monotonic and reversed plastic zone sizes. The results reported here are similar to the results obtained by Bathias (8). The monotonic plastic zone sizes which are reported in Figure 15 are in good agreement with the theoretical sizes given by the equation $R_m = A(\frac{\Delta K}{\sigma_y})^2$. The values of σ_y were obtained from low strain rate tensile tests. The experimental value of 0.053 for A is one half of the value found by Hahn et al for a Fe-3Si alloy (12) and one third of the theoretical value of 0.157 given by Levy et al (13) for the plane strain plastic zone size of a non-hardening plastic material. The difference between the measured and theoretical values of A could be related to the high monotonic workhardening

exponent of the stainless steels. When the reversed plastic zone was large enough to be measured by microhardness indentations, the zone was approximately one fourth of the size of the monotonic plastic zone which is in agreement with Rice's model of reversed yielding at the tip of a fatigue crack. (14)

The only alloy which exhibited cyclic softening at the crack tip was the warm-worked 301 stainless steel at a test temperature near M_d. This softening behaviour could be predicted from the value of the ratio of UTS to σ_y. At θ = 95°C (Table 2), this ratio is 1.05, which is lower than the critical value of 1.2 for cyclic stability (15). At 25°C, the same alloy undergoes cyclic hardening because the martensitic transformation at the crack tip offsets the cyclic softening of the warm-worked austenite. The difference between cyclic softening at 95°C and cyclic hardening at 25°C is not reflected in a marked change in the slopes of the da/dN - ΔK curves (see Fig. 8).

2. Crack Growth Rate in Stable Austenite

2:1 Influence of SFE and deformation modes on FCGR

By comparing the FCGR of different copper base alloys, some authors (16-19) have concluded that a decrease in intrinsic stacking fault energy (SFE) will lower the fatigue crack growth rate. Since the SFE of the austenitic steels used here were known, it is worthwhile to compare the FCGR of the alloys on the basis of SFE levels.

The austenitic alloys studied here can be conveniently grouped in two classes, depending upon their SFE:

(i) the SFE of the Fe-Ni alloys is greater than 50 ergs/cm^2 and they deform only by slip. The yield strength of these ferromagnetic austenites is relatively high.

(ii) the SFE of the two stainless steels is much lower than the Fe-Ni

alloys. It is of the order of 25 - 30 ergs/cm^2 at M_d (1,5). This low value for the SFE results in plastic deformation by a) twinning at 90°C for the 16-13 alloy; b) twinning and $\gamma \rightarrow \varepsilon$ martensitic transformation at 95°C for the 301 steel.

The FCGR of the Fe-34Ni and the annealed 301 alloy are comparable, although the SFE and deformation modes are quite different. On the other hand, a comparison of the FCGR of the two Fe-Ni alloys and the two annealed stainless steels shows that the FCGR decreases with increasing yield stress (Fig. 16). It is well known that this correlation is not observed in quenched and tempered high strength steels such as maraging steels (8,9). which usually work soften at the crack tip. However, the warm-worked 301 steel which work-softens at 85°C shows a higher FCGR than the annealed material although their yield strengths differ by a factor of 5.

It is tentatively concluded that the FCGR decreases with increasing tensile yield stress as long as the alloy undergoes cyclic hardening or is cyclically stable.

2:2 Macroscopic and microscopic FCGR

A detailed comparison between da/dN and the striation spacing (i) was made for the two stainless steels. The crack propagation rates (da/dN) measured in these two alloys near the M_d temperature are similar to those reported for different stable commercial stainless steels tested at 25°C (8, 10, 20, 21).

The FCGR behaviour of 301 steel is typical, that is at low ΔK, i < da/dN and i > da/dN at high ΔK. At low ΔK, the difference between i and da/dN shows that crack growth is discontinuous along the crack front. At high ΔK, static fracture modes such as ductile void formation accelerate the growth rate, and the transition where the i and da/dN versus ΔK curves cross

over corresponds to the appearance of voids on the fracture surfaces. In 16-13 alloy, it is more difficult to compare the microscopic and macroscopic growth rates because of the extensive density of secondary cracks.

It is worthwhile to note that the same $i - \Delta K$ dependence was found for both alloys (Fig. 13, 14) and that the slopes of the $i - \Delta K$ curve are greater than the value of 2 which is predicted by a simple crack growth model based on the crack opening displacement (COD) concept. Slopes greater than 2 have also been measured by Weber and Hertzberg (21) in a 305 stainless steel. Moreover, the experimental values for i are at least one order of magnitude lower than the values predicted by the COD model, that is $i \approx 0.25 \frac{\Delta K^2}{E\sigma_{yc}}$, taking a cyclic yield strength σ_{yc} of 115 ksi for a 301 steel (22).

3. Influence of Strain -induced Martensitic Transformation on FCGR

Since the influence of the strain-induced phase transformation on the FCGR was studied by varying the test temperature, we must first determine the effect of a temperature change on the mechanical and physical properties which could affect the FCGR.

For stainless steels, the variation of the SFE (γ) with temperature is given by $d\gamma/dT \approx -0.10$ ergs/cm^2° K (5,23,24). Thus, in the relatively narrow temperature range used here, the value of γ changes by a factor less than 2. Furthermore, as discussed above , it is felt that the SFE is not a critical factor in controlling the FCGR. The Young modulus (E) will increase by about 3% for a decrease in temperature of 100 to 150°C. This variation of E will not markedly affect the COD or the elastic strain distribution near the crack tip.

It can therefore be concluded that the change in FCGR with temperature is unambiguously due to the strain induced martensitic transformation. The

temperature dependence appears to be related to the relative amount of martensite formed near the crack tip. Metallographic observations and X-ray diffraction analysis of the plastic zone show that the amount of α' martensite increases with decreasing temperature. It remains then to explain how the phase transformation will lead to a lower FCGR and to a decrease in the da/dN - ΔK slope with decreasing temperature. This change of slope was observed only in the 301 stainless steel which exhibited the larger volume fraction of transformed α'.

The lower growth rates with a greater amount of phase transformation are not due to the fact that the FCGR in martensite is lower than the FCGR in austenite. On the contrary, the results on Fe-31.5Ni alloy showed that the FCGR in the fully austenitic condition was lower than in the fully martensitic condition. However, in this alloy, the slope of the da/dN - ΔK curve is lower in martensite than in austenite. This difference in slopes could explain the lower slopes observed in 301 steel when the test temperature is decreased.

The influence of the strain-induced phase transformation on the FCGR can best be explained by considering the concomittant changes of the monotonic and cyclic work hardening coefficients. The marked increase in the cyclic work hardening coefficient due to $\gamma \rightarrow \alpha'$ phase transformation was reported previously (22). Currently, there is no complete FCGR theory which takes into account the influence of both the monotonic (n) and the cyclic (n') work hardening coefficients. The theoretical models of the da/dN - ΔK laws can be conveniently grouped in two broad classes; a) the work hardening or integrated damage theories, and b) the COD theories based on a plastic deformation and fracture criteria at the crack tip. In all these theories, higher monotonic and cyclic hardening coefficients will lower the FCGR.

The theory of Head (25), which represents the plastic zone at the crack tip by rigid work hardening elements, shows da/dN varying as $\frac{1}{UT - \sigma_y}$. In the 301 steel, this ratio increases by a factor of 3 between 95°C and -30°C, while the growth rate decreases by a factor of 20 for $\Delta K \geq 40$ ksi.

It can also be shown that an increase of the monotonic and cyclic work hardening coefficients will lead to a decrease of the strain gradient in the plastic zone near the crack tip. For instance, for a work hardening material $\sigma = A\varepsilon_p^{n}$, the monotonic strain distribution in the plastic zone will be given by $\varepsilon_p = \varepsilon_y(\frac{R}{r} - 1)^{1/1-n}$, where R is the plastic zone size and r the distance to the crack tip (26). Due to the fact that n' increases as well as n, the cyclic plastic strains distribution within the plastic zone will also be more uniform. Thus, the integrated damage criteria proposed by McClintock (27) should lead to a decreasing FCGR when n and n' increase.

Although the COD model cannot accurately account for the observed propagation rates (cf. 2:2), it is worthwhile to use this concept to estimate qualitatively the influence of the martensitic transformation on the cyclic yield stress and on the work hardening exponent. The phase transformation at the crack tip results in a marked increase in the cyclic elastic limit which lowers the COD at a given ΔK level. For instance, the cyclic stress strain curves of a 301 type steel showed that σ_{yc} at -30°C is 3 to 6 times higher at -30°C than at 90°C. σ_{yc} depends strongly upon the value of the permanent offset plastic strain at which it is measured. McClintock also showed that, theoretically, the COD decreases when the monotonic work hardening coefficient increases (28).

However, these predicted changes of the FCGR due to the variation of σ_{yc} and of the work hardening coefficients are not as large as the observed variations of FCGR with decreasing temperatures, particularly at high ΔK

levels. It is felt that the residual stresses near the crack tip and along the flanks of the crack behind the tip may play an important role in controlling the FCGR when strain induced $\gamma \rightarrow \alpha'$ phase transformation is taking place. The role of residual stresses has been demonstrated by the work of Elber, who introduced the concept of effective stress intensity factor (29,30). At this time, we do not have any theoretical approach to predict the distribution of residual stresses. We can only say qualitatively that the high cyclic yield and ultimate tensile stresses resulting from the α' phase transformation could lead to very high residual stresses which would lower the value of ΔK effective for a given ΔK applied. These residual stresses appear to be very stable and to resist any cyclic shakedown due to reversed plastic deformation within the plastic zone.

CONCLUSIONS

1. The FCGR of metastable stainless steels were found to be strongly temperature dependent in the M_s-M_d temperature range. At a given ΔK level, the FCGR decrease as the volume fraction of strain-induced $\gamma \rightarrow \alpha'$ phase transformation at the crack tip increases with decreasing temperature.

2. In the stable austenites, the FCGR do not depend upon the intrinsic stacking fault energy or upon the deformation modes of the austenites. It is found that in the annealed austenites, the FCGR will decrease when the monotonic tensile yield stress increases.

3. In a Fe-31.5Ni alloy, the FCGR is higher in the martensitic structure than in the annealed austenite for $\Delta K \leq 25$ ksi $\sqrt{in}$.

4. A 301 type stainless steel has a lower fatigue crack growth resistance in the high strength warm-worked condition than in the annealed austenitic condition for $\Delta K \leq 40$ ksi $\sqrt{in}$.

5. The monotonic and reversed plastic zone sizes which were determined by

microhardness measurements are in good agreement with the sizes predicted from theoretical models.

6. The influence of the strain-induced martensitic phase transformation on the FCGR in the M_s-M_d range is attributed to the strong concomittant variations of cyclic and monotonic work hardening exponents and to residual stresses left near the crack tip and along the flanks of the fatigue fracture surfaces.

ACKNOWLEDGMENTS

This work was supported by DAHC 15-73C-0316.

The X-ray measurements were performed by Professor Van Der Sande, Dept. of Metallurgy, M.I.T.

REFERENCES

1. F. Lecroisey and A. Pineau, Met. Trans, 1972, Vol. 3, p. 387.
2. F. Abrassart, F. Lecroisey and A. Pineau, Mem. Sci. Rev. Met., 1969, Vol. 66, p. 805.
3. ASTM Standard E 99 - 70T.
4. B.D. Cullity, Elements of X-ray Diffraction, Addison-Wesley Co. (1967), p. 388.
5. F. Abrassart, Thesis (Sc.D), University of Nancy, 1972.
6. G.F. Bolling and R.H. Richman, Phil. Mag., 1969, Vol. 19, p. 247.
7. J.P. Bressanelli and A. Moskowitz, ASM Trans Quart., 1966, Vol. 59, p. 223.
8. C. Bathias and R.M. Pelloux, Met. Trans, 1973, Vol. 4, p. 1265.
9. L.F. van Swam, Thesis, (Sc.D), M.I.T., Cambridge, 1973.
10. P. Shahinian, H.E. Watson and H.H. Smith, J^{al} of Materials, 1972, p. 527.
11. G.R. Chanani, D.S. Antolovich and W.W. Gerberich, Met. Trans, 1972, Vol.3, p. 2661.
12. G.T. Hahn, M. Sarrate and A.R. Rosenfield, Int^{al} Jal of Fract. Mech., 1971, Vol. 7, p. 435.
13. N. Levy, P.V. Marcal, W.J. Ostergren and J.R. Rice, Int^{al} Jal of Fract. Mech., 1971, Vol. 7, p. 142.
14. J.R. Rice, ASTM STP 415, 1966, p. 247.
15. R.W. Smith, M.H. Hirschberg, S.S. Manson, NASA TND -1574, 1963.
16. A.J. McEvily and R.C. Boettner, Acta Met., 1963, Vol. 11, p. 725.
17. G.A. Miller, D.H. Avery and W.A. Backofen, Trans. AIME, 1966, Vol. 236, p. 1667.
18. H. Ishii and J. Weertman, Met. Trans., 1971, Vol. 2, p. 3441.
19. C.M. Wan and J.G. Byrne, "Fracture", Brighton Conf. 1969, p. 598.
20. L.E. James and E.B. Schwenk, Met. Trans., 1971, Vol. 2, p. 491.

21. J.H. Weber and R.W. Hertzberg, Met. Trans.,1973, Vol. 4, p. 595.

22. A. Pineau, L.F. van Swam and R.M. Pelloux, Scripta Met., 1973, Vol. 7, p. 657.

23. F. Lecroisey and B. Thomas, Phys. Stat. Sol. (a), 1970, Vol. 2; K.217

24. R.M.Latanisonand A.W. Ruff, Met. Trans., 1971, Vol. 2, p. 505

25. A.K. Head, Phil. Mag., 1956, Vol. 44, Ser. 7, p. 925.

26. J.R. Rice and G.F. Rosengren, Jal Mech. Phys. Solids, 1968, Vol. 16, p.1.

27. F.A. McClintock, Fracture of Solids. John Wiley, New York, 1963, p. 65.

28. F.A. McClintock, Fracture, Academic Press, New York and London, 1971, Vol. 3, p. 47.

29. W. Elber, ASTM STP 486, p. 230.

30. W. Elber, Eng. Fracture Mechanics, 1970, Vol. 2, p. 37.

TABLE I

Alloy compositions (weight %) - Heat treatments - Austenite grain sizes - Transformation temperatures

Type	Composition				M_s (°C)	M_d (°C)	Water-quenched	grain size (microns)
	Ni	Cr	C	Fe				
Fe-34Ni	34.09		0.005	Bal	<-196		1000°C (1 1/2 hr)	70
Fe-31.5Ni	31.41		0.004	"	-45	5	1000°C (1 1/2 hr)	70
16-13	12.50	15.8	0.010	"	-75	80	1100°C (1 hr)	80
301	6.50	18.25	0.19	"	-100	100	1120°C (1 hr)	110

TABLE II

Tensile properties of alloy 301 warm-worked 65% at 450°-500°C

Test temperature (°C)	Yield strength (ksi)	Ultimate tensile strength (ksi)	Total Elongation	Test direction
95	148	154.6	15.1	longitudinal
25	153.5 164	188.5 188.5	45.5 40.3	longitudinal transverse

TABLE III

Plastic zone sizes measurements

Alloy	Condition	Test temperature(°C)	ΔK MPa $\sqrt{m}$	Rm (mm)	Rr (mm)	Rm/Rr	Cyclic behaviour
Fe-34Ni	Annealed	25	27.8	1	0.20	5	hardening
"	Annealed	25	41.4	2.30	0.40	5.8	hardening
301	Annealed	25	28.9	0.80	0.18	4.4	hardening
"	Annealed	25	42.9	2.25	0.50	4.5	hardening
301	warm-worked	90	52.6	0.150			softening
"	warm-worked	25	41	0.150			hardening
"	warm-worked	25	70	0.350	0.08	4.4	hardening

Figures

Fig. 1 - Alloy 301: α' martensite imbedded in ε platelets bands following quenching to -196°C.

Fig. 2 - Fe-Ni alloys: tensile stress-strain curves at 25°C.

Fig. 3 - Alloy 301: tensile stress-strain curves and magnetization (J) - strain curves at different test temperatures - (100% martensite corresponds to J ≈ 14,000 gauss).

Fig. 4 - Alloy 16-13: tensile stress-strain curves and magnetization (J) - strain curves at different test temperatures - (100% martensite corresponds to J ≈ 14,000 gauss).

Fig. 5 - Elongation δ versus test temperature: uniform tensile elongation versus test temperature for alloys 16-13 and 301.

Fig. 6 - Fe-Ni alloys : fatigue crack growth rates as a function of ΔK at 20°C.

Fig. 7 - Alloy 16-13 : fatigue crack growth rates as a function of ΔK at different temperatures.

Fig. 8 - Alloy 301 : fatigue crack growth rates of annealed and warm-worked 301 steel at various temperatures. At θ = 20°C, the warm-worked 301 alloy was tested in the transverse direction (TD) and longitudinal direction (LD).

Fig. 9 - Alloy Fe-34Ni: plastic zone size determination by microhardness measurements at two ΔK levels.

Fig. 10 - Alloy 301 : metallographic evidence of the reversed plastic zone size below the fracture surface. (a) θ = 25°C, ΔK = 26.7 ksi $\sqrt{in}$; (b) ΔK = 42.6 ksi $\sqrt{in}$, θ = -30°C. The edges of the plastic zones are indicated by an arrow.

Fig. 11 - Alloy 301 : typical fracture lamellae which are associated with the transformed martensitic structures (θ = 25°C). (a) ΔK = 43 ksi $\sqrt{in}$; (b) ΔK = 26.5 ksi $\sqrt{in}$.

Fig. 12 - Alloy 16-13 : typical fracture features at 90°C. The density and residual opening of the secondary cracks are higher in fig. 12b (ΔK = 31.6 ksi $\sqrt{in}$) than in fig. 12a (ΔK = 23.3 ksi $\sqrt{in}$).

Fig. 13 - Alloy 16-13 : comparison of the macroscopic and microscopic (i) crack growth rates at 90° and 20°C.

Fig. 14 - Alloy 301 : comparison of the macroscopic and microscopic (i) crack growth rates at 95° and 20°C.

Fig. 15 - Measurements of monotonic plastic zone sizes (Rm) versus $(\Delta K/\sigma_y)^2$.

Fig. 16 - Fatigue crack growth rates of different stable austenites as a function of ΔK. The tensile yield strength of each alloy is given for reference.

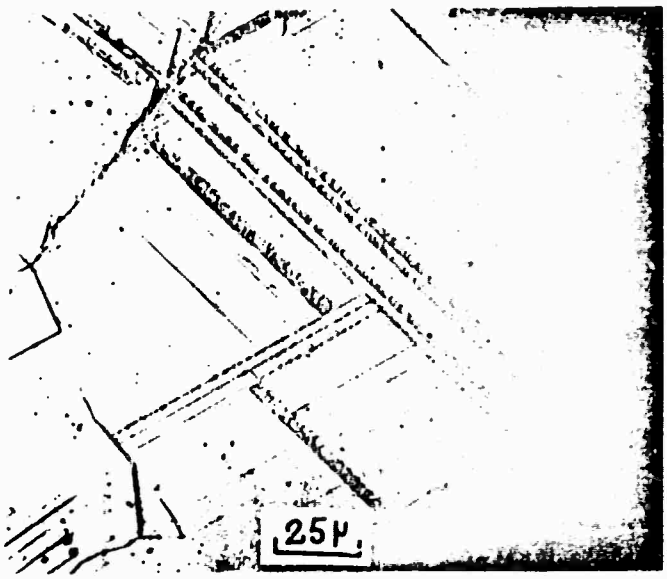

Fig. 1

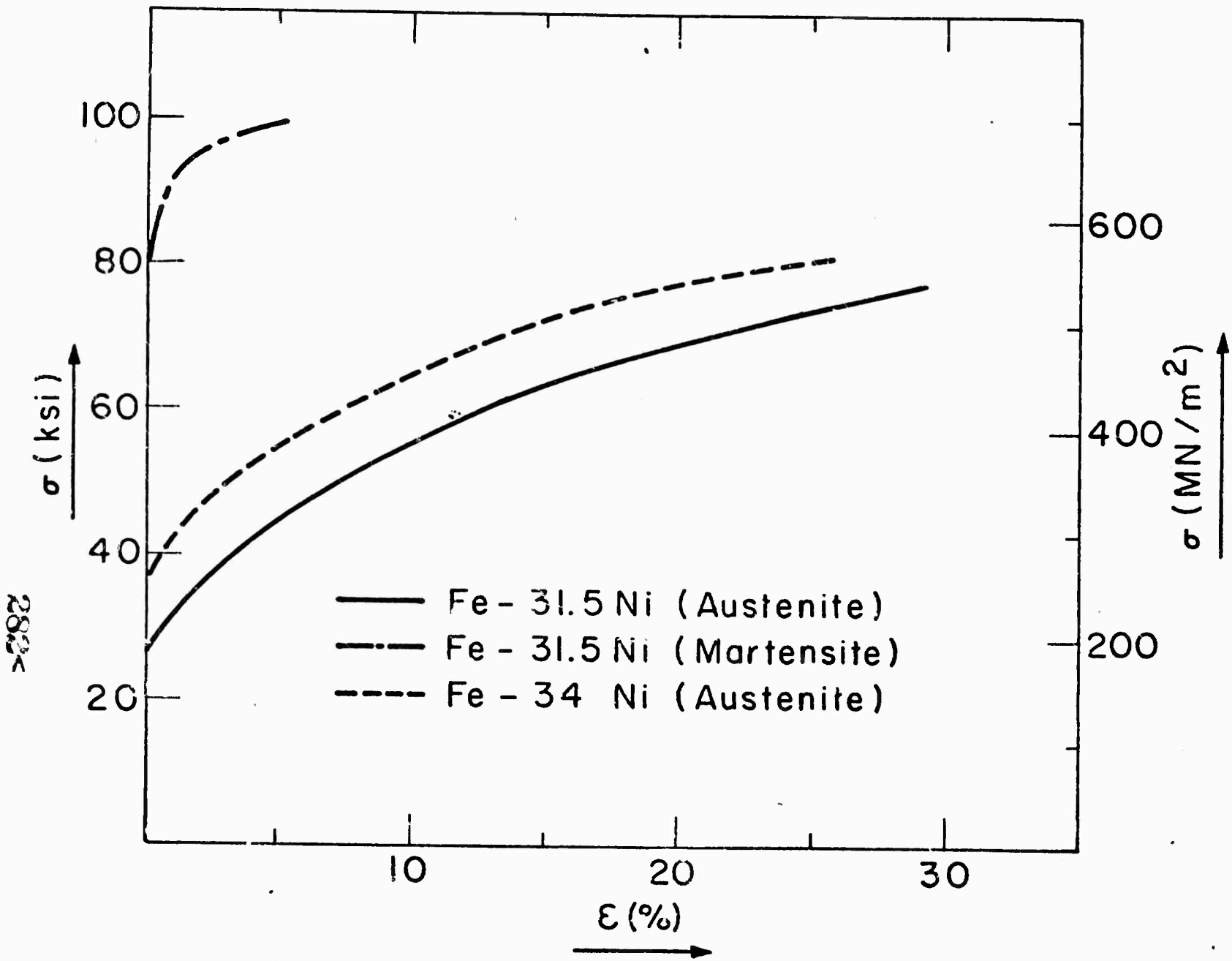
100
80
60
40
20
σ (ksi)
600
400
200
σ (MN/m²)
10
20
30
ε (%)
Fe - 31.5 Ni (Austenite)
Fe - 31.5 Ni (Martensite)
Fe - 34 Ni (Austenite)

Fig. 2

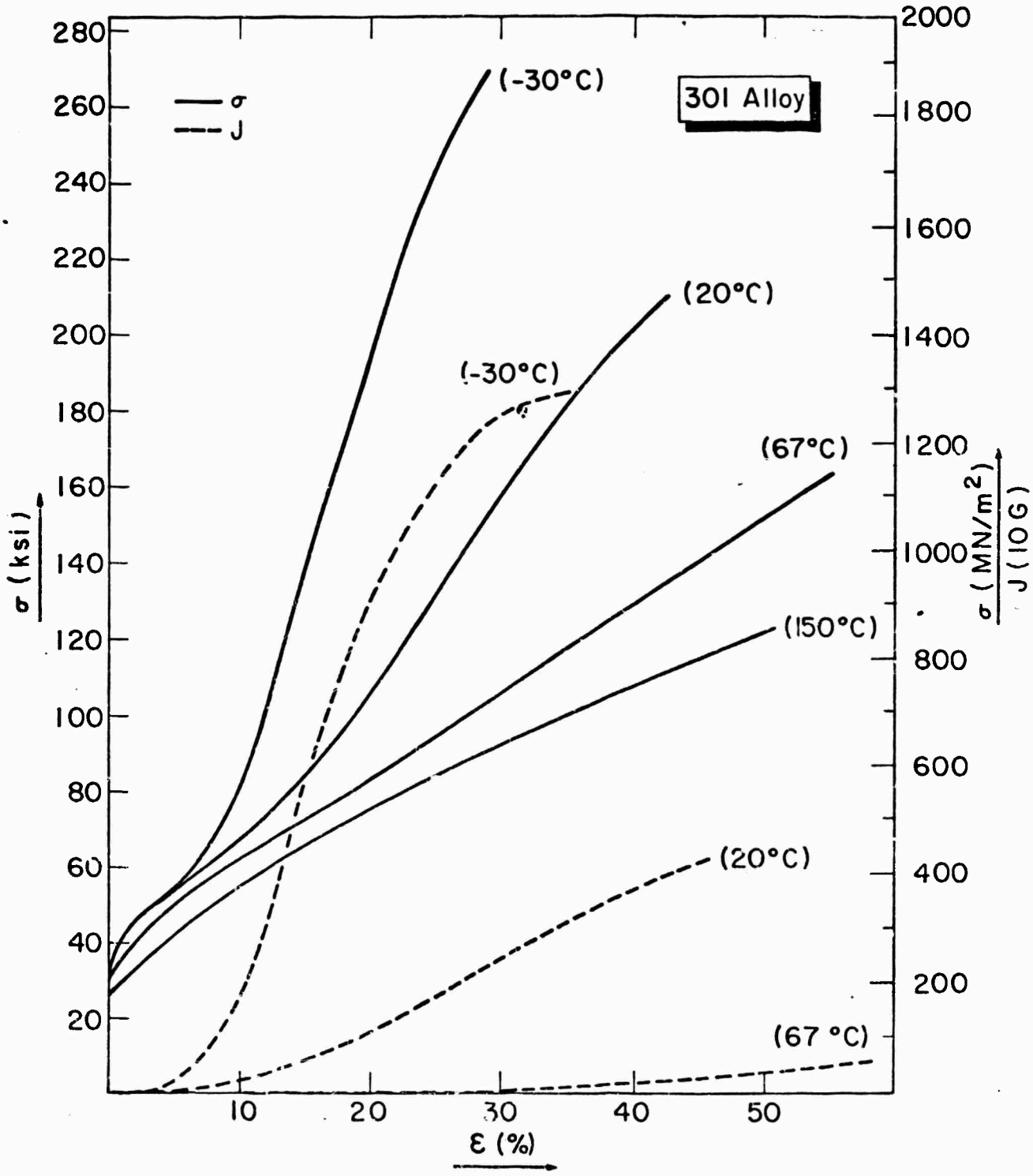
σ
J
301 Alloy
(-30°C)
(20°C)
(-30°C)
(67°C)
(150°C)
(20°C)
(67 °C)
σ (ksi)
σ (MN/m²)
J (10 G)
ε (%)
280
260
240
220
200
180
160
140
120
100
80
60
40
20
2000
1800
1600
1400
1200
1000
800
600
400
200
10
20
30
40
50

Fig. 3

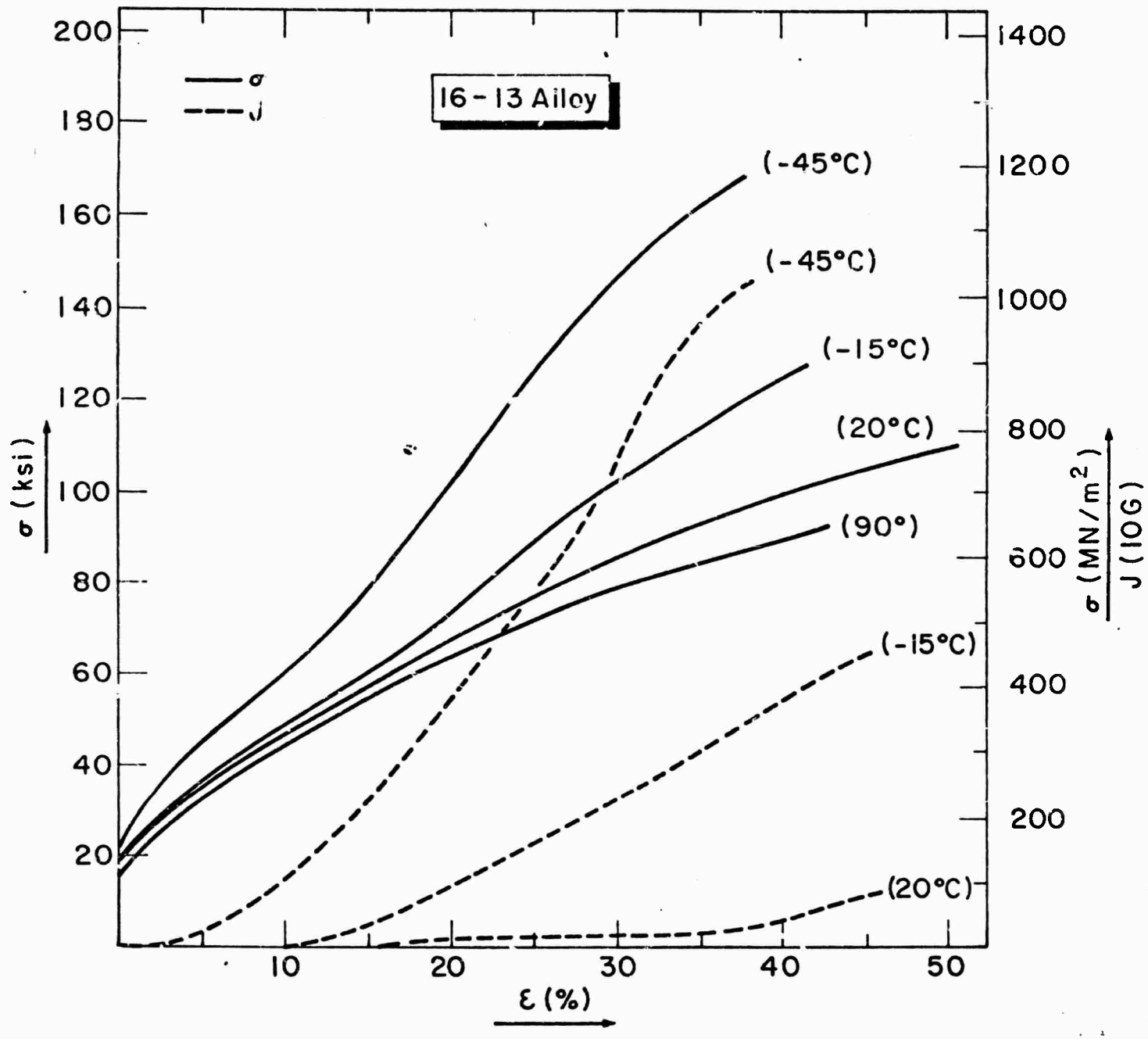
16 - 13 Alloy
σ
J
(-45°C)
(-45°C)
(-15°C)
(20°C)
(90°)
(-15°C)
(20°C)
σ (ksi)
σ (MN/m²)
J (10G)
ε (%)
200
180
160
140
120
100
80
60
40
20
1400
1200
1000
800
600
400
200
10
20
30
40
50

Fig. 4

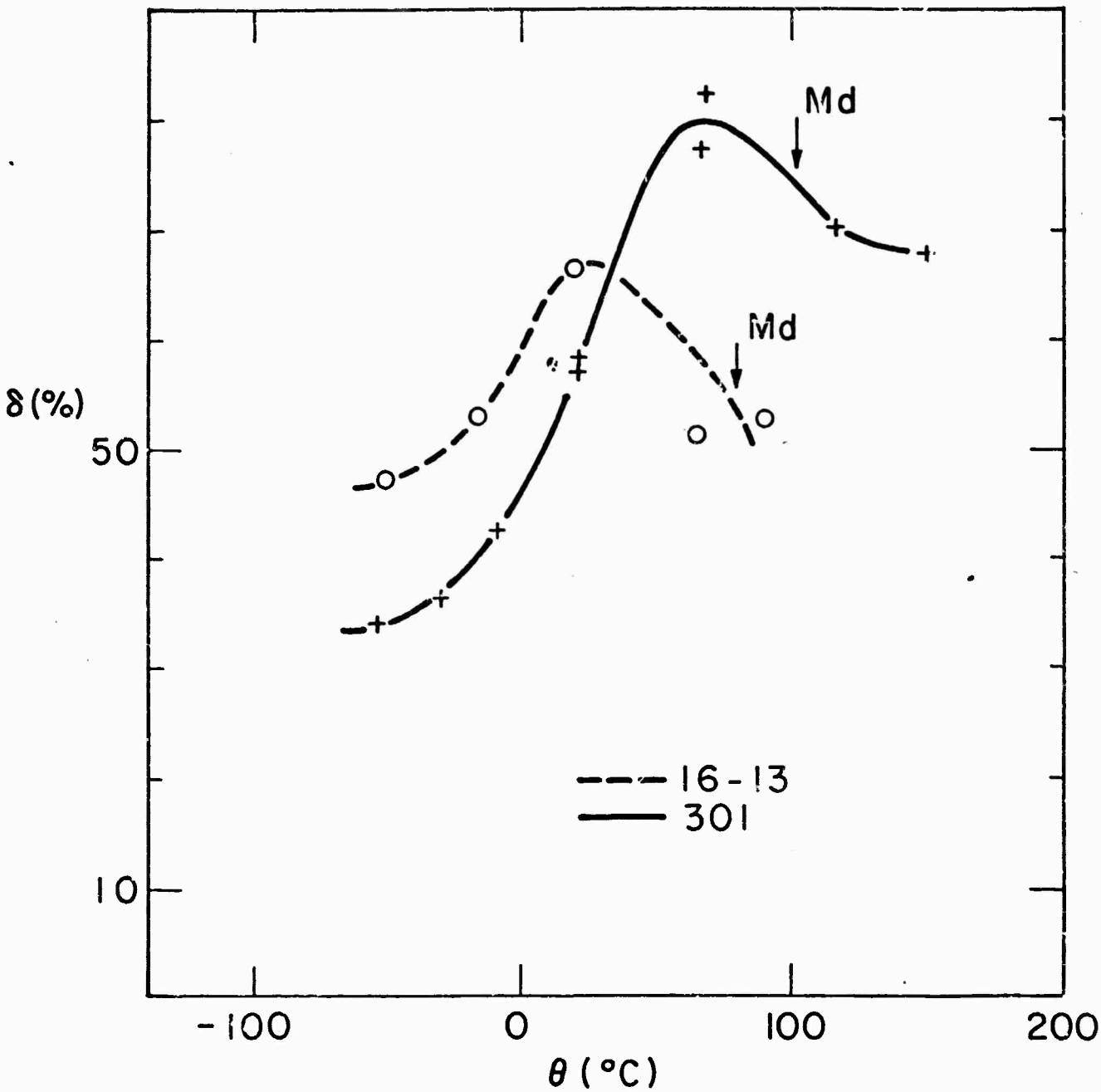

Fig. 5

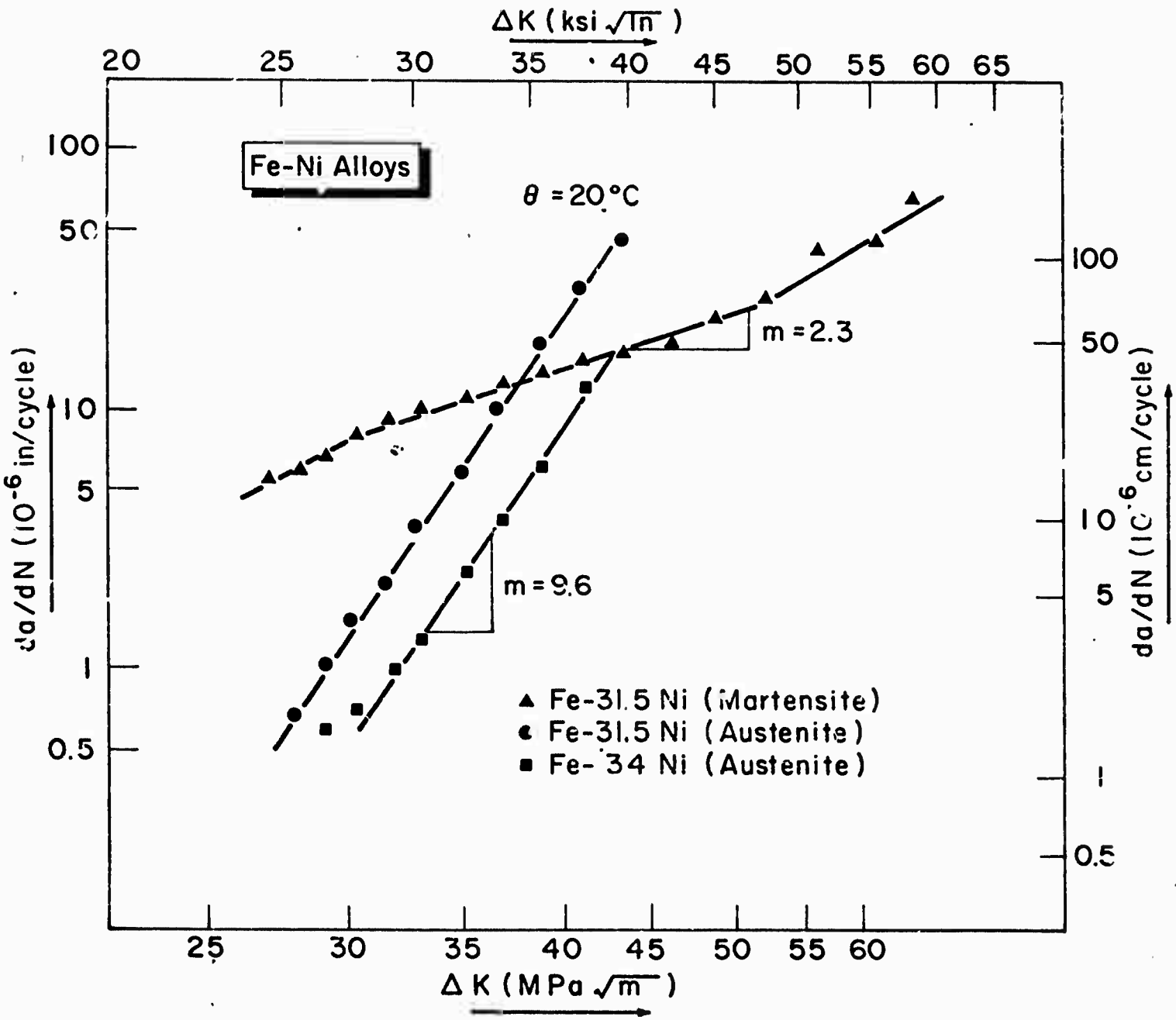
ΔK (ksi √in)
20
25
30
35
40
45
50
55
60
65
Fe-Ni Alloys
θ = 20°C
m = 2.3
m = 9.6
▲ Fe-31.5 Ni (Martensite)
● Fe-31.5 Ni (Austenite)
■ Fe-34 Ni (Austenite)
da/dN (10⁻⁶ in/cycle)
100
50
10
5
1
0.5
da/dN (10⁻⁶ cm/cycle)
100
50
10
5
1
0.5
25
30
35
40
45
50
55
60
ΔK (MPa √m)

Fig. 6

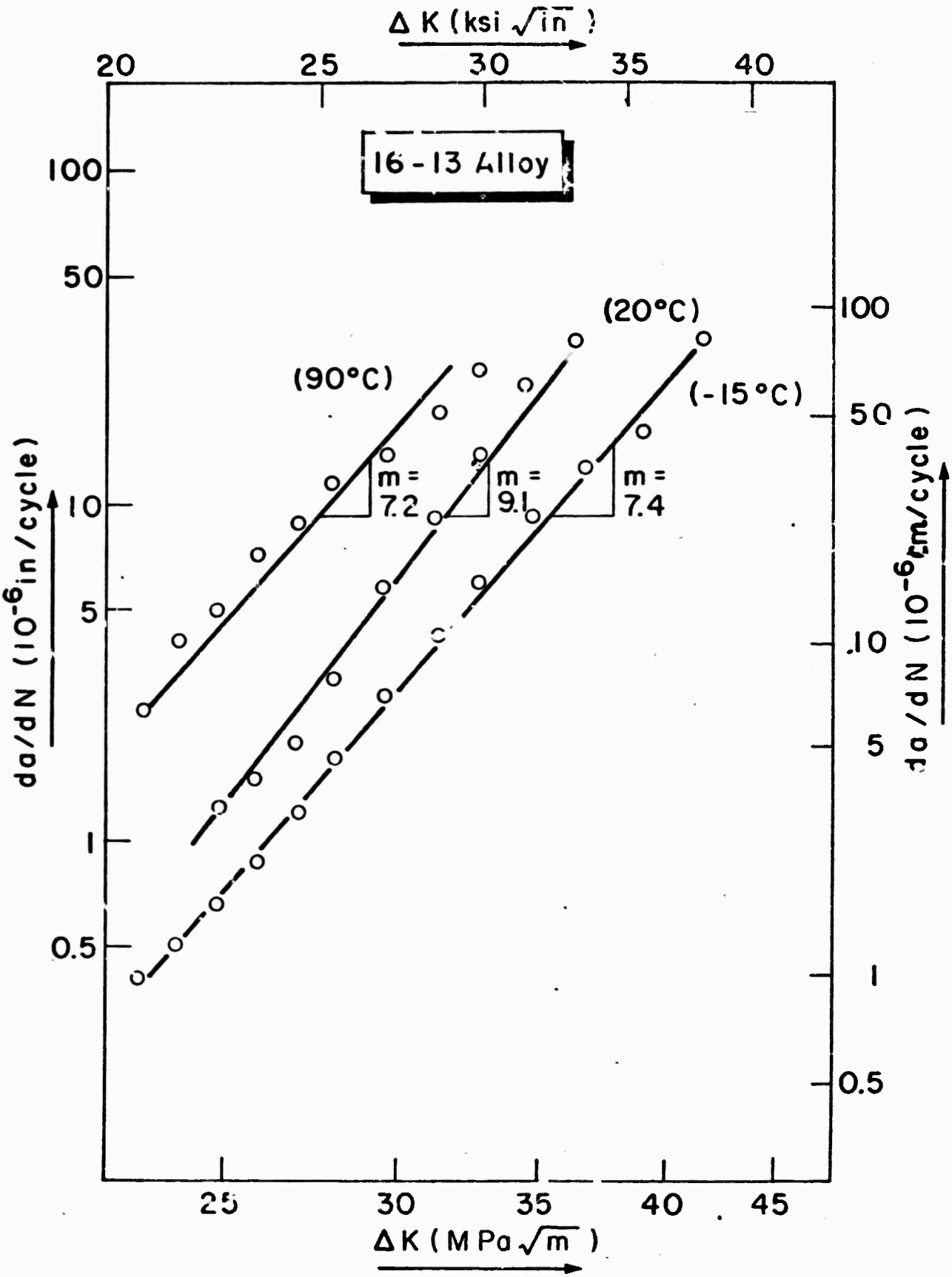
ΔK (ksi √in)
20
25
30
35
40
16-13 Alloy
100
50
10
5
1
0.5
(90°C)
(20°C)
(-15°C)
m = 7.2
m = 9.1
m = 7.4
da/dN (10⁻⁶ in/cycle)
da/dN (10⁻⁶ cm/cycle)
100
50
10
5
1
0.5
25
30
35
40
45
ΔK (MPa √m)

Fig. 7

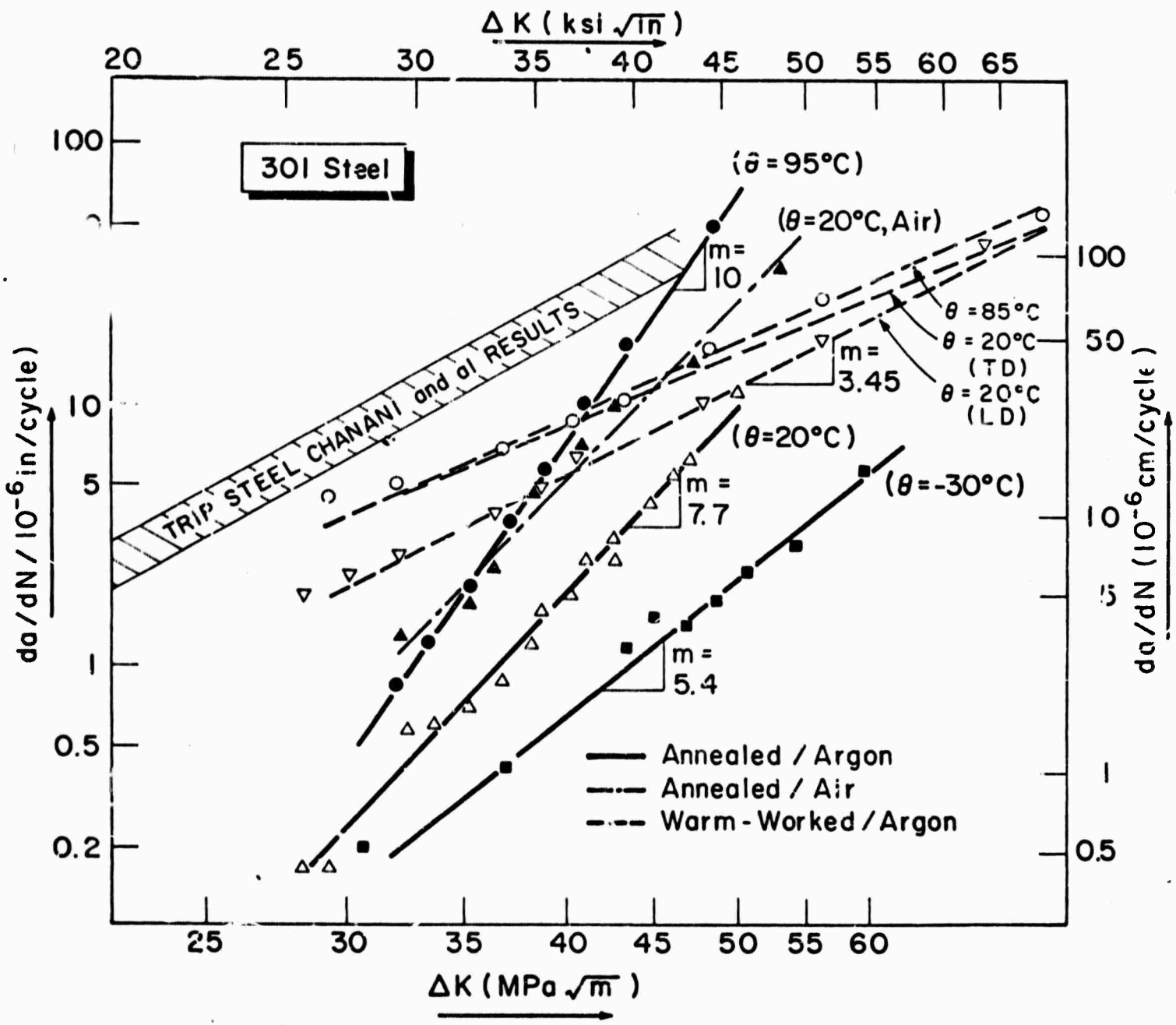
ΔK (ksi √in)
20
25
30
35
40
45
50
55
60
65
301 Steel
(θ = 95°C)
(θ=20°C, Air)
m = 10
TRIP STEEL CHANANI and al RESULTS
θ = 85°C
θ = 20°C (TD)
θ = 20°C (LD)
m = 3.45
(θ=20°C)
m = 7.7
(θ=-30°C)
m = 5.4
Annealed / Argon
Annealed / Air
Warm - Worked / Argon
da/dN / 10^-6 in/cycle)
100
10
5
1
0.5
0.2
da/dN (10^-6 cm/cycle)
100
50
10
5
1
0.5
25
30
35
40
45
50
55
60
ΔK (MPa √m)

Fig. 8

(a) (b)

Fig. 10

(a)

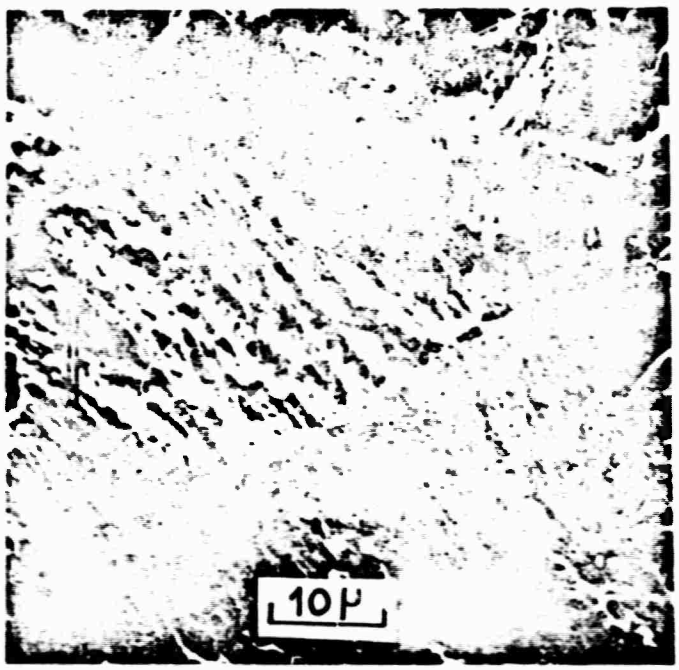

(b)

Fig. 11

(a) (b)

Fig. 12

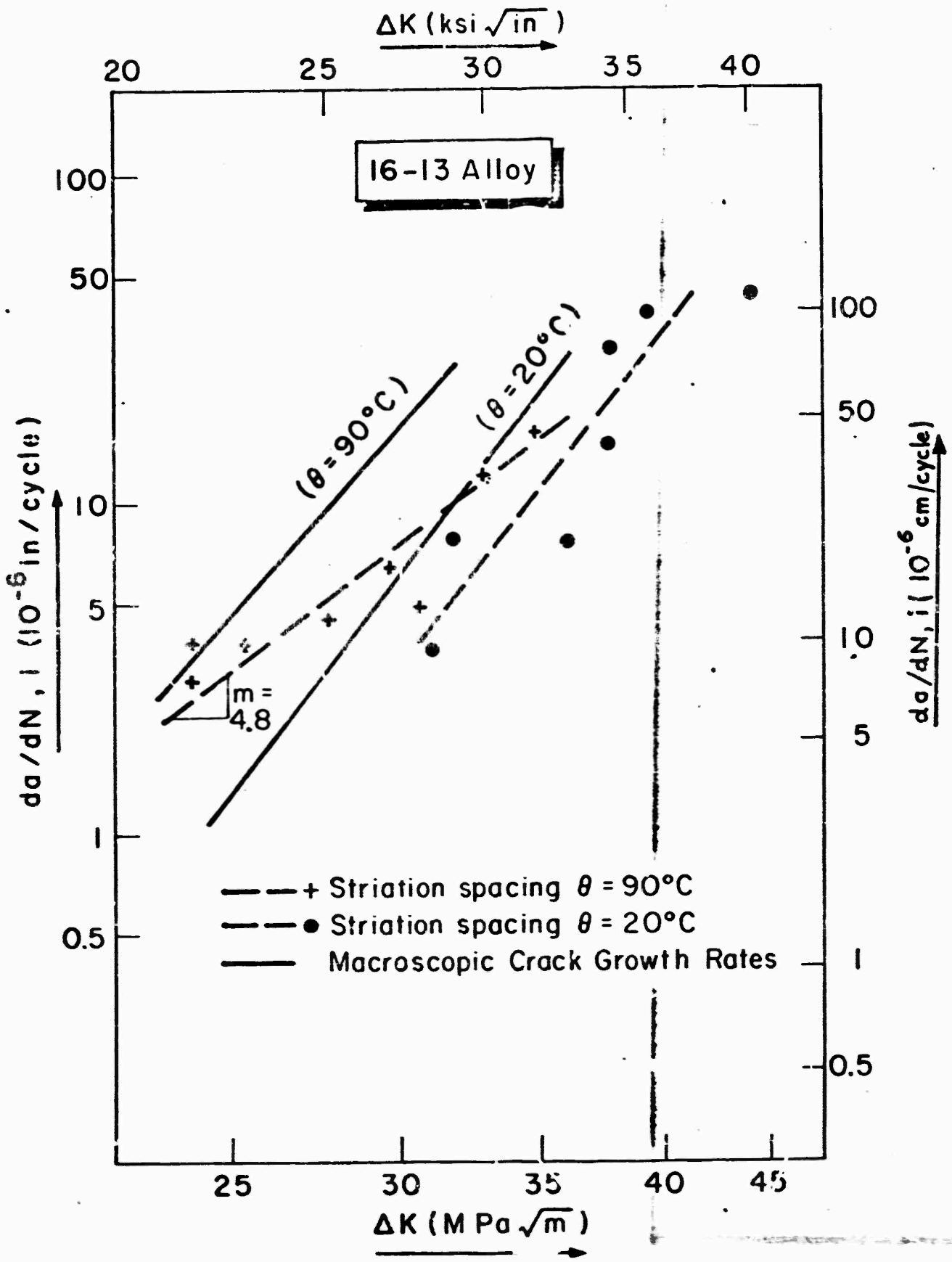
ΔK (ksi √in)
20
25
30
35
40
16-13 Alloy
100
50
10
5
1
0.5
(θ=90°C)
(θ=20°C)
m = 4.8
da/dN, i (10⁻⁶ in/cycle)
da/dN, i (10⁻⁶ cm/cycle)
+ Striation spacing θ = 90°C
● Striation spacing θ = 20°C
Macroscopic Crack Growth Rates
25
30
35
40
45
ΔK (M Pa √m)

Fig. 13

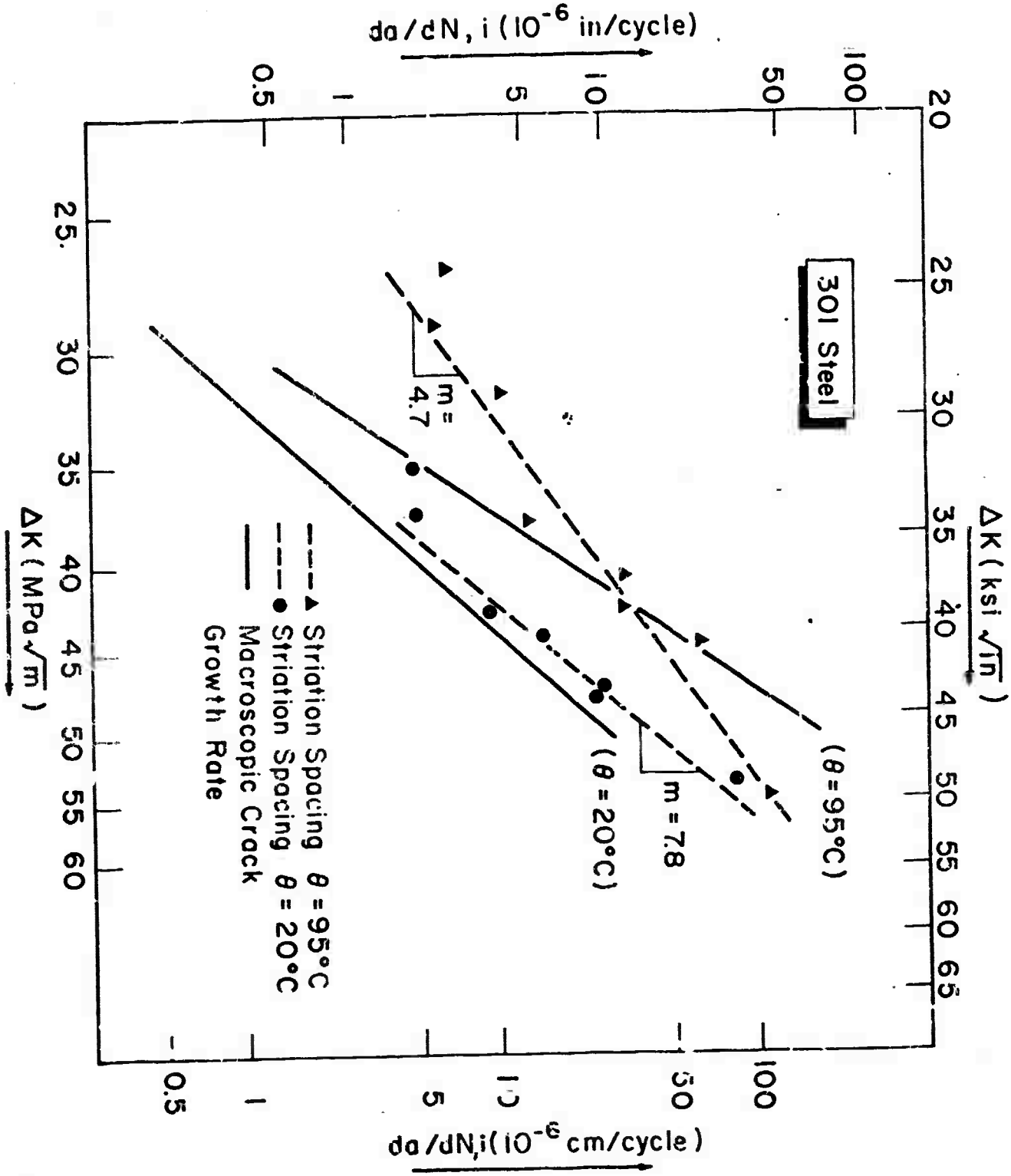
301 Steel
ΔK (ksi √in)
da/dN, i (10^-6 in/cycle)
da/dN,i(10^-6 cm/cycle)
ΔK (MPa √m)
(θ = 95°C)
(θ = 20°C)
m = 7.8
m = 4.7
Striation Spacing θ = 95°C
Striation Spacing θ = 20°C
Macroscopic Crack Growth Rate

Fig. 14

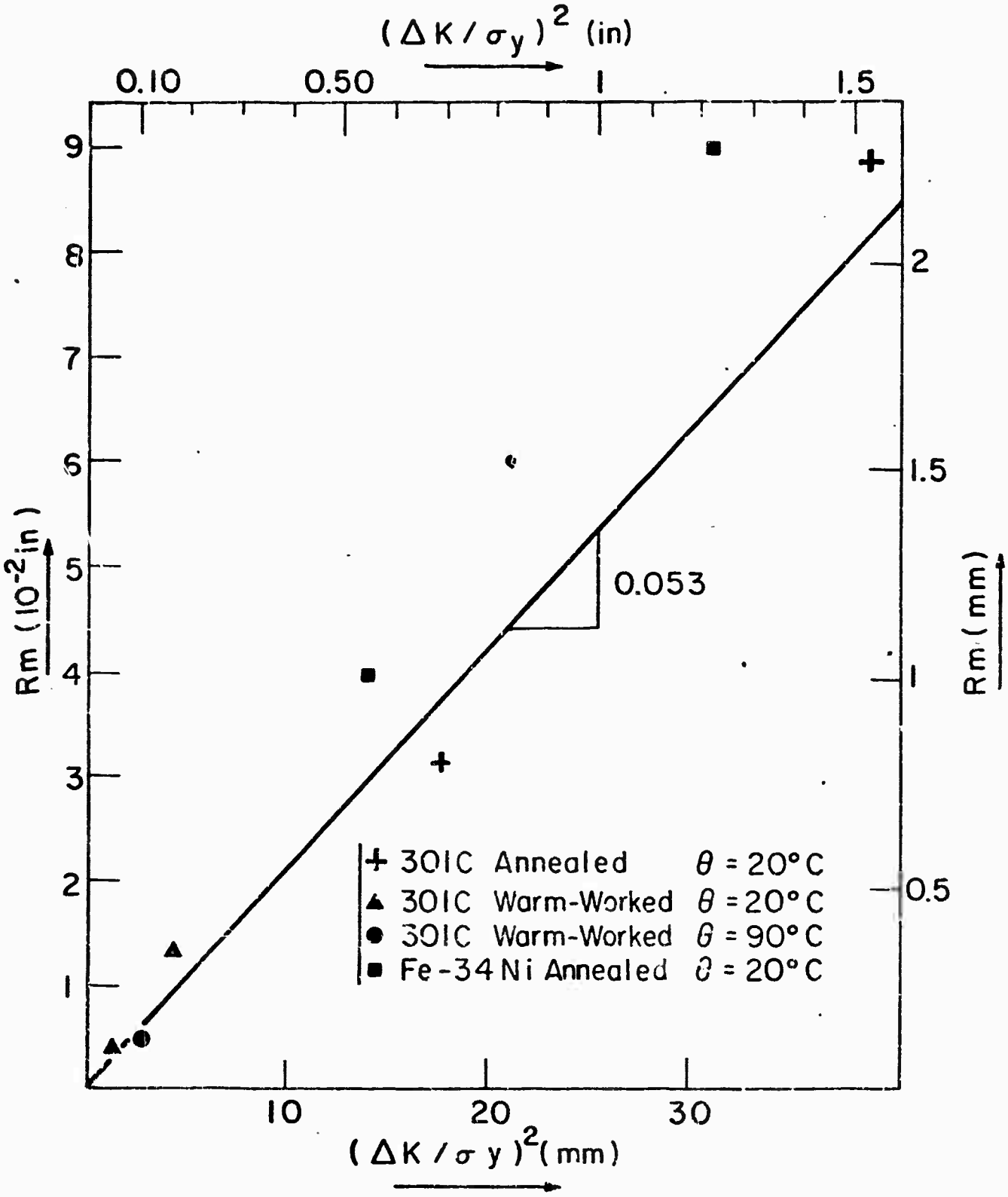
(ΔK / σy)² (in)
0.10
0.50
1
1.5
9
8
7
6
5
4
3
2
1
Rm (10⁻² in)
2
1.5
1
0.5
Rm (mm)
0.053
+ 301C Annealed θ = 20°C
▲ 301C Warm-Worked θ = 20°C
● 301C Warm-Worked θ = 90°C
■ Fe-34 Ni Annealed θ = 20°C
10
20
30
(ΔK / σ y)²(mm)

Fig. 15

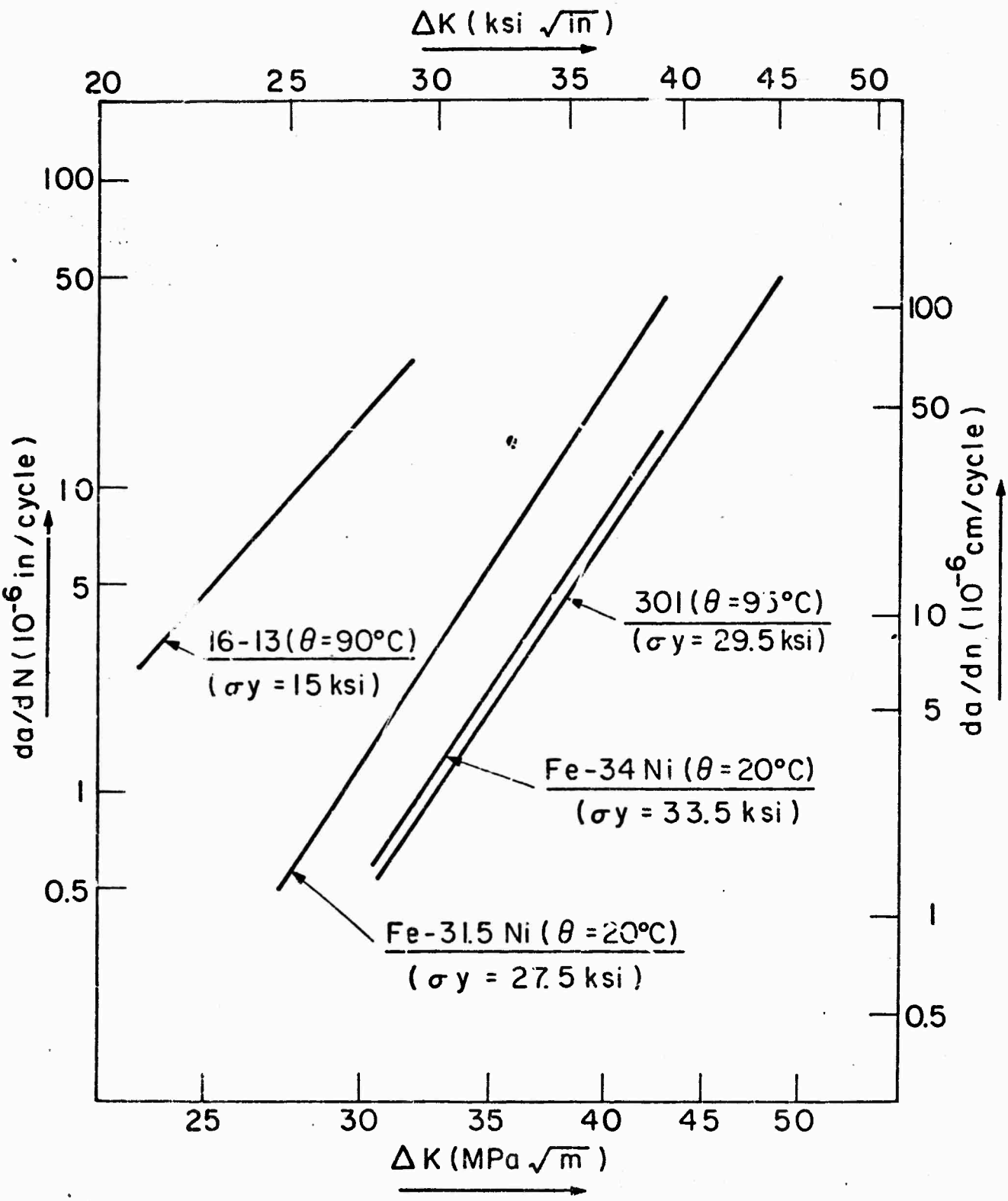
ΔK (ksi √in)
20
25
30
35
40
45
50
100
50
10
5
1
0.5
da/dN (10^-6 in/cycle)
100
50
10
5
1
0.5
da/dn (10^-6 cm/cycle)
16-13 (θ=90°C)
(σy = 15 ksi)
301 (θ=95°C)
(σy = 29.5 ksi)
Fe-34 Ni (θ=20°C)
(σy = 33.5 ksi)
Fe-31.5 Ni (θ=20°C)
(σy = 27.5 ksi)
25
30
35
40
45
50
ΔK (MPa √m)

Fig. 16

SEMI-ANNUAL TECHNICAL REPORT #1

Period: July 1, 1973 - Dec. 31, 1973

Title: Research in Materials Sciences

Project Title: Materials Characterization Using Laser Light Scattering Spectroscopy

Contract Number: DAHC 15-73-C-0316

ARPA Order Number: 2469

Program Code Number: 3D10

Name of Contractor: Massachusetts Institute of Technology
Cambridge, Mass. 02139

Principal Investigator: N.J. Grant (617) 253-5638

Project Scientists or Engineers: George B. Benedek (617) 253-4828

Effective Date of Contract: June 1, 1973

Contract Expiration Date: May 31, 1974

Amount of Contract: $425,000

Amount of Project: $ 72,500

Sponsored By

Advanced Research Projects Agency

ARPA Order No. 2469

SEMI-ANNUAL TECHNICAL REPORT

July 1 - Dec. 31, 1973

George B. Benedek

During the period July 1 - Dec. 31 our work has been devoted to three major areas.

a) Characterization of the viscoelastic properties of gels from the quasi-elastic spectrum of the scattered laser light.

b) The measurement of the equation of state of a two-dimensional monolayer "gas".

c) The study of the onset and structure of turbulence from the spectrum of light, microwaves or sound waves scattered from the fluid.

We shall report here on the progress of each of these in turn.

a) Dr. T. Tanaka and D. L. Hocker have succeeded in measuring the spectrum of laser light scattered from poly-acrylamide gels as a function of the gel density, scattering angle, and the temperature. They have been able to interpret their data in terms of a theory whose principal parameters are the elastic constant of the gel fiber network, and the friction factor between the fiber network and the gel liquid. In fact from their measurements they were able to measure the ratio of these quantities, and the temperature dependence of this ratio. By means of painstaking mechanical measurements they were able to measure macroscopically both the elastic constant and friction factor and were able to demonstrate that the values so determined were in excellent agreement with those found from the light scattering spectra. They also showed that the temperature dependence of the elastic constant, as obtained from the light scattering measurements was not quite linearly proportional to the temperature. This measurement of the departure from linearity has important consequences for the theory of random polymer chains. This work

has been written up and has appeared in the Journal of Chemical Physics, 59, 5151, 1973. Dr. Hocker is now at the Lincoln Laboratories of M.I.T.

b) Dr. Gilbert Hawkins has measured the pressure-area isotherms of a two-dimensional gas of pentadecylic acid molecules resting on the surface of water. He designed, and brought into operation, an apparatus for this purpose whose sensitivity exceeded by a factor 10 previous studies of surface monolayers. With this apparatus Dr. Hawkins demonstrated for the first time the existence of a critical point in a gas-liquid type of transition, for a two-dimensional system. He also measured the shape of the "gas-liquid" coexistence curve and the exponent which describes the divergence of the compressibility. The results were interpreted in terms of a mean field theory which succeeds in predicting the exponents characterizing the divergence of the compressibility and the shape of the coexistence curve. The mean field description is consistent with the existence of long-range interactions between the polar molecules of pentadecylic acid. This work represents the first measurement, of the equation of state of a two-dimensional monolayer and should stimulate the investigation of the rich range of phase transitions which are possible in such two-dimensional systems.

This work has just been written up for publication as a Physical Review Letter. The manuscript was submitted in Dec. 1973. Dr. Hawkins is now a Miller Institute Fellow in Physics at the University of California at Berkeley.

c) Mr. Ben Ross and Professor G. Benedek are now reviewing the literature on experimental and theoretical studies of the transition between laminar and turbulent fluid flow. Since the development of light scattering spectroscopy, it has been clear that a new technical instrument now exists for the accurate measurement of velocity and velocity correlations in fluid flow. That instrument is the detection of Doppler shifts in the flowing fluid by the methods of optical mixing spectroscopy. The subject of the laminar-turbulent transition is one of

great practical and theoretical importance. We are now endeavoring to determine what is known about the complex phase boundaries of the transition, and the characteristics of the flow whose measurement is of principle importance. At this stage we are in a literature search and discussion phase.

Report Summary

In the period July 1 - Dec. 31 we have completed two separate investigations. The first is a study of the spectrum of light scattered quasi-elastically from gels. The second is the accurate measurement of the equation of state of a two-dimensional gas of pentadecylic acid water molecules on the surface of water. We are now in the process of analysis of the problem of the accurate characterization of the laminar-turbulent flow transition in high speed flow. The experimental method employed would be that of optical mixing spectroscopy, or if the characteristic size of fluctuation requires it, we will use microwave or ultrasonic waves for the scattering spectroscopy.